

ISTANBUL TECHNICAL UNIVERSITY ★ INFORMATICS INSTITUTE

**BIOMECHANICAL MODELING OF GROWTH AND REMODELING
PROCESS IN SOFT BIOLOGICAL TISSUE**



Ph.D. THESIS

Gürsan ÇOBAN

Computational Science and Engineering Department

Computational Science and Engineering Program

SEPTEMBER 2016

ISTANBUL TECHNICAL UNIVERSITY ★ INFORMATICS INSTITUTE

**BIOMECHANICAL MODELING OF GROWTH AND REMODELING
PROCESS IN SOFT BIOLOGICAL TISSUE**

Ph.D. THESIS

**Gürsan ÇOBAN
(702072004)**

Computational Science and Engineering Department

Computational Science and Engineering Program

Thesis Advisor: Prof. Dr. M. Serdar ÇELEBİ

SEPTEMBER 2016

İSTANBUL TEKNİK ÜNİVERSİTESİ ★ BİLİŞİM ENSTİTÜSÜ

**YUMUŞAK DOKULARDA BÜYÜME VE YENİDEN-MODELLEME
SÜREÇLERİNİN BİYOMEKANİK OLARAK MODELLENMESİ**

DOKTORA TEZİ

**Gürsan ÇOBAN
(702072004)**

Hesaplamalı Bilim ve Mühendislik Anabilim Dalı

Hesaplamalı Bilim ve Mühendislik Programı

Tez Danışmanı: Prof. Dr. M. Serdar ÇELEBİ

EYLÜL 2016

Gürsan ÇOBAN, a Ph.D. student of ITU Informatics Institute Engineering and Technology 702072004 successfully defended the thesis entitled “BIOMECHANICAL MODELING OF GROWTH AND REMODELING PROCESS IN SOFT BIOLOGICAL TISSUE”, which he/she prepared after fulfilling the requirements specified in the associated legislations, before the jury whose signatures are below.

Thesis Advisor : **Prof. Dr. M. Serdar ÇELEBİ**
İstanbul Technical University

Jury Members : **Prof. Dr. M. Serdar ÇELEBİ**
İstanbul Technical University

Prof. Dr. Tuncer TOPRAK
Bahçeşehir University

Prof. Dr. Can YÜCESOY
Boğaziçi University

Prof. Dr. Ata MUĞAN
İstanbul Technical University

Doc. Dr. Kerem PEKKAN
Koç University

Date of Submission : **2 May 2016**

Date of Defense : **9 September 2016**





To Gülçin and İpek,



FOREWORD

I would thank to my thesis advisor Serdar Çelebi, the thesis' committee members Tuncer Toprak and Can Yücesoy who greatly contributed to shaping the technical details and the realization of this thesis.

Additionally, I gratefully thank my wife Gülçin and my family who provided me an exceptional moral support. Without them, the completion of this work would not be possible.

9 September 2016

Gürsan ÇOBAN



TABLE OF CONTENTS

	<u>Page</u>
FOREWORD	ix
TABLE OF CONTENTS	xi
ABBREVIATIONS	xv
SYMBOLS	xvii
LIST OF TABLES	xxiii
LIST OF FIGURES	xxv
SUMMARY	xxix
ÖZET	xxxii
1. INTRODUCTION	1
1.1 Randomness, Cellular Functions, and Cellular Mechanics	8
1.2 Purpose of Thesis	9
1.3 Literature Review	12
2. THEORETICAL BACKGROUND	17
2.1 Kinematics and Analysis of Deformation	17
2.2 Continuum Mass, Force, and Stress Concepts	18
2.2.1 Continuum bodies.....	18
2.2.2 Force	19
2.2.3 Stress concept	24
2.3 Balance Laws.....	26
2.3.1 Conservation of mass.....	26
2.3.2 Balance of linear and angular momentum.....	27
2.3.3 Balance of mechanical energy	28
2.3.4 Entropy inequality	29
3. EVOLUTION OF STRUCTURAL TENSORS	31
3.1 Purpose	31
3.2 Constitutive Framework for the General Theory of Growth	31
3.2.1 Multiplicative decomposition of the deformation gradient	38
3.2.1.1 Growth and remodeling formulations for the evolution of mass density	39
3.2.1.2 Notes on the algorithmic update procedures of the growth and remodeling variables.....	40
3.3 Mechanical Evolution Laws for the Growth and Remodeling Process	43
3.3.1 Evolution of growth and structural tensor	44
3.3.2 Micro-Structural evolution of the growth and remodeling processes and its relationship with governing constitutive equations.....	46
3.4 Current Approaches That Aim to Understand the Evolution of the Structural Tensors in a Growth and Remodeling Process	49

3.4.1	The time-dependent fiber reorientation approach based on the mechanically motivated vector differential equations	51
3.4.2	Remodeling of the fiber directions via the evolution of angular parameters.....	53
3.4.3	Fiber remodeling approaches based on n -chain networks	54
3.5	Time Dependent Evolution of the Statistically Dispersed Fiber Directions...	59
3.5.1	Evolution of the orientation density distribution of the fiber dispersion	59
3.5.2	Biologically motivated approaches.....	62
3.5.3	κ -based remodeling approaches for the evolution of the generalized structural tensor (GST).....	65
4.	A PRELIMINARY FORMULATION: A COMPUTATIONAL MODEL TO PREDICT THE EVOLUTION OF HYDROXYPROLINE CONCENTRATION AND TRANSITION STRETCH IN FIBRIN GELS	67
4.1	Purpose and Motivation.....	67
4.2	Theoretical Framework.....	67
4.2.1	Essential kinematics and constitutive equations.....	67
4.2.2	Evolution of collagen production based on the modulation transition stretch	69
4.2.3	A locally linear fiber remodeling formulation based on langevin force.	71
4.3	Model Parameters and Their Intervals.....	76
4.3.1	Problem specification	76
4.3.2	Material parameters for fibrin-based engineered tissue.....	77
4.3.3	Collagen remodeling and transition stretch.....	79
4.3.4	Rotation rate	81
4.4	Numerical Implementation: Solution Method and Software	81
4.5	Results and the Validation of the Algorithm	82
4.5.1	Evaluation of the experimental validation of the framework	84
5.	A NOVEL FIBER REMODELING FORMULATION BASED ON LANGEVIN FORCE.....	95
5.1	Purpose	95
5.2	Theoretical Framework.....	95
5.2.1	Essential kinematics and constitutive equations.....	95
5.2.2	A locally linear fiber remodeling formulation based on a Langevin force.....	98
5.2.3	Interpretation of the functional forms of drift and diffusion terms	101
5.2.4	Comparison of the proposed algorithm with existing modeling approaches	103
5.2.4.1	Ornstein-Uhlenbeck interpretation of the evolution of statistical dispersion.....	103
5.2.4.2	Computational efficiency of the algorithm	108
5.3	Numerical Implementation.....	109
5.3.1	Deformation of a “single layered” and “internally pressurized” axisymmetric cylindrical artery tube	109
5.3.2	Model parameters	115
5.4	Application and Results.....	116
6.	CONCLUSION AND FUTURE PERSPECTIVES.....	125

6.1 General Comments on Simulations, Numerical Problems and Future Perspectives	125
6.1.1 Perspectives on growth and remodeling models	130
6.1.2 Perspectives on numerical problems	130
6.1.3 Perspectives on experimental validation related issues	131
6.1.4 Interdisciplinary reflections to other scientific fields (complex systems, social sciences and paleontology)	132
6.1.4.1 Profitable utilization by randomness in social systems	132
6.1.4.2 Complex systems	133
6.1.4.3 Separation of evolutionary time scale from the growth and remodeling time scale	134
6.2 Closure.....	135
REFERENCES.....	137
APPENDICES.....	145
CURRICULUM VITAE.....	152





ABBREVIATIONS

ECM	: Extra Cellular Matrix
GR	: Growth and Remodeling
AAA	: Abdominal Aortic Aneurysm
SF	: Stress Fiber
MMP	: Matrix Metalloproteinases
TIMP	: Tissue Inhibitor Metalloproteinases
GAG	: Glycosaminoglycan
Hyp	: Hydroxyproline
UTS	: Ultimate Tensile Stress
DNA	: Deoxyribonucleic Acid
Fb	: Fibrinogen
Tb	: Thrombin
GST	: Generalized Structural Tensor (sGST for the symmetric definition)
AI	: Angular Integration
TGF-β	: Transforming Growth Factor beta
APE	: Absolute Percentage Error
MAPE	: Mean Absolute Percentage Error
Adj-R^2	: Adjusted R -square
SED	: Strain Energy Density
TL	: Total Lagrangian



SYMBOLS

\mathbf{n}_i^C	: i^{th} eigenvector of $C \in \mathcal{V}^2$
λ_i^C	: i^{th} eigenvalue of $C \in \mathcal{V}^2$
φ	: Deformation mapping (chapter 2 and 3)
Π	: Deformation mapping (chapter 4 and 5)
\mathcal{B}	: Deforming body (physical), an open subset of Euclidian space
Ω_0	: Material configuration
\mathbf{X}	: Vector of a material point
\mathbf{x}	: Vector of a spatial point
$\partial\Omega$: Configuration of the boundary layer that surrounds Ω
$\underline{\Omega}^{(k)}$: k^{th} intermediate configuration
$\tilde{\Omega}_t$: The spatial configuration at time t
$\tilde{\nabla}$: The gradient operator defined w.r.t $\tilde{\Omega}_t$
∇_0	: The gradient operator defined w.r.t Ω_0
\mathbf{P}	: First Piola-Kirchhoff stress tensor $\mathbf{P} \in \mathcal{V}^2$
\mathbf{S}	: Second Piola-Kirchhoff stress tensor $\mathbf{S} \in \mathcal{V}^2$
\mathbf{M}	: Mandel stress tensor $\mathbf{M} \in \mathcal{V}^2$
$\boldsymbol{\sigma}$: Cauchy stress tensor $\boldsymbol{\sigma} \in \mathcal{V}^2$
$\boldsymbol{\tau}$: Kirchoff stress tensor $\boldsymbol{\tau} \in \mathcal{V}^2$
\mathbf{N}	: Normal vector on $\partial\Omega_0$ (also \mathbf{N}_0)
\mathbf{n}	: Normal vector on $\partial\tilde{\Omega}$ (also $\tilde{\mathbf{n}}$)
$\partial\Omega'$: The virtual boundary layer that a traction vector is normal to
\mathbf{t}	: True Cauchy traction
\mathbf{T}	: Nominal Piola-Kirchhoff traction
\mathbf{F}	: Deformation Gradient Tensor
\mathbf{C}	: Right Cauchy-Green deformation tensor
\mathbf{b}	: Left Cauchy-Green deformation tensor
\mathbf{E}	: Green-Lagrange material strain tensor
$\boldsymbol{\varepsilon}$: Euler-Almansi spatial strain tensor (also \mathbf{e})
\mathbf{v}	: Spatial velocity (also $\tilde{\mathbf{v}}$)
\mathbf{l}	: Spatial velocity gradient (also $\tilde{\mathbf{l}}$)
\mathbf{L}	: Material version of spatial velocity gradient
J	: Jacobian of deformation gradient \mathbf{F}
$\dot{(\mathbf{u})}$: Material time derivative of \mathbf{u}
$\overset{\circ}{(\mathbf{h})}$: Objective rate of a second order tensor \mathbf{h}
$\underset{\nabla}{(\mathbf{h})}$: Truesdel rate of a second order tensor \mathbf{h}
$\det\{\mathbf{A}\}$: Determinant of a second order tensor \mathbf{A}
$\text{tr}\{\mathbf{A}\}$: Trace of a second order tensor \mathbf{A}
$\text{dev}\{\mathbf{A}\}$: Deviatoric part of \mathbf{A} , $\text{dev}(\cdot) = (\cdot) - (1/3)\text{tr}(\cdot)\mathbf{I}$
$\text{sym}\{\mathbf{A}\}$: Symmetric part of \mathbf{A}
$\text{skw}\{\mathbf{A}\}$: Skew symmetric part of \mathbf{A}
$(\cdot) : (\cdot)$: Double contraction operator

$\text{mass}[\cdot]$: Mass of (\cdot)
$\text{vol}[\cdot]$: Volume of (\cdot)
$\text{vol}[\tilde{\Omega}(\mathbf{X}_\epsilon)]$: Volume of a configuration of the infinitesimal hyperball with radius ϵ at center \mathbf{X}
\mathbf{b}	: $\mathbf{b} : \Omega \rightarrow \mathcal{V}$ body force field
\mathbf{r}_b	: Resultant force $\int_\Omega \mathbf{b}(\mathbf{X})d\Omega$
torque(\mathbf{b})	: Torque created by the force field \mathbf{b}
$\mathbf{u}(\mathbf{X})$: $\mathbf{u} : \Omega_0 \rightarrow \mathcal{V}$ displacement at \mathbf{X}
\mathbf{R}	: Rotation matrix as an element of the polar decomposition
\mathbf{U}, \mathbf{V}	: Stretch matrices as the elements of polar decomposition
$(\cdot)_0$: A material magnitude (i.e. a tensor $(\cdot) : \Omega \rightarrow \mathcal{V}^n$)
(\cdot)	: A spatial magnitude (i.e. a tensor $(\cdot) : \Omega \rightarrow \mathcal{V}^n$)
λ	: Stretch of a spatial direction (chapter 2 and 3)
\mathbf{D}	: The symmetric part of the velocity gradient tensor, as $\mathbf{v} \otimes (\nabla)_{sym}$
$\mathcal{I}_i^{(\cdot)}$: i^{th} invariant of the mechanical magnitude (\cdot) in a continuum configuration
$\mathcal{I}_i^{(\cdot)*}$: The dispersed κ - based invariant
\mathbf{L}	: Total linear momentum
\mathbf{J}	: Total angular momentum
\mathbf{F}	: Forces
\mathbf{M}	: Moment of the forces
\mathcal{P}_{ext}	: External mechanical power
\mathcal{K}	: Kinetic energy
\mathcal{P}_{int}	: The rate of internal mechanical work
\mathcal{S}	: The total entropy
$\tilde{\eta}$: The entropy per unit spatial volume
\mathcal{D}_{int}	: The internal dissipation function
\mathcal{T}	: The absolute temperature (in chapter 2 and 3), the transfer function (in chapter 5)
Ψ, Ψ_H	: Helmholtz free energy
$\Psi(\cdot)$: Definition of the Helmholtz free energy specified by (\cdot)
u_{int}	: The internal free energy (without the dissipation term)
$\{\underline{\Omega}^i\}_{i=1}^n$: The splitting of the time-dependent configuration of the motion into n number of intermediate virtual steps
$\mathbf{F}_e, \mathbf{F}_g$: The elastic and growth parts of the total deformation gradient,
$(\cdot)_e$: The elastic part of a mechanical magnitude (\cdot)
$(\cdot)_g$: The growing part of a mechanical magnitude (\cdot)
$\Gamma_{(\cdot)}$: The flux of the material quantity (\cdot) that is defined for $\partial\Omega_0$
$\gamma_{(\cdot)}$: The flux of the spatial quantity (\cdot) that is defined for $\partial\tilde{\Omega}$ (chapter 3)
γ	: The random force parameter for the ratio of principal strains (chapter 4)
$R_{(\cdot)}(\mathbf{X})$: The internal source of (\cdot) in configuration Ω_0 located at \mathbf{X}
$r_{(\cdot)}(\mathbf{x})$: The internal source of (\cdot) in configuration $\tilde{\Omega}$ located at \mathbf{x}
\mathbf{p}_0	: Volume specific momentum density
Υ^i, Υ_i	: i^{th} internal variable that is defined with respect to per unit current mass
Υ_0^i	: i^{th} internal variable that is defined with respect to per unit initial mass
f_k	: Thermodynamic forces conjugate to the fluxes $d\Upsilon_k/dt$
$\rho(\mathbf{x}), \tilde{\rho}(\mathbf{x})$: Mass density at \mathbf{x} in $\tilde{\Omega}_t$ (in chapter 2 and 3)
$\rho_0(\mathbf{X})$: Mass density at \mathbf{X} in Ω_0 (in chapter 2 and 3)
$\rho^g(\mathbf{X})$: Mass density in the intermediate configuration

$\rho_0^g(\mathbf{X})$: The growing density in reference configuration
\mathcal{P}	: The rate of work done by the external and internal forces
\mathbf{q}	: The rate of work that is related to the heat flux \mathbf{q} across the surface element $\mathbf{n} dS$
w	: The rate of heat input per unit current mass
\mathcal{R}_g	: The thermodynamic conjugate variable that is associated to the rate of mass-growth which is sourced by the spatial mass source r_g
r_η	: Entropy production rate
η	: Entropy per unit mass
\mathbf{L}_g	: Growth velocity gradient
\mathbf{H}^*	: Homeostatic equilibrium condition for structural tensor
\mathbf{H}_p	: The set of structural tensors $p = \overline{1, n}$ that defines the fabric of the material domain $\mathbf{H} : \Omega_0 \rightarrow \mathcal{V}^2$
α	: Integration parameter for the Euler evolution (chapter 3)
$(\cdot)^{algo}$: The field quantity (\cdot) is considered to be the element of an "algorithmic update" procedure
$\{\mathbf{\Gamma}_\eta^{\Upsilon_k}\}_k$: The external entropy flux vector term for the k^{th} internal variable Υ_k
$\{R_\eta^{\Upsilon_k}\}_k$: The internal point-wise entropy source term
ν_{iso}, ν_{aniso}	: Isotropic and anisotropic growth parameters that are related to the growth deformation gradient tensor
\mathbf{Q}	: Rotation tensor that belongs to the symmetry group $SO(\dim)$
$\omega^{\tilde{\mathbf{n}}_t}$: Axis of rotation with respect to the spatial $\tilde{\mathbf{n}}_t$
$\angle(a, b)$: Angle between a, b
\mathbf{n}_{max}^C	: Homeostatic position vector which is the eigenvector associated with the maximum principal strain value
$\tau(\cdot)$: Characteristic remodeling time labeled by the subscript (\cdot)
$\text{Pr}(\cdot)$: Probability of (\cdot)
N_f	: Number of fiber families
n_c	: Number of distinct linear parts of a long polymer chain
l_c	: Length of the distinct parts in a polymer chain
d_r	: End-to-end distance characterizing the geometric macro-molecular conformation
L_c	: The total length of a macro-molecule
$\overline{d_{r-out}^2}$: The mean square value of the conformations that are the un-cross-linked free chains out of the polymer network
$\overline{d_{r-in}^2}$: The mean square value of the conformations that are the cross-linked chains in the polymer network
μ_c	: Shear modulus for the Neo-Hookean material
p_h	: Hydrostatic pressure
M_n	: n^{th} statistical moment of a probability density distribution
dS, dA	: Infinitesimal surface patches
$\text{Pr}(x \mu, k)$: Conditional probability of observing x when μ, k are given
b_{mig}	: Basal migration coefficient
b_{cell}	: Basal proliferation coefficient
q in \mathbf{H}^q	: The sensitivity parameter for the cell contact guidance
κ	: The dispersion parameter for the generalized structural tensor
E	: Green-Lagrange strain
\overline{E}	: Isochoric component of the Green-Lagrange strain

N_{cell}	: Total number of cells in a volume V
M_{DNA}	: Mass of DNA per cell
M_{coll}	: Mass of the collagen content
R_{hyp}^{coll}	: The collagen volume fraction constant
(η, ξ)	: The conversion constants of hydroxyproline and collagen (chapter 4)
E_M	: Elastic Modulus
C_1, D_1	: Shear and bulk modulus (chapter 4)
λ_h	: Homeostatic residual strain generated by the cellular activities (chapter 4)
λ_g	: Growth stretch (chapter 4)
τ_g	: Characteristic remodeling time constant for the transition stretch (chapter 4)
τ_w	: Characteristic remodeling time constant for fiber orientation (chapter 4)
φ_{max}	: Target concentration (max) in terms of hydroxyproline and DNA mass (chapter 4)
φ_{min}	: Target concentration (min) in terms of hydroxyproline and DNA mass (chapter 4)
λ_u	: Upper bound for the fiber stretch to activate φ_{max} (chapter 4)
λ_l	: Lower bound for the fiber stretch to activate φ_{min} (chapter 4)
$\frac{\tau_g}{(\cdot)}$: Characteristic time for the hydroxyproline synthesis (chapter 4)
$\overline{\mathbf{F}}$: Isochoric component of a mechanical magnitude (\cdot)
$\overline{\mathbf{F}}$: Isochoric component of the deformation gradient tensor \mathbf{F}
$U(J)$: Volumetric component of the strain energy density function
$\overline{\Psi}$: Isochoric component of the strain energy density function
\mathcal{H}	: Heaviside step function
$\mathbf{\Gamma}$: The random Langevin force term (chapter 5)
θ_μ	: The angle between the preferred direction and the current mean fiber orientation
$\hat{\kappa}$: Estimation of κ (chapter 5)
V	: Variance (chapter 5)
$\widetilde{\text{Pr}}$: Transition probability (chapter 5)
$\rho^{cell,coll}$: The mean vector length of the cell and collagen orientation (chapter 5)
τ_μ	: Characteristic evolution time for the mean vector (chapter 5)
τ_s	: Characteristic evolution time for the variance (chapter 5)
$\lambda_{r,\theta,z}$: Stretch components in cylindrical coordinates (chapter 5)
\mathbf{a}_μ	: The mean fiber orientation of the dispersed fiber distribution (chapter 5)
$R_{i,m,0}$: The inner, medial and outer radii of an artery in the undeformed reference configuration (chapter 5)
$r_{i,m,0}$: The inner, medial and outer radii of an artery in the deformed current configuration (chapter 5)
λ	: The axial pre-stretch (chapter 5)
Λ	: The residual stress definition (chapter 5)
P_0, p_0	: Internal blood pressure in kPa's (chapter 5)
\wedge	: The symbol for logical "or"
β	: The angle between the axial direction and preferred direction (chapter 5)
φ	: The angle between the mean fiber direction and axial direction (chapter 5)
E_z	: Axial direction
\sum	: The dispersion force term
\mathcal{M}	: Modulation function
$dW(t)$: Wiener process (chapter 4)

- ζ_u : Upper bound for the random force (chapter 4)
 γ : Nonlinearity exponent for the diffusion force (chapter 4)
 φ_{coll} : Collagen volume fraction (chapter 4)
 ν, ν_{ss} : The current and steady-state hydroxyproline concentrations (chapter 4)





LIST OF TABLES

	<u>Page</u>
Table 4.1 : Previous works that describe the mechanical properties of fibrin gels (<i>NA</i> : Not Available).	83
Table 4.2 : The predefined parameters, their descriptions and test intervals that are used in simulations.....	84
Table 5.1 : Constitutive parameters for isotropic and anisotropic contributions in the strain energy density function according to [1].	116
Table 5.2 : Parameter set used for media and adventitia, and remodeling simulation (see [1]).	116
Table 5.3 : Initial condition sets that are used for simulating six trial cases.....	117
Table A.1 : Approximating $\hat{\kappa}(s)$ functions for $\kappa - s$ transformation. ϵ represents the global error statistics.	149



LIST OF FIGURES

	<u>Page</u>
Figure 1.1 : Conceptual classification of the adaptive forces and their elements that are common in a thermodynamic system.	3
Figure 1.2 : The time-dependent change in structure can be considered as the finite deformation of a structure, donated by an evolution “function”, where the initial deformation process is triggered by an external “fluctuation”.	6
Figure 1.3 : Spatial and temporal scales that are observed in a growing and remodeling biological domain (adapted from [2]).	7
Figure 1.4 : As being the three main conceptual phenomena, growth-remodeling and morphogenesis give rise to the ontological formation of biological pattern formation and development.	10
Figure 1.5 : The three layers that are observed in many artery tissues. The layers are distinctively differentiated from each other by their preferred main fiber direction and biological elements (from [3]). ...	14
Figure 3.1 : Representation of the multiplicative decomposition of deformation gradient into its elastic and growth parts in the configuration space. The intermediate configuration is assumed to be a stress free one which permits independent deformation (and evolution) of the individual local body partitions in the configuration space. Each local body partition is deformed in a geometrically incompatible way via F_g . The final geometrically compatible body domain is constructed by the elastic deformation supplied by F_e	32
Figure 3.2 : A mass flux representation based on a virtual configuration Ω which has a point mass source at \boldsymbol{x}' . The mass flux is assumed to be observed through the boundary layer $\partial\Omega$ with a normal vector \boldsymbol{N}	33
Figure 3.3 : Representation of the multiplicative decomposition of the deformation gradient into its elastic and growth parts in the configuration space. The density relations that depend on the Jacobian of the transformations are presented as a function mapping.	39
Figure 3.4 : Graphical representation of the configuration mapping $\varphi : \Omega_0 \rightarrow \tilde{\Omega}_t$, and the successive intermediate configurations set.	42

Figure 3.5	: A transversely isotropic description of the anisotropic mass growth based on a characteristic direction \mathbf{a} which is mapped between configurations. The anisotropic growth is expressed by two growth parameters which correspond to the evolution of the eigenvalues of an ellipsoid representation of the growth deformation gradient.....	48
Figure 3.6	: The molecular conformations and corresponding end-to-end distance d_r . The distance d_r is a direct indicator for the probability of a geometric conformation. The molecules are represented by flexible lines.	55
Figure 3.7	: Fiber dispersion parameters are based on a circular probability distribution. A fiber direction vector \mathbf{a}^i is defined with respect to the Cartesian e_1 axis where $\phi^i = \angle(\mathbf{a}^i, e_1)$. The fiber orientation density Φ_f is a circular weight associated with the angular measurement ϕ and a circular dispersion parameter k . The figure is adapted from [4].....	61
Figure 4.1	: A sample drawing of the experiment samples and strip geometry. (a) Experimental design of a set of strips located on a fibrin block. (b) Rough geometry of the samples and their constrained regions.	77
Figure 4.2	: Experimentally observed hydroxyproline concentration data [5] and the best logistic type nonlinear growth fitting curve.	80
Figure 4.3	: Representation of the finite element discretization of strip geometry with 1848 hexahedral 8-node elements. A single node has been selected for data demonstration purposes. u_y is the displacement variable that belongs to the sample node.	81
Figure 4.4	: Representative True stress - Engineering strain curves for experimental UTS and modulus (a). The effect of the variation of anisotropic parameter k_2 compared with the layout of experimental UTS and modulus (b).	85
Figure 4.5	: Simulation results for the hydroxyproline production. The effects of varying φ_{max} , τ_g and t_ω on the evolution of hydroxyproline concentration (a and b).	86
Figure 4.6	: Simulation results for the Cauchy Stress σ_{xx} element. The effects of varying τ_g and φ_{max} on the evolution of stress measurements while λ_h and τ_ω are fixed (a). The effects of varying φ_{max} while φ_{max} τ_ω are fixed (b).....	87
Figure 4.7	: Simulation results for the Cauchy Stress u_y element. The effects of varying τ_g and φ_{max} on the evolution of displacement measurements while λ_h and τ_ω are fixed (a). The effects of varying φ_{max} while φ_{max} τ_ω are fixed (b).....	88
Figure 4.8	: Simulation results for the anisotropy ratio $(1 - \Lambda_{max-1}^H / \Lambda_{max}^H)$. The effects of varying τ_g and φ_{max} on the evolution of anisotropy ratio while λ_h and τ_ω are fixed (a). The effects of varying φ_{max} while φ_{max} and τ_ω are fixed (b).	89
Figure 4.9	: Simulation results for the evolution of the anisotropy ratio at days 0.5,14,21 and 28.	90

Figure 4.10	: Simulation results for the evolution of mean fiber direction \mathbf{a}_μ at days 0.5,2,10,20 and 30.	91
Figure 4.11	: Simulation results for the transition stretch λ_g . The effects of varying τ_g and φ_{max} on the evolution of λ_g while λ_h and τ_ω are fixed (a). The effects of varying φ_{max} while τ_g and τ_ω are fixed (b).	92
Figure 4.12	: Experimental validation of the model framework in accordance with the hydroxyproline production. The model could explain the experimental data for $\varphi_{max} = 490$ and the parameters can be fine-tuned in order to obtain exact compaction levels.	93
Figure 5.1	: (a) Statistical mean vector \mathbf{a}_μ of dispersed fiber bundle family in spherical parameterization $\mathbf{a}_\mu = \mathbf{a}_\mu(\Theta, \phi)$ according to the Cartesian basis $(\mathbf{e}_1, \mathbf{e}_2, \mathbf{e}_3)$ on reference configuration. (b) Rotation path of p^{th} fiber cluster accumulated around \mathbf{a}_μ towards its desired homeostatic position vector \mathbf{n} , where $\cos^{-1}(\mathbf{a}_\mu \cdot \mathbf{n}) = \theta^{(p)}$ and $\theta^{(p)} < \pi/2$, according to arbitrary orthogonal basis (η_i, η_j, η_k)	99
Figure 5.2	: Model fitting results of the mean collagen (θ_μ^{coll}) and mean cell (θ_μ^{cell}) orientation by using two parameter relationship $\theta_\mu(t) = \theta_0 \exp(-t/\tau_\mu)$. (a) best model fit ($\theta_0 = 17.98^\circ$, $\tau_\mu^{coll} = 17.93h$) for the mean collagen orientation and (c) natural logarithm of the dependent axis of the same analysis. (b) best model fit ($\theta_0 = 10.75^\circ$, $\tau_\mu^{cell} = 37.08h$) for the mean cell orientation and (d) natural logarithm of the dependent axis of the same analysis. The data in circles ((a)-(b)) are evaluated as the statistical outliers for the analysis by performing a Cook's distance analysis (from [6]).	105
Figure 5.3	: Model fitting results of the collagen (ρ^{coll}) and cell (ρ^{cell}) mean vector lengths by using the relationship in equation 5.30 with fixed characteristic remodeling time τ_μ (obtained from the previous analysis). (a) best model fits for the collagen orientation dispersion: comparison of the proposed approach and existing assumption of "equal characteristic times". (b) best model fit for the cell orientation dispersion: comparison of the proposed approach and existing assumption of equal characteristic times (from [6]).	106
Figure 5.4	: Model fitting results of the collagen (κ^{coll}) and cell (κ^{cell}) structural parameters by using the approximation in Table A.1. (a) Best model fits for the collagen orientation κ parameter: comparison of the proposed approach and existing assumption of equal characteristic times. (b) Best model fit for the cell orientation κ parameter: comparison of the proposed approach and existing assumption of "equal characteristic times" (from [6]).	106
Figure 5.5	: Model fitting absolute percentage errors (APE) for the collagen and the cell orientation κ parameter: (a) comparison of the proposed approach and the existing assumption of "equal characteristic times" for cell, (b) comparison of the proposed approach and the existing assumption of "equal characteristic times" for collagen orientation (from [6]).	107

Figure 5.6	: (a) Kinematics of an arterial wall with respect to final deformed configuration under internal pressure. (b) Geometry of the stress free configuration in cylindrical coordinates (R, Θ, Z) with an opening angle of Θ_0 and internal radius R_m . (c) Solution domain of the internally pressurized thick cylinder and corresponding principals λ_{Θ} and λ_z . For each artery layer, it is assumed that the dispersion of fibers are clustered around a mean direction which is very close to the reference vector \mathbf{n} and \mathbf{n}' (from [6])......	110
Figure 5.7	: The layout of mean fiber orientation vector \mathbf{a}_μ , spatial stimulus direction vector $\mathbf{n}^{\lambda\sigma}$ and angular measurement θ_μ between these two vectors (from [6]).	113
Figure 5.8	: Converged mechanical magnitudes with respect to the changes in the applied internal pressure P_0 based on the strain stimulus (Σ_λ) . The internal pressure steps for the simulation are $P_0 = 2, 5, 10, 15, 20, 30$ (kPa). At every pressure step, the evolution of mechanical magnitudes are tracked for 30 days, and final converged values are represented in the graphics. Initial condition sets for the six simulation cases corresponding to the six pressure steps are given in Table 5.3. The time step for the simulation is set as $\Delta t = 0.2$ days (from [6]).	119
Figure 5.9	: Evolution of mechanical magnitudes in time based on strain stimulus (Σ_λ) . The model parameters for this simulation are $\lambda = 1.265$ and $\Lambda = 1.0$, with the initial conditions $s_0 = 0.1\pi$ and $\varphi_0 = 85^\circ$. The time step for the simulation is $\Delta t = 0.04$ days (from [6]).	120
Figure 5.10	: Evolution of mechanical magnitudes in time based on strain stimulus (Σ_λ) . The model parameters for this simulation are $\lambda = 1.265$ and $\Lambda = 1.0$, with the initial conditions $s_0 = 0.9\pi$ and $\varphi_0 = 5^\circ$. The time step for the simulation is $\Delta t = 0.04$ days . ..	121
Figure 5.11	: Evolution of mechanical magnitudes in time based on stress stimulus (Σ_σ) . The model parameters for this simulation are $\lambda = 1.265$ and $\Lambda = 1.0$, with the initial conditions $s_0 = 0.9\pi$ and $\varphi_0 = 70^\circ$. The time step for the simulation is $\Delta t = 1$ days (from [6]).	122
Figure A.1	: The graph of $\kappa - s$ function which transforms the normal variance parameter s into the transversally isotropic dispersion parameter κ by \mathcal{T}^{-1} by means of the parameterization of k	149

BIOMECHANICAL MODELING OF GROWTH AND REMODELING PROCESS IN SOFT BIOLOGICAL TISSUE

SUMMARY

In this work, we constructed a novel collagen fiber remodeling algorithm that incorporates the complex nature of random evolution acting on single fibers causing macroscopic fiber dispersion. The proposed framework is different from the existing remodeling algorithms, in a way that the microscopic random force on cellular scales causing a rotational-type Brownian motion alone is considered as an aspect of vascular tissue remodeling. A continuum mechanical framework for the evolution of local dispersion and how it could be used for modeling the evolution of internal radius of biaxially strained artery structures under constant internal blood pressure are presented. A linear evolution form for the statistical fiber dispersion is employed in the model. The random force component of the evolution, which depends on the mechanical stress stimuli, is described by a single parameter. Although the mathematical form of the proposed model is simple, it has been considered that there is a strong link between microscopic evolution of collagen dispersion on the cellular level and its effects on macroscopic visible world through mechanical variables. We believe that the proposed algorithm utilizes a better understanding of the relationship between the evolution rates of the mean fiber direction and fiber dispersion. The predictive capability of the algorithm is presented using experimental data. A preliminary version has been tested by the prediction of the mechanical magnitudes and chemical concentrations that are given by a fibrin-based gel experiment. For this purpose we apply the algorithm by means of a finite element framework. The model has been simulated by solving a single layered axisymmetric artery (adventitia) deformation problem. The algorithm performed well for estimating the quantitative features of the experimental anisotropy, mean fiber direction vector and dispersion (κ) measurements under the strain dependent evolution assumptions. The convergence and uniqueness of the solutions have been analyzed by altering the initial conditions set for both validation of the fibrin-gel experiment and artery deformation problem. The uniqueness has been achieved for the strain based remodeling framework, whereas the results for the stress based framework is convergent but not unique.



YUMUŞAK DOKULARDA BÜYÜME VE YENİDEN-MODELLEME SÜREÇLERİNİN BİYOMEKANİK OLARAK MODELLENMESİ

ÖZET

Biyomekanik genel olarak mekaniğin biyolojiye uygulanması olarak şeklinde tanımlanır. Temel amacı insan sağlığının ve sağlık şartlarının iyileştirilmesidir. Sağlık şartlarının iyileştirilmesine yönelik olarak kimyasal ve fiziksel tüm ardalın bilgilerinin ortak bir paydada birleştirilebileceği sürekli bir ortam ve bağlantılı bir çatı yaratılması esas odak noktasıdır. Asıl vurgunun genellikle matematik ve biyokimya olması da bu düşünsel akıştan kaynaklanmaktadır. Doğrusal olmayan sürekli ortamlar mekaniğinin 1940'lı yıllardan sonrası hızlı gelişimi sonucunda elde edilen kinematik çatı, polimer fiziğinin bulguları ile birleştirilerek biyolojik dokuların davranışına ilişkin ilk rasyonel sonuçların irdelenmesine fırsat sağlamıştır. Bu sayede daha önce anlaşılabilir görülen geri dönüşsüz ve karmaşık zaman patikalarına sahip deneysel gözlemlerin, aslında bir hayli derin analitik bağlantılar içeren öngörülebilir termodinamik bir sistemin uzantıları olabileceğine dair tespitler artmıştır. Doğa, ve onun bir parçası olan biyolojik sistemler içsel ve dışsal devinimler altında sürekli olarak daha karmaşığa ve karmaşıklığın anlaşılmasını bir nebze de olsa kolaylaştıran çok katmanlı yapılara doğru evrilen bir dinamik eğilim sergilemektedir. Bu evrilmenin yönetici denklemlerine yönelik temel biyokimyasal anlayışın matematiksel bir dışavurumu olarak Turing'in morfojen kavramı örnek verilebilir. Bir tepkime-yayıma (reaction-diffusion) denkleminde yönlendirici tepkime terimi sistemin evrilimini kesinleştirici bir hedef noktaya yöneltirken, yayılma terimi de bu sistemin yönelimindeki belirsizliği arttıran bir etkiye bulunmaktadır. Biyolojik sistemlerdeki bu ikili (dual) ilişki canlılığın doğasına yönelik temel bakış açılarından bir tanesidir.

Çok küçük ölçeklerde organların temel yapıtaşı olarak hücreler ve onun dış ortamını oluşturan hücre-dışı ortam (ECM), hücreler arası kısa ve uzun erimli iletişimin ve mekanik iç gerilmelerdeki bilgi taşıyıcı unsurların ana kaynağıdır. Hücreler bu ortam içinde tutunabilmekte, rastgele şekilde hareket edebilmekte ve içinde buldukları çevre ile çift-yönlü geri besleme kanalları üzerinden buldukları ortamı şekillendirmektedirler. Mekanik ortamla etkileşim içinde bulunan ve ortamdaki sağladığı verileri kendi protein sentez mekanizmasına dahil eden (mechano-transduction) hücreler, salgıladıkları uzun polimer zincirlerini (kolajen, elastin, fibronektin, GAGs glycosaminoglycans), dokuların dayanımını optimize edecek şekilde yeniden biçimlendirmektedirler. Bu ortamlar matematiksel olarak modellenmelerini için polimer fiziği kaynaklı hiperelastik (Neo-Hookean) varsayımların kullanılmasına izin verir. Bir karışım teorisi (mixture theory) üzerinden toplamsal şekilde tanımlanabilen hücresel ortamın mekanik davranışı, aynı zamanda ortama salgılanan proteinlerin bağımsız olarak incelenebilmesine olanak sağlamaktadır. Hücrelerin içinde buldukları ortamın mekanik özelliklerini uzun vadeli bir biçimde belirlemeleri, dokudaki kütle artışı ve dokunun iç biçim ve örüntüsünün yeniden-modellenmesi (remodeling), büyüme ve yeniden-modelleme

(growth and remodeling) başlığı altında incelenmektedir. Büyüyen ve kütlesi artan bir ortamdaki yoğunluk değişimlerinin evrilimi deformasyon tensörünün ara konfigürasyonlar (intermediate configuration) üzerinden yapılan tanımlamalarına bağlı şekilde verilebilir. Biyolojik dokularda kütsel büyüme yaklaşımlarının türevi olan kavramların (örneğin yüzey alanı artışı ve fiber uzaması) teorik sınırları artık iyi bilinmekte olup, günümüzdeki çabaların odak noktası fenomenolojik kavramlardan mekanistik yaklaşımlara doğru kayarak, biyolojik sistemlerin bir hayli karmaşık, transkripsiyon süreçlerini de içeren sinyal-patikalarının derin ardalan ilişkilerine doğru ilerlemektedir. Fenomenolojik yaklaşımlarda ise, makroskopik mekaniğin kabullerine dayanılarak büyüme ve yeniden modelleme çalışmalarının ayırım sınırları çizilmiştir. Buna göre büyüme kütle artışını içeren bir değişme ve yeniden-modelleme ise doku içi örüntüyü tanımlayan matematiksel büyüklüklerin zaman evrilimine yönelik sürekli ortamlar mekaniği yorumundan oluşmaktadır. Biz bu çalışmada büyümenin sınırlı kaldığı ve yeniden-modelleme olgusunun dokunun iç mekanik gerilme durumunu önemli ölçüde belirlediği bir durumda, yapısal tensörlerin evrilme denklemlerinin hangi formlarda tasvir edilebileceği üzerine eğilmekteyiz.

Bir serbest enerji denklemi aynı zamanda doku içinde gömülü bulunan *tercih edilen yapısal yönlerin* (preferred structural direction/orientation) objektif bir fonksiyonudur. Dokudaki uzun vadeli değişimlerin mekanik kökenleri bu tercih edilen yönlerin termodinamik ve kinematik kısıtlar altındaki evrilme denklemleri ile ilişkilidir. Bu evrilme denklemleri, örneğin, kalp-damar sistemi hastalıklarının patolojik kökenlerine ait kavramların ayrıştırılması için kullanılmaktadır. Sıvı mekaniğinin genel varsayımlarından yararlanıldığında, yüksek tansiyon altında, damar dokusundaki uzun vadeli değişimlerde tercih edilen kolajen lif yönlerinin dokunun yeniden yapılanması için önemli olduğu görülür. Buradaki yapılanma kavramı karşım teorlerinde kullanılan protein yarı ömrü ile yakından ilişkilidir. Buna göre lifler zaman içinde ön-gerilmeli (pre-strained) bir şekilde ortamda yapılanırken, mekanik haberleşme ile tetiklenen bir moleküler-patika (MMP,TIMP,TGF- β pathways) ile proteinlerin çözünmesi ve gerilmenin evrilmesi sağlanabilmektedir. Bu mekanik konfigürasyonlar arasında geçmişe gecikmeli-bağımlı (viscous) bir sürecin oluşmasını sağlar.

Her ne kadar kolajen liflerin kütsel veya hacim oranı artışının modellenmesi (volume fraction) önemli ise de, matematiksel açıdan kolajen liflerin yöne bağlı (anisotropic) ve yönden-bağımsız/izotropik (isotropic) evrilme özelliklerinin incelenmesi kritiktir. Bunun nedeni liflerin izotropik yapılanma evriliminin iç gerilmelerin büyüklüklerine olası katkısıdır. Son 30 yıldaki deneysel veriler, doku içindeki yük taşıyıcı makro-moleküllere ait saçılımın izotropik kısmının doku mekaniğinin asli bir unsuru olduğunu ve iç-gerilme üzerinde etkili olduğunu göstermiştir. İç gerilmenin yeniden-modellemeye bağlı evriliminin tam olarak anlaşılabilmesi için yük taşıyıcı unsurların saçılımına ait izotropik komponentin evrilimine ilişkin bütüncül bir yaklaşım gereklidir. Burada bütüncülden kasıt hücrenin bireyselliğinin ortadan kaldırılarak (çoğu deneyde bireyseldir) eylemlerinin içinde bulunduğu ortam ile eşanlı ve geri-beslemeli bir biçimde incelenmesi ve ortamda meydana gelen değişimlerin hem makroskopik (tissue scale) hem de mikroskopik (cell scale) ölçekteki biyolojik amaç ve hedeflerinin incelenmesini gerektirmektedir. Benzer şekilde bu algoritmaların hesaplamalı özelliklerinin, olguların karmaşıklığı altında hızlı sonuç vermesinin önünü açacak yeni yaklaşımlara da ihtiyaç bulunmaktadır.

Günümüzde kolajen lif saçılımının hesaplamalı modellerine yönelik genel uygulamalar lif ögelerinin ayrı doğrultular olarak ele alınarak, her bir doğrultuya ait evrilme denkleminin sonuçtaki toplamsal bir serbest enerji formunun içine gömülmesi şeklindedir. Bu yaklaşım açısız integrasyon (angular integration AI) olarak bilinir. Günümüzde sık kullanılan, hesaplama yükü ağır, fakat gerilme doğrultularından bağımsız gürbüz bir yöntemdir. Kolajen liflerin saçılımının evrilmesine yönelik ikinci temel yaklaşım ise yapısal tensörün ayrı kolajen liflerin bir toplamsal gösterilimi şeklinde betimlenmediği, lif dağılımının doğrultulanma yoğunluk fonksiyonuna (orientation density function) bağlı az sayıda parametre üzerinden, genelleştirilmiş yapısal bir tensör (generalized structural tensor (GST)) ile tanımlanmasıdır. Bu yaklaşım kullanılarak hesaplama yükü azaltılabilir. Damar kolajen liflerine ait yapısal tensörün genelleştirilmiş formları her ne kadar belirli bir dağılım formu esas alınarak türetilse de, bu varsayım deneysel veriler ile tutarlıdır. Saçılım için tek bir parametre gerektiğinde model yaklaşımı κ -GST ile betimlenebilir. κ -GST yaklaşımı tek eksenli gerilme durumları için gürbüz değilse de, çift eksenli gerilmelerde, gerilmelerin oranının birbirine yakın olduğu durumlarda gürbüzdür. Bu nedenle damar sisteminin eksenel-bakışık silindirik geometrilerinde kullanılabilir. Kolajen liflerin κ -GST zaman evrilim denklemleri için ise mikroskopik kaynaklı gözlemler kullanılabilir. Buna göre uzun zaman adımlarına sahip ara konfigürasyonların evriliminde lif rotasyonunun mikroskopik denklemlerine bozucu bir terim eklenerek, makroskopik evrilimdeki etkileri gözlenebilir. Bu durumda saçılım evriminin, tercih edilen yapısal ortalama yönün (mean preferred structural direction) evrilimine göre daha hızlı dengeye varması beklenir. Bu yaklaşım makroskopiktir ve olgunun hızlı değişen alt ögelerinin (örneğin kimyasal) daha üst ölçeklerdeki yansımaları ihmal edilmektedir. Aynı zamanda bu bozucu etkiler bir kuvvet terimi gibi evrilim denklemlerine toplamsal olarak etki edebildiğinden, bozucu terim ile onun makroskopik yansıması arasında bir geçiş fonksiyonu tanımlayacağı göz ardı edilemez. Bu geçiş fonksiyonu en basit şekli ile bu tez kapsamında verilmiştir. Fonksiyon bozucu etkilerin doku içindeki mekanik bir tanımlayıcısıdır.

Bu çalışmada, biz, mikroskopik fiber dağılımının karmaşık doğasını tanımlayan özgün bir kolajen fiber yeniden-modelleme algoritmasını, canlıların biyomekaniksel gelişiminin daha iyi anlaşılması için önermekteyiz. Burada önerilen form varolan algoritmalarından farklı olarak, mikroskopik ölçekteki rastgele etkiler sonucu ortaya çıkan açısız tipteki Brownian hareketin kendisinin, damar yeniden-modellemesinin asli bir unsuru olduğu şeklindeki bir yaklaşımı savunmaktadır. Yerel saçılım dinamiklerinin sürekli ortamlar mekaniği çatısına dayalı evrimsel yapısına ait bir model, kan basıncına maruz kalarak iki yönlü eksenel kuvvetler altında gerilen damarın yarıçap değişimini modellemek için hangi şekillerde kullanılacağı belirtilmiştir.

Fiberlerin istatistiksel dağılımını modellemek için doğrusal bir yaklaşım kullanılmıştır. Değişim denklemlerinin stress uyarana bağlı rastgele kısmının modellenmesi için tek parametreden yararlanılmıştır. Modelin matematiksel formu basit olsa da, mekanik değişkenler analizi, hücresel düzeyde mikroskopik kolajen fiber dağılımını ile makroskopik düzeydeki fiber değişimi arasında güçlü bir bağ olduğunu düşündürmektedir. Önerilen algoritmanın fiber saçılım dinamiklerini ve ortalama fiber yönünün evrimini aydınlatan bir şekilde, daha iyi bir modelleme aracı olduğunu savunulmuştur.

İki farklı algoritmik form üstünde çalışılmıştır. Öncül olarak türetilen denklemler sonlu elemanlar yöntemi kullanılarak fibrin-jel deneyinden elde edilen kimyasal bileşenlerin tahmini için kullanılmıştır. İntegrasyon noktası tabanlı sonlu elemanlar yönteminde Toplamsal Lagrangian (Total lagrangian) yaklaşımıyla çözülen problemde sonuçlar düğüm noktalara interpolate edilerek verilmiştir. Burada bir hassaslık analizi vasıtasıyla mekanik simülasyon sonuçları kimyasal konsantrasyon patikasına uydurulmuştur. Bu model pek çok başlangıç şartı için tekrar edildiğinden gerilme tabanlı algoritmanın iyi sonuç verdiği söylenebilir.

İkinci model öncül modelin kavramsal çatısının iyileştirilerek yeniden kurgulanması ile elde edilmiştir. Modelin nümerik kararlılığı ve tekil sonuçları tek tabakalı damar modelinin şekil değişimi üzerinde gösterilmiştir. Modelin zamana bağlı sonuçları ve ulaştığı son parametrik değerler, ortalama fiber yönü ve κ dağılım istatistikleri, gerilme tabanlı uyaran için deneysel gözlemlerle uyumludur. Bu deneysel veriler çeşitli hastalardan alınan κ istatistiklerinin ortalaması şeklindedir. Algoritma sonuçları gerilim (stress) ve gerilme (strain) tabanlı denge durum evrilimleri için incelenmiştir. Gerilme (strain) tabanlı algoritma farklı başlangıç şartları için, beklenen şekilde aynı denge durumuna evrilmiştir. Bununla beraber gerilim tabanlı algoritma farklı başlangıç sonuçları için eşsiz olmayan fakat yakınsak sonuçlar sağlamıştır. Sonuç olarak algoritmanın gerilme tabanlı kullanılması uygundur.

1. INTRODUCTION

Philosophical principles we live in the world has been inherited from the philosopher of science Rene Descartes and his period. Rendering rationalism and perceptible natural phenomena into understandable forms, scientific thinking has been carried out by fitting the one-way linear reductionist perspective of a scientific approach on to natural events in the 17th century. Descartes' famous '*I think therefore I am*' approach that distinguish the nature and mental processes has led the scientific ideology that all kinds of natural phenomena can be evaluated via objective reductionist perspective. Thus, we live in the era of science and the impact of reductionism has been great. According to this understanding, each natural event should have been divided into small pieces before an implicit perception. Every piece of nature must be understood through an explicit objective analysis process supported by experimentation. Then, implicit knowledge of the natural phenomena should be a summary of functioning as a mathematical model of the machine frame compatible with the explicitly agreed parts. This machine analogy, especially via the widespread use of differential calculus after Newton, is rated as the only acceptable truth within the world of science. Briefly, the intuition has been replaced by experimental evidence which is an element of the deterministic Cartesian perspective.

The science of this deterministic and reproducible machine analogy which can be observed to this day assayed a great success in areas such as physics and chemistry. Similarly, the reductionist approach has made major advances in biology in which the experimental approach can be used partly. From the 17th century, accumulated medical and anatomical information on the human body, intuitively, led researchers to imagine the human body like a highly detailed machine that converts certain entries to the outputs. One of the basic principles behind this perception was the fact that living organisms work in an integrated framework consisting of multi-tiered hierarchical nested structures. Accordingly, long chain polymers form cellular organelles and cellular groups form macroscopic organs. Life arises from complex interactions within

the multi-scaled structure of these organelles and organs. The sources of the diseases are the predictable disruptions and distortions in the body organs interacting with each other. For example in this era, Louis Pasteur's discovery of the role of the single-celled organisms in the formation of the diseases has made a revolution in the field, especially in biology and medicine community adopting a reductionist view. Accordingly, the source of functional disorders seen in the macro-scale could be the ecological problems at the micro scale, and the way of thinking would have demonstrated the usefulness of the hierarchical system approach. In this way, the teachings and beliefs of the diseases based on the reductionist approach has seriously serve medicine current in the 18th and 19th centuries. Diseases were functional disorders, and the largest shareholders were the interactions at the cellular level.

In fact, Louis Pasteur and his followers were ecological thinkers, and the source of viability problems encountered by the surge was believed to be the environmental conditions which have vital importance. Environmental condition is another important aspect of the evolutionary biology, as being one of the main conceptual tools. According to the evolutionary perspective, organisms have reached their present multi-layered structure through a long genetic variation and natural elimination process. The concept of *functional adaptation* in gaining this structure should also be required at the cellular level, in which the concept is seated at the head corner in the formation of macroscopic phenotype features. In particular, from the examination of the phenotype characteristics both in terms of biological and mathematical point of view, it is easy to notice that the first attempts at modeling were carried out in this context. By the help of a number of isomorphic geometric transformations, Darcy Thomson has shown that the average phenotype of the same family of animal species can be explained by the non-linear transformations where its impact in the field of developmental biology continues even today.

Understanding of the molecular causes of functional adaptation could be proceeded after the second world war when the advanced imaging techniques in medical treatments spread and universal behavior of polymer physics (and related phase transformation phenomena) was clarified. One of the most important conceptual problems in evolutionary biology is how the energy efficient living systems able to continue functioning within an extraordinary complex environment that is giving

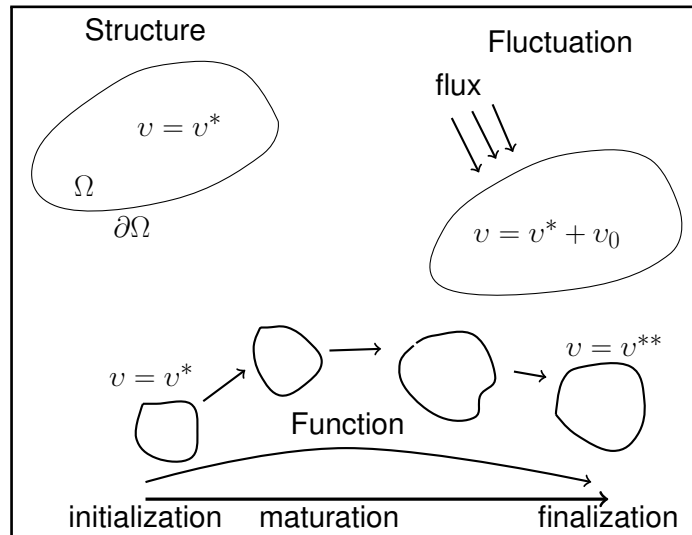


Figure 1.1: Conceptual classification of the adaptive forces and their elements that are common in a thermodynamic system.

rise to the organizational layers appear today. Aside from the animal and plant kingdom, biological interactions have a high level of complexity, even for single-celled organisms. Considering the structure and form of this complexity, it is away from linearity, programmed and at the very large scale (planetary scale) is seen to adhere to certain universal laws.

When systems with life or including life (social, political, economic) are concerned, most of the events are seen to be vulnerable to catastrophic conditions and navigating away from equilibrium. These features also apply to biological systems. According to Ilya Prigogine, the item 'history' is located only in humanities such as economics, sociology, psychology and for biology. There is no history element in the basic sciences of physics and chemistry. From an evolutionary perspective, history element in biology, the events are considered to follow a constructive path that requires an understanding of the premise. As a result, the phenotypes observed in short-term fluctuations showing a limited change in months and years are, in fact, a snapshot of the biological formation, representing an evolutionary motion of the system examined for millions of years. In addition, by observing some chemical reactions, Prigogine was the first to reveal that chemical reactions may have its own history and may lead to complex structures in an irreversible manner. According to him, there are three interdependent basic concepts associated with determining the history path of dissipative structures: *function, structure, and fluctuations* (Figure 1.1). Basic

determiners for a biological development process are as follows: “structure” is a continuous or discontinuous physical domain that the problem is being evaluated on. Without physical laws, the structure is just a conceptual representation of boundaries. “Fluctuation” is an initial event or triggering activity that gives rise to a continuous development process. “Functions” are force fields like chemical gradients, magnetic fields, morphogenetic activities, internal stress-strain fields that are generated as a result of the boundary conditions (such as mass flux). The shape and intensity of the fluctuations in the environment have been writing the history of a specific kind of reaction, and the mathematical form of the reaction is of central importance here. Turing (1952) showed mathematically that the chemical reactions at the cellular level could affect the animal’s morphology and give them a new differentiated form. Diffusion equations, in general, are seen as a function that leads to building a more stable system, such as heat dissipation. However, the chemicals called morphogens can exhibit diffusive interactions that lead to highly detailed visual results under certain boundary conditions. As a result, an irreversible history of chemical reactions is possible in a way that these reactions are those corresponding to the morphogen that can influence the animal’s morphology with complex outputs. This is one of the intersection points of biology and mathematics. Low-dimensional mathematical equations corresponding to the biochemical processes could produce complex outputs. Since the second half of the 20th century, the developed non-linear dynamic systems approach and chaos terms are used for this purpose. Such equations give rise to the formation of the self-determined unstable orbits, and the future of the system can be created depending on the trajectory path to evolve into one of these unstable orbits.

For all its complexity, chemical reactions continue at all scales in the cellular viability, on the large scale, however, it can be expressed by a number of parameters. For example, the massive growth path of many vertebrates living on the earth’s surface is the same with a high level of confidence. As a result, on the basis of the evolution of very complex systems, a small number of variables of the systems owned right to speak in accessing to the homeostatic state, is one of the basic assumptions of a finite growth process. In this case, simplicity could represent the complexity of nature. After this semi-philosophical introduction, now, the context of the cellular level that is the basic building block of life must be evaluated.

Cells are the basic building blocks of vertebrate and invertebrate animals and plants. Cells are closed forms that contain organelles including the nucleus and surrounded by a phospholipid based membrane containing a viscous liquid. Since the scope of this thesis is focused more on mathematical evolution and the mechanical strength, the historical development of the cells has not been discussed. As a brief summary, the emergence of cellular life is considered to begin with the occurrence of self-replicating long-chain molecules and information-encoder polymers guaranteeing the transfer of biological inheritance. Until an unusual ice age covering the whole world, there have been only single-celled organisms. After this period, an increase in the diversity of life called Cambrian explosion appeared and it was the turning point for the bio-mechanical design and organization. The competition among creatures, as they grow in mass, was moved to a biomechanical field in the same time. The first *collagen* molecule is produced in the bodies of marine sponge. With the emergence of embryo, the role of the mechanical instability as well as the chemicals in the first phase of biological development has been revealed.

Cells are mechanically stable structures. The geometric shape of eukaryotic cells and their response to environmental conditions are provided by the bony structures (cytoskeleton) in the cytoplasm. These structures are the networks of fibers in the form of protein. One of these structures, which connects the cytoplasm to the plasma membrane is the actin micro-filaments. Microtubules stabilize the organelles and cell shape while intermediate filament provides a support for the cytoskeleton.

Because the molecular biology of the cells is an extremely wide area and the scientific perception includes interdisciplinary concepts, the items included here are for only to evaluate the terms of the mechanics of cells and the basic elements of biomechanics. In this case, 'what the biomechanics is' should be emphasized and in what direction, it is separated from pure mechanics.

Biomechanics is in general defined as the application of mechanics in biology'. Its main goal is the improvement of human health and the health conditions. As for the improvement of health conditions, chemical and physical information of all backgrounds can be combined to create a common ground associated with a *continuum* framework. Therefore, the main emphasis is on the mathematical and physical roof, geometric boundaries, and biochemical inputs. The continuum domain is related to the

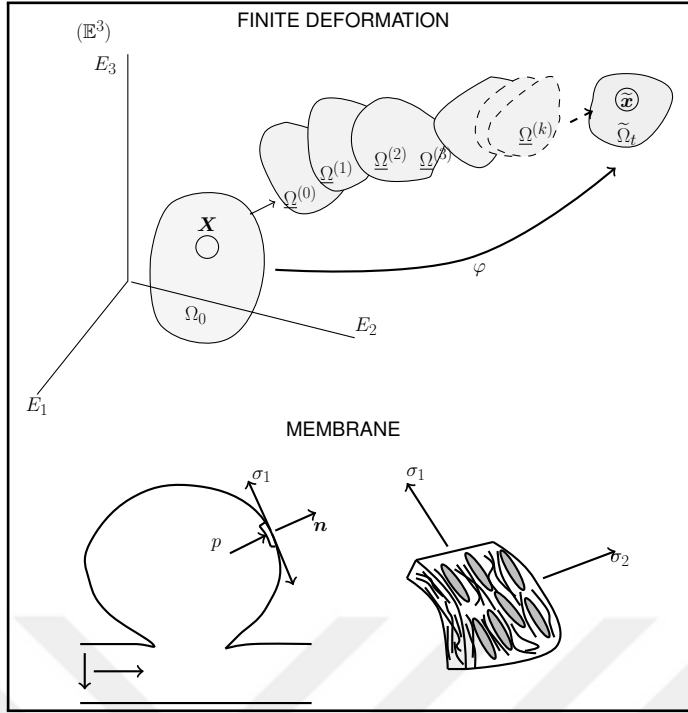


Figure 1.2: The time-dependent change in structure can be considered as the finite deformation of a structure, denoted by an evolution “function”, where the initial deformation process is triggered by an external “fluctuation”.

“structure” concept. Thus, the evolution of biological domain includes the perception of a time-dependent finite deformation of the structure in a quasi-static manner (Figure 1.2). The rapid development of nonlinear continuum mechanics after the second world war combined with the findings of polymer physics in the 50s and 60s, the first models of the mechanical behavior of tissue were opened to discussion. For example, Fung has suggested the existence of a three-dimensional strain energy function by evaluating the exponential characteristics of the experimental data, giving the term pseudo-elasticity to the literature

$$\Psi = c(e^Q - 1). \quad (1.1)$$

Here c is a material constant and Q is a function of elastic strains in tissue. Many experimental data on the functioning of this simple approach has proved that the mechanical behavior of complex layered macroscopic soft tissue structures could be explained by few constants. It is mentioned that at microscopic scales cells and its external environment making up the extra-cellular matrix are the basic building block of organs (Figure 1.3). Smaller in scale, the complexity of physical nature changes greatly. There are 200 kinds of cells in the human body that can be located in 4 main tissue categories: muscle, epithelial, connective and nerve. The cells are in

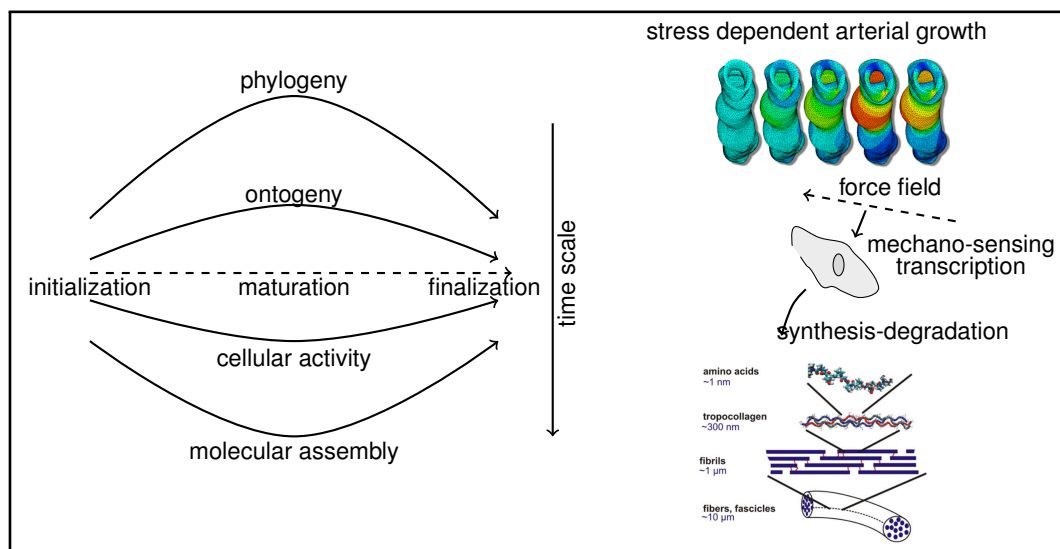


Figure 1.3: Spatial and temporal scales that are observed in a growing and remodeling biological domain (adapted from [2]).

exchange of information with the extracellular matrix environment (ECM) which they are embedded in, and the formation of the external environment plays an active role in mobility. Because cells are movable within this environment, they can adhere to a surface or displace randomly. Therefore, ECM also has an impact on the shape and orientation of the cells as a two-way relationship. Scientific advances in the last 20 years of imaging techniques have shown that extracellular mechanical pattern is not independent of the cytoskeletal patterns of intracellular and subcellular organization. The ECM collagen fiber orientation seems to be connected to the shape of the cells as a delayed feedback. ECM is composed of various long chain polymers (collagen, elastin, and fibronectin), glycosaminoglycans (GAGs) and water. GAGs forming covalent bonds with proteins form proteoglycans. Three basic protein chain that enables the mechanical strength of ECM are collagen, elastin, and those proteoglycans. These types of proteins have half-life period which can vary sharply according to the cell-signaling mechanisms (days or months). In that sense, ECM is a continuum filler where the propagating mechanical signals are felt with the aid of cell receptors. Therefore, the degree of formation of a protein, its concentration and geometric orientation in the ECM are setting items that influence the rigidity and cell-signaling mechanism. Microscopic anisotropy itself seems to be a basic determiner in the evolution of the fiber reinforced structural fabrics based on cellular feedback.

When we examine the current approaches, it is seen that two important mathematical propositions made on the viability of the growth and development and mechanical organization are found to be effective in dynamic feedback. (1) Reaction-diffusion type equations can affect cell behavior with its organization and morphogenetic effects make complex forms possible. (2) Mechanical conditions perturbed by cells may lead to distortion and instability. In such cases, the mechanical effects gain long-range character. Especially in bending situations, the instability helps to transfer of knowledge mechanically without the presence of chemical morphogens. In the early stages of the embryonic development of vertebrates, instability is the one the primary factors of the embryonic growth patterns. These growth patterns are proposed to be based on a biological terminology, the so-called hyper-restoration hypothesis. Discussions on this issue have not been finalized.

1.1 Randomness, Cellular Functions, and Cellular Mechanics

Tissue cells are individual entities that can be considered independently from the environment in which they are embedded in. As a result, when they left from their environment, under in vitro experiments, the functional behavior they exhibit is similar to the one in the tissue. This is an indicator of their decision-making behavior and individuality. By these types of experiments, the complex processes of cells could be described by simple equations. Some typical well-known animal cell behavior is briefly discussed here.

Cells can adhere extremely strongly to a surface. Cell adhesion function performs with a very low number of receptor-ligand bonds, which is unusual that the number of bonds is so low that the deterministic behavior can not be described by an average (mean field) model. The behavior is stochastic in nature which is associated with microscopic scale. The number of receptor-ligand bonds of adherent cells is a discrete, time dependent and randomly fluctuating variable.

Cells can evaluate local mechanical, chemical or electromagnetic forces to assess their local environment or they can also develop their own response to eliminate the effects of these forces. For example, fibroblast cells under cyclic stress may exhibit rotation perpendicularly to the direction of stretching from outside, or they may provide buckling on man-made of elastic material. Similarly, cells move randomly in

the direction of the cathode under a voltage stress, or they can follow the chemical gradient signals. Most of these examples are based on well-known experimental works that investigate the mechanism of cellular movement.

The basis of the facts mentioned here is the existence of molecular motor dynamics that enable cellular motion. Cellular movement and orientation are one of the basic features of life. Indeed, Taber said it well: “*During many cellular processes, cell movement is more important than cell division. ...abnormal cell division is bad, but abnormal cell motion is often worse (metastasis)*”. Just as in adhesion events (and in numerous other cellular processes), cellular orientation movement features the basics of the Brownian nature. For example, the fundamental dynamics of the cellular engine model called Brownian Ratchets use the rectified energy of Brownian motion. This probabilistic approach has played a crucial role in the understanding of a number of other low-level processes. For example, it is taking place around the cell membrane, such as protrusive filopodia and lamellipodia events. Filopodia is an event governed by the Brownian nature, which is important for the modeling of cellular migration. Animal cells can also detect the long-range behavior of other cells by means of elongate protrusions. In this case, cell movement patterns have led to the utilization of a biharmonic partial differential equation that belongs to a special type of diffusion equation. The overall perspective is that this form of cellular movement is an anisotropic diffusion. Today, Brownian effect became one of the basic assumptions to model the cellular motion.

1.2 Purpose of Thesis

Mechanisms of cell's actions can be considered within a holistic approach with its environment where their individuality is abolished. The evolutionary changes that occur in that environment will require an examination of both the microscopic and the macroscopic scale biological goals and objectives. In this case, basically, three different evolutionary processes can be reduced to mathematical equations seen gliding through layered structures for living tissues. These include a description of the mass increase called as *growth*, the changes in the internal structure of the material properties and forms called as *remodelling*, and the *morphogenesis* in which the epigenetic concepts and genetic elements have an impact on the morphology of the living things. The first two of these concepts are inseparable since the conversion

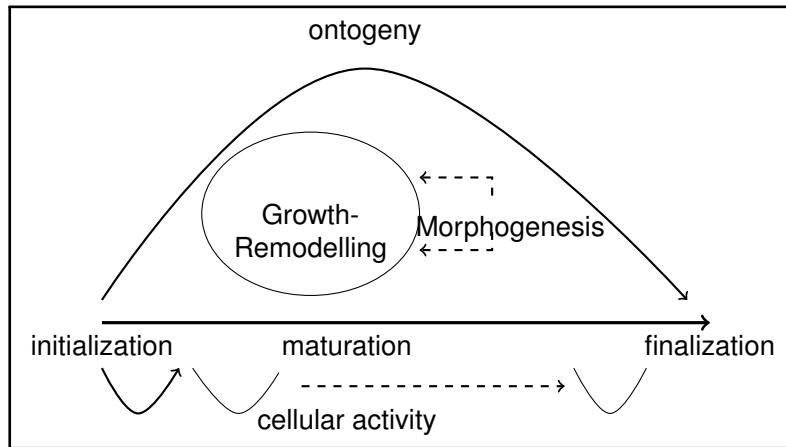


Figure 1.4: As being the three main conceptual phenomena, growth-remodeling and morphogenesis give rise to the ontological formation of biological pattern formation and development.

reaction of substances in different phases with each other is related to both growth and remodelling at the cellular level. Nevertheless, the concepts are interrelated with each other and there is feedback (Figure 1.4). In this study, by evaluating the mathematical findings of developmental patterns that have been developed so far, and by making an interpretation of the randomness observed at the cellular level inside the animal tissue, how this randomness should be shown in the macroscopic constitutive equations has been discussed. Here, as an important element, the distorting effects called the random *Langevin force* is considered to be an essential and a new kind of internal tissue force similar to the concepts of strain and stress. The tissue is evolving to an optimal state of equilibrium through the measurable outcomes of Langevin force, by adjusting its internal structure. The validity of the situation has been analyzed with some experimental data. Another case presented here is that the randomness of the small scale affects the optimal situation on the large scale, and a mathematical form called 'transfer function' is a clear and pure representation of this effect.

Evaluation of this present work states that, in particular, the randomness of events and its properties inside the tissue, affects the structural changes for the future. This is the collagen fiber remodelling managed by fibroblasts in vascular tissue. In the body, the remodelling includes the mechanochemical events involving an intense feedback which depends on environmental factors. These events, intracellular and extracellular processes, in some cases (e.g., diseases) also, create an irreversible memory of the tissue history by configuring the structural pattern. Structural characteristics of the

tissue stored in its history can be traced to a certain extent by mathematical techniques. An important part of this modelling techniques has now brought proposals for the dynamics of the fiber dispersion mechanisms for the patterned texture. However, the undeniable presence of Brownian phenomena in microscopic scales affecting the overall characteristics of the subject of equations was not addressed in any way connected with the macroscopic constitutive equations. One of the reasons may be the simplifying assumptions in the macroscopic constitutive equations as an imitation of the unifying theories. However, as indicated by Stuart Kauffmann advocating the exploratory phenomenological approach, evolutionary steps are very dependent to the current reference, and to biology, a 'grand unified theory' does not exist. It may be the only thing to do then, it is to create a form compatible with the microscopic and macroscopic equations.

The reason that we're working on the area of vascular tissue is the fact that this is one of the most apparent places of the randomness in the formation of collagen fibers' distributional structure. Especially after the 90s, since the structural randomness within the tissue is known to affect stresses significantly, related works have been concentrated on this subject. In addition, the diseases associated with the blood vessels and veins are the cases with high mortality, however, unlike cancer, clinical findings for vascular diseases indicate that the mechanical ones are much more effective than other factors. Similarly, the geometric boundary conditions of blood circulation are very clear. This means that the effects of the anomalies under the relevant boundary conditions may be dominant on the behavior of the fluid and the constitutive equations rather than chemical reactions. Such that, the source of the diseases suggest that the main reason can be the geometric perspective (curvatures, bifurcations).

Considering the trend underlying biomechanics is to improve people's health conditions, in particular, it is important to know how they appear and spread in the form of the diseases. Since collagen is found in abundance in the human body, diseases related to its deficiency reduce the quality of life seriously. Such as Keratoconus is a genetically oriented corneal disease that occurs in the eyes predisposing to the development of irregular collagen fibril evolution which causes the thinning of the lens continuously. Although riboflavin injection stops the disease, it is not possible to return

to a completely healthy condition. Similarly, Marfan syndrome is a disease of genetic origin characterized by the highly scattered irregular collagen fiber patterns in tissue.

Pathological conditions that are related to the growth and development of collagenous vascular tissue is a vital concept and it is very common in society, due to the fact that the problems are an extension of epigenetic factors rather than the genetic ones. The age, as being an important factor of such diseases, is an important ingredient of the technical assumptions made on the elasticity and the mechanical strength of the tissue. For example, cardiac hypertrophy occurs as a result of the loss of elasticity under the pressure load in the face of long-term hypertension. On the other hand, our main consideration is the aneurysm phenomena.

An aneurysm is a focal dilatation of the arterial wall structure. Although a certain pathogenesis is not known, degeneration in a portion of vascular tissue followed by a time-dependent reduction of medial smooth muscle cells is believed to be the triggering factor. A typical example is the intracranial saccular aneurysm that occurs near the Circle of Willis. Another example is the abdominal aortic aneurysm (AAA) which is very common in industrial societies (9% of the population). Clinical and computational works state that the main reason of the pathology is due to the mechanical factors. The vascular lesions' position relative to the blood flow line may influence the rupture potential. Heterogeneous distribution of the wall shear stresses on the artery face can trigger the local weakness by affecting the levels of collagen production locally. In both vascular diseases, the concentration and the orientation of collagen fibers within configurations change the course of the disease over time and determine the patient's life expectancy. Simple and computational efficient ways that give rise to the identification of predictive mechanisms are important from a mathematical point of view, which is the aim of observing the physical relationships.

1.3 Literature Review

Biological adaptation is a crucial element of complex evolutionary processes observed in the life cycle of cellular organisms. An adaptation process, which occurs at diverse spatial and temporal scales, genetically drives dense feedback mechanisms including chemical and mechanical information flow. Due to this fact, the long-term change in morphology by mechanical effects existing in, and adaptation process of,

biological systems is being investigated through the concepts of growth, remodeling and morphogenesis ([7]). A noteworthy number of recent works try to analyze the mechanical nature of growth and remodeling process through evolution equations. Especially, the random nature of the evolution of tissue structure becomes an important heading. In order to obtain a predictive computational model, it is essential to include the effects of microscopic ingredients in the cellular environment (such as proteins, chain reactions) that act over short time scale.

The mechanical strength of biological materials, soft tissue or engineered scaffolds, is highly related to the continuous cycle of synthesis and degradation of the directed macromolecular assembly, such as elastin and collagen fibers, that brings an anisotropic characteristic. The anisotropy can be seen in each layer of the artery structure which has a distinctive fiber distribution with an angle of preferred main direction (see Figure 1.5). It has a high level of ultimate tensile strength where fibers are embedded in a mechanically isotropic matrix environment. Since the tensile strength depends on the “load carrying” anisotropic *fiber* component, it is expected that in order to balance the external mechanical conditions, the “long term” remodeling of the tissue structure requires the change in the physical characteristics of fibers. In natural events, structural change is linked to the mass growth of the tissue. In pathological cases, the physiological properties of collagen deposition play role in many diseases. For instance, during the progression of atherosclerosis, smooth muscle cells have transitions from contractile to matrix synthetic phenotype where the accumulation of collagen has significant a role in plaque formation. In some pathologies, such as abdominal aortic aneurysm, not only the deposition of collagen but also the volumetric growth of the collagenous environment with pre-existing collagen formation plays an important role. In opposition to the atherosclerotic case, according to histological observations, tissues having intracranial aneurysm show a decreased number of endothelial cells, degradation of the internal elastic lamina and thinning of the medial layer. In advanced cases, the only mechanical barrier between turbulent blood flow and brain tissue is the very thin adventitia layer. It is believed that the elastin/collagen fiber reconstitution mechanism plays a major role in aneurysm wall weakening. Thus, understanding the natural evolution of a collagen-rich tissue environment, and developing new computational frameworks, have become inevitable

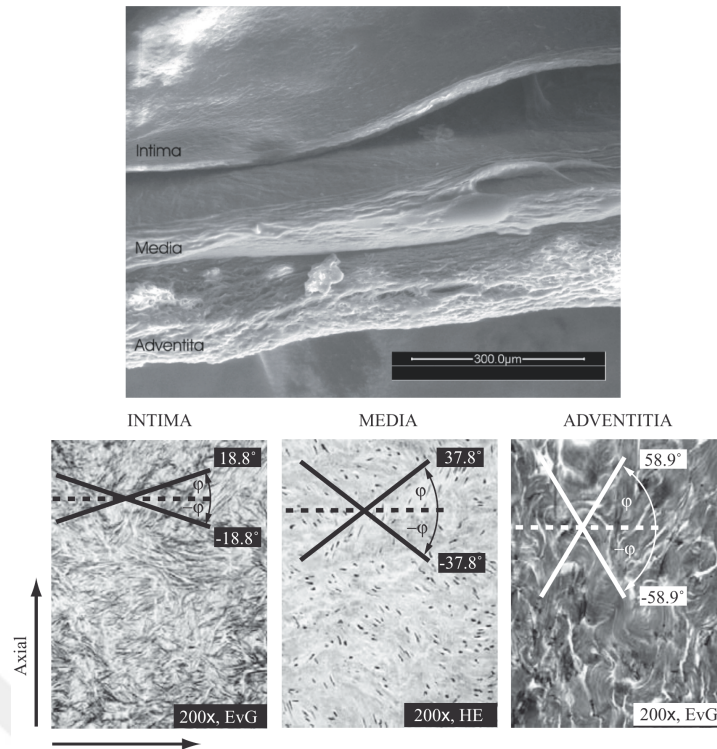


Figure 1.5: The three layers that are observed in many artery tissues. The layers are distinctively differentiated from each other by their preferred main fiber direction and biological elements (from [3]).

in biomechanics. Here, we have limited our considerations to collagen fibers and their dispersion. In general, the remodeling of collagen fibers oriented towards a certain direction has two main headings: the fiber volume fraction of the tissue and fiber reorientation ([8], [9]). The concept of fiber reorientation requires a basic assumption for the desired homeostatic orientation, which is usually to align in the principal stress/strain direction. Collagen fibers can be assumed to lie in between principal strain directions ([10]). Axial and biaxial experiments on collagenous samples have verified that the rotation of fibers in fibroblast populated regions is triggered by the applied strain ([11, 12, 13, 14, 15]) and applied stress. [16] developed a strain dependent theoretical model for the traction-induced formation and organization of collagen alignment and extra-cellular matrix composition. Since strain is a directly observable quantity, the rate of rotation and dispersion due to the contractility of fibroblasts could be measured quantitatively ([11]). Although visual observations state that the rotation of fibers is related to the rotation of single cells (see [14]), this phenomenon was recently proposed to be a result of “intracellular” formation of stress fibers (SF) comprised of F-actin and myosin ([17]). Strain-dependent experiments showed that

stress fiber alignment depends on boundary conditions ([18]). Then, the formation of stress fibers aligned with the collagen fiber directions can be used efficiently for the modeling of compaction evolution in collagen gels ([19]). The direction of principal stress can also be selected as the main driving source for reorientation ([20]), due to the coaxially assumption. To summarize, the axial cellular formation can either be modeled through the rotation of cells or by evaluating the formation of SF's based on principal strain/stress, or both (see for example [21]).

In addition to the concept of orientation towards a homeostatic state, the rate of remodeling and the existing level of dispersion are crucial for anisotropic models. The derivation of evolution equations, which incorporate the effects of random structure, has been one of the major problems so far. In [4], it is proposed that the evolution of the rotation component and dispersion can be thought as distinct events that are modeled by first-order differential equations. Here, dispersion is assumed to be a circular Gaussian, π -periodic Von-Mises distribution, discussed by [22]. An approach utilizing this assumption can be employed to estimate the fiber dispersion in cardiovascular tissue components ([9, 23]). The *generalized structural tensor (GST)* concept explained by [22, 23, 24, 25] was utilized in the work of [26] to obtain the evolution equation of a structural tensor. The evolution of tensor forms, that are based on an exponential strain energy density, is supported by supplementary variables describing the form of the orientation distribution ([26]). If one tries to split the microscopic rotation components of the aforementioned structural tensor, the anisotropic formulation of individual micro level evolution equations should be present. [27] gave a formulation of evolution equations based on the spherical integration of individual directions through a stereographic projection. Their technique adopts the worm-like chain model in which the strain energy depends on persistence length and thermodynamic variables for the polymer based constituent (see [28]). The anisotropic microsphere model has been evaluated for collagen remodeling process by [29]. [30] have shown that, due to the ellipsoid representation of tensorial fiber orientations, the rate of change in structural tensor can be considered as an eigenvector evolution determined by the recruitment (transition) stretch. The theoretical work of [31] concerns the fiber dispersion as a diffusion-like continuum evolution of the orientation density. The remodeling approach of [19] differs in its point of view with

an assumption made on linking cellular stress fiber formation to extracellular fiber alignment. The works concerning the evolution of statistical dispersion assume the existence of a “deterministic type” evolution form controlling the dispersion that is supposed to originate from a continuum source.

In this work, we formulated a novel collagen fiber remodeling algorithm that incorporates the complex nature of random evolution acting on single fibers causing macroscopic fiber dispersion. The proposed framework is different from the existing remodeling algorithms, such that the microscopic random force on cellular scales causing a rotational-type Brownian motion alone is considered as an aspect of vascular tissue remodeling. A continuum mechanical framework for the evolution of local dispersion and how it could be used for modeling the evolution of internal radius of biaxially strained artery structures under constant internal blood pressure are presented. The chapters are organized as follows: In chapter 2, we explain the basic mathematical definitions that are commonly used in continuum biomechanics. In chapter 3, common mathematical approaches utilized in growth and remodeling phenomena have been described. In chapter 4, we have proposed a preliminary formulation of a linear evolution equation for the statistical fiber dispersion based on random perturbation term. In chapter 5, an extended version of the preliminary formulation has been given. The numerical solution scheme used for an axisymmetric deformation problem, and the parameter sets in tabular form used in simulations, are presented. The simulation results are displayed and explained. We discuss some validity concepts and future directions in chapter 6.

2. THEORETICAL BACKGROUND

2.1 Kinematics and Analysis of Deformation

Kinematics deal with the analysis of motion and deformation without referencing the cause of the event. Then, natural laws and interpretations are out of consideration, while geometric principles and physical analogies of abstract mapping functions are of interest. In the field of biomechanics, hard tissue elements can be modelled by linear material laws. In these cases, the infinitesimal assumptions made on strain give rise to the neglect of any kind of geometric motion. On the other hand, soft tissues often exhibit large deformation characteristics, not infinitesimal but, finite magnitudes. Large rotations or “large” translations of material space vector \mathbf{X} in Ω_0 are a part of geometric nonlinearity. Materials having linear stress-strain curves undergoing large deformations also belong to the nonlinear continuum analysis. Nonlinear continuum mechanics basically includes the headings below ([32]):

- the study of motion and deformation (kinematics)
- the study of stress in a continuum (internal forces)
- the material description of the fundamental laws of physics governing the motion of a continuum body (balance principles).

Our aim here is to represent the logical flow of the mathematical basis and definitions related to the derivation of constitutive equations for the growth and remodeling phenomena. Secondly, it is important to understand how biological modelling approaches are based on a continuum hypothesis and which apriori assumptions are made for the simplification of the framework.

The basic assumptions for a continuum body can be related to the concept of the nonfluctuating (at least piece-wise continuous) field variables, such as density,

temperature, and stress where one has the ability to track the gradient of a searched quantity.

2.2 Continuum Mass, Force, and Stress Concepts

The main focus here is on the evaluation of the continuity and physical characteristics of the investigated domain Ω which can be scaled down to the degree of atomistic level. In the case of negligible level of density fluctuations, the whole domain can be evaluated as a whole unique subset where the same principles of the basic laws of physics are valid. These laws are generally in a Newtonian manner where the exact deterministic evolution of the system could be determined. Beyond atomistic levels, through much smaller scales, the Newtonian assumptions are not valid and field equations are derived to cover the underlying uncertain nature of the subatomic relationships. Here, in this work, the concepts are limited by the boundaries of atomistic scale, and our main aim will be to discuss the cellular and tissue scale continuum events. For this purpose, the basic concepts of the physical laws, balance principles and the logical connections of these principles with a phenomenological description of the living organisms should be discussed. Continuum assumption provides a computational modeling approach without dealing the complex hierarchical micro-structure of the domain. That is why the phenomenology discussed here is often considered as a macroscopic approach.

2.2.1 Continuum bodies

The ignorance of the density fluctuations of the physical domain greatly simplifies the analytical description of basic laws. By assuming an infinitely divisible material domain, we obtain a homogeneous open subset \mathcal{B} of Euclidean space \mathbb{E}^3 as a moving frame in Cartesian space. Each virtual material point $\mathbf{X} \in \mathcal{B}$ on this frame supplies a neighborhood relationship between different points. \mathcal{B} is called the configuration of the body in \mathbb{E}^3 . All its own material points $\mathbf{X} = (X_i) \in \mathfrak{R}^{n_{dim}}$ are represented according to the natural basis. In this case, \mathcal{B} is called “regular” according to,

- \mathcal{B} consists of a finite number of open disjoint and bounded components.

- the bounding surface of $\partial\mathcal{B}$ is piece-wise smooth and consists of a finite number of components.
- each component is orientable since it has two sides.

As a physical property of matter, the quantification of the resistance of matter towards acceleration, mass density field for a continuum body can be considered as an integration over an open subset of $\overset{\circ}{\Omega}$ of Ω . Then, the 'mass density field' per unit volume is given by, $\rho : \Omega \rightarrow \mathfrak{R}_+$,

$$\text{mass}[\overset{\circ}{\Omega}] = \int_{\overset{\circ}{\Omega}} \rho(\mathbf{X}) dV_{\mathbf{X}}, \quad (2.1)$$

where $dV_{\mathbf{X}}$ denotes the infinitesimal volume element at $\mathbf{X} \in \overset{\circ}{\Omega}$. Specifically, the volume of $\overset{\circ}{\Omega}$ is,

$$\text{vol}[\overset{\circ}{\Omega}] = \int_{\overset{\circ}{\Omega}} dV_{\mathbf{X}}. \quad (2.2)$$

The mass density field is defined as,

$$\rho(\mathbf{X}) = \lim_{\epsilon \rightarrow 0} \frac{\text{mass}[\overset{\circ}{\Omega}_{\epsilon}(\mathbf{X})]}{\text{vol}[\overset{\circ}{\Omega}_{\epsilon}(\mathbf{X})]}, \quad (2.3)$$

for $\forall \epsilon > 0$ and $\text{vol}[\overset{\circ}{\Omega}_{\epsilon}(\mathbf{X})] \rightarrow 0$ as $\epsilon \rightarrow 0$. The concepts does not change for material frames under continuous motion, where there exists a bijective mapping φ for $\Omega_0 \xrightarrow{\varphi} \Omega_t$ and for $\mathbf{x} \rightarrow \varphi(\mathbf{X})$. The mass conservation enforces $\overline{\text{mass}[\Omega_0]} = \overline{\text{mass}[\Omega_t]} = 0$. If the density does not depend on $\mathbf{X} \in \Omega_0$ and if $\nabla \rho_{\Omega_0}(\mathbf{X}) = 0$, then the configuration is said to be homogeneous, a typical assumption made in continuum biomechanics.

2.2.2 Force

By definition, there are four basic forces which govern interactions between real particles. These are the gravitation, electromagnetism, weak nuclear interaction and strong nuclear interaction. These forces are the body forces acting on each point in a material space independently from any kind of material mapping φ . In relation with the deformation of a material body, surface forces are exerted on internal surfaces between separate parts of a continuum body, or an external boundary layer. Body forces depend on the distance from the source of potential. The external influence of a body force \mathbf{b} is defined by the field $\mathbf{b} : \Omega \rightarrow \mathcal{V}$, where $\mathcal{V}^{n_{\text{dim}}}$ is the set of n_{dim} -dimensional tensor

space. The resultant force defined on the configuration Ω due to a body force per unit volume is,

$$r_{\mathbf{b}} = \int_{\Omega} \mathbf{b}(\mathbf{X}) d\Omega, \quad (2.4)$$

and the resultant torque on Ω about a point \mathbf{Z} is,

$$\text{torque}_{\mathbf{b}} = \int_{\Omega} (\mathbf{X} - \mathbf{Z}) \mathbf{b}(\mathbf{X}) d\Omega. \quad (2.5)$$

The resultant torque vanishes, if the body force is applied to all neighborhood of material points \mathbf{X} .

At this point, geometric and functional relationships between two successive configurations, namely Ω_0 and Ω_t , have been briefly discussed. The collection of material particles forms a physical body \mathcal{B} surrounded by the boundary layer $\partial\mathcal{B}$. As body moves from one position to another in space, it occupies a finite number of successive configurations (regions) denoted by $\Omega_0, \dots, \Omega_t$. All material points in \mathcal{B} will also occupy the translated images of the previous configurations, yielding a collective motion of the whole domain from one reference configuration Ω_0 (also called initial or material) to the final destination, called the spatial (current) configuration $\tilde{\Omega}_t$. For clarity, here and in the following chapters, a configurational variable with the superscript “tilde” sign ($\tilde{(\cdot)}$) defines a variable in the spatial coordinates. The reference configuration is furnished by the Cartesian basis $E_{\{1,2,3\}}$ constructing \mathbb{E}^3 , and a spatial variable is defined with respect to the basis $e_{\{1,2,3\}} = \mathbf{e}^3$. The detailed concepts of the curvilinear representations of the configurations with respect to an arbitrary basis set are omitted. Then, $\mathbf{X} = (X_i) = X_i E_i$ and $\mathbf{x} = (x_i) = x_i e_i$ and E_i, e_i are identical ($i = 1, 2, 3$).

If the mapping φ is bijective (one-to-one and on-to) in $\varphi : \Omega_0 \rightarrow \tilde{\Omega}_t$, then the mapping corresponds to a motion of the body. The motion changes the geometric relationships of the material points giving rise to a smooth deformation. Thus, φ is a deformation map relative to the reference configuration Ω_0 . Due to the bijection, material coordinates of a particle have an indirect representation as $\mathbf{X} = \varphi^{-1}(\mathbf{x})$ for $\mathbf{x} \in \tilde{\Omega}_t$. Since the distance between any two particles is altered, it can be characterized by the displacement field $\mathbf{u} : \Omega_0 \rightarrow \mathcal{V}$,

$$\mathbf{u}(\mathbf{X}) = \varphi(\mathbf{X}) - \mathbf{X}. \quad (2.6)$$

The mapping is one-to-one and on-to, $\det(\nabla\varphi(\mathbf{X})) > 0, \forall \mathbf{X} \in \Omega_0$.

A crucial concept in nonlinear deformation mappings is the “deformation gradient tensor” which describes the local geometric evolution of a material point \mathbf{X} and its neighborhood $\Omega_{\mathbf{X}}^\epsilon$. An open ball of radius $\epsilon > 0$ centered at $\mathbf{X}_0 \in \Omega_0$ has been defined as $\Omega_{\mathbf{X}}^\epsilon$. Under the deformation φ , the point $\mathbf{X}_0 \in \Omega_0$ is mapped to $\mathbf{x}_0 = \varphi(\mathbf{X}_0)$. Any relative difference in the geometrical shape caused by the mapping process $\varphi : \Omega_0 \rightarrow \Omega_t$ in the limit $\epsilon \rightarrow 0$ is called the strain at \mathbf{X}_0 . The source of the strain is the local deformation in the neighborhood of a material point. A technical approach to characterize the local deformation of a configuration $\Omega_{\mathbf{X}_0}^\epsilon$ is supplied by the definition of the deformation gradient. The deformation gradient is a second order tensor field $\mathbf{F} : \Omega_0 \rightarrow \mathcal{V}^2$, which is defined by

$$\mathbf{F}(\mathbf{X}) = \nabla \varphi(\mathbf{X}). \quad (2.7)$$

The field supplies information about the local behavior of the deformation φ . For $\mathbf{X}_0 \in \Omega_0$, Taylor expansion around \mathbf{X}_0 yields,

$$\varphi(\mathbf{X}) = \varphi(\mathbf{X}_0) + \mathbf{F}(\mathbf{X}_0)(\mathbf{X} - \mathbf{X}_0) + \mathcal{O}(|\mathbf{X} - \mathbf{X}_0|^2). \quad (2.8)$$

Thus, in the local neighborhood of a material point, the deformation gradient depends on the material configuration, which is in fact a ‘two-point’ tensor involving points from the two different configurations. Formally,

$$\mathbf{F}(\mathbf{X}, t) = \frac{\partial \varphi(\mathbf{X}, t)}{\partial \mathbf{X}} = \nabla_0 \mathbf{x}(\mathbf{X}, t) = \sum F_{iI} e_i \otimes E_I \quad (i, I = \overline{1, n_{\text{dim}}}). \quad (2.9)$$

Deformation gradient can be inverted,

$$\mathbf{F}^{-1}(\mathbf{x}, t) = \frac{\partial \varphi^{-1}(\mathbf{x}, t)}{\partial \mathbf{x}} = \tilde{\nabla} \mathbf{X}(\mathbf{x}, t), \quad (2.10)$$

where $\tilde{\nabla}$ is defined with respect to the spatial configuration. Due to bijection, the change in the body volume V_0 in Ω_0 is related to the volume v at $\tilde{\Omega}_t$ as,

$$dv = J(\mathbf{X}, t) dV_0 \quad J(\mathbf{X}, t) = \det(\mathbf{F}(\mathbf{X}), t) > 0. \quad (2.11)$$

If the motion is affine, $\mathbf{F} = \mathbf{I}$ and $\det(\mathbf{F}) = 1$, then the motion is called isochoric (volume-preserving). Deformation mapping not only translates the position of points, but also affects the deformation related high dimensional tensors. There is a polar decomposition of the deformation gradient,

$$\mathbf{F} = \mathbf{R}\mathbf{U} = \mathbf{V}\mathbf{R}, \quad (2.12)$$

where U, V are the stretch tensors and R is a rotation tensor. Naturally, a vector in material configuration \mathbf{a}_0 can be transformed into spatial version $\tilde{\mathbf{a}}$ via ,

$$\tilde{\mathbf{a}} = \mathbf{F}\mathbf{a}_0 . \quad (2.13)$$

Norm of a stretch vector, $\|\tilde{\mathbf{a}}\| = \lambda$, in spatial configuration is the result of a deformation, when $\|\mathbf{a}_0\| = 1$. Similarly, $\|\tilde{\mathbf{a}}\|^2 = \|\mathbf{F}\mathbf{a}_0\|\|\mathbf{F}\mathbf{a}_0\|$. Then,

$$\lambda^2 = (\mathbf{F}\mathbf{a}_0)^T \mathbf{F}\mathbf{a}_0 , \quad (2.14)$$

$$\lambda^2 = \mathbf{a}_0^T (\mathbf{F}^T \mathbf{F}) \mathbf{a}_0 , \quad (2.15)$$

in which $\mathbf{C} = \mathbf{F}^T \mathbf{F}$ is the right Cauchy-Green deformation tensor. \mathbf{C} is a symmetric positive definite tensor defined for each $\mathbf{X} \in \Omega_0$, then $\mathbf{a}^T \cdot \mathbf{C} \cdot \mathbf{a} > 0$, $\forall \mathbf{a} \neq 0$. An important extension, which is widely used in Fung type materials, is the Green-Lagrange strain tensor \mathbf{E} defined by,

$$\mathbf{E} = \frac{1}{2}(\mathbf{C} - \mathbf{I}) . \quad (2.16)$$

Both \mathbf{C} and \mathbf{E} are material tensors. Their spatial counter versions are the Finger tensor $\mathbf{b} = \mathbf{F}\mathbf{F}^T$, and the Euler-Almansi strain tensor $\mathbf{e} = \frac{1}{2}(\mathbf{I} - \mathbf{b}^{-1})$. The inverse of the deformation mapping gives the advantage of defining the tensor related quantities in both configurations via the push-forward and the pull-back operations. For example, the push-forward operation $\varphi_* = \Omega_0 \rightarrow \tilde{\Omega}_t$ is defined for the Almansi strain,

$$\mathbf{e} = \varphi_*(\mathbf{E}) = \mathbf{F}^{-T} \mathbf{E} \mathbf{F}^{-1} , \quad (2.17)$$

and the pull-back of the same tensor from spatial coordinates to the material one yields,

$$\mathbf{E} = \varphi_*^{-1}(\mathbf{e}) = \mathbf{F}^T \mathbf{E} \mathbf{F} . \quad (2.18)$$

Not all deformation mappings cause strain at the spatial configuration. A deformation is called translation if,

$$\varphi(\mathbf{X}) = \mathbf{X} + \mathbf{c} , \quad (2.19)$$

for some constant vector $\mathbf{c} \in \mathcal{V}$. The deformation is called an extension at \mathbf{X}_0 in the direction of a unit vector \mathbf{a} , if

$$\varphi(\mathbf{X}) = \mathbf{X}_0 + \mathbf{F}(\mathbf{X} - \mathbf{X}_0) \quad \mathbf{F} = \mathbf{I} + (\lambda - 1)\mathbf{a} \otimes \mathbf{a} , \quad (2.20)$$

for some $\lambda \in \mathfrak{R}_+$. The last equation shows us the appropriate application of the stretch variable λ on the direction of \mathbf{a} . The situation can be analyzed for a general case via spectral decomposition of the deformation tensor \mathbf{C} . Cauchy-Green tensor \mathbf{C} can be represented by its spectral decomposition including an eigenvalue (Λ_i^C) and an eigenvector set (\mathbf{n}_i^C). Thus,

$$\mathbf{C} = \sum_{i=1}^{n_{\text{dim}}} \Lambda_i^C (\mathbf{n}_i^C \otimes \mathbf{n}_i^C) . \quad (2.21)$$

Lagrangian (material) and Eulerian (spatial) strain tensors have the decomposition,

$$\mathbf{E} = \frac{1}{2} \sum_{i=1}^{n_{\text{dim}}} \left((\Lambda_i^C)^2 - 1 \right) (\mathbf{n}_i^C \otimes \mathbf{n}_i^C) , \quad (2.22)$$

$$\mathbf{e} = \frac{1}{2} \sum_{i=1}^{n_{\text{dim}}} \left(1 - (\Lambda_i^b)^2 \right) (\mathbf{n}_i^b \otimes \mathbf{n}_i^b) , \quad (2.23)$$

respectively. For $\Lambda_i^C = (\Lambda_i^b)^{-1}$, it yields $\mathbf{R}^T \mathbf{R} = \mathbf{I}$.

While evaluating the time-dependent spatial evolution of a deforming body \mathcal{B} , the rates of the deformation tensor gain attention. The geometric consideration assumes a spatial dimension $1 \leq n_{\text{dim}} \leq 3$, so the mapping should also cover a time configuration (time frame) $t \in \mathbb{I}$, $\mathbb{I} = [0, \infty) \subset \mathfrak{R}_+$. Then, the mapping is defined by $\varphi : \Omega_0 \times \mathbb{I} \rightarrow \mathbb{E}^{n_{\text{dim}}}$, where for each fixed $t \geq 0$, φ_t maps the reference configuration onto a selected spatial configuration, $\Omega_t = \varphi_t(\Omega_0)$. Similar to the displacement field (\mathbf{u}), any kind of physical quantity can be represented with respect to a selected configuration. For example, chemical density ρ_c , may be a description in the material coordinates $\rho_c = \rho_c(\mathbf{X}, t)$ or in the spatial one $\tilde{\rho}_c = \tilde{\rho}_c(\mathbf{x}, t)$. The time rate of the spatial field variables should be evaluated by considering the simultaneously deforming current configuration. For the spatial chemical field,

$$\begin{aligned} \dot{\tilde{\rho}}_c &= \frac{\partial}{\partial t} \tilde{\rho}_c(\varphi(\mathbf{X}, t), t) , \\ &= \frac{\partial \tilde{\rho}_c(\mathbf{x}, t)}{\partial t} + \frac{\partial \tilde{\rho}_c(\mathbf{x}, t)}{\partial x} \cdot \frac{\partial \varphi(\mathbf{X}, t)}{\partial t} . \end{aligned} \quad (2.24)$$

The second additional term in equation 2.24 is a result of the simultaneous deformation. The spatial time derivative concept can be related to the velocity of the deformation. Assume, $\varphi : \Omega_0 \times \mathbb{I} \rightarrow \mathbb{E}^3$ describes the motion of a continuum configuration Ω . The material (\mathbf{v}) and spatial ($\tilde{\mathbf{v}}$) velocity at time t are expressed by

$$\mathbf{v}(\mathbf{X}, t) = \frac{\partial \varphi(\mathbf{X}, t)}{\partial t} \quad \tilde{\mathbf{v}}(\mathbf{x}, t) = \tilde{\mathbf{v}}(\varphi^{-1}(\mathbf{X}, t), t) , \quad (2.25)$$

and the acceleration is $\mathbf{a} = \partial^2 \varphi(\mathbf{X}, t) / \partial t^2$. Formally, for a continuum motion $\varphi : \Omega \times \mathbb{I} \rightarrow \mathbb{E}^3$ with the spatial velocity field $\tilde{\mathbf{v}}$, and an arbitrary vector field $\tilde{\mathbf{q}} = \tilde{\mathbf{q}}(\mathbf{x}, t)$ is given by

$$\dot{\tilde{\mathbf{q}}} = \frac{\partial}{\partial t} \tilde{\mathbf{q}} + \left(\tilde{\nabla} \tilde{\mathbf{q}} \right) \cdot \tilde{\mathbf{v}}. \quad (2.26)$$

Similarly, the spatial velocity gradient is given by

$$\tilde{\mathbf{l}} = \frac{\partial \tilde{\mathbf{v}}(\mathbf{x}, t)}{\partial \mathbf{x}} = \tilde{\nabla} \tilde{\mathbf{v}}. \quad (2.27)$$

The spatial velocity gradient can be decomposed into its symmetric and anti-symmetric parts as

$$\tilde{\mathbf{l}} = \tilde{\mathbf{d}} + \tilde{\mathbf{w}}, \quad (2.28)$$

where $\tilde{\mathbf{d}} = (\tilde{\mathbf{l}} + \tilde{\mathbf{l}}^T) / 2$ and $\tilde{\mathbf{w}} = (\tilde{\mathbf{l}} - \tilde{\mathbf{l}}^T) / 2$, are the symmetric and the skew-symmetric rate of the deformation respectively.

2.2.3 Stress concept

In this section, the concept of stress is summarized. The motion of a continuum body is a geometric transformation causing strains which has effects on the geometric positions of continuum particles. Strain creates an internal force field inside the material, and that should be balanced by a virtual opposing force field. When external forces are applied on the boundary $\partial\Omega$ of the body, internal forces start acting on the virtual boundary layers $\partial\Omega'$ at any point inside the body. If the body is continuously deforming, there appears an inside flux of resultant force which brings out a time dependent traction vector $\mathbf{t} = \mathbf{t}(\mathbf{x}, t, \tilde{\mathbf{n}})$ in the direction of the normal $\tilde{\mathbf{n}}(\mathbf{x}, t) \perp \partial\tilde{\Omega}'(\mathbf{x}, t)$. $\mathbf{t} = \mathbf{t}(\mathbf{x}, t, \tilde{\mathbf{n}})$ is called the true Cauchy traction vector and $\mathbf{T} = \mathbf{T}(\mathbf{X}, t, \mathbf{n})$ is the first Piola-Kirchhoff (nominal) traction. Due to the law of action-reaction, $\mathbf{t}(\mathbf{x}, t, \tilde{\mathbf{n}}) = -\mathbf{t}(\mathbf{x}, t, -\tilde{\mathbf{n}})$. The following lines are known as the Cauchy's stress theorem. Let $\mathbf{t} : \mathcal{N} \times \tilde{\Omega}' \rightarrow \mathcal{V}$ be the traction function for a configuration $\tilde{\Omega}'$ whose volume tends to zero (\mathcal{N} is the set of all normal vectors with respect to a boundary layer). Then, $\mathbf{t}(\mathbf{x}, \tilde{\mathbf{n}})$ is linear in \mathbf{n} , that is, for each $\mathbf{x} \in \tilde{\Omega}'$ there exists a second-order tensor $\mathbf{S}(\mathbf{x}) \in \mathcal{V}^2$,

$$\mathbf{t}(\mathbf{x}, \tilde{\mathbf{n}}) = \mathbf{S}(\mathbf{x}) \cdot \tilde{\mathbf{n}}. \quad (2.29)$$

The field $\mathbf{S} : \tilde{\Omega}' \rightarrow \mathcal{V}^2$ is called as the Cauchy stress field for $\tilde{\Omega}'$. The relationship between the Cauchy ($\boldsymbol{\sigma}$) and Piola (\mathbf{P}) stresses is given by,

$$\mathbf{P} = J\boldsymbol{\sigma}\mathbf{F}^{-T}. \quad (2.30)$$

Another spatial stress quantity is the Kirchhoff stress tensor $\boldsymbol{\tau}$, and it is related to the Cauchy stress via the Jacobian of the mapping by,

$$\boldsymbol{\tau} = J\boldsymbol{\sigma}. \quad (2.31)$$

In many computational applications, the symmetric definitions of the stress tensors are crucial for reducing the computational complexity of the simulations. The symmetric second Piola-Kirchhoff tensor is defined for the material configuration which may be obtained via the pull-back of the Cauchy stress,

$$\mathbf{S} = J\mathbf{F}^{-1}\boldsymbol{\sigma}\mathbf{F}^{-T}. \quad (2.32)$$

For growing biological domains, the Mandel stress is defined with respect to the coordinate system of the intermediate configuration $\underline{\Omega}$. It is preferred for the evolution equations of the internal variables, due to its relationship with the thermodynamic magnitudes (energetically conjugate pairs). Mandel stress \mathbf{M} is defined as,

$$\mathbf{M} = \mathbf{C}\mathbf{S}, \quad (2.33)$$

where \mathbf{C} is the Green deformation and \mathbf{S} is the second Piola-Kirchhoff stress tensor. In many applications of the developmental biomechanics, the main consideration may be to determine the maximum stress level at a point $\mathbf{x} \in \Omega_t$ in order to evaluate the excessive loads inside the body. The problem is the determination of the eigenvalues of a stress tensor. For instance, the equation $(\boldsymbol{\sigma} - \Lambda_i^\sigma \mathbf{I}) \cdot \mathbf{n}_i^\sigma = 0$ yields the characteristic polynomial

$$\Lambda_i^\sigma - I_1\Lambda_i^\sigma + I_2\Lambda_i^\sigma - I_3 = 0 \quad i = \overline{1, n_{\text{dim}}}, \quad (2.34)$$

with the set of principal stress invariants I_i of the tensor $\boldsymbol{\sigma}$,

$$\begin{aligned} I_1(\boldsymbol{\sigma}) &= \text{tr}(\boldsymbol{\sigma}), \\ I_2(\boldsymbol{\sigma}) &= \frac{1}{2}((\text{tr}(\boldsymbol{\sigma}^2)) - \text{tr}(\boldsymbol{\sigma})^2), \\ I_3(\boldsymbol{\sigma}) &= \det(\boldsymbol{\sigma}). \end{aligned} \quad (2.35)$$

The spectral decomposition of the stress tensor $\boldsymbol{\sigma}$ yields

$$\boldsymbol{\sigma} = \sum_{i=1}^{n_{\text{dim}}} \sigma_i (\mathbf{n}_i^\sigma \otimes \mathbf{n}_i^\sigma). \quad (2.36)$$

2.3 Balance Laws

For a consistent analysis of the motion of a continuum body \mathcal{B} , the kinematic process should obey some universal laws that guarantee the existence of an equilibrium configuration $\tilde{\Omega}_t$. Since the behavior of the macroscopic continuum elements depends on the applied internal or external forces, the final equilibrium configuration is determined by the magnitude of these forces. The effects of the forces may be absorbed by the body potentially (without heat production) or it may be exerted to the movement kinetically. At least some quantity, defining the potential or kinetic behavior of the output, should be preserved to obtain the steady-state equilibrium conditions. In this section, five fundamental balance laws are analyzed in order to denote the time-dependent configurational mapping with the consistent universal laws, where any continuum body does inevitably obey. These are the conservation equations of the mass, linear momentum, angular momentum, and the stored energy for the configuration $\tilde{\Omega}_t$. The fifth law is the entropy inequality. The inequality defines a definite restriction, a natural boundary, for the thermodynamic processes.

2.3.1 Conservation of mass

Some aspects of mass have been previously discussed in section 2.2. The focus of this work is in low energy physics, in which the integrity of elemental particles is preserved, and the mass of continuum domain does not change. Thus, for a closed system \mathcal{B} , the mass of the initial configuration is

$$\text{mass}[\tilde{\Omega}_0] = \text{mass}[\tilde{\Omega}_t] > 0 \quad \forall t \in \mathbb{I}. \quad (2.37)$$

The principle is called the conservation of mass. Similarly, for $\varphi : \Omega_0 \rightarrow \tilde{\Omega}_{t \in \mathbb{I}}$, the spatial mass density $\tilde{\rho} = \tilde{\rho}(\mathbf{x}, t)$ changes with time since $dv = J(\mathbf{x}, t) dV$, $\rho_0(\mathbf{x}) dV = \tilde{\rho}(\mathbf{x}, t) J dV$. Thus, for a constant material density $\dot{\rho}_0 = 0$, one obtains

$$\frac{d}{d}(\rho J) = \dot{\rho} J + \rho J (\tilde{\nabla} \cdot \tilde{\mathbf{v}}). \quad (2.38)$$

For the volume preserving motions, $\tilde{\nabla} \cdot \tilde{\mathbf{v}} = 0$ equality inevitably dictates $\dot{\rho} = 0$ for $J = 1$. In many applications of vascular biomechanics, soft tissue is assumed to be incompressible or nearly incompressible due to the abundance of water.

2.3.2 Balance of linear and angular momentum

Let $\varphi : \Omega_0 \times \mathbb{I} \rightarrow \mathbb{E}^3$ be a deformation field for $\mathbf{x} = \varphi(\mathbf{X}, t)$, the spatial mass density is $\tilde{\rho} = \tilde{\rho}(\mathbf{x}, t)$, and spatial velocity field is $\tilde{\mathbf{v}} = \tilde{\mathbf{v}}(\mathbf{x}, t)$. The total linear momentum \mathbf{L} is defined by the vector valued function $\mathbf{L} : \mathcal{V} \rightarrow \mathcal{V}$ as,

$$\mathbf{L}(t) = \int_{\Omega_t} \tilde{\rho}(\mathbf{x}, t) \tilde{\mathbf{v}}(\mathbf{x}, t) dv = \int_{\Omega_0} \rho_0(\mathbf{X}, t) \mathbf{v}_0(\mathbf{X}, t) dV, \quad (2.39)$$

and the total angular momentum $\mathbf{J}(t)$ relative to a fixed point \mathbf{x}_0 is defined as,

$$\mathbf{J}(t) = \int_{\Omega_t} \mathbf{r} \times \tilde{\rho}(\mathbf{x}, t) \tilde{\mathbf{v}}(\mathbf{x}, t) dv = \int_{\Omega_0} \mathbf{r} \times \rho_0(\mathbf{X}, t) \mathbf{v}_0(\mathbf{X}, t) dV, \quad (2.40)$$

for $\mathbf{r}(\mathbf{x}) = \mathbf{x} - \mathbf{x}_0 = \varphi(\mathbf{X}, t) - \mathbf{x}_0$ [32]. The time rates give $\dot{\mathbf{L}}(t) = \mathbf{F}(t)$ and $\dot{\mathbf{J}}(t) = \mathbf{M}(t)$ are the forces and moment of the forces. They define two sets of balance equation as,

$$\mathbf{F}(t) = \frac{d}{dt} \int_{\Omega_t} \tilde{\rho}(\mathbf{x}, t) \tilde{\mathbf{v}}(\mathbf{x}, t) dv = \int_{\partial\Omega} \mathbf{t} ds + \int_{\Omega} \mathbf{b} dv, \quad (2.41)$$

$$\mathbf{M}(t) = \frac{d}{dt} \int_{\Omega_t} \mathbf{r} \times \tilde{\rho}(\mathbf{x}, t) \tilde{\mathbf{v}}(\mathbf{x}, t) dv = \int_{\partial\Omega_t} \mathbf{r} \times \mathbf{t} ds + \int_{\Omega} \mathbf{r} \times \mathbf{b} dv. \quad (2.42)$$

The necessary and sufficient condition for the linear and angular momentum equations to be valid is the existence of a tensor field $\boldsymbol{\sigma}$, where $\mathbf{t} = \mathbf{t}(\mathbf{x}, t, \tilde{\mathbf{n}}) = \boldsymbol{\sigma}(\mathbf{x}, t) \cdot \tilde{\mathbf{n}}$. From the divergence theorem,

$$\mathbf{t} = \mathbf{t}(\mathbf{x}, t, \tilde{\mathbf{n}}) = \boldsymbol{\sigma}(\mathbf{x}, t) \cdot \tilde{\mathbf{n}}, \quad (2.43)$$

$$\int_{\partial\Omega_t} \mathbf{t}(\mathbf{x}, t, \tilde{\mathbf{n}}) ds = \int_{\partial\Omega_t} \boldsymbol{\sigma}(\mathbf{x}, t) \cdot \tilde{\mathbf{n}} ds = \int_{\Omega_t} \tilde{\nabla} \cdot \boldsymbol{\sigma}(\mathbf{x}, t) dv, \quad (2.44)$$

where $\boldsymbol{\sigma}$ is the Cauchy stress. Substituting the integration yields,

$$\int_{\Omega_t} \left(\tilde{\nabla} \cdot \boldsymbol{\sigma}(\mathbf{x}, t) + \mathbf{b}(\mathbf{x}, t) - \rho \dot{\tilde{\mathbf{v}}}(\mathbf{x}, t) \right) dv = 0, \quad (2.45)$$

which can be reduced into the Cauchy's equation of motion $\tilde{\nabla} \cdot \boldsymbol{\sigma} + \mathbf{b} = \rho \dot{\tilde{\mathbf{v}}}$. For a very slow quasi-static evolution of growing bodies, the acceleration term is assumed to vanish. Thus,

$$\tilde{\nabla} \cdot \boldsymbol{\sigma} + \mathbf{b} = 0. \quad (2.46)$$

If not strictly required, internal body forces (i.e. gravity) is not critical for the long-term biological changes. Thus, the balance of linear momentum simplifies into the form $\tilde{\nabla} \cdot \boldsymbol{\sigma} = 0$, pointing the status of self-equilibrium. The balance of angular momentum is satisfied by the symmetry restriction of the Cauchy stress,

$$\boldsymbol{\sigma} = \boldsymbol{\sigma}^T. \quad (2.47)$$

2.3.3 Balance of mechanical energy

The balance of energy can be supposed to be an extension of the Cauchy's equation of motion. A dynamic process based on a tensor field $\boldsymbol{\sigma} : \tilde{\Omega}_t \rightarrow \mathcal{V}^2$ and a deformation field $\varphi : \Omega_0 \rightarrow \tilde{\Omega}_t$ for $\boldsymbol{x} = \varphi(\boldsymbol{X}, t)$ is assumed. Since the whole process depends on the $(\boldsymbol{\sigma}, \varphi)$ tuple, the energy based derivations assume that the accumulation of the internal potential is dynamically influenced by only the stress field. Then, there is a natural distinction between external and internal energy sources. The external mechanical power, which is the rate of an external mechanical work is defined by,

$$\mathcal{P}_{ext}(t) = \int_{\partial\tilde{\Omega}_t} \boldsymbol{t} \cdot \tilde{\boldsymbol{v}} ds + \int_{\tilde{\Omega}_t} \boldsymbol{b} \cdot \tilde{\boldsymbol{v}} dv, \quad (2.48)$$

is the power of input in a region $\tilde{\Omega}_t$ realized by the system forces $(\boldsymbol{t}, \boldsymbol{b})$. The kinetic energy \mathcal{K} in the $\tilde{\Omega}_t$ region is

$$\mathcal{K}(t) = \int_{\tilde{\Omega}_t} \frac{1}{2} \rho \tilde{\boldsymbol{v}}^2 dv = \int_{\tilde{\Omega}_t} \frac{1}{2} \rho \tilde{\boldsymbol{v}} \cdot \tilde{\boldsymbol{v}} dv. \quad (2.49)$$

The rate of the internal mechanical work \mathcal{P}_{int} in a region $\tilde{\Omega}_t$ created by a stress field is defined by,

$$\mathcal{P}_{int}(t) = \int_{\tilde{\Omega}_t} \boldsymbol{\sigma} : \boldsymbol{d} dv = \int_{\tilde{\Omega}_t} \text{tr}(\boldsymbol{\sigma}^T \boldsymbol{d}) dv. \quad (2.50)$$

By substituting the previous definitions, the total balance of mechanical energy in the spatial configuration yields,

$$\frac{d}{dt} \mathcal{K}(t) + \mathcal{P}_{int}(t) = \mathcal{P}_{ext}(t). \quad (2.51)$$

Then,

$$\int_{\tilde{\Omega}_t} \frac{1}{2} \rho \tilde{\boldsymbol{v}}^2 dv + \int_{\tilde{\Omega}_t} \boldsymbol{\sigma} : \boldsymbol{d} dv = \int_{\partial\tilde{\Omega}_t} \boldsymbol{t} \cdot \tilde{\boldsymbol{v}} ds + \int_{\tilde{\Omega}_t} \boldsymbol{b} \cdot \tilde{\boldsymbol{v}} dv. \quad (2.52)$$

The balance of mechanical energy in the material configuration is represented by [32],

$$\int_{\Omega_0} \frac{1}{2} \rho_0 \boldsymbol{V}_0^2 dV + \int_{\Omega_0} \boldsymbol{P} : \dot{\boldsymbol{F}} dV = \int_{\partial\Omega_0} \boldsymbol{T} \cdot \boldsymbol{V}_0 dS + \int_{\Omega_0} \boldsymbol{B} \cdot \boldsymbol{V}_0 dV, \quad (2.53)$$

where $\mathbf{B}(\mathbf{X}, t) = J(\mathbf{X}, t)\mathbf{b}(\mathbf{x}, t)$, $T(\mathbf{X}, t, \mathbf{n}_0) = \mathbf{P}(\mathbf{X}, t) \cdot \mathbf{n}_0$ and $\mathbf{V}_0(\mathbf{X}, t)$ is the velocity of the deformation field at \mathbf{X} . The total energy is conserved during the dynamical process $(\boldsymbol{\sigma}, \varphi)$.

2.3.4 Entropy inequality

A continuum configuration which possesses both mechanical and thermal energy is called a *thermodynamic continuum*. The time evolution of a continuum is governed by the *state variables*, where the relationship between them are described by the *constitutive equations*. The second law of thermodynamics sets a physical boundary for the evolution of thermodynamic systems. The energy transfer from one system to another exhibits some level of irreversible energy loss (as heat), due to the random nature and disorder in the microscopic partitions of the system. The total entropy of a continuum configuration can be expressed by $\mathcal{S}(t)$,

$$\mathcal{S}(t) = \int_{\tilde{\Omega}_t} \tilde{\eta}(\mathbf{x}, t) dv = \int_{\Omega_0} \eta(\mathbf{x}, t) dV, \quad (2.54)$$

where $\tilde{\eta}(\mathbf{x}, t)$ and $\tilde{\eta}(\mathbf{X}, t)$ stands for the entropy per unit spatial and material volume. The second law of thermodynamics known as the Clausius-Planck inequality is

$$\mathcal{D}_{int} = \mathbf{P} : \dot{\mathbf{F}} - \dot{\Psi} - \eta \dot{\mathcal{T}}, \quad (2.55)$$

where \mathcal{D}_{int} is called the internal dissipation, \mathcal{T} is the absolute temperature and Ψ is the Helmholtz free energy $\Psi = u_{int} - \eta\mathcal{T}$, for an internal energy term u_{int} . The $(\mathbf{P}, \dot{\mathbf{F}})$ tuple remarks that the dissipative process is a deformation driven one.



3. EVOLUTION OF STRUCTURAL TENSORS

3.1 Purpose

In this section, a general framework for growing continuum domains which is influenced by a mass source (or flux) will be discussed. Some references will be emphasized from the theoretical background in chapter 2. Many equations that are related to the mass growth is similar to the behavior of any physical field that belongs to the non-relativistic continuum mechanics. Mass growth may be the reason for the residual stresses in a biological environment. Thus, an intermediate virtual configuration $\underline{\Omega}$ is utilized for the volumetric growth cases in order to obtain a stress-free configuration.

3.2 Constitutive Framework for the General Theory of Growth

The splitting of the time-dependent deformation and motion into an n number of virtual steps, constructs a virtual configuration set $\{\underline{\Omega}^i\}_{i=1}^n$, is a basic description for the continuously remodeling continuum bodies. The mass growth in a continuum body \mathcal{B} is considered to be a non-elastic action, where the deformation gradient of the mapping possesses a permanent residual component. The residual component supplies information about the inelastic (plastic) strains stored in the deformation field φ . A non-complex description of the deformation field, which is split into its elastic and plastic parts, can be represented by the multiplicative decomposition, known as the Kroner-Lee decomposition [33],

$$\mathbf{F} = \mathbf{F}_e \mathbf{F}_g, \quad (3.1)$$

where \mathbf{F} is the total deformation gradient, \mathbf{F}_e is the elastic recoverable part, and \mathbf{F}_g is the inelastic growing part of the total deformation. Similar multiplicative decompositions also apply for nonliving materials such as crystal structures as being the continua. In Figure 3.1, it is shown that the deformation mapping from the initial configuration Ω_0 to the final one $\tilde{\Omega}_t$ can be decomposed into its elastic and plastic

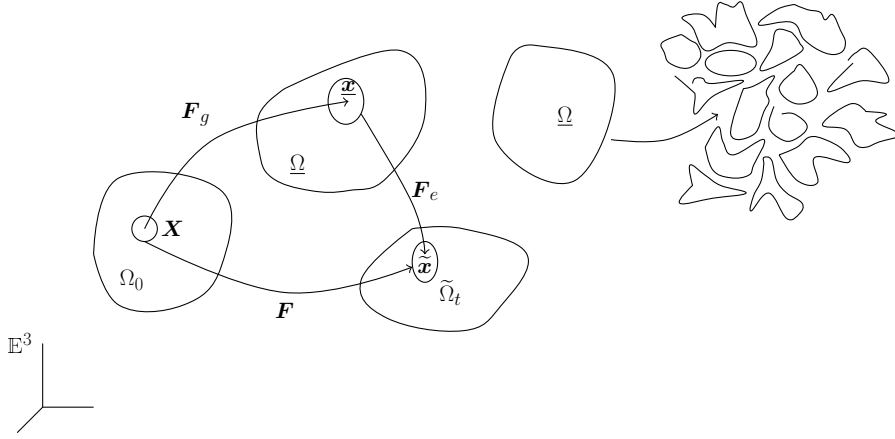


Figure 3.1: Representation of the multiplicative decomposition of deformation gradient into its elastic and growth parts in the configuration space. The intermediate configuration is assumed to be a stress free one which permits independent deformation (and evolution) of the individual local body partitions in the configuration space. Each local body partition is deformed in a geometrically incompatible way via \mathbf{F}_g . The final geometrically compatible body domain is constructed by the elastic deformation supplied by \mathbf{F}_e .

parts. There is still a theoretical discussion on the existence of a decomposition of the deformation mapping (φ) itself. However, for computational purposes, the decomposition of the deformation gradient matrix finds a wide range of application. Assume that, φ is the deformation mapping, such that, $\varphi : \Omega_0 \times \mathbb{I} \rightarrow \mathbb{E}^3$ and $\varphi : \Omega_0 \rightarrow \tilde{\Omega}_t$ in which the deformation gradients are $\mathbf{F}_g = \partial \underline{\mathbf{x}} / \partial \mathbf{X}$ and $\mathbf{F}_e = \partial \tilde{\mathbf{x}} / \partial \underline{\mathbf{x}}$ which yields $\mathbf{F}_e = \partial \tilde{\mathbf{x}} / \partial \mathbf{X}$ in global. The chain rule supplies the mentioned form in equation 3.1. The decomposition of the gradient is not uniquely defined since arbitrary rotations between $\Omega_0 \rightarrow \underline{\Omega}$ may yield the same unstressed intermediate configuration. Since, $\mathbf{F} = \mathbf{F}_e \mathbf{F}_g$, the polar decomposition yields $\mathbf{F} = \mathbf{V}_e (\mathbf{R}_e \mathbf{R}_g) \mathbf{U}_g$. For an isotropic strain energy density function (SED), the stresses inside the body depend on the principal stretches that are based on $\mathbf{C}_e = \mathbf{F}_e^T \mathbf{F}_e$. For simplicity, $\mathbf{R}_g = \mathbf{I}$ can be assumed. In this case, the growth part of the deformation gradient depends only on the stretches that appear on the path of $\Omega_0 \rightarrow \underline{\Omega}$. The simplest case is the independent isotropic growth of individual local partitions in the $\underline{\Omega}$ configuration, and $\mathbf{U}_g = \nu \mathbf{I}$ for $\nu \in \mathfrak{R}$. When the material body is transversely isotropic, the transverse layout of the fibers enforces the existence of a preferred direction embedded in the fabric structure. It is usual to assume that the mass growth, which has potential to generate the additional stresses due to the rotation of the local preferred direction, does not affect

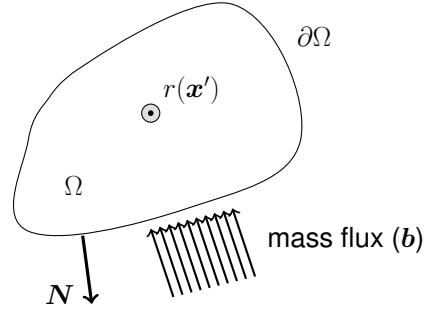


Figure 3.2: A mass flux representation based on a virtual configuration Ω which has a point mass source at \mathbf{x}' . The mass flux is assumed to be observed through the boundary layer $\partial\Omega$ with a normal vector \mathbf{N} .

the fabric structure ([34, 35]). Here, we will present the generally accepted settlement of the continuum theory of open system thermodynamics, balance equations, and the relationship between the continuum deformation of the material domain (continuum domain as the “structure”) and the evolution of the fabric structure (remodeling as the “function”). The mass flux can be evaluated as a physical process where the source of a mass change in a continuum body \mathcal{B} is related to both an external mass flux through $\partial\Omega$ and an internal mass source $R(\mathbf{x})$ located at \mathbf{x} in Ω . Then, the mass density ρ is related to the mass sources as,

$$\frac{D}{Dt} \int_{\Omega_0} \rho_0 dV = \int_{\Omega_0} R(\mathbf{X}) dV + \int_{\partial\Omega_0} \Gamma_{mass} dV, \quad (3.2)$$

where ρ_0 is the mass density in the reference configuration, R is a smooth volumetric source term and Γ_{mass} is the mass flux through the boundary layer $\partial\Omega$, and $\mathbf{\Gamma}_{mass}$ is the mass flux vector defined by a normal vector $\Gamma_{mass} = \mathbf{N} \cdot \mathbf{\Gamma}_{mass}$. From Cauchy’s theorem,

$$\frac{\partial}{\partial t} \rho_0(\mathbf{X}) = R(\mathbf{X}) + \nabla_0 \cdot \mathbf{\Gamma}_{mass}, \quad (3.3)$$

for the material configuration. Piola transformation which yields $r(\mathbf{x}) = J^{-1} R(\mathbf{X})$ uses the Jacobian J of the deformation gradient \mathbf{F} (see Figure 3.2). Similarly, in the spatial configuration, $\gamma_{mass}(\mathbf{x}) = J^{-1} \mathbf{F} \mathbf{\Gamma}_{mass}$. The spatial density ρ is related to ρ_0 as

$$\rho = \rho_0 J^{-1}, \quad J = \det(\mathbf{F}). \quad (3.4)$$

It is clear that the current density is determined by ρ_0 and J tuple where $\dot{\rho} = 0$ is also possible. The following balance law describes the evolution of ρ as a remodeling event in $\tilde{\Omega}_t$

$$\frac{d}{dt} \rho(\mathbf{x}) = r(\mathbf{x}) + \tilde{\nabla} \cdot \gamma_{mass}(\mathbf{x}) - \rho \tilde{\nabla} \cdot \tilde{\mathbf{v}}(\mathbf{x}), \quad (3.5)$$

where $\tilde{\mathbf{v}}$ is the spatial velocity of the deformation at \mathbf{x} ([34, 35]). Then, a density preserving spatial evolution is described by ([36])

$$r(\mathbf{x}) + \tilde{\nabla} \cdot \gamma_{mass}(\mathbf{x}) - \rho \tilde{\nabla} \cdot \tilde{\mathbf{v}}(\mathbf{x}) = 0. \quad (3.6)$$

For an open system thermodynamic equilibrium, the concept of the “reduced” form of quantities are of special importance ([37]). Similar in rocket movements, the reduced quantities in an open system correspond to the hot gas flow that is excluded from the closed system of the rocket and gas union. Then, for an open system, there are reversible conserved magnitudes which do not leave the system, and some portion of the flux is lost (irreversible) since it leaves the system forever. One typical example is the migration of cellular clusters, entering in a closed region Ω through its boundary $\partial\Omega$ as a cell flux Γ_{cell} , where some portion of the flux $\bar{\Gamma}_{cell}$ is again exerted from the boundary $\partial\Omega$, leaving a reversible portion of the migration. Then, the total momentum flux (Γ) including the reduced flux is $\Gamma = \bar{\Gamma} + \mathbf{v} \otimes R$ where $\mathbf{v} = D\varphi(\mathbf{X}, t)/Dt$ ([37]). Similarly, $\gamma = \bar{\gamma} + \tilde{\mathbf{v}} \otimes r$ for the spatial configuration. The momentum source is defined by $b_0 = \bar{b}_0 + \mathbf{v} R_{mass} - \nabla \mathbf{v} \cdot \Gamma_{mass}$ in which R_{mass} is a source function supplying the rate of material production and Γ_{mass} is a mass influx. According to the derivations of the balance equations for volume-specific and mass specific versions, the mass-specific balance laws can be reformulated in order to incorporate the change in mass. Unlike any other internal variable, change in mass itself has a direct effect on the form of conservation relationships. For the *volume-specific* case, the material version of the momentum balance equation is the classical Cauchy’s equation, with the replacement of Γ ,

$$\frac{D}{Dt} \mathbf{p}_0 = \nabla_0 \mathbf{P} + \mathbf{b}_0, \quad (3.7)$$

which is associated with a set of Piola transformations,

$$\mathbf{p}_0 = J \tilde{\mathbf{p}} \quad \mathbf{b}_0 = J \tilde{\mathbf{b}} \quad \mathbf{P} = J \boldsymbol{\sigma} \mathbf{F}^{-T}, \quad (3.8)$$

where \mathbf{p}_0 is the volume-specific momentum density, and \mathbf{P} is the first Piola-Kirchhoff stress tensor standing for the momentum flux. Momentum can be expressed as a function of the spatial velocity as $\mathbf{p}_0 = J \tilde{\rho} \tilde{\mathbf{v}}$. For the spatial configuration, the momentum balance is

$$\frac{d}{dt} \tilde{\mathbf{p}} + \tilde{\nabla} (\tilde{\mathbf{p}} \otimes \tilde{\mathbf{v}}) = \tilde{\nabla} \boldsymbol{\sigma} + \tilde{\mathbf{b}}. \quad (3.9)$$

In an open system the external mass source is the only phenomena that effects the shape of the balance equations,

$$\mathbf{P} \cdot \mathbf{N} = \mathbf{t}_0^{closed} + \mathbf{t}_0^{open} \quad , \quad \mathbf{t}_0^{open} = \bar{\mathbf{t}}_0^{open} + (\mathbf{p} \otimes R) \cdot \mathbf{N} \quad , \quad (3.10)$$

$$\boldsymbol{\sigma} \cdot \mathbf{n} = \tilde{\mathbf{t}}^{closed} + \tilde{\mathbf{t}}^{open} \quad , \quad \tilde{\mathbf{t}}^{open} = \tilde{\bar{\mathbf{t}}}^{open} + (\mathbf{p} \otimes r) \cdot \mathbf{n} \quad , \quad (3.11)$$

for \mathbf{n} being the normal vector for the mass flux in the spatial configuration, and \mathbf{t} is the Cauchy traction. Upper indices state the source of the magnitudes whether it is coming from a closed or an open system. It is clear that the effects of an external mass flux contribution are only seen via the change in variable $\bar{\mathbf{t}}^{open}$. Similar to the traction, the external mass source is defined by the equations [37]

$$\mathbf{b}_0 = \mathbf{b}_0^{closed} + \mathbf{b}_0^{open} \quad , \quad \mathbf{b}_0^{open} = \bar{\mathbf{b}}_0^{open} + \mathbf{p} \mathcal{R}_0 - \nabla_0 \mathbf{p} \cdot R \quad , \quad (3.12)$$

$$\tilde{\mathbf{b}} = \tilde{\mathbf{b}}^{closed} + \tilde{\mathbf{b}}^{open} \quad , \quad \tilde{\mathbf{b}}^{open} = \tilde{\bar{\mathbf{b}}}^{open} + \mathbf{p} \tilde{\mathbf{R}} - \tilde{\nabla} \mathbf{p} \cdot r \quad , \quad (3.13)$$

where \mathbf{b} is the external mass source term. Addition of the external mass flux into the dynamic system can be defined explicitly by the point-wise modification the $\bar{\mathbf{b}}^{open}$ term. In the volume-specific formulations, density is related to the deformation itself if $\mathbf{b}^{open} = 0$, and the external mass source is in its classical version that is observed in closed systems, $\mathbf{b} = \mathbf{b}^{closed}$. The mass-specific formulations are identical to the volume- case, and much shorter representations can be achieved (see [37] for discussions). The energy balance and the entropy inequality are analyzed in a similar way.

A simple case includes an example of the continuum system with a growing mass through the activities of the internal sources ([34]). If $r_g(\boldsymbol{x})$ is the time rate of mass growth per unit volume, and ρ is the mass density, such that

$$\frac{d}{dt}(dm) = r_g dv \quad , \quad \rho = \frac{dm}{dv} \quad , \quad (3.14)$$

in which, d/dt stands for the material time derivative. For $r_g > 0$ the mass growth occurs. Then the evolution of the material density with a growing mass is given by,

$$\frac{d}{dt} \rho + \rho \tilde{\nabla} \cdot \tilde{\mathbf{v}} = r_g \quad . \quad (3.15)$$

For incompressible materials $d\rho/dt = 0$ and $\tilde{\nabla} \cdot \tilde{\mathbf{v}} = r_g/\rho$ and for the volume preserving cases $\tilde{\nabla} \cdot \tilde{\mathbf{v}} = 0$. The time rate of the mass growth per unit reference

volume R_g can be obtained by $r_g dv = R_g dV$. Thus, $R_g = r_g J$, since $dv = J dV$. Similarly, $d(\rho J)/dt = R_g$ for $\rho_0^g = \rho J$, where ρ_0^g is the path dependent growing density in the reference configuration. The time evolution yields,

$$\rho J = \rho_0 + \int_0^t R_g dt'. \quad (3.16)$$

Essentially, for biological structures, if the volume is preserved throughout the evolution of a remodeling event, then $J = 1$, $\rho_0^g = \rho$, $R_g = r_g$, and $\rho = \rho_0 + \int_0^t R_g dt'$ as observed commonly in bone tissue. If the material is incompressible, the density is preserved and $\rho = \rho_0$, $\rho_0^g = \rho_0$ are kept constant. Then,

$$J = 1 + \frac{1}{\rho_0} \int_0^t R_g dt', \quad (3.17)$$

as commonly observed in vascular systems when mass growth occurs. The approach can be generalized for various internal variables. Assume Υ^i is the i^{th} internal variable which is defined with respect to the per unit current mass. Υ_0^i is the corresponding variable defined for the per unit initial mass. Then, $\Upsilon^i \rho dv = \Upsilon_0^i \rho_0 dV$. Since $dv = J dV$, it follows that $\Upsilon^i \rho J = \Upsilon_0^i \rho_0$. By using the identity in equation 3.16, it yields

$$\Upsilon^i \left(1 + \frac{1}{\rho_0} \int_0^t R_g dt' \right) = \Upsilon_0^i, \quad (3.18)$$

for the internal variable Υ^i . For quasi-static analysis, the linear and angular balance of momentums are similarly evaluated as in the non-growing cases which do not include mass-growth. The material form of the Cauchy's law of motion can be reduced into the balance law,

$$\nabla_0 \mathbf{P} + \rho_0 \mathbf{b}_0 = \rho_0^g \frac{d\mathbf{v}}{dt}, \quad (3.19)$$

for the nominal Piola-Kirchhoff stress \mathbf{P} . For long time periods, when the transient elastic waves vanish, and the accelerations are negligible $d\mathbf{v}/dt \approx 0$, ρ_0^g has no effect on the balance. The angular balance of momentum for the mass-growth case is again satisfied by the symmetry constraint of the Cauchy's stress tensor, $\boldsymbol{\sigma} = \boldsymbol{\sigma}^T$.

The first law of thermodynamics (conservation of energy) for the case of growing mass can be represented by,

$$\frac{d}{dt} \int_v \rho \left(\frac{1}{2} \mathbf{v} \cdot \mathbf{v} + u \right) dv = \mathcal{P} + \mathcal{Q} + \int_v r_g \left(\frac{1}{2} \mathbf{v} \cdot \mathbf{v} + u \right) dv + \int_v \rho \mathcal{R}_g r_g dv, \quad (3.20)$$

and the rate of the work done by the external and body forces is given by,

$$\mathcal{P} = \int_v \left(\rho \frac{d}{dt} \left(\frac{1}{2} \mathbf{v} \cdot \mathbf{v} \right) + \boldsymbol{\sigma} : \mathbf{D} \right) dv \quad \mathbf{D} = (\mathbf{v} \otimes \nabla)_{sym}, \quad (3.21)$$

where \mathbf{D} is the symmetric part of the spatial velocity gradient tensor. The rate of the work is related to the heat flux \mathbf{q} across a surface element $\mathbf{n}dS$, and the rate of the heat input per unit current mass w is defined by,

$$\mathcal{Q} = - \int_v \mathbf{q} \cdot \mathbf{n} dv + \int_v \rho w dv = \int_v (-\nabla \cdot \mathbf{q} + \rho w) dv. \quad (3.22)$$

In equation 3.20, the term $\mathcal{R}_g r_g$ represents the rate of chemical energy per unit current mass. Then, \mathcal{R}_g is considered as the conjugate variable associated with the rate of mass-growth that is supplied by the term r_g . The term u stands for the rate of internal energy associated with the current mass growth. The time derivative of u has an explicit representation,

$$\frac{d}{dt}u = \frac{1}{\rho} \boldsymbol{\sigma} : \mathbf{D} - \frac{1}{\rho} \nabla \cdot \mathbf{q} + w + \mathcal{R}_g r_g, \quad (3.23)$$

which depends on the internal stresses, heat flux and a chemical potential, are all sourced from the mass growth.

The second law of thermodynamics (entropy inequality) for the case of growing mass can be related to the dissipation due to the structural changes (i.e. fabric). The rate of the dissipation per unit mass accompanying structural remodeling can be described by,

$$\sum_k f_k \frac{d\mathcal{I}_k}{dt}, \quad (3.24)$$

where \mathcal{I}_k ($k = 1, \dots, n$) are the internal variables that describe the structural changes due to the deformation, and f_k are the thermodynamic forces that are conjugate to the fluxes $d\mathcal{I}_k/dt$ ([34]). The thermodynamic conjugate reserved for the mass source r_g is f_g . The integral form of the entropy inequality for the continuum domain in spatial configuration with a growing mass is then,

$$\frac{d}{dt} \int_v \rho \eta dv = - \int_S \frac{1}{\mathcal{T}} \mathbf{q} \cdot \mathbf{n} dS + \int_v \frac{w}{\mathcal{T}} \rho dv + \int_v \rho r_\eta dv, \quad (3.25)$$

η is the entropy per unit mass, \mathcal{T} is the absolute temperature and r_η is the entropy production rate. The second law of thermodynamics restricts that $r_\eta > 0$, and the total rate of the dissipation is given by,

$$\mathcal{T} r_\eta = f_g r_g + \sum_k f_k \frac{d\mathcal{I}_k}{dt} \geq 0. \quad (3.26)$$

There is a direct relationship between the time rate of entropy production and the rate of mass production,

$$\frac{d\eta}{dt} = -\frac{1}{\rho} \nabla \cdot \left(\frac{1}{\mathcal{T}} \mathbf{q} \right) + \frac{1}{\mathcal{T}} \left(w + f_g r_g + \sum_k f_k \frac{d\mathcal{I}_k}{dt} \right). \quad (3.27)$$

From equation 3.23, the reversible partition of the rate of internal energy is defined by,

$$\frac{du}{dt} = \frac{1}{\rho} \boldsymbol{\sigma} : \mathbf{D} + \mathcal{T} \frac{d\eta}{dt} + (\mathcal{R}_g - f_g) r_g - \sum_k f_k \frac{d\Upsilon_k}{dt}. \quad (3.28)$$

It is clear that a sound description of the internal energy per unit mass may be represented in the form of

$$u = u(\mathbf{E}, \eta, \rho_0^g, \Upsilon_k), \quad (3.29)$$

for the Green-Lagrange strain tensor \mathbf{E} . Introduction of the Helmholtz free energy gives,

$$\Psi(\mathbf{E}, \mathcal{T}, \rho_0^g, \Upsilon_k) = u(\mathbf{E}, \eta, \rho_0^g, \Upsilon_k) - \mathcal{T} \eta, \quad (3.30)$$

which is crucial for the definitions of the growing entropic material domains, such as the long-chain polymer based extra cellular matrix environment in soft biological tissues. Once an acceptable form of the free energy is explicitly stated, via experiments or so, then the dissipation and its conjugate terms can be associated with the mechanical potential as,

$$\frac{d\Psi}{dt} = \frac{\partial \Psi}{\partial \mathbf{E}} : \frac{d\mathbf{E}}{dt} - \eta \frac{d\mathcal{T}}{dt} + (\mathcal{R}_g - f_g) r_g - \sum_k f_k \frac{d\Upsilon_k}{dt}, \quad (3.31)$$

in which,

$$\eta = -\frac{\partial \Psi}{\partial \mathcal{T}}, \quad \mathcal{R}_g - f_g = J \frac{\partial \Psi}{\partial \rho_0^g}, \quad f_k = -\frac{\partial \Psi}{\partial \Upsilon_k}. \quad (3.32)$$

These could be the basic relationships that define the thermodynamic state of a biological material. The determination of the exact form of the potential, which depends on a large number of internal variables $k \gg 1$, may be problematic for the biological structures.

3.2.1 Multiplicative decomposition of the deformation gradient

The biomechanical applications which incorporates the growth and remodeling process in soft biological tissue, the decomposition of the deformation gradient \mathbf{F} into its elastic and growth parts is crucial for the compact representation of the evolution equations. Some preliminary information about the decomposition has been given in previous paragraphs. It should be emphasized that the decomposition in equation 3.1 is not uniquely defined. Arbitrary local material rotations can be applied onto the rotational part of \mathbf{F}_g preserving the same unstressed state of the intermediate configuration $\underline{\Omega}$. However, an explicit definition of the growth part of \mathbf{F} supplies the

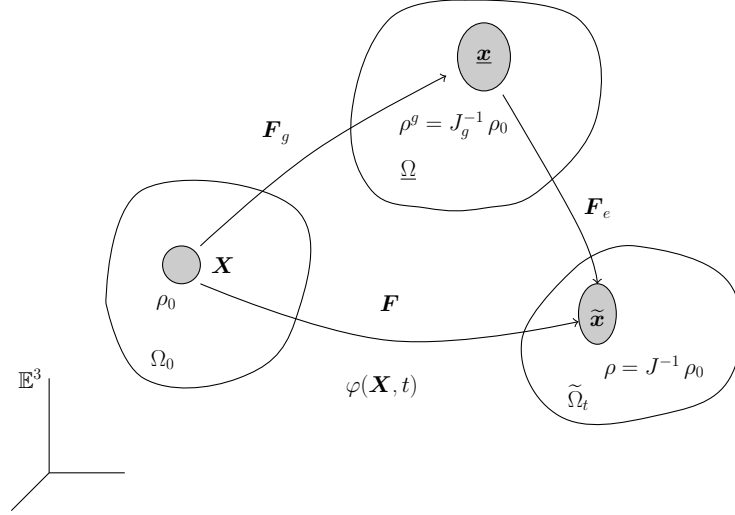


Figure 3.3: Representation of the multiplicative decomposition of the deformation gradient into its elastic and growth parts in the configuration space. The density relations that depend on the Jacobian of the transformations are presented as a function mapping.

sufficient freedom for the continuum formulations. Similar to the non-growing cases, in a growing media, the Lagrangian definition of the strain measures are given by,

$$\mathbf{E}_e = \frac{1}{2} (\mathbf{F}_e^T \mathbf{F}_e - \mathbf{I}), \quad \mathbf{E}_g = \frac{1}{2} (\mathbf{F}_g^T \mathbf{F}_g - \mathbf{I}), \quad (3.33)$$

where \mathbf{E}_e is the elastic and \mathbf{E}_g is the (permanent) growth strain. The total strain can be expressed as,

$$\mathbf{E} = \frac{1}{2} (\mathbf{F}^T \mathbf{F} - \mathbf{I}) = \mathbf{E}_g + \mathbf{F}_g^T \cdot \mathbf{E}_e \cdot \mathbf{F}_g, \quad (3.34)$$

and the decomposition does not supply an additive splitting, $\mathbf{E} \neq \mathbf{E}_g + \mathbf{E}_e$.

3.2.1.1 Growth and remodeling formulations for the evolution of mass density

Biological structures in the body of a living organism exhibit mechanical anisotropy. These structures are characterized by a set of structural tensor and related variables that describe the fabric of the domain. A usual example is the fiber reinforced vascular tissue. As in the case of the non-growing deformation mapping, the Jacobian of the deformation that maps the mass density from initial configuration to the grown intermediate-configuration is $\det(\mathbf{F}_g) = J_g$, and the elastic Jacobian is $\det(\mathbf{F}_e) = J_e$. Thus, $J = J_e J_g$. The local mass density around a fixed point can be associated with the growth deformation gradient, as shown in Figure 3.3. The density in the intermediate configuration is given by $\rho^g(\mathbf{x}) = J_g^{-1} \rho_0(\mathbf{X})$. The time evolution for the density in

spatial configuration is,

$$\frac{d\rho}{dt} + \rho \operatorname{tr} \left(\dot{\mathbf{F}} \cdot \mathbf{F}^{-1} \right) = r_g, \quad (3.35)$$

and in the intermediate configuration it is,

$$\frac{d\rho_g}{dt} + \rho_g \operatorname{tr} \left(\dot{\mathbf{F}}_g \cdot \mathbf{F}_g^{-1} \right) = r_g J_e. \quad (3.36)$$

The evolution equation for the reference mass density ρ_0 is defined by

$$\dot{\rho}_0 = -\rho_0 J_g (\dot{J}_g^{-1}) = \rho_0 \operatorname{tr} (\mathbf{L}_g), \quad (3.37)$$

with the velocity gradient $\mathbf{L}_g = \dot{\mathbf{F}}_g \cdot \mathbf{F}_g^{-1}$ in intermediate configuration. If there is no mass flux $\nabla_0 \cdot \Gamma_{mass} = 0$, then $R_g = \rho_0 \operatorname{tr} (\mathbf{L}_g)$. The total velocity gradient in the reference configuration can be represented in terms of the growth velocity gradient,

$$\mathbf{L} = \dot{\mathbf{F}} \cdot \mathbf{F}^{-1} = \dot{\mathbf{F}}_e \cdot \mathbf{F}_e^{-1} + \dot{\mathbf{F}}_e \cdot \left(\dot{\mathbf{F}}_g \cdot \mathbf{F}_g^{-1} \right) \cdot \mathbf{F}_e^{-1}. \quad (3.38)$$

Considering equation 3.30, a plausible free-energy description for the biological tissue can be summarized in a compact form,

$$\Psi = \Psi (\mathbf{F}, \mathbf{F}_g, \mathbf{H}_p, \rho_0, \mathcal{T}), \quad (3.39)$$

where \mathbf{H}_p is the set of structural tensors with $p = \overline{1, n}$. A typical element of this set is the outer product $\mathbf{H} = \mathbf{a} \otimes \mathbf{a}$ where \mathbf{a} is a vector determining the preferred direction of the elastic anisotropy. When there is no external mass flux, \mathbf{F}_g is only affected by an internal mass source which defines the rate of mass growth. Naturally, the relationship between other mechanical magnitudes can be represented by,

$$R_g = R_g (\mathbf{F}, \mathbf{F}_g, \mathbf{H}_p, \rho_0, \mathcal{T}). \quad (3.40)$$

In the following passages, the theoretical connections between a growing hyper-elastic domain and the remodeling of a structural fabric in time are discussed.

3.2.1.2 Notes on the algorithmic update procedures of the growth and remodeling variables

Our main consideration here is that the biological growth is considered to be a process of the large time scales. When it is compared with the time scale of the process of the arteries undergoing large deformation due to the blood pressure, the viscoelastic effects inside the artery wall are considered as transient ones. On the larger time

scales, the viscoelastic effects are negligible and the tissue can be assumed to obey the hyper-elastic constitutive laws ([38]). For an isothermal process $\dot{\mathcal{T}} \approx 0$, the growth and remodeling is a history dependent evolutionary event which can be analyzed similarly by the internal variable update procedures applied in computational plasticity. Then, the evolution of the internal structure (fabric) and the mass evolution of the continua can be represented by the constitutive functions that predict the global behavior of the domain. Here, the global constitutive model for the structure is assumed to be an hyper-elastic one. If the fabric of the structure is defined by a single tensor-field, $\mathbf{H} : \Omega_0 \rightarrow \mathcal{V}^2$, the Eulerian counter-part is defined by $\mathbf{H} = \mathbf{F}^T \mathbf{h} \mathbf{F}$. Then, the Lagrangian description of the hyper-elastic law states,

$$\mathbf{S} = \mathbf{S}(\mathbf{F}, \mathbf{H}), \quad (3.41)$$

with the Lagrangian internal variable \mathbf{H} . The stress-like quantity \mathbf{S} satisfies $\mathbf{S}(\mathbf{Q}\mathbf{F}, \mathbf{H}) = \mathbf{S}(\mathbf{F}, \mathbf{H})$ for $\forall \mathbf{Q} \in SO(3)$. Then, for a growth and remodeling event, \mathbf{H} has the evolution equation,

$$\dot{\mathbf{H}} = \mathbf{h}(\mathbf{F}, \mathbf{H}) \quad \text{with} \quad \mathbf{H}|_{t_n} = \mathbf{H}_n, \quad (3.42)$$

and function \mathbf{h} satisfies the objectivity requirement $\mathbf{h}(\mathbf{Q}\mathbf{F}, \mathbf{H}) = \mathbf{h}(\mathbf{F}, \mathbf{H})$. From a computational point of view, for $[t_n, t_{n+1}] \in \mathbb{I}$, the internal variable is updated by ([39]),

$$\mathbf{H}_{n+1} = \mathbf{H}_n + \Delta t ((1 - \alpha)\mathbf{h}(\mathbf{F}_n, \mathbf{H}_n) + \alpha\mathbf{h}(\mathbf{F}_{n+1}, \mathbf{H}_{n+1})), \quad (3.43)$$

where $\Delta t = t_{n+1} - t_n$ and α is the integration parameter. The update procedure $\mathbf{H}_{n+1} = \hat{\mathbf{H}}^{algo}(\mathbf{F}_{n+1}; \{\mathbf{F}_n, \mathbf{H}_n\})$ is called the ‘‘deformation-driven algorithmic Lagrangian state-update’’ algorithm. Similarly, stress update is given by

$$\begin{aligned} \mathbf{S}_{n+1} &= \hat{\mathbf{S}}^{algo}(\mathbf{F}_{n+1}; \{\mathbf{F}_n, \mathbf{H}_n\}), \\ &= \hat{\mathbf{S}}^{algo}\left(\mathbf{F}_{n+1}; \hat{\mathbf{H}}^{algo}(\mathbf{F}_{n+1}; \{\mathbf{F}_n, \mathbf{H}_n\})\right). \end{aligned} \quad (3.44)$$

The Lagrangian state-update and stress-update algorithms are *incrementally objective*. For the spatial configuration, an incrementally objective algorithm requires the definition of the Oldroyd rate of the Eulerian tensor field $\mathbf{h} : \tilde{\Omega}_t \rightarrow \mathcal{V}^2$ which is given by the definition of Lie derivative (\mathcal{L}),

$$\mathcal{L}_v\{\mathbf{h}\} : \mathbf{F}^{-T} \dot{\mathbf{H}} \mathbf{F}^{-1} = \dot{\mathbf{h}} + \mathbf{h}\mathbf{l} + \mathbf{l}^T \mathbf{h}, \quad (3.45)$$

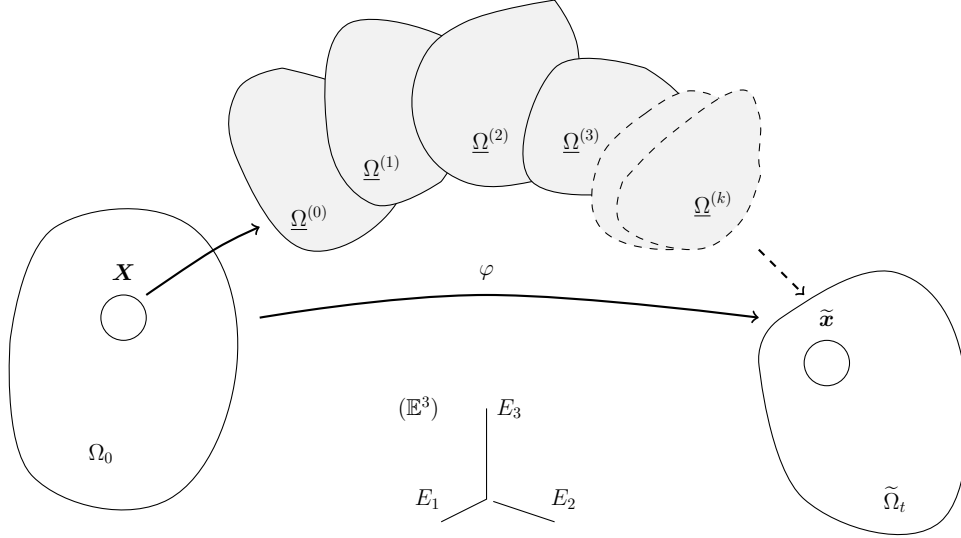


Figure 3.4: Graphical representation of the configuration mapping $\varphi : \Omega_0 \rightarrow \tilde{\Omega}_t$, and the successive intermediate configurations set.

formulated in terms of the spatial velocity gradient $\mathbf{l} = \dot{\mathbf{F}}\mathbf{F}^{-1} = \nabla\mathbf{v}$. Consequently, $\mathcal{L}_v\{\mathbf{h}\} : \mathbf{F}^{-T}\mathbf{H}\mathbf{F}^{-1} = \dot{\mathbf{h}} + \mathbf{h}\dot{\mathbf{F}}\mathbf{F}^{-1} + \mathbf{F}^{-T}\dot{\mathbf{F}}^T\mathbf{h}$. The algorithmic update for \mathbf{h} is given by,

$$\begin{aligned} \mathbf{h}_{n+1} &= \mathbf{F}_{n+1}^{-T} (\mathbf{F}_n^T \mathbf{h}_n \mathbf{F}_n) \mathbf{F}_{n+1}^{-1} \\ &+ \Delta t ((1 - \alpha) \mathbf{F}_{n+1}^{-T} (\mathbf{F}_n^T \mathbf{h}(\mathbf{F}_n, \mathbf{h}_n) \mathbf{F}_n) \mathbf{F}_{n+1}^{-1} \\ &+ \alpha \mathbf{h}(\mathbf{F}_{n+1}, \mathbf{h}_{n+1})), \end{aligned} \quad (3.46)$$

which supplies an objective rate of the internal variable evolution. Then, $\mathbf{h}_{n+1} = \mathbf{h}^{algo}(\mathbf{F}_{n+1}; \{\mathbf{F}_n, \mathbf{h}\})$. Spatial stress-update is calculated in a similar way,

$$\boldsymbol{\sigma}_{n+1} = \hat{\boldsymbol{\sigma}}^{algo}(\mathbf{F}_{n+1}; \{\mathbf{F}_n, \mathbf{h}_n\}) = \hat{\boldsymbol{\sigma}}^{algo}(\mathbf{F}_{n+1}; \hat{\boldsymbol{\sigma}}^{algo}(\mathbf{F}_{n+1}; \{\mathbf{F}_n, \mathbf{h}_n\})). \quad (3.47)$$

It is observable that the rate of change of \mathbf{h} from t_n to t_{n+1} depends on the mapping $\mathbf{F}_{n+1}^{-T} (\mathbf{F}_n^T (\mathcal{Y})_n \mathbf{F}_n) \mathbf{F}_{n+1}^{-1}$ which belongs to the internal variable \mathcal{Y} . This is a semi-implicit mapping in time which gathers information from both previous and current time steps (see Figure 3.4). When the time step is close to zero $\Delta t \approx 0$, then $\mathbf{F}_n \approx \mathbf{F}_{n+1}$, and the successive dynamic steps coincide with the material configuration with a displacement vector close to zero $\mathbf{u} \approx 0$. This assumption is useful for computational evaluation of the balance of momentum via considering $\mathbf{v} \approx 0$ [10, 38], for slowly evolving systems. The algorithmic update is related to the spatial velocity gradient as $(\mathbf{F}_{n+1} - \mathbf{F}_n) = \Delta t \cdot \mathbf{l} = \Delta t \nabla \mathbf{v} \cdot \mathbf{F}_{n+1}$, and spectral decomposition of a

symmetric $\Upsilon = \mathbf{h} : \tilde{\Omega}_t \rightarrow \mathcal{V}^2$ yields,

$$(\mathbf{I} - \Delta t \nabla \mathbf{v})^T \cdot \left(\sum_i \lambda_i^h \mathbf{n}_i^h \otimes \mathbf{n}_i^h \right) \cdot (\mathbf{I} - \Delta t \nabla \mathbf{v}), \quad (3.48)$$

and,

$$\left(\sum_i \lambda_i^h (\mathbf{I} - \Delta t \nabla \mathbf{v})^T \mathbf{n}_i^h \otimes \mathbf{n}_i^h (\mathbf{I} - \Delta t \nabla \mathbf{v}) \right), \quad (3.49)$$

which shows the effect of the time step.

3.3 Mechanical Evolution Laws for the Growth and Remodeling Process

The mathematical investigations of the growing domains have shown that the constitutive evolution equations of a growth process may be classified in one of three main titles. These titles are ([40]) itemized as,

- the tensorial evolution of growth,
- the homeostatic equilibrium of growth,
- the micro-structural evolution of growth.

Constitutive relationships that govern the rate of change in the fabric related tensor quantities are usually thought to be related to the balance laws. The balance of linear momentum has been previously mentioned in equation 3.19 for an existing mass source. When a mass in flux or out flux exists on the boundary layer of the domain, then the linear momentum balance is specified by,

$$\rho_0 \dot{\mathbf{v}} = \nabla_0 (\mathbf{P} - \mathbf{v} \otimes \Gamma_{mass}) + \rho_0 \mathbf{b} + R_0 \mathbf{v} + \dot{\mathbf{F}} \cdot \Gamma_{mass}. \quad (3.50)$$

For slowly evolving quasi-static events, $\dot{\mathbf{v}} = 0$, the linear momentum in reference configuration is the classical equation,

$$\mathbf{0} = \nabla_0 \mathbf{P} + \rho_0 \mathbf{b}, \quad (3.51)$$

which is the usual equation to be solved for the computational growth and remodeling processes. The entropy inequality for the isothermal conditions states that ([41, 38])

$$\rho_0 \mathcal{D} = \mathbf{P} : \dot{\mathbf{F}} - \rho_0 \dot{\Psi} + \mathcal{T} (\nabla_0 \Gamma_\eta - \Gamma_\eta) \geq 0, \quad (3.52)$$

which is the short representation of the Clausius-Duhem inequality in terms of the dissipation functional \mathcal{D} . The relationship between the internal variables and the time rate of the free energy Ψ has been given in equation 3.31. The additional term $r_\eta = (\nabla_0 \Gamma_\eta - R_\eta)$ denotes the external entropy fluxes $\Gamma_\eta = \{\Gamma_\eta^{T_k}\}_k$ and the internal entropy sources (reference) $R_\eta = \{R_\eta^{T_k}\}_k$ as being given similarly in equation 3.26. For the constitutive equations, the Helmholtz free energy can be represented as

$$\Psi(\mathbf{F}, \mathbf{F}_g, \mathbf{H}, \rho_0, \mathcal{T}) = u(\mathbf{F}_e, \mathbf{H}, \rho_0, \eta) - \mathcal{T}\eta, \quad (3.53)$$

which assumes that the fabric structure depends only on the preferred direction, $\mathbf{H} = \mathbf{a} \otimes \mathbf{a}$. For soft tissues, $\dot{\mathcal{T}} \approx 0$ is a typical assumption. The deformation driven dissipation function finally takes the form ([40]),

$$\begin{aligned} \rho_0 \mathcal{D} &= \left[\mathbf{P} - \rho_0 \frac{\partial \Psi}{\partial \mathbf{F}} \right] : \dot{\mathbf{F}} - \rho_0 \frac{\partial \Psi}{\partial \mathbf{F}_g} : \dot{\mathbf{F}}_g \\ &\quad - \rho_0 \frac{\partial \Psi}{\partial \mathbf{H}} : \dot{\mathbf{H}} \\ &\quad - \rho_0 \frac{\partial \Psi}{\partial \rho_0} (\nabla_0 \cdot \Gamma_{mass} - R_{mass}) + \mathcal{T} (\nabla_0 \Gamma_\eta - R_\eta) \geq 0. \end{aligned} \quad (3.54)$$

3.3.1 Evolution of growth and structural tensor

A focus on the growth tensor \mathbf{F}_g in equation 3.54 interprets that,

$$\begin{aligned} \rho_0 \frac{\partial \Psi}{\partial \mathbf{F}_g} : \dot{\mathbf{F}}_g &= - \left(\rho_0 \frac{\partial \Psi}{\partial \mathbf{F}_g} \cdot \dot{\mathbf{F}}_g^T \right) : \left(\dot{\mathbf{F}}_g \cdot \mathbf{F}_g^{-1} \right), \\ &= - \left(\mathbf{P}_e : \frac{\partial \mathbf{F}_e}{\partial \mathbf{F}_g} \cdot \mathbf{F}_g^T \right) : \mathbf{L}_g, \\ &= \left(\mathbf{F}_e^T \cdot \mathbf{P}_e \right) : \mathbf{L}_g = \mathbf{M}_e : \mathbf{L}_g, \end{aligned} \quad (3.55)$$

where \mathbf{M}_e is the elastic Mandel stress and \mathbf{P}_e is the pull back of the first Piola-Kirchhoff stress in to the intermediate configuration $\underline{\Omega}$. As a result, the evolution of the growth tensor is considered to be a function of the elastic Mandel stress, and the relationship between the conjugates can be represented as $\left(\partial_{\mathbf{F}_g} \Psi(\mathbf{F}, \mathbf{F}_g, \mathbf{H}, \rho_0, \mathcal{T}), \dot{\mathbf{F}}_g \right) \Leftrightarrow (\mathbf{M}_e, \mathbf{L}_g)$. This approach is based on pure thermodynamic concerns. Thus, modified functional assumptions can be made for the determiner variables of the velocity gradient in $\underline{\Omega}$ and for other growth magnitudes, such that, $\mathbf{L}_g = \mathbf{L}_g(\mathbf{F}, \mathbf{F}_g, \mathbf{H}, \rho_0, \mathcal{T})$ instead of $\mathbf{L}_g = \mathbf{L}_g(\mathbf{M}_e, \mathbf{H}, \rho_0, \mathcal{T})$.

Evolution of the structural tensors can be analyzed by a similar logic. The conjugate analysis of the second law gives the conjugate pair $\left(-\rho_0 \partial_{\mathbf{H}} \Psi, \dot{\mathbf{H}} \right)$ for the term

$-\rho_0 \frac{\partial \Psi}{\partial \mathbf{H}} : \dot{\mathbf{H}}$. Then, due to the thermodynamic restrictions of the second law, the evolution law of a structural tensor \mathbf{H} can given by

$$\dot{\mathbf{H}} = \dot{\mathbf{H}}(-\rho_0 \partial_{\mathbf{H}} \Psi, \mathbf{H}, \rho_0, \mathcal{T}), \quad (3.56)$$

where $-\rho_0 \partial_{\mathbf{H}} \Psi$ is the thermodynamic conjugate term for the evolution of \mathbf{H} in the second law. This form is suitable for a stress dependent evolution law since the value of $\partial_{\mathbf{H}} \Psi$ may be altered even if the configuration's geometry is fixed in time. Similarly, for a strain dependent law,

$$\dot{\mathbf{H}} = \dot{\mathbf{H}}(\mathbf{F}, \mathbf{F}_g, \mathbf{H}, \rho_0, \mathcal{T}). \quad (3.57)$$

The tensorial evolution laws are driven by purely mathematical restrictions. Soft tissues exhibit a large number of chemical interactions that appear in short time intervals. Thus, the effects of these interactions inevitably possess additional weights on the terms of the evolution equations, at least in a statistical sense. The statistical averaging is usually referred as a homogenization scheme, which is applied to reduce the complexity of the biomechanical problem. Consequently, the proposals made for the tensor evolution laws based on the thermodynamic conjugates are in fact abstract idealizations of the underlying complex processes. However, at least, it is supposed to be useful to determine the core functional forms of the law. *Homeostatic equilibrium* is the most accepted phenomena in the biomechanics community where it is believed that the tissue evolution serves for the governing of the internal fabric evolution towards an optimal equilibrium point in order to reduce the effects of the excessive internal mechanical loads. A technical description of the equilibrium has been proposed by Stephen Cowin ([42]), such that, the homeostatic equilibrium is described by the coaxiality of the symmetric stress tensor \mathbf{S} and the fabric tensor \mathbf{H} . In the coaxial case,

$$\mathbf{H} \cdot \mathbf{S} = \mathbf{S} \cdot \mathbf{H}, \quad (3.58)$$

where the eigenvectors of the multiplications in both sides coincide for the homeostatic equilibrium condition, $\mathbf{n}_i^{H \cdot S} = \mathbf{n}_i^{S \cdot H}$.

In addition to these, the existence and uniqueness of the solution of the evolution is another concept that is related to the homeostatic conditions. It is observable that similar mechanical boundary conditions applied on to the artificial in vitro cell-seeded

gel structures yield close final mechanical magnitudes and fabric orientations. There seems to be a tendency to reach a pre-programmed mechanical equilibrium in living biological tissues. The existence of a unique equilibrium condition is still questionable [42] for some types of tissue. The utilization of the mechanical instability is sometimes useful to obtain the certain morphologies such as wrinkled surfaces of skin or alveolars. On the other hand, the mechanical models using small-strain assumption for the bone remodeling theory have suggested that a large class of the strain based remodeling events is expected to have unique solutions, and the homeostatic equilibrium seems to be a desired property for the mathematical investigations. Some theoretical discussions have recently begun to seek for the reason of the mechanical equilibrium for the structural tensors, in order to enlighten the concept of homeostatic optimality conditions for a fabric evolution (see [43]).

3.3.2 Micro-Structural evolution of the growth and remodeling processes and its relationship with governing constitutive equations

The focus of this section is based on the analysis of the micro-structural evolution of biological tissues. Here, we define the structural evolution as the time evolution of a fabric tensor \mathbf{H} that approaches to a homeostatic equilibrium labeled by the tensor \mathbf{H}^* . The fabric tensor is usually characterized by a characteristic direction vector \mathbf{a} defining the anisotropy, such that, $\mathbf{H} = \mathbf{a} \otimes \mathbf{a}$. In this section, first, an isotropic mass growth is analyzed. Then, secondly, the formulations of an anisotropic mass growth in the direction of preferred vector are detailed. In equation 3.53, a free energy definition has been given by $\Psi(\mathbf{F}, \mathbf{F}_g, \mathbf{H}, \rho_0, \mathcal{T})$ which is equivalent to $\underline{\Psi}(\mathbf{F}_e, \underline{\mathbf{H}}, \rho_0, \mathcal{T})$, where $\underline{\mathbf{H}} = \underline{\mathbf{a}} \otimes \underline{\mathbf{a}}$ defines the anisotropy in the intermediate configuration. Then, Piola stress is

$$\mathbf{P} = \mathbf{P}_e \cdot \mathbf{F}_g^{-1}, \quad (3.59)$$

$$\mathbf{P}_e = 2\rho_0 \mathbf{F}_e \sum_{k=1}^7 \frac{\partial \underline{\Psi}(\mathcal{I}_k^{\mathbf{C}_e}, \mathcal{I}_{1,2,3}^{\underline{\mathbf{H}}}, \rho_0, \mathcal{T})}{\partial \mathcal{I}_k^{\mathbf{C}_e}} \cdot \frac{\partial \mathcal{I}_k^{\mathbf{C}_e}}{\partial \mathbf{C}_e}, \quad (3.60)$$

with $\mathbf{C}_e = \mathbf{F}_e^T \mathbf{F}_e$ and $\underline{\mathbf{H}} = \mathbf{F}_g^T \cdot \mathbf{H} \cdot \mathbf{F}_g$ is the push forward on $\Omega_0 \rightarrow \underline{\Omega}$.

The set of strain invariants \mathcal{I}_k in equation 3.60 is given as,

$$\begin{aligned}
\mathcal{I}_i^{C_e} &= \text{tr}(\mathbf{C}_e^i) & i &= 1, 2, 3 \\
\mathcal{I}_4^{C_e} &= \text{tr}(\mathbf{C}_e \cdot \underline{\mathbf{H}}) & \mathcal{I}_5^{C_e} &= \text{tr}(\mathbf{C}_e^2 \cdot \underline{\mathbf{H}}) \\
\mathcal{I}_6^{C_e} &= \text{tr}(\mathbf{C}_e \cdot \underline{\mathbf{H}}^2) & \mathcal{I}_7^{C_e} &= \text{tr}(\mathbf{C}_e^2 \cdot \underline{\mathbf{H}}^2) \\
\mathcal{I}_j^{\underline{\mathbf{H}}} &= \text{tr}(\underline{\mathbf{H}}^j) & j &= 1, 2, 3
\end{aligned} \tag{3.61}$$

which can characterize the anisotropy in a material. For isotropic materials, the strain energy density is an isotropic function of the elastic strain tensor \mathbf{C}_e ,

$$\Psi(\mathbf{C}, \mathbf{C}_g, \rho_0, \mathcal{T}) = \underline{\Psi}(\mathbf{C}_e, \rho_0, \mathcal{T}) = \underline{\Psi}(\mathcal{I}_{1,2,3}^{C_e}, \rho_0, \mathcal{T}). \tag{3.62}$$

The principal invariants $\mathcal{I}_i^{C_e}$ are expanded as ($\mathbf{C}_e = \mathbf{F}_e^T \mathbf{F}_e$),

$$\mathcal{I}_1^{C_e} = \text{tr}(\mathbf{C}_e), \quad \mathcal{I}_2^{C_e} = \frac{1}{2} (\text{tr}(\mathbf{C}_e^2) - (\text{tr}(\mathbf{C}_e))^2), \quad \mathcal{I}_3^{C_e} = \det(\mathbf{C}_e) = J_e^2. \tag{3.63}$$

A function \mathcal{G} is said to be isotropic if $\mathcal{G} : \mathcal{V}^2 \rightarrow \mathcal{V}^2$ is,

$$\mathbf{Q} \cdot \mathcal{G}(\mathbf{C}) \cdot \mathbf{Q}^T = \mathcal{G}(\mathbf{Q} \cdot \mathbf{C} \cdot \mathbf{Q}^T), \tag{3.64}$$

for all $\forall \mathbf{A} \in \mathcal{V}^2$ and for all norm preserving rotation tensors \mathbf{Q} belonging to a rotation group labeled by $\mathbf{Q} \in SO(\dim(\mathbf{Q}))$. If $\mathcal{G} : \mathcal{V}^2 \rightarrow \mathcal{V}^2$ maps symmetric tensors to the symmetric ones, then there exists functions $c_k : \mathfrak{R} \rightarrow \mathfrak{R}$,

$$\mathcal{G}(\mathbf{C}) = c_0(\mathcal{I}^C) \mathbf{I} + c_1(\mathcal{I}^C) \mathbf{C} + c_2(\mathcal{I}^C) \mathbf{C}^2. \tag{3.65}$$

For the isotropic mass growth, a simple assumption can be made for the functional form of the growth deformation gradient as,

$$\mathbf{F}_g = \nu_g \mathbf{I}, \tag{3.66}$$

where ν_g is the isotropic growth parameter. Additionally, ν_g is the isotropic permanent stretch ratio which defines the growth Jacobian of the volumetric mass growth, such that $J_g = (\nu_g)^3$. The velocity gradient \mathbf{L}_g is given by,

$$\mathbf{L}_g = \dot{\mathbf{F}}_g \mathbf{F}_g^{-1} = \frac{\dot{\nu}_g}{\nu_g} \mathbf{I}. \tag{3.67}$$

The association of \mathbf{L}_g with the Mandel stress in the form of $\mathbf{M}_e : \mathbf{L}_g$ gives the evolution laws of the isotropic growth based on thermodynamic conjugates

$$\mathbf{M}_e : \mathbf{L}_g = \frac{\dot{\nu}_g}{\nu_g} \mathcal{I}_1^{M_e}, \quad \mathbf{C}_e : \mathbf{L}_g = \frac{\dot{\nu}_g}{\nu_g} \mathcal{I}_1^{C_e}, \tag{3.68}$$

$$\dot{\nu}_g = \frac{k_{\nu_g}}{\nu_g} \mathcal{I}_1^{M_e}, \quad \dot{\nu}_g = \frac{k_{\nu_g}}{\nu_g} \mathcal{I}_1^{C_e}, \tag{3.69}$$

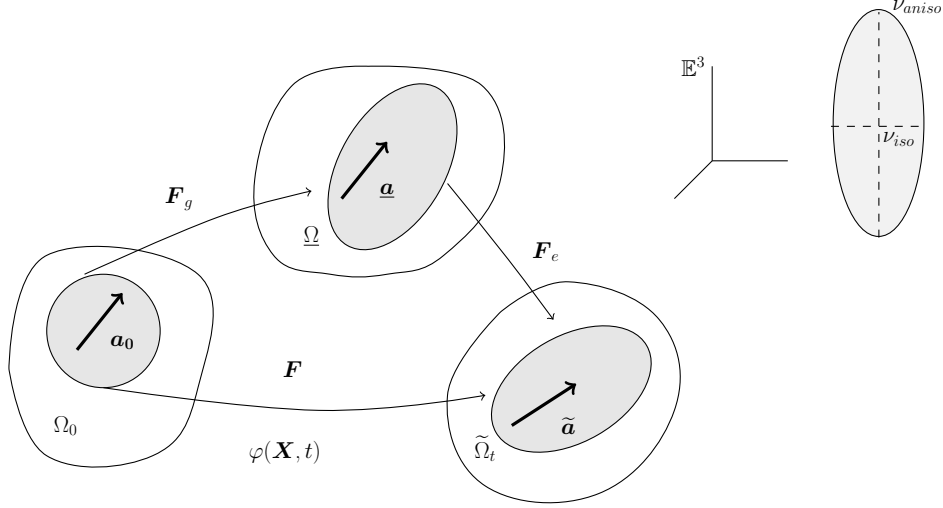


Figure 3.5: A transversely isotropic description of the anisotropic mass growth based on a characteristic direction \mathbf{a} which is mapped between configurations. The anisotropic growth is expressed by two growth parameters which correspond to the evolution of the eigenvalues of an ellipsoid representation of the growth deformation gradient.

where \mathcal{I}_1 is the first invariant of the associated mechanical tensor and k_{ν_g} is a parameter controlling the saturation type convergence towards a maximum or minimum limit ([34, 38]). When both anisotropic and isotropic mass growth occur, the effect of the mass growth in the direction of a micro-structural preferred direction is characterized by an additional parameter (Figure 3.5). When the structural tensor is given by $\mathbf{H} = \mathbf{a} \otimes \mathbf{a}$, the growth deformation gradient tensor is defined in the form of

$$\mathbf{F}_g = \nu_{iso} \mathbf{I} + (\nu_{aniso} - 1) \mathbf{a} \otimes \mathbf{a}, \quad (3.70)$$

for $\|\mathbf{a}\| = 1$. The isotropic growth that appears through every direction is controlled by the parameter ν_{iso} . The isotropic growth is weighted by an additional anisotropic parameter by ν_{aniso} . Since \mathbf{F}_g is symmetric, the rotational part is excluded. If the characteristic direction is preserved during growth, then $\dot{\mathbf{F}}_g = \dot{\nu}_{iso} \mathbf{I} + (\dot{\nu}_{aniso} - 1) \mathbf{a} \otimes \mathbf{a}$. The stress and strain dependent stimuli which are based on the growth velocity gradient are given by,

$$\begin{aligned} \mathbf{M}_e : \mathbf{L}_g &= \dot{\nu}_{iso} \left(\frac{\mathcal{I}_1^{M_e}}{\nu_{iso}} - \frac{\nu_{aniso} - 1}{\nu_{iso} (\nu_{iso} + \nu_{aniso} - 1)} \mathcal{I}_4^{M_e} \right) \\ &+ \dot{\nu}_{aniso} \left(\frac{1}{\nu_{iso} + \nu_{aniso} - 1} \mathcal{I}_4^{M_e} \right), \end{aligned} \quad (3.71)$$

$$\begin{aligned} \mathbf{C}_e : \mathbf{L}_g &= \dot{\nu}_{iso} \left(\frac{\mathcal{I}_1^{C_e}}{\nu_{iso}} - \frac{\nu_{aniso} - 1}{\nu_{iso} (\nu_{iso} + \nu_{aniso} - 1)} \mathcal{I}_4^{C_e} \right) \\ &+ \dot{\nu}_{aniso} \left(\frac{1}{\nu_{iso} + \nu_{aniso} - 1} \mathcal{I}_4^{C_e} \right). \end{aligned} \quad (3.72)$$

For $\nu_{iso} = 1$, a set of unidirectional fiber growth stimuli is obtained,

$$\mathbf{M}_e : \mathbf{L}_g = \dot{\nu}_{aniso} \left(\frac{1}{\nu_{aniso}} \mathcal{I}_4^{\mathbf{M}_e} \right), \quad (3.73)$$

$$\mathbf{C}_e : \mathbf{L}_g = \dot{\nu}_{aniso} \left(\frac{1}{\nu_{aniso}} \mathcal{I}_4^{\mathbf{C}_e} \right). \quad (3.74)$$

For this special case, a fiber elongation accompanying the mass growth is seen. Then, the growth deformation gradient represents a one-dimensional elongation rather than an expanding ellipsoid. These brief evolution forms supply a generally accepted framework for the growing biological domains. In the next section, the growth and remodeling laws intended for the structural tensor will be discussed.

3.4 Current Approaches That Aim to Understand the Evolution of the Structural Tensors in a Growth and Remodeling Process

In a mathematical sense, the evolution of the anisotropic direction \mathbf{a} via rotation is usually treated as a distinct mechanical process of the structural evolution that is separated from the overall growth phenomena. Mechanical growth is a consequence of the density evolution via mass flux or mass source. If $\dot{\rho}_0 \neq 0$, the process is also evaluated as a remodeling one where the fabric may remain unchanged, but the density gradient is time dependent. The preferred direction may evolve into a new state, while the total mass of the system is preserved or not. In this section, we analyze the current advancements in the theoretical modeling of the evolution of structural tensors. Specifically, we focus on the approaches that are related to the statistical nature of the fiber dispersion in a collagen-rich soft tissue. We classify the basic algorithmic methods which describe the evolution law of the statistical parameters. At the end of the section, we propose a new theoretical approach and position it among other previously proposed approaches. We discuss how the proposal fills the theoretical needs in order to supply a new framework for the biomechanical modeling demands.

Due to the widespread concepts in growth and remodeling theories we limit the discussion with the mathematical evolution forms, in special, the forms of the time rate of structural tensors. We define the structural tensor as a material description in the micro-scale (μm) environment where the internal web of the preferred structural directions is embedded into the set of these tensors. Structural tensors describe the

anisotropic behavior of the material domain in addition to the isotropic components of the media which are defined by an additive decomposition of the SED function.

A non-complex representation of the structural tensor is the outer product of the preferred directions in the material space $\mathbf{H} = \mathbf{a}_0 \otimes \mathbf{a}_0$. Then, the evolution of \mathbf{H} strictly depends on the evolution of \mathbf{a}_0 . For a unit vector $\mathbf{n}_0 = \mathbf{a}_0 / \|\mathbf{a}_0\|$, the rotation of \mathbf{n}_0 is realized by an orthogonal rotation matrix \mathbf{Q} as,

$$\tilde{\mathbf{n}}_t = \mathbf{Q} \cdot \mathbf{n}_0, \quad (3.75)$$

which preserves unity. The time rate of \mathbf{n} is expressed by,

$$\dot{\tilde{\mathbf{n}}}_t = \dot{\mathbf{Q}} \cdot \mathbf{n}_0, \quad (3.76)$$

where \mathbf{n}_0 is fixed in Ω_0 and $\tilde{\mathbf{n}}_t$ is a vector in $\tilde{\Omega}_t$ configuration. Since \mathbf{Q} is a norm preserving matrix, its polar decomposition yields only a rotational component whereas its derivative yields the rate of the rotation (spin tensor) part,

$$\dot{\tilde{\mathbf{n}}}_t = \dot{\mathbf{Q}} \cdot \mathbf{n}_0 \Rightarrow \boldsymbol{\omega}^{\tilde{\mathbf{n}}_t} \times \tilde{\mathbf{n}}_t. \quad (3.77)$$

The rate of a spatial unit vector depends on the selection of an axis of rotation $\boldsymbol{\omega}^{\tilde{\mathbf{n}}_t}$ vector. The target direction of the rotation, which is called as stimulus, can be assumed to depend on the strain or stress tensors,

$$\boldsymbol{\omega}^{\tilde{\mathbf{n}}_t} = \frac{1}{\tau_c} \tilde{\mathbf{n}}_t \otimes \mathbf{n}_{max}^{M_e}, \quad \boldsymbol{\omega}^{\tilde{\mathbf{n}}_t} = \frac{1}{\tau_c} \tilde{\mathbf{n}}_t \otimes \mathbf{n}_{max}^{C_e}, \quad (3.78)$$

$$\mathbf{M}_e = \sum_i^{n_{dim}} \lambda_i^{M_e} \mathbf{n}_i^{M_e} \otimes \mathbf{n}_i^{M_e}, \quad \mathbf{C}_e = \sum_i^{n_{dim}} \lambda_i^{C_e} \mathbf{n}_i^{C_e} \otimes \mathbf{n}_i^{C_e}, \quad (3.79)$$

where τ_c is the characteristic remodeling time, and $\mathbf{n}_{max}^{(\cdot)}$ is one of the principal directions associated with the maximum principal value of (\cdot) tensor. The evolution of rotation is given by,

$$\dot{\tilde{\mathbf{n}}}_t = \frac{1}{\tau_c} (\mathbf{I} - \tilde{\mathbf{n}}_t \otimes \tilde{\mathbf{n}}_t) \cdot \mathbf{n}_{max}^{M_e}, \quad \dot{\tilde{\mathbf{n}}}_t = \frac{1}{\tau_c} (\mathbf{I} - \tilde{\mathbf{n}}_t \otimes \tilde{\mathbf{n}}_t) \cdot \mathbf{n}_{max}^{C_e}. \quad (3.80)$$

If we consider the case in equation 3.70 with $\mathbf{n}_{max}^{C_e}$ being the stimulus, the time evolution of growth deformation tensor with respect to Ω_0 is,

$$\dot{\mathbf{F}}_g = \dot{\nu}_{iso} \mathbf{I} + \dot{\nu}_{aniso} (\tilde{\mathbf{n}}_t \otimes \tilde{\mathbf{n}}_t) + \nu_{aniso} (\dot{\tilde{\mathbf{n}}}_t \otimes \tilde{\mathbf{n}}_t + \tilde{\mathbf{n}}_t \otimes \dot{\tilde{\mathbf{n}}}_t), \quad (3.81)$$

$$\begin{aligned} \dot{\mathbf{F}}_g &= \dot{\nu}_{iso} \mathbf{I} + \dot{\nu}_{aniso} (\tilde{\mathbf{n}}_t \otimes \tilde{\mathbf{n}}_t) + \frac{\nu_{aniso}}{\tau_c} \\ &\times ((\mathbf{I} - \tilde{\mathbf{n}}_t \otimes \tilde{\mathbf{n}}_t) \cdot \mathbf{n}_{max}^{C_e} \otimes \tilde{\mathbf{n}}_t + \tilde{\mathbf{n}}_t \otimes (\mathbf{I} - \tilde{\mathbf{n}}_t \otimes \tilde{\mathbf{n}}_t) \cdot \mathbf{n}_{max}^{C_e}). \end{aligned} \quad (3.82)$$

It is clear that the additional anisotropic contribution comes from the evolution of rotation. Consequently, the rotation of a micro-structural direction effects the rate of change in the permanent growth-strain \mathbf{E}_g . The information which can be related to the speed of fabric rotation is inevitably stored in the intermediate configuration temporarily. That speed is controlled by the angular distance between $\angle(\mathbf{n}_{max}^{C_e}, \tilde{\mathbf{n}}_t)$ and its effect on \mathbf{F}_g is weighted by ν_{aniso}/τ_c . During the growth process, due to the irreversible bio-mechanochemical interactions between the growth deformation gradient and the deposition or degradation rate of the local proteins, the temporal information has the potential to be stored permanently on the whole remodeling system.

3.4.1 The time-dependent fiber reorientation approach based on the mechanically motivated vector differential equations

Time dependent fiber reorientation is assumed to be a rotation of the fabric related vectors towards the biological stimulus. The rotation process is completed by reaching a homeostatic equilibrium condition. The rotation phenomena is not restricted with the biological domains and it may be observed in the cases of liquid crystal formation as well as the polarization of piezoceramic materials. For a deformation $\varphi : \Omega_0 \rightarrow \tilde{\Omega}_t$, the spatial coordinates of a particle is defined by $\mathbf{x} = \varphi(\mathbf{X}, t)$. In a hyper-elastic transversely isotropic domain, the structural tensor, which is defined by $\mathbf{H} = \mathbf{a}_0 \otimes \mathbf{a}_0$, $\|\mathbf{a}_0\| = 1$ in Ω_0 , is associated with the fabric direction \mathbf{a}_0 . If the mass is preserved during the remodeling, the free energy is described by $\Psi(\mathbf{C}, \mathbf{H}) = \Psi(\mathbf{Q}\mathbf{C}\mathbf{Q}^T, \mathbf{Q}\mathbf{H}\mathbf{Q}^T)$, $\forall \mathbf{Q} = SO(\dim(\mathbf{Q}))$. The symmetry group is defined by the tensor valued set $\mathcal{G} = \{\mathbf{Q} \in SO(\dim(\mathbf{Q})) | \mathbf{Q}\mathbf{A}\mathbf{Q}^T = \mathbf{A}\}$. The transversely isotropic description of the SED function based on the strain invariants can be described by $\Psi(\mathbf{C}, \mathbf{H}) = \Psi(\mathcal{I}_{1,\dots,5}^C)$. The Clasius-Duhem inequality states that [44],

$$\mathcal{D}_0 = \frac{1}{2} \mathbf{S} : \dot{\mathbf{C}} - \dot{\Psi}(\mathbf{C}, \mathbf{H}) - \mathcal{T}(\nabla_0 \Gamma_\eta - R_\eta) \geq 0, \quad (3.83)$$

$$\mathbf{S} = 2 \frac{\partial \Psi}{\partial \mathbf{C}}. \quad (3.84)$$

where \mathbf{S} is the second Piola-Kirchhoff stress tensor. During the reorientation of the fiber fabric while keeping the term $\nabla_0 \Gamma_\eta - R_\eta \approx 0$, the second law may be violated. Thus, an additional entropy flux and entropy source term that is related to the biological

domain is conceptually utilized, in order to enforce the second law being inherently satisfied. In fact, the physical limitations and characterization of the external entropy source term seems to be an important part of the evolving biological domains. This concept may be linked intuitively to the irreversibility of the growth and remodeling processes, where it is definitely known that “*an arrow of time*” is present.

The evolution form derived in [44] depends mostly on kinematic quantities making this approach widely applicable. For a rigid body motion $\mathbf{x}(\mathbf{X}, t) = \mathbf{c}(t) + \mathbf{R}(t) \cdot \mathbf{X}(t)$ the spatial velocity gradient has the decomposition $\mathbf{l} = \mathbf{d} + \mathbf{w}$. Then, there is a norm preserving rotation of the fiber with additional properties of $\mathbf{d} = 0$ and $\mathbf{w} = \dot{\mathbf{R}}\mathbf{R}^T$, \mathbf{R} being an orthogonal rotation tensor. The variation of a spatial line element with respect to itself describes the rotation

$$d\dot{\mathbf{x}} = \frac{\partial \dot{\mathbf{x}}}{\partial \mathbf{x}} \cdot d\mathbf{x} = \nabla_0 \mathbf{v} \cdot d\mathbf{x} = \dot{\mathbf{F}} \cdot \mathbf{F}^{-1} \cdot d\mathbf{x}. \quad (3.85)$$

Thus, $d\dot{\mathbf{x}} = \mathbf{w} \cdot d\mathbf{x} = \boldsymbol{\omega}^{dx} \times d\mathbf{x}$, since \mathbf{w} is skew-symmetric. The time evolution of a unit fiber vector (defines the fabric) is

$$\frac{\partial}{\partial t} (\mathbf{a}_0 \cdot \mathbf{a}_0) = 0 \quad \Rightarrow \quad \dot{\mathbf{a}}_0 \cdot \mathbf{a}_0 = 0, \quad (3.86)$$

which states that the time rate of the fiber orientation is perpendicular to the fiber direction itself. Then the evolution of a fiber direction is,

$$\dot{\mathbf{a}}_0 = \boldsymbol{\omega}^{a_0} \times \mathbf{a}_0, \quad (3.87)$$

where the superscript in $\boldsymbol{\omega}^{a_0}$ states that the axis of the rotation is determined perpendicular to \mathbf{a}_0 . The axis direction can be linked to the strain based mechanical stimulus,

$$\boldsymbol{\omega}^{a_0} = \frac{\pi}{2\tau_c} \mathbf{a}_0 \times \mathbf{n}_{max}^C. \quad (3.88)$$

Finally, the rotation of a fiber direction vector is given by,

$$\dot{\mathbf{a}}_0 = \frac{\pi}{2\tau_c} (\mathbf{I} - \mathbf{a}_0 \otimes \mathbf{a}_0) \cdot \mathbf{n}_{max}^C. \quad (3.89)$$

It should be noted that the direction \mathbf{a}_0 is defined with respect to the material configuration. Then, the time evolution is a permanent update procedure for the remodeling of the structural tensor. This approach is a basic description for the vector-valued differential equation that governs the evolution of a single fiber direction.

The tensor-based finite element derivations are straight forward since it is formulated in the vector form. A disadvantage of the approach is the existence of a singular point near $\mathbf{a}_0 \cdot \mathbf{n}_{max}^C = 0$. Although the time evolution is inherently nonlinear, this approach does not reflect the effect of the stimulus magnitude on the time evolution pattern.

3.4.2 Remodeling of the fiber directions via the evolution of angular parameters

According to the basic deterministic model described by Driessen et.al. in [45], N_f number of fiber families associated with a frequency distribution for each one can be represented by a single structural fibre reorientation tensor \mathbf{H}_0 . In the undeformed initial configuration it is defined by,

$$\mathbf{H}_0 = \sum_{i=1}^{N_f} \text{Pr}(i) (\mathbf{a}_0^i \otimes \mathbf{a}_0^i), \quad (3.90)$$

where Pr is a probability density distribution and $\text{Pr}(i)$ stands for the partitioned observation probability associated with the direction i . Then, the sum of the partitions yield $\sum_{i=1}^{N_f} \text{Pr}(i) = 1$. This approach is supposed to be the first model which describes a distinct evolution equation for each fiber direction. The time evolution of \mathbf{H}_0 in the spatial configuration is given by,

$$\overset{\nabla}{\widetilde{\mathbf{H}}} + 2 \left(\mathbf{l} : \widetilde{\mathbf{H}} \right) \cdot \widetilde{\mathbf{H}} = 0, \quad (3.91)$$

where $\overset{\nabla}{(\bullet)}$ is the objective Truesdell derivative of the spatial (\bullet) tensor. The objective evolution with respect to the spatial configuration is defined by $\overset{\nabla}{\widetilde{\mathbf{H}}} = \overset{\cdot}{\widetilde{\mathbf{H}}} - \mathbf{l} \cdot \widetilde{\mathbf{H}} - \widetilde{\mathbf{H}} \cdot \mathbf{l}^T$. \mathbf{l} is the spatial velocity gradient and $\overset{\cdot}{\widetilde{\mathbf{H}}}$ stands for the ordinary material derivative. $\widetilde{\mathbf{H}}$ is the spatial mapping of the material \mathbf{H}_0 defined by the push-forward operation,

$$\widetilde{\mathbf{H}} = \frac{\mathbf{F} \mathbf{H}_0 \mathbf{F}^T}{\Lambda_f^2}. \quad (3.92)$$

The normalization is supplied by Λ_f^2 which is the sum of square fiber stretches $\Lambda_f^2 = \sum_{i=1}^{N_f} \lambda_i^2 = \text{tr}(\mathbf{F} \mathbf{H}_0 \mathbf{F}^T)$. The fiber stretch is defined as $\lambda_i^2 \widetilde{\mathbf{a}}^i = \mathbf{F} \cdot \mathbf{a}_0^i$, for $\|\widetilde{\mathbf{a}}^i\| = 1$. The normalization division is applied in order to eliminate any initial fictitious strains. The fibre evolution is extended to include an internal governing stimuli by adding the term,

$$\overset{\nabla}{\widetilde{\mathbf{H}}} + 2 \left(\mathbf{l} : \widetilde{\mathbf{H}} \right) \cdot \widetilde{\mathbf{H}} = \frac{1}{\tau_c} \left(\widetilde{\mathbf{H}}^* - \widetilde{\mathbf{H}} \right). \quad (3.93)$$

where $\widetilde{\mathbf{H}}^*$ is a spatial stimulus tensor. In quasi-static deformations ($\mathbf{L} = 0$), equation 3.93 reduces to a first order rate equation,

$$\dot{\widetilde{\mathbf{H}}} = \frac{1}{\tau} \left(\widetilde{\mathbf{H}}^* - \widetilde{\mathbf{H}} \right). \quad (3.94)$$

Based on the objectivity principle, the spatial target tensor $\widetilde{\mathbf{H}}^*$ is assumed to be a function of the fiber strain \mathbf{b} . Then, the anisotropy of the tissue is expected to develop from the macroscopic kinematic quantities,

$$\widetilde{\mathbf{H}}^* = \frac{\mathbf{b}^v}{\text{tr}(\mathbf{b}^v)}, \quad (3.95)$$

with the constant parameter v . The reorientation of the fiber vectors can be represented by the evolution of the angle between stimulus direction and the vector itself, $\theta_i \angle (\mathbf{a}_0^i, \mathbf{n}_{max}^C)$. The differential change in $\theta < \pi/2$ for the i^{th} fiber family is,

$$\frac{d\theta_i}{dt} = \frac{1}{\tau_c} (1 - \cos(\theta_i)). \quad (3.96)$$

The update of the the new orientation can be obtained by an explicit or implicit scheme, as $\theta_i = \theta_i + d\theta_i$.

3.4.3 Fiber remodeling approaches based on n -chain networks

The collagen fiber remodeling approaches based on n -chain networks have been summarized in [28]. This remodeling framework differs from the previously mentioned existing approaches since its mechanism is based on the developments of the long-chain polymer physics whose background goes back to 1940's. Living tissue is a chemically active environment supported by a complex structural hierarchy. For biological structures, the main structural blocks are made of various long-chain polymers which support the mechanical load bearing of the macroscopic organism. One example for the polymer based structural material is the extra cellular-matrix (ECM) environment that constructs an intermediate media for the flow of intra-cellular information. ECM plays role in the physical synthesis and remodeling of the additional structures. Before proceeding to the model, a brief explanation of the relationship between the Neo-Hookean free energy and ECM is presented.

Living organisms are carbon-based beings. Carbon is the fourth most abundant element on earth. Carbon can form a covalent bond with other carbon atoms to

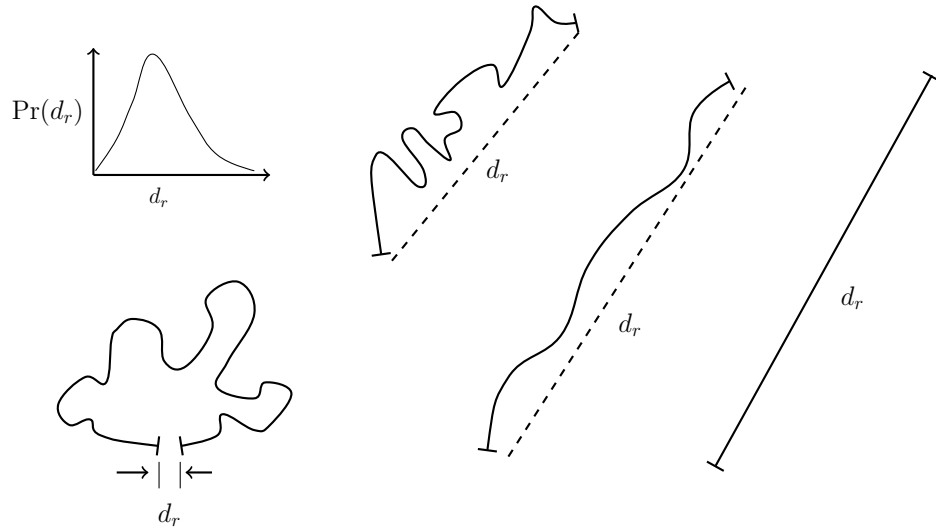


Figure 3.6: The molecular conformations and corresponding end-to-end distance d_r . The distance d_r is a direct indicator for the probability of a geometric conformation. The molecules are represented by flexible lines.

construct macro-molecular chains consisting of thousands of atoms. Collagen-I is a typical example for this. In biological systems, the variety of the complexity and the geometrical formation of the carbon-based long-chain polymers increase. As being the basis for the structural integrity, the organic polymer compounds increase the stiffness of the extracellular matrix making the concept crucial for fiber remodeling approaches. In the ECM, the long polymer chains may be cross-linked to produce advanced chain structures with the desired mechanical properties, such as the tropocollagen. The fiber reinforced continuum can be imagined to include long macro-molecules that occupy a certain geometric characteristic (conformation) in the material configuration space. The geometrical conformations of the molecules can be analytically investigated by assigning them in to specific categories. The categories are labeled as the n -chain networks where n represents the number corresponding to a specific geometric type of the individual structural elements integrating the network. Long polymer chains with n_c distinct independent parts with length l_c is characterized by the so-called end-to-end distance (d_r) between the two tie points of the polymer (Figure 3.6). Here, for the simplification of the discussion, it is assumed that the molecule does not exhibit any branching and it can be represented by a flexible line element. Then the total length of the chain is $L_c = n_c l_c$.

The distance d_r is an indicator for the number of geometric possibilities of the full chain. For $d_r = L_c$ there is only one molecular conformation as the straight line

element. The mean square value $\overline{d_r^2}$ for a Gaussian chain with n freely moving joints is given by, ($r \ll L$),

$$\overline{d_r^2} = n_c l_c^2. \quad (3.97)$$

The probability of a conformation which has an end-to-end distance d_r is given by [32],

$$\text{Pr}(d_r) d d_r = \left(4 \frac{b^3}{\pi^{\frac{3}{2}}}\right) d_r^2 \exp(-b^2 d_r^2) d d_r, \quad (3.98)$$

which is of Gaussian type. Probability of a thermodynamic state of a single chain conformation can be calculated by the Boltzmann's equation,

$$\eta_i = a + k_B \ln(\text{Pr}(d_r)), \quad (3.99)$$

for a constant a and the Boltzmann constant $k_B = 1.38 \times 10^{-23} \text{Nm/K}$. Then, the entropy of a single chain is obtained as,

$$\eta_i = c - k_B b^2 d_r^2, \quad (3.100)$$

for $c = a + k_B \ln(b^3/\pi^{\frac{3}{2}})$. Here b is a parameter which is related to the end-to-end distances as $b^2 = 3 / \left(2 \overline{d_{r-out}^2}\right)$ and $\overline{d_{r-out}^2}$ is the mean square value of the conformations that includes the un-cross-linked free chains out of the network. When the chain is deformed from one state to another, i.e the material is stretched or compressed, the number of microscopic probable states (entropy by conformations) the molecules geometrically occupy inevitably change. A simple stretching can be defined by the affine mapping $x_i = \lambda_i X_i$ from the undeformed ($\mathbf{X} = X_i$) to the deformed configuration ($\mathbf{x} = x_i$). If one tip of the chain is fixed at $\mathbf{X}' = \mathbf{0}$, then the other end moves from \mathbf{X} to \mathbf{x} . The difference in entropy with the change in d_r is given by,

$$\Delta \eta_i = \sum_j^{n_{\text{dim}}} -k_B b^2 ((\lambda_j^2 - 1) X_j^2), \quad (3.101)$$

with $\prod_i \lambda_i = 1$ satisfying incompressibility. The extension is applied to all N_c number of macro-molecular chains in a molecular network. Then, from the summation of the entropies, $\Delta \eta = \sum_i^{N_c} \Delta \eta_i$ is,

$$\begin{aligned} \Delta \eta &= -k_B b^2 [(\lambda_1^2 - 1) \sum_i X_{i,1}^2 \\ &+ (\lambda_2^2 - 1) \sum_i X_{i,2}^2 + (\lambda_3^2 - 1) \sum_i X_{i,3}^2], \end{aligned} \quad (3.102)$$

for subscript $X_{i,j}$ stands for the j^{th} end tip coordinate element of the i^{th} chain. If the material has no preferred direction within the fabric structure, it acts as an isotropic one. Thus, $\sum_i X_{i,1} = \sum_i X_{i,2} = \sum_i X_{i,3}$ under the assumption that the molecular configurations are all randomly oriented. Then, $\sum_{i=1}^{N_c} X_{i,1}^2 = \overline{d_{r-in}^2}/3$ is defined where $\overline{d_{r-in}^2}$ is the average over cross-linked chains at the beginning of the deformation. Finally,

$$\Delta\eta = -\frac{1}{2}N_c k_B \frac{\overline{d_{r-out}^2}}{\overline{d_{r-in}^2}} (\lambda_1^2 + \lambda_2^2 + \lambda_3^2 - 3) . \quad (3.103)$$

The change in Helmholtz free energy Ψ_H is,

$$\Psi_H = u - \eta\mathcal{T} , \quad (3.104)$$

$$\Delta\Psi_H = \Delta u - \Delta\eta\mathcal{T} , \quad (3.105)$$

$$\Psi_H = \frac{1}{2}N_c k_B \frac{\overline{d_{r-out}^2}}{\overline{d_{r-in}^2}} (\lambda_1^2 + \lambda_2^2 + \lambda_3^2 - 3) , \quad (3.106)$$

which defines a material property where long polymer elongations in the material space are randomly oriented. Such material can be described by an incompressible Neo-Hookean material with the shear modulus μ_c for the complete chain network,

$$\Psi = \mu_c (\lambda_1^2 + \lambda_2^2 + \lambda_3^2 - 3) , \quad (3.107)$$

and the Cauchy stress for the isotropic model is,

$$\boldsymbol{\sigma} = -p_h \mathbf{I} + \mu_c \mathbf{F} \mathbf{F}^T , \quad (3.108)$$

for an unknown hydrostatic pressure p_h . Since ECM matrix is mostly proteoglycan based and has isotropic material properties, it is common to approximate its behavior by a Neo-Hookean material model. For non-Gaussian freely joint cases with finite extensions, the formulations are altered greatly. This concept, which is supposed to be crucial for highly sensitive industrial applications, is out of the scope of our discussions on biological structures.

The evolution of the structural peculiarities is based on the remodeling of the long chain polymer elements. The rotation based chain remodeling is a common example that the free energy depends on the alteration in the geometric conformations. In order to give an ordered framework for the geometric behavior, Arruda-Boyce 8-chain model can be utilized for the free energy definitions. An 8-chain model is a wormlike-chain approach where the chain may bend under thermal fluctuations. The

theoretical wormlike-chain model has been discussed in [28]. The model is separated in to three different length-scales. The smallest scale for the collagen remodeling algorithm is the molecular level of collagen. The free energy Ψ_{chain} of a single collagen fiber is given by,

$$\Psi_{chain} = \Psi_{0,chain} + k_B \mathcal{T} \left(\frac{L_f}{4A} \right) \left(2 \frac{d_r}{L_f^2} + \frac{1}{1 - \frac{d_r}{L_f}} - \frac{d_r}{L_f} \right), \quad (3.109)$$

where $\Psi_{0,chain}$ shows the initial unperturbed energy level of the chain, d_r is the end-to-end distance and L_f is the length of the collagen fiber ($\mathcal{T} = 310$ K). A is the persistence length which is described as the projection of the conformation in the direction of the first bond ($l_f \ll A \ll L_f$). The constant A is an indicator for the bending stiffness.

On the ECM level, the total free energy of the extra cellular media and collagen fiber bundles is given by,

$$\Psi = \Psi_{iso} + \Psi_{chain} + \Psi_{rep}, \quad (3.110)$$

with a repulsive energy contribution Ψ_{rep} . The expansion of the energy contributions is given as,

$$\Psi_{iso} = \frac{1}{2} \lambda_{Lame} \ln(J) + \frac{1}{2} \mu_{Lame} (\mathcal{I}_1^C - n_{dim}) - \mu_{Lame} \ln(J), \quad (3.111)$$

$$\Psi_{chain} = k_B \mathcal{T} n_f L_f \left(2 \frac{d_r}{L_f^2} + \frac{1}{1 - \frac{d_r}{L_f}} - \frac{d_r}{L_f} \right), \quad (3.112)$$

$$\Psi_{rep} = k_B \mathcal{T} \frac{n_f}{4A} \left(\frac{1}{4} + \frac{1}{4d_{0,r} \left(1 - \frac{d_{0,r}}{L_f} \right)} - \frac{1}{4d_{0,r}} \right) \bar{\Psi}_{rep}, \quad (3.113)$$

for the material constants $\lambda_{Lame}, \mu_{Lame}$, initial end-to-end distance $d_{0,r}$, strain invariant $\mathcal{I}_1^C = \mathbf{C} : \mathbf{I}$, $\mathbf{C} = \mathbf{F}^T \mathbf{F}$ and $J = \det(\mathbf{F})$. The total length of a fiber is $L_f = n_f l_f$. It is clear that the model inherently includes the thermoelastic behavior of the chain deformations. $\bar{\Psi}_{rep}$ is defined as the function of the strain nonstandard invariants formulated for the 8-chain deformation elements in order to eliminate the effects of the initial $d_{0,r}$ distances. The Cauchy stress is,

$$\boldsymbol{\sigma} = \boldsymbol{\sigma}_{iso} + \boldsymbol{\sigma}_{chain} + \boldsymbol{\sigma}_{rep}, \quad (3.114)$$

The principal axes of the chain network remodels towards the principal axes of the stress tensor as similarly in the previous remodeling approaches.

3.5 Time Dependent Evolution of the Statistically Dispersed Fiber Directions

In previous subsections, the structural tensor is assumed to be an outer product of a single fiber direction vector. In reality, various kinds of biological materials in the tissue show a high level of dispersion through the tissue volume. The dispersion in the target domain can be characterized by the analytic probability distribution functions. In the following subsections, the free energy approaches that define the mathematical relationship between the statistical dispersion of the fiber directions and their effects on the stresses are briefly summarized.

3.5.1 Evolution of the orientation density distribution of the fiber dispersion

The micro-sphere approach is a homogenization technique where the dispersion of the fiber directions are integrated over the unit sphere to obtain a structural tensor. If the orientation density ρ of the variable \mathcal{Y} between $A, A + dA$ is known, the total orientation density can be obtained by the integration on a unit sphere. In the case of the fiber distributions, the orientation density satisfies $\rho(\mathbf{a}) = \rho(-\mathbf{a}), \forall \mathbf{a} \in \mathbb{S}^2$ and $(4\pi)^{-1} \int_{\mathbb{S}^2} \rho(\mathbf{a}) dA = 1$. The ‘‘average’’ of a direction dependent internal variable \mathcal{Y} over the unit sphere is given by [29],

$$\langle \mathcal{Y} \rangle = \frac{1}{4\pi} \int_{\mathbb{S}^2} \mathcal{Y} dA \approx \sum_{i=1}^{N_w} w_i \mathcal{Y}_i, \quad (3.115)$$

where the integration is applied on the two dimensional surface \mathbb{S}^2 of the sphere. The brackets $\langle \rangle$ define a homogenization operation [27]. w_i are the numerical integration weights corresponding to a finite number of unique directions ($i = \overline{1, N_w}$). A soft tissue reinforced by an anisotropic fiber dispersion that is embedded in an isotropic incompressible media can be defined by its free energy representation,

$$\Psi(\mathbf{C}, \mathbf{a}_0^i) = \Psi_{vol}(J) + \Psi_{iso} + \Psi_{aniso}(\overline{\mathbf{C}}, \mathbf{a}^i) \quad i = \overline{1, N_f}. \quad (3.116)$$

The term Ψ_{aniso} can be approximated by the *angular integration* (AI) scheme,

$$\Psi_{aniso}(\overline{\mathbf{C}}, \mathbf{a}^i) \approx \Psi_{aniso}(\overline{\mathbf{C}}, \mathbf{y}^j) \quad i = \overline{1, N_f}, \quad j = \overline{1, N_w}, \quad (3.117)$$

$$\begin{aligned} \Psi_{aniso}(\overline{\mathbf{C}}, \mathbf{y}^j) &= \frac{1}{4\pi} \int_{\mathbb{S}^2} n_f \rho \Psi_{aniso}(\overline{\lambda}) dA, \\ &\approx \sum_{j=1}^{N_w} (n_f \rho_j w_j \Psi_{aniso}(\overline{\lambda}_j)), \end{aligned} \quad (3.118)$$

$\bar{\lambda}_j = \sqrt{\mathbf{y}^j \cdot \bar{\mathbf{C}} \cdot \mathbf{y}^j}$ is the stretch on the direction of a fiber (integration) vector, and \mathbf{y}^j and ρ_j are the probabilistic values for each direction \mathbf{y}^j . n_f is the fibril number density. The same term can be approximated by the *generalized structural tensor* approach (GST)

$$\Psi_{aniso}(\bar{\mathbf{C}}, \mathbf{a}^i) \approx \Psi_{aniso}(\bar{\lambda}) \frac{1}{4\pi} \int_{\mathbb{S}^2} \rho(\mathbf{a}) (\mathbf{a} \otimes \mathbf{a}) dA. \quad (3.119)$$

If the probability of observing a single fiber direction is uniformly distributed, then,

$$\begin{aligned} \Psi_{aniso}(\bar{\mathbf{C}}, \mathbf{a}^i) &\approx \Psi_{aniso}(\bar{\lambda}) \frac{1}{4\pi} \int_{\mathbb{S}^2} \rho(\mathbf{a}) (\mathbf{a} \otimes \mathbf{a}) dA, \\ &= \Psi_{aniso}(\bar{\lambda}) \sum_{i=1}^{N_f} (\mathbf{a}^i \otimes \mathbf{a}^i). \end{aligned} \quad (3.120)$$

The evolution of the orientation density distribution can be formulated by using the rate equations of the statistical moments. A probability distribution $\Pr(x)$ has an infinite number of moments M_n , $n \in \mathbb{Z}_+$ around fixed $c \in \mathfrak{R}$ defined by,

$$M_n = E(x^n) = \int_{-\infty}^{+\infty} (x - c)^n \Pr(x) dx. \quad (3.121)$$

Statistical distributions that are commonly used in the modeling of the fiber dispersion are the functions of the first two moments of the distributed random variable. For example, the circular von-Mises probability distribution, which is the analogue of the Gaussian probability density on a spherical domain, is given by,

$$\Pr(x|\mu, k) = \frac{\exp(\cos(x - \mu))}{2\pi I_0(k)}, \quad (3.122)$$

where μ is the mean of the density, k is the magnitude of the dispersion and $I_0(k)$ is the modified Bessel function of order 0. The evolution of the fiber directions is identical to the modeling of the distinct evolution of the moment parameters. When the distribution depends only on the average and the variance measure of the probability density, the mechanical evolution includes two independent/dependent rate equations. It is obvious that such a remodeling approach assumes a static form of the probability distribution. During the evolution, the shape of the probability density function is not related to any other moment parameters (Figure 3.7). Instead of assuming the distinction between individual fiber directions, as mentioned in micro-sphere approach, simple idealizations can be made for the modeling of the angular evolution of the statistical

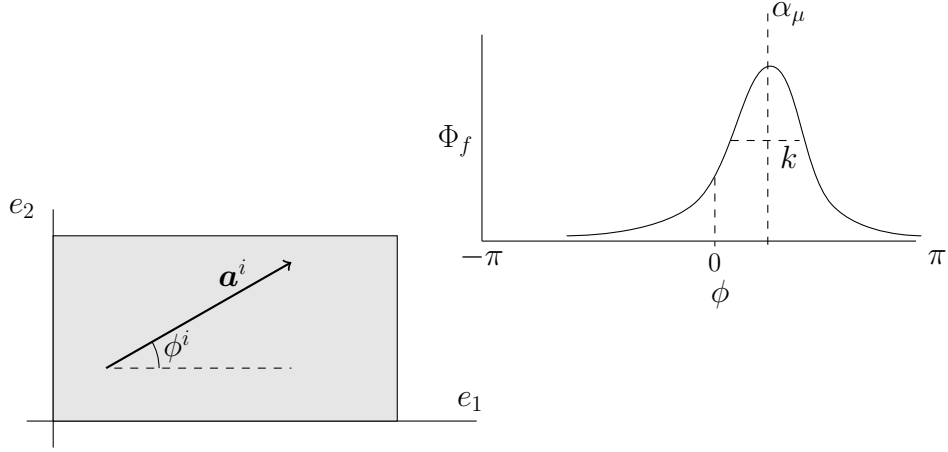


Figure 3.7: Fiber dispersion parameters are based on a circular probability distribution. A fiber direction vector \mathbf{a}^i is defined with respect to the Cartesian e_1 axis where $\phi^i = \angle(\mathbf{a}^i, e_1)$. The fiber orientation density Φ_f is a circular weight associated with the angular measurement ϕ and a circular dispersion parameter k . The figure is adapted from [4].

fiber dispersion. One example is the Driessen et.al.'s work on the angular deviation of the fibers discussed in [4]. The total stress includes an isotropic and anisotropic part,

$$\boldsymbol{\sigma} = -p_h \mathbf{I} + \boldsymbol{\sigma}_{iso} + \boldsymbol{\sigma}_{aniso}, \quad (3.123)$$

$$\boldsymbol{\sigma}_{aniso} = \sum_{i=1}^{N_f} \Phi_f^i (\sigma_f^i (\lambda_f^i) - \tilde{\mathbf{a}}^i \cdot \boldsymbol{\sigma}_{iso} \cdot \tilde{\mathbf{a}}^i) \tilde{\mathbf{a}}^i \otimes \tilde{\mathbf{a}}^i, \quad (3.124)$$

where σ_f^i is the i^{th} fiber's stress depending on the fiber stretch λ_f^i , and Φ_f^i is the associated orientation density on a spatial direction $\tilde{\mathbf{a}}^i = \mathbf{F} \cdot \mathbf{a}_0^i$. The partition of the orientation density is analogous to the integration weights utilized in micro-sphere approach. The weights of the orientation density depends on the circular probability distribution as,

$$\Phi_f^i (\phi^i) = A \exp \left(\frac{\cos(2(\phi^i - \alpha_\mu)) + 1}{k} \right). \quad (3.125)$$

α_μ is the main fiber direction and k is the variance parameter of the distribution. A is a scaling factor that guarantees $\sum_i \Phi_f^i = \Phi_f$. In general, the evolution of the angle and dispersion parameters obey first order equations,

$$\frac{d\alpha_\mu}{dt} = \frac{1}{\tau_\alpha} (\alpha_p - \alpha_\mu), \quad (3.126)$$

$$\frac{dk}{dt} = \frac{1}{\tau_k} (k_p - k), \quad (3.127)$$

τ_α, τ_k are the *characteristic remodeling times*. The target homeostatic condition parameters α_p, k_p are determined by the target stimuli definitions which are not detailed here.

To summarize, the statistical evolution of the dispersion in a fiber reinforced soft tissue can be related to the evolution of a finite number of distinct fibers associated with a probability density function. In a micro-sphere like approximation, additional evolution equations for each integration direction should be developed in order to be able to write down the whole evolution process [27]. On the other hand, the evolution of the dispersion can be reduced to the evolution of only one single parameter (k) to define the overall statistical dispersion. The local fluctuations common in natural processes may yield non-Gaussian density forms. Then, multiple distributions for distinct fiber families may be a way to overcome the problem. On the other hand, the assumption of the existence of one single dispersion parameter has taken place in many experimental works, and the models gave satisfactory results (see for example [46]).

3.5.2 Biologically motivated approaches

The fiber remodeling algorithms that are discussed so far are motivated by the acceptance of a mechanical stimulus such as the principal stress and strain. In reality, the cellular scale microscopic phenomena are the main cause of the micro-scale remodeling. It is experimentally validated that the evolution of the fiber orientation vectors may depend on both strain and stress. However, the time evolution of such dependency is highly related to the sub-processes having extreme complexity. In this subsection, we emphasize some basic approaches and well-known models that are trying to explain the aforementioned cellular activities.

An important development in the field of modeling the structural remodeling in collagen gels may be attributed to the research of Barocas and Tranquillo ([16]). The model is developed for predicting the time evolution of the collagen gel remodeling. The collagen gels are obtained by a carefully designed incubation procedure including a cell seeding process. After the seeding process, the gel evolves into its homeostatic mechanical conditions via the cell migration, which can be modeled by an anisotropic diffusion process. The anisotropic cell migration can be modeled by,

$$\frac{dc}{dt} + c (\nabla \cdot \mathbf{v}_n) = \nabla \cdot (b_{mig} \mathbf{H}_c \cdot \nabla) + b_{cell} c, \quad (3.128)$$

where b_{mig} is a basal migration, b_{cell} is a basal proliferation coefficient and \mathbf{H}_c is a tensor that defines the cell alignment (orientation) of the cells. \mathbf{v}_n is the velocity of

the fibrillar network which is embedded in an interstitial fluid component. The cell alignment is supposed to be related to the fibril alignment in the extra-cellular matrix domain. Due to the concept of the contact guidance, the cell alignment tensor \mathbf{H}_f is a monotonous function of the fibril alignment tensor \mathbf{H}_f as,

$$\mathbf{H}_c = \frac{n_{\text{dim}}}{\text{tr}(\mathbf{H}_f)^q} (\mathbf{H}_f)^q, \quad (3.129)$$

q is a sensitivity parameter for the cell contact guidance. A typical value is $q \approx 4$ ([10, 16]). The fibril alignment tensor is given by,

$$\mathbf{H}_f = \frac{3}{2\pi} \int_0^{\frac{\pi}{2}} \int_0^{2\pi} \text{Pr}(\zeta, \Xi) (\mathbf{a}(\zeta, \Xi) \otimes \mathbf{a}(\zeta, \Xi)) \sin(\zeta) d\zeta d\Xi, \quad (3.130)$$

for the fibril direction $\mathbf{a}(\zeta, \Xi) \in \mathbb{S}^2$ in spherical coordinates.

The criticism of the model can be summarized as follows,

- As observed in some experimental situations [6], the relationship between time evolution of $\mathbf{H}_{c,f}$ can be indirectly related. For instance, assume that $\mathbf{H}_f = \kappa \mathbf{I} + (1 - \kappa n_{\text{dim}}) \mathbf{e}_1 \otimes \mathbf{e}_1$, then $\mathbf{H}_c \approx A \mathbf{H}_f^q = A \text{diag}((1 - \kappa(n_{\text{dim}} - 1))^q, \kappa^q, \kappa^q)$, A being any normalizer. When $q \approx 1$, the principal directions of \mathbf{H}_c and \mathbf{H}_f coincide in time, which means that their evolution speeds are the same. If the distribution is a transversely isotropic one defining an ellipsoid, the rotation of \mathbf{e}_1 does not effect the interpretation. However, as we discuss in chapter 5, the evolution of structural tensors for the cell and fibril orientations is shifted in time. In addition, the evolution of the mean fiber rotation and dispersion rates are time shifted [11]. Thus, the mechanical equations should be based on these observations.
- According to the concept of cell contact guidance, the evolution of migration and fibril alignment is inter-dependent processes. Fibril alignment itself is not only a consequence of the current deformation field but also the cellular migration field. Cellular migration type (i.e. ameboid) also affect fibril alignment pattern. Then, at least, a feedback approach which translates the random information propagating in the ECM environment should be present in the model.

Another class of the collagen remodeling models depends on the mechanistic evolution of the anisotropy due to the synthesis of proteins and the stiffness evolution. Such models cover a great volume of the derived novel approaches published in the field

in the last decade. In the growth and remodeling frameworks, some concepts are widely accepted and now they are settled as the state-of-the-art principles. One of the principles is related to the *loss of balance* between the production and degradation of the ECM constituents (collagen, elastin, proteoglycans) which are considered to be influential for bio-mechanochemical processes. Pathological cases may be related to the loss of balance. During the evolution of the vascular remodeling, hemodynamic conditions could trigger a black-box mechanism which starts protein synthesis via transcription in cells. Growing in mass, the accumulated protein deposition alter the mechanical magnitudes locally. This two-sided feedback process starts a fluctuating events chain until the adaptation is completed by reaching a homeostatic condition. For collagen-based vascular tissue, the balance mechanism can be effected by the chemical agents such as TGF- β (transforming growth factor). The release of TGF- β from the smooth muscle cells is associated with the deposition of the pro-collagen molecule. In addition, the ratio of the metalloproteinase enzymes (MMP) and the tissue inhibitors of the metalloproteinase (TIMP) is a quantifier of the degradation level. In hypertension, the level of MMP decreases in accordance with the degradation of collagen. A typical approach to characterize this event is to use a first order rate equation for the mentioned chemical agents [47],

$$R_{\text{TGF-}\beta} = \dot{\rho}_{\text{TGF-}\beta} = c_{\text{TGF-}\beta} \left[\frac{\rho_{\text{TGF-}\beta}}{\rho_{\text{TGF-}\beta}^*} \right]^{-m_{\text{TGF-}\beta}} \Psi_{\text{SMC}}(\mathcal{I}_4) - \Psi_{\text{TGF-}\beta}^*, \quad (3.131)$$

for the source term R . The density evolution of a system is represented by,

$$\dot{\rho} = R, \quad R = \left[\frac{\rho}{\rho^*} \right]^{-m} \Psi(\mathbf{C}) - \Psi^*, \quad (3.132)$$

with $2 < m < 3$. Ψ^* is the energy that exists in the equilibrium state, and ρ^* is the density of the homeostatic conditions. Similarly,

$$R_{\text{TIMP}} = \dot{\rho}_{\text{TIMP}} = c_{\text{TIMP}} \left[\frac{\rho_{\text{TIMP}}}{\rho_{\text{TIMP}}^*} \right]^{-m_{\text{TIMP}}} \Psi_{\text{SMC}}(\mathcal{I}_4) - \Psi_{\text{TIMP}}^*, \quad (3.133)$$

where c_{TIMP} is a rate parameter. Then, the evolution of the collagen fiber density can be given by,

$$R_{\text{coll}} = \dot{\rho}_{\text{coll}} = c_0 R_{\text{TGF-}\beta} + c_1 R_{\text{TIMP}}, \quad (3.134)$$

which links the production and the degradation rates. The collective rate of change of various protein chains can be handled in a similar way. If the chemicals

diffuse very slowly in the media, the spatial dimension affects the time-dependent propagation of the chemicals, and the ordinary rate equations are extended in to their reaction-diffusion forms including the additional diffusion rate constants.

3.5.3 κ -based remodeling approaches for the evolution of the generalized structural tensor (GST)

In this section, the generalized structural tensor (GST) based remodeling approaches are briefly discussed. A generalized structure definition of a fiber reinforced collagen tissue [22] based on the statistical orientation parameter κ is given by,

$$\mathbf{H}(\mathbf{a}_0, \kappa) = \kappa \mathbf{I} + (1 - 3\kappa) \mathbf{a}_0 \otimes \mathbf{a}_0, \quad (3.135)$$

where the formal definition is,

$$\mathbf{H} = \frac{1}{4\pi} \int \rho(\mathbf{a}_0(\zeta, \Xi)) \mathbf{a}_0(\zeta, \Xi) \otimes \mathbf{a}_0(\zeta, \Xi) \sin(\zeta) d\zeta d\Xi, \quad (3.136)$$

$$1 = \frac{1}{4\pi} \int \rho(\mathbf{a}_0(\zeta, \Xi)) \sin(\zeta) d\zeta d\Xi, \quad (3.137)$$

and $\rho(\mathbf{a}_0) = -\rho(\mathbf{a}_0)$, where \mathbf{a}_0 is defined in Eulerian space coordinates as,

$$\mathbf{a}_0(\zeta, \Xi) = \sin(\zeta) \cos(\Xi) \mathbf{e}_1 + \sin(\zeta) \sin(\Xi) \mathbf{e}_2 + \cos(\zeta) \mathbf{e}_3, \quad (3.138)$$

$\text{span}\{\mathbf{e}_1, \mathbf{e}_2, \mathbf{e}_3\} = \mathbb{E}^3$. \mathbf{H} is a linear mixture of isotropic \mathbf{I} and a directed component $\mathbf{a}_0 \otimes \mathbf{a}_0$ weighted by an assigned probability. Then, \mathbf{H} has positive eigenvalues. For the transversely isotropic distribution of the fibers in space, κ can be reduced into the short form,

$$\kappa = \frac{1}{4} \int_0^\pi \rho(\zeta) \sin^3(\zeta) d\zeta, \quad (3.139)$$

$\rho(\zeta)$ is usually modeled as a circular normal distribution, such as, π -periodic von-Mises distribution. Then, $\rho(\zeta)$ is,

$$\rho(\zeta) = 4 \sqrt{\frac{b}{2\pi}} \frac{\exp(b \cos(2\zeta) + 1)}{\text{erfi}(\sqrt{2b})}, \quad (3.140)$$

and b is the concentration parameter. The energy function can be represented as,

$$\Psi = \Psi_{iso} + \sum_{i=1}^p \Psi_f(\widehat{\lambda}_f^i), \quad (3.141)$$

or $\widehat{\lambda}_f^i = (\mathbf{H}_i : \mathbf{C})^{\frac{1}{2}}$ is the average stretch definition based on the structural tensor \mathbf{H}_i accompanying strain tensor \mathbf{C} . A superscript hat symbol is utilized in order to

make a distinction between the deterministic stretch from the statistical distribution based stretch (in average sense). Then, unlike formulations discussed in [4], the distribution is integrated to obtain the structural tensor. $\widehat{\lambda}_f^i$ is an average description for the dispersed stretch which appears on the direction of the mean orientation of the total fiber layout. Thus, there is a loss of information coming from the second moment of the distribution. For very low dispersion magnitudes, the loss of information is negligible. For a three-dimensional transversely isotropic von-Mises type orientation distribution function, the integration is reduced into the form of equation 3.135 for $0 \leq \kappa \leq 1/3$. In this case, time rate of \mathbf{H} depends on κ and \mathbf{a}_0 . The preferred mean direction vector rotates according to the concepts discussed in previous sections. The parameter κ remodels according to a first order equation,

$$\dot{\kappa}^i = \frac{1}{\tau_\kappa} (\kappa^* - \kappa^i) , \quad (3.142)$$

where κ^* is the target dispersion and κ^i is the i^{th} dispersion parameter in the fiber network.

Mathematical models proposed for the evolution of fiber dispersion achieved a great amount of success, however, all these algorithms have similar conceptual backgrounds to model the complex interactions in a tissue. All of them assume the existence of a deterministic nature, except migration based approaches. At the very small scale, the cellular migration and related phenomena seems to be a direct indicator of the existence of a fluctuating non-deterministic microscale environment. The clues about this fact can be followed to explain the evolution of the macroscopic fiber reinforced structures.

In the following sections, a new remodeling framework based on the random Langevin force is proposed. The proposed framework emphasizes that not only the quantitative evolution of the mechanical magnitudes but also the speed of the evolution of mean orientation and dispersion should be the basic concept. The random Langevin force can restrict the evolution speeds of the distinct distribution moments, if the process is coming from a Gaussian one.

4. A PRELIMINARY FORMULATION: A COMPUTATIONAL MODEL TO PREDICT THE EVOLUTION OF HYDROXYPROLINE CONCENTRATION AND TRANSITION STRETCH IN FIBRIN GELS

4.1 Purpose and Motivation

In this section, we construct a *preliminary* version of the collagen fiber remodeling algorithm that incorporates the complex nature of the random evolution and macroscopic fiber dispersion. We also present a continuum mechanical framework for the evolution of local dispersion and how it could be coupled with the transition stretch and collagen production. A locally linear evolution form for the statistical fiber dispersion was proposed. The random force component of the evolution is described by two parameters. The bounds of the constitutive model parameters are determined by considering the experimental modulus and ultimate tensile stress data. We validate the consistency of the whole algorithm by determining the optimal model parameters that explain a four-week evolution of the Hydroxyproline concentration in a fibrin gel experiment. The whole algorithm performed well for estimating the “qualitative” features of anisotropy ratio distribution and four-week evolution of the collagen volume fraction. The evolution equation parameters that control the maximum level of Hydroxyproline concentration and remodeling time for the transition stretch are determined to be critical for the evolution of compaction and collagen production.

4.2 Theoretical Framework

4.2.1 Essential kinematics and constitutive equations

The deformation of an undeformed initial configuration \mathcal{B}_0 to deformed current configuration \mathcal{B}_t at time t is described by one-to one mapping of Π . Then, transformation (mapping) of the coordinates of material particles $\mathbf{X} \in \mathcal{B}_0 \subset \mathbb{E}^3$ to the spatial coordinates $\mathbf{z} \in \mathcal{B}_t \subset \mathbb{E}^3$ is represented by $\mathbf{x} = \Pi(\mathbf{X}, t)$. The deformation gradient (\mathbf{F}) that stores the information of the relative infinitesimal rate

of change of the displacement field between the material and spatial space is given by $\mathbf{F}(\mathbf{X}) = \nabla \Pi = \partial \Pi(\mathbf{X}) / \partial \mathbf{X}$ (the details are discussed in chapter 2). The Cauchy-Green tensor is denoted by \mathbf{C} ,

$$\mathbf{C} = \mathbf{F}^T \mathbf{F}. \quad (4.1)$$

The fibres are assumed to be embedded in an isotropic nonlinear hyperelastic matrix environment and its angular orientation is characterized by the reference unit vector defined on the surface of the unit sphere $\mathbb{S}^2 = (\mathbf{a} \in \mathbb{R}^3, \|\mathbf{a}\| = 1)$. The deformation gradient maps the fiber orientation from the material configuration to the spatial one as,

$$\lambda \underline{\mathbf{a}} = \mathbf{F} \mathbf{a}, \quad \lambda = \sqrt{\mathbf{a}^T \mathbf{C} \mathbf{a}}, \quad (4.2)$$

where λ is the fiber stretch on the direction of \mathbf{a} . In material space, the stretch λ , defined in equation 4.2 is supposed to be applied on the current preferred direction of the collagen orientation $\tilde{\mathbf{a}}$. For the anisotropic behavior of the material with the statistically dispersed fiber orientations, we consider the definitions in [22] based on the additive splitting of the strain energy density function into its isotropic and anisotropic contributions originally described in [48]. In this case, the strain energy function for the dispersed structure can be defined as (φ is the volume fraction of the constituent),

$$\psi(\mathbf{C}, \mathbf{H}_i) = \varphi_{iso} \psi_{iso}(\mathbf{C}) + \varphi_{aniso} \sum_{i=1}^{N_f} \psi_{aniso}(\mathbf{C}, \mathbf{H}_i(\mathbf{a}_\mu^i, \kappa_i)), \quad (4.3)$$

in which \mathbf{H}_i is the i^{th} structural tensor of N_f fiber families with the mean orientation \mathbf{a}_μ^i and for some dispersion parameter κ_i . The symmetric generalized structural tensor (sGST) \mathbf{H} is defined as a function of the orientation density $\rho(\mathbf{a}) = \rho(-\mathbf{a})$ integrated through the surface of the unit sphere $\Omega(\Theta, \Phi) \in \mathbb{S}^2$,

$$\mathbf{H} = \frac{1}{4\pi} \int_{\mathbb{S}^2} \rho(\mathbf{a}(\Theta, \Phi)) \mathbf{a}(\Theta, \Phi) \otimes \mathbf{a}(\Theta, \Phi) dS. \quad (4.4)$$

In equation 4.4, $\mathbf{a}(\Theta, \Phi) = \sin \Theta \cos \Phi \mathbf{e}_1 + \sin \Theta \sin \Phi \mathbf{e}_2 + \cos \Theta \mathbf{e}_3$ is defined in Eulerian angles where $\mathbf{e}_{1,2,3}$ is the Cartesian basis set. Thus, $[\mathbf{H}]_{k,l} = b_{k,l} \mathbf{e}_k \otimes \mathbf{e}_l$ for some $b_{k,l}$ which define the orientation based average quantities. The explicit mathematical form of the total potential can be determined as a function of the Green-Lagrange strain-like quantity $E = \mathbf{H} : \mathbf{C} - 1$. For one fiber family,

$$\psi(\mathbf{C}, \mathbf{H}) = \varphi_{iso} \psi_{iso}(\mathbf{C}) + \mathcal{H}(E) \varphi_{aniso} \psi_{aniso}(\mathbf{C}, \mathbf{H}, \beta), \quad (4.5)$$

$$\psi_{aniso} = \frac{k_1}{2k_2} (E)^{k_2}, \quad (4.6)$$

where β represents a set of material parameters. ψ_{aniso} is the so-called anisotropic fibre potential activated by the Heaviside step function \mathcal{H} , whereas ψ_{iso} is the isotropic potential ([22, 24]). $\mathcal{I}_4^* = \mathbf{H} : \mathbf{C}$ is an invariant of \mathbf{C} which might be used in equation 4.5 too. The first derivative of the scalar function $\psi(\mathcal{I}_4^*(\mathbf{C}, \mathbf{H}))$ of \mathcal{I}_4^* with respect to \mathbf{C} is given by ($\mathbf{H} \in \mathfrak{R}^{m \times m}$),

$$\frac{\partial \psi(\mathcal{I}_4^*(\mathbf{C}, \mathbf{H}))}{\partial \mathbf{C}} = \frac{\partial \psi(\mathcal{I}_4^*(\mathbf{C}, \mathbf{H}))}{\partial \mathcal{I}_4^*} \mathbf{H}. \quad (4.7)$$

The identity in equation 4.7 can be utilized to obtain the second Piola-Kirchhoff stress tensor (\mathbf{S}) by,

$$\mathbf{S} = \mathbf{S}_{iso} + \mathbf{S}_{aniso}, \quad (4.8)$$

$$\mathbf{S}_{iso} = C_1(\text{tr}(\mathbf{C}) - \ln(\det(\mathbf{C})) - 3) + D_1(\ln(\det(\mathbf{C})))^2, \quad (4.9)$$

$$\mathbf{S}_{aniso} = 2 \frac{\partial \psi_{aniso}(\mathcal{I}_4^*(\mathbf{C}, \mathbf{H}))}{\partial \mathbf{C}}, \quad (4.10)$$

$$\mathbf{S}_{aniso} = k_1 (E)^{k_2-1} \mathbf{H}. \quad (4.11)$$

Equation 4.10 has a the desired mathematical form that the stress can be represented as the product of a scalar with the generalized structure tensor. The implication points that the stress evolution corresponding to the anisotropic remodeling depends directly on the evolution of \mathbf{H} . Surely, the convexity of the potential for arbitrary functional forms of ψ is essential. The convexity of the polynomial type potentials under similar circumstances has been investigated in [24].

4.2.2 Evolution of collagen production based on the modulation transition stretch

Collagen fibers align in the direction of the principal stretch to optimally bear the internal stress load. The strain-dependent remodeling process is supported by the synthesis and degradation of the collagen. Matrix proteins such as matrix metalloproteinases (MMP) and tissue inhibitor metalloproteinases (TIMPs) are important in the remodeling of collagenous tissue. MMPs are supposed to be activated by the mechanical stimuli and their excessive production may point an abnormal event, such as pathological situations and remodeling ([49]). The concentration of these agents increases with stretch. This results in an increase in collagen level in terms of the net amount of *hydroxyproline* (Hyp) content ([5]) (see section 4.3). The final collagen level is expected to saturate towards the homeostatic position to be in balance with the final deformation field.

There are mechanistic models which defines the cellular signaling pathways and transduction mechanisms for the collagen synthesis and secretion. If the concentration or collagen volume fraction data has a highly oscillating complex evolution pattern, mechanistic approaches should (inevitably) be preferred in order to capture the oscillations. However, here, we apply a phenomenological evolution equation for the collagen synthesis. The layout of the hydroxyproline concentration data of the fibrin scaffold does not show a complicated growth pattern, and we consider those phenomenological models being able to capture the rate of change in the time-dependent evolution of hydroxyproline (see Figure 4.2).

Then, the steady state of the concentration of hydroxyproline content (ϑ_{ss}) can be assumed to be linearly related to the square of the fiber stretch (λ^2). The collagen content is limited by the lower value ϑ_{\min} activated by a minimum stretch λ_l , and the upper value ϑ_{\max} activated by a maximum stretch λ_u [9]. Thus,

$$\vartheta_{ss} = \begin{cases} \vartheta_{\min} & \text{if } \lambda < \lambda_l, \\ \vartheta_{\max} & \text{if } \lambda > \lambda_u, \\ \left(\frac{\vartheta_{\max} - \vartheta_{\min}}{\lambda_u^2 - \lambda_l^2} \right) (\lambda^2 - \lambda_l^2) + \vartheta_{\min} & \text{if } \lambda_l < \lambda < \lambda_u. \end{cases} \quad (4.12)$$

The evolution of the hydroxyproline concentration can be given as a first order linear differential equation,

$$\frac{d\vartheta}{dt} = \frac{1}{\tau_{coll}} (\vartheta_{ss}(\lambda^2) - \vartheta). \quad (4.13)$$

In equation 4.13 $d\vartheta/dt$ is the collagen net turnover as a result of synthesis and degradation process. It is assumed that λ_u has a certain upper bound, since excessive strain levels inhibit collagen production rate (see [8, 9] and references therein). Experimental observations support that the tissue compaction in cellular scales is one of the leading mechanisms for the molecular machinery of the remodeling process [12]. From one point of view ([30]), the contractile motions of cells in the ECM are utilized for the stretched assembly of the load carrying collagen fibers making them pre-strained, residually via the transition stretch, which may be the reason for the compaction observed in collagen and fibrin based structures. Here, we follow the same assumption with a slight modification due to the dispersion. The pre-stretched assembly assumption requires the definition of an intermediate remodeled continuum configuration (Π_g), which acts only on the anisotropic constituent of the structure.

Then, the current transition stretch (λ_g) evolves according to equation 4.14.

$$\frac{d\lambda_g}{dt} = \frac{1}{\tau_g} (\lambda_0 - \lambda_g) . \quad (4.14)$$

The target transition stretch is defined by the multiplicative decomposition yielding the remodeling and elastic stretches (equation 4.15).

$$\lambda_0 = \frac{\sqrt{\mathbf{H} : \mathbf{C}}}{\lambda_h} , \quad (4.15)$$

$$E = \lambda_g^{-2} (\mathbf{H} : \mathbf{C}) - 1 . \quad (4.16)$$

The desired homeostatic stretch (λ_h) is supposed to be the final stretch level of the pre-strained dispersed fibers. Naturally, the final stretch of the dispersed directions depend on $\mathbf{H} : \mathbf{C}$ which is the average quantity obtained from every single fiber direction. We finally define the Green-Lagrange strain like quantity E (see [22]) in the remodelled intermediate configuration as in equation 4.16. When λ_g decreases, the fibers evolves towards a residually strained configuration through the time steps, due to an increase in E .

4.2.3 A locally linear fiber remodeling formulation based on langevin force

In this work, we consider the observed dispersion characteristics of the collagen fiber orientations as not being a static structure of the soft tissue, but as a stationary state of a transient dynamic mechanism. Our main goal is to derive the macroscopic remodeling of fiber dispersion and give a consistent evolution equation for the time-dependent evolution of generalized structural tensor \mathbf{H} . An evolution form has been previously given by [26] whereas we will be focusing on the analytical form to account the random force term. In this case, the overall collagen remodeling problem on hand intrinsically assumes the existence of an underlying spatio-temporal diffusion mechanism, that can be originated from a random force acting on the fast time scale. The remodeling process also includes a deterministic driving force which *drifts* the process towards a mechanically determined direction. The microscopic description of a stochastic dynamics disturbed by the random Langevin can be represented by the *Langevin Equation*. A general form of the nonlinear Langevin equation for the M -dimensional state vector variable $\boldsymbol{\xi}$ is given by ([50, 51]),

$$\frac{d\boldsymbol{\xi}(t)}{dt} = \mathbf{h}(\boldsymbol{\xi}(t), t) + \mathbf{g}(\boldsymbol{\xi}(t), t)\boldsymbol{\Gamma}(t) , \quad (4.17)$$

where $\boldsymbol{\xi} = \boldsymbol{\xi}(t)$ for $\boldsymbol{\xi} : \mathfrak{R}^M \rightarrow \mathfrak{R}^M$ is a stochastic variable and $\mathbf{h}(\boldsymbol{\xi}, t) : \mathfrak{R}^M \rightarrow \mathfrak{R}^M$, $\mathbf{g}(\boldsymbol{\xi}, t) \in \mathfrak{R}^{M \times M}$ are drift and diffusion terms consecutively. $\boldsymbol{\Gamma}(t) \in \mathfrak{R}^M$ is the random Langevin force. Its components are assumed to be of Gaussian type with zero mean and δ -correlation having the properties

$$\langle \Gamma_k(t) \rangle = 0, \quad \langle \Gamma_l(t) \Gamma_k(t') \rangle = \delta_{lk} \delta(t - t'). \quad (4.18)$$

The evolution of $\boldsymbol{\xi}$ depends on the applied random force $\boldsymbol{\Gamma}(t)$, where $\mathbf{g}(\boldsymbol{\xi})$ determines the magnitude and the rotation of the random force vector. To obtain the microscopic description of the time-dependent remodeling of collagen orientation, we use the heuristic derivation approach explained in [50]. Since the remodeling process outcomes with observed statistical quantities that are represented by probability distributions, the probability distribution of collagen orientation can be obtained by investigating the effects of microscopic Langevin force on the drifting mechanism [52]. As a result, we have a microscopic definition of the remodeling process driven by the deterministic drift (h). The functional form of $\mathbf{h} : \mathfrak{R}^M \rightarrow \mathfrak{R}^M$, $\mathbf{h} = \mathbf{h}(\mathbf{a}, \mathbf{C}, t)$, $\mathbf{a} \in \mathfrak{R}^M$ can be selected to give the rate of the rotation as described in [44],

$$\mathbf{h}(\mathbf{a}, \mathbf{C}, t) = f(\mathbf{a}, \Lambda_{max}^{\mathbf{C}}) (\mathbf{I} - \mathbf{a} \otimes \mathbf{a}) \mathbf{n}_{max}^{\mathbf{C}}, \quad (4.19)$$

where f is a scalar function, and $\Lambda_i^{\mathbf{C}}$ is the i^{th} eigenvalue of \mathbf{C} corresponding to the eigenvector $\mathbf{n}_i^{\mathbf{C}}$. Then, a probabilistic evolution of \mathbf{a} can be proposed as described in equation 4.20.

$$\frac{d\mathbf{a}(t)}{dt} = f(\mathbf{a}, \Lambda_{max}^{\mathbf{C}}) (\mathbf{I} - \mathbf{a} \otimes \mathbf{a}) \mathbf{n}_{max}^{\mathbf{C}} + \mathbf{g}(\mathbf{a}(t), t) \boldsymbol{\Gamma}(t). \quad (4.20)$$

It is possible to represent the time-dependent evolution of \mathbf{H} through equation 4.20. We use the probabilistic definition in order to estimate the \mathbf{H} matrix. The probability density function $\text{Pr}(\mathbf{x})$ in equation 4.22 describes the geometric layout (orientation) of a fiber density distribution that gives the probability of a single fiber being in the interval $(\mathbf{x}, \mathbf{x} + d\mathbf{x})$. By applying an approach similar to the “*sample covariance matrix estimator*”, the integration of the individual fiber directions can be calculated by the discrete sums. The covariance matrix of a random \mathbf{x} vector is defined by ($\mathbf{COV}(\mathbf{x}, \mathbf{x})$) (\otimes is the outer product),

$$\mathbf{COV}(\mathbf{x}, \mathbf{x}) = \mathbb{E}(\mathbf{x} \otimes \mathbf{x}) - \mathbb{E}(\mathbf{x}) \otimes \mathbb{E}(\mathbf{x}), \quad (4.21)$$

$$= \int_{\mathbf{x}} p(\mathbf{x}) \mathbf{x} \otimes \mathbf{x} d\mathbf{x} - \mathbb{E}(\mathbf{x}) \otimes \mathbb{E}(\mathbf{x}). \quad (4.22)$$

The integration of the continuous form $\int_{\mathbf{x}} \text{Pr}(\mathbf{x}) \mathbf{x} \otimes \mathbf{x} d\mathbf{x}$ can be approximated by the discrete sums including a sample of n independent vectors from the same distribution.

$$\int_{\mathbf{x}} \text{Pr}(\mathbf{x}) \mathbf{x} \otimes \mathbf{x} d\mathbf{x} = \mathbb{E}(\mathbf{x} \otimes \mathbf{x}) \approx \frac{1}{n} \sum_{i=1}^n \mathbf{x}_i \otimes \mathbf{x}_i, \quad (4.23)$$

where i is the sample index for a random vector. In the asymptotic case $n \rightarrow \infty$, the sum approaches to the exact matrix obtained from the continuous form. Since the integration corresponds to the expectation calculated from all microscopic directions \mathbf{a}^i , then

$$\mathbf{H} = \frac{1}{4\pi} \int_{\mathbb{S}^2} \rho(\mathbf{a}) \mathbf{a} \otimes \mathbf{a} dS, \quad (4.24)$$

$$\approx \lim_{N \rightarrow \infty} \frac{1}{N} \sum_{i=1}^N \mathbf{a}^i \otimes \mathbf{a}^i, \quad (4.25)$$

for ρ being the orientation density distribution that source from the definition of Pr, and

$$\frac{1}{4\pi} \int_{\mathbb{S}^2} \rho(\mathbf{a}) dS = 1. \quad (4.26)$$

From equation 4.20 and from the definition of \mathbf{H} in equation 4.27 we get,

$$\dot{\mathbf{H}} = \lim_{N \rightarrow \infty} \frac{1}{N} \sum_{i=1}^N \dot{\mathbf{a}}^i \otimes \mathbf{a}^i + \mathbf{a}^i \otimes \dot{\mathbf{a}}^i, \quad (4.27)$$

$$\begin{aligned} \dot{\mathbf{H}} &= \lim_{N \rightarrow \infty} \frac{1}{N} \sum_{i=1}^N [(f(\mathbf{a}^i, \Lambda_{max}^C) (\mathbf{I} - \mathbf{a}^i \otimes \mathbf{a}^i) \mathbf{n}_{max}^C \\ &+ \mathbf{g}(\mathbf{a}^i, t) \mathbf{\Gamma}(t)) \otimes \mathbf{a}^i \\ &+ \mathbf{a}^i \otimes (f(\mathbf{a}^i, \Lambda_{max}^C) (\mathbf{I} - \mathbf{a}^i \otimes \mathbf{a}^i) \mathbf{n}_{max}^C \\ &+ \mathbf{g}(\mathbf{a}^i, t) \mathbf{\Gamma}(t))], \end{aligned} \quad (4.28)$$

which might not be represented in simplified tensor forms for nonlinear f and g . The whole sum should be calculated to obtain $\dot{\mathbf{H}}$. An approach using the integration over the unit sphere to calculate the total effect of individual fibers has been recently applied in many studies [19, 30, 47, 27]. However, we focus on the homogenized average effects of the process. The evolution in equation 4.27 can be transformed in to a compact tensor form if an appropriate form of \mathbf{h} is chosen. The linearization of

equation 4.19 around \mathbf{a}_0 at time t yields,

$$\mathbf{h}(\mathbf{a}) = \mathbf{h}(\mathbf{a}_0) + \nabla(\mathbf{h}(\mathbf{a}_0)) \cdot (\mathbf{a} - \mathbf{a}_0) + \mathcal{O}(\|\mathbf{a} - \mathbf{a}_0\|), \quad (4.29)$$

$$\nabla \mathbf{h} = \nabla_{\mathbf{a}} (f(\mathbf{a}, \Lambda_{max}^{\mathbf{C}}) (\mathbf{I} - \mathbf{a} \otimes \mathbf{a}) \mathbf{n}_{max}^{\mathbf{C}}), \quad (4.30)$$

$$\begin{aligned} &= f(\mathbf{a}, \Lambda_{max}^{\mathbf{C}}) \nabla_{\mathbf{a}} ((\mathbf{I} - \mathbf{a} \otimes \mathbf{a}) \mathbf{n}_{max}^{\mathbf{C}}) \\ &\quad + ((\mathbf{I} - \mathbf{a} \otimes \mathbf{a}) \mathbf{n}_{max}^{\mathbf{C}}) \otimes \nabla_{\mathbf{a}} f(\mathbf{a}, \Lambda_{max}^{\mathbf{C}}). \end{aligned} \quad (4.31)$$

Keeping $f(\mathbf{a}) = \pi/2 \tau_{\omega}$ as a constant value is effective for the numerical simulations.

Finally the linearization is given by,

$$\begin{aligned} \mathbf{h}(\mathbf{a}, t) &= \frac{\pi}{2 \tau_{\omega}} \left(\mathbf{n}_{max}^{\mathbf{C}} + \mathbf{a}_0^T \mathbf{n}_{max}^{\mathbf{C}} \mathbf{a}_0 \right. \\ &\quad \left. - \left((\mathbf{n}_{max}^{\mathbf{C}})^T \mathbf{a}_0 \mathbf{I} + \mathbf{a}_0 \otimes \mathbf{n}_{max}^{\mathbf{C}} \right) \mathbf{a} \right), \end{aligned} \quad (4.32)$$

$$= \mathbf{B}(\mathbf{a}_0) \mathbf{a} + \mathbf{c}(\mathbf{a}_0), \quad (4.33)$$

in which $\mathbf{B} \in \mathfrak{R}^{M \times M}$, $\mathbf{c} \in \mathfrak{R}^M$ for $\mathbf{a} \in \mathfrak{R}^M$, and τ_{ω} is the characteristic remodeling time of rotation. \mathbf{a}_0 can be considered as the previous direction of the fiber in the reference configuration which is algorithmically updated by the incremental Newton iterations to a newly remodeled direction. By incorporating the linear form with equation 4.20, it is possible to give an integrated version (equation 4.35) and the differential form of the fiber orientation evolution including the random effects,

$$\begin{aligned} \mathbf{a}(t + \Delta t) &= \mathbf{a}(t) + \int_t^{t+\Delta t} \mathbf{h}(\mathbf{a}(t'), t') dt' \\ &\quad + \int_t^{t+\Delta t} \mathbf{g}(\mathbf{a}(t'), t') \mathbf{\Gamma}(t') dt', \end{aligned} \quad (4.34)$$

$$d\mathbf{a}(t) = (\mathbf{B}(t) \mathbf{a}(t) + \mathbf{c}(t)) dt + \sqrt{\Sigma} d\mathbf{W}(t), \quad (4.35)$$

where $d\mathbf{W}(t)$ is a Wiener process ([50, 51]) with the property,

$$\mathbf{W}(t + \Delta t) - \mathbf{W}(t) = \int_t^{t+\Delta t} \mathbf{\Gamma}(t') dt', \quad (4.36)$$

$$d\mathbf{W} = \sqrt{\Delta t} \mathbf{\Gamma}(t), \quad (4.37)$$

and $\mathbf{g}(\mathbf{a}, t)$, as given in equation 4.20, is taken to be $\sqrt{\Sigma}$. In equation 4.36, due to random nature of $\mathbf{\Gamma}$, the integration is calculated by the probabilistic approaches (Itô

rule). As previously mentioned, $\mathbf{\Gamma}(t) \in \mathfrak{R}^M$ is distributed according to the Gaussian distribution defined by the probability density function $\text{Pr}(\mathbf{\Gamma})$,

$$\text{Pr}(\mathbf{\Gamma}) = \frac{1}{\sqrt{(2\pi)^M}} \exp\left(-\frac{1}{2}\mathbf{\Gamma} \cdot \mathbf{\Gamma}\right). \quad (4.38)$$

The expected value of the mean orientation (\mathbf{a}_μ) can be calculated by utilizing the infinitesimal increase on the expectation function $\mathbb{E}(\mathbf{x}) = \int_{\mathbf{x}} \text{Pr}(\mathbf{x}) \mathbf{x} d\mathbf{x}$. Since $\mathbb{E}(d\mathbf{W}(t)) = \mathbf{0}$

$$d\mathbf{a}_\mu = \mathbb{E}(\mathbf{a} + d\mathbf{a}) - \mathbb{E}(\mathbf{a}), \quad (4.39)$$

$$= \mathbf{B}(t)\mathbf{a}_\mu(t)dt + \mathbf{c}(t)dt. \quad (4.40)$$

We want to estimate the expectation of the structural tensor through the derived identities as in equation 4.40. Generalized structure tensor can be defined by the expected value of the variance-covariance matrix $\mathbf{V} = \mathbb{E}(\mathbf{a} \otimes \mathbf{a}) - \mathbb{E}(\mathbf{a}) \otimes \mathbb{E}(\mathbf{a})$. Thus,

$$\dot{\mathbf{V}} = \dot{\mathbf{H}} - \overline{\dot{\mathbf{a}}_\mu \otimes \mathbf{a}_\mu}. \quad (4.41)$$

From $\mathbb{E}(\sqrt{\Sigma}d\mathbf{W}(t) \otimes \sqrt{\Sigma}d\mathbf{W}(t)) = \Sigma \mathbf{I} dt$ ($d\mathbf{W}$ is isotropic) and assuming a constant dispersion term $\Sigma \in \mathfrak{R}$, one obtains the time-dependent matrix differential equation for the evolution of \mathbf{V} (and \mathbf{H}).

$$\begin{aligned} d\mathbf{V}(t) &= \mathbb{E}((\mathbf{a} + d\mathbf{a} - \mathbf{a}_\mu - d\mathbf{a}_\mu) \otimes (\mathbf{a} + d\mathbf{a} - \mathbf{a}_\mu - d\mathbf{a}_\mu)) \\ &- \mathbb{E}((\mathbf{a} - \mathbf{a}_\mu) \otimes (\mathbf{a} - \mathbf{a}_\mu)), \end{aligned} \quad (4.42)$$

$$= \mathbf{B}(t) \otimes \mathbf{V}(t)dt + \mathbf{V}(t) \otimes \mathbf{B}(t)dt + \Sigma \mathbf{I}dt + \mathcal{O}(dt^2). \quad (4.43)$$

There is an advantage of the linearity that the update procedures can be given analytically for the nonlinear Newton iterations. The update equations from t to $t + \Delta t$ for \mathbf{a}_μ , \mathbf{V} and \mathbf{H} is given in equation 4.44.

$$\mathbf{a}_\mu(t + \Delta t) = e^{\Delta t \mathbf{B}} \mathbf{a}_\mu(t) + \int_0^{\Delta t} e^{(\Delta t - s)\mathbf{B}} \mathbf{c} ds, \quad (4.44)$$

$$\mathbf{a}_\mu(t + \Delta t) = \mathbf{a}_\mu(t + \Delta t) / \|\mathbf{a}_\mu(t + \Delta t)\|, \quad (4.45)$$

$$\begin{aligned} \mathbf{V}(t + \Delta t) &= e^{\Delta t \mathbf{B}} \mathbf{V}(t) e^{\Delta t \mathbf{B}^T} \\ &+ \int_0^{\Delta t} e^{(\Delta t - s)\mathbf{B}} \Sigma \mathbf{I} e^{(\Delta t - s)\mathbf{B}^T} ds, \end{aligned} \quad (4.46)$$

$$\begin{aligned} \mathbf{H}(t + \Delta t) &= \frac{1}{\sum_{i=1}^M \Lambda_i^{H(t+\Delta t)}} \\ &\times (\mathbf{V}(t + \Delta t) + \mathbf{a}_\mu(t + \Delta t) \otimes \mathbf{a}_\mu(t + \Delta t)). \end{aligned} \quad (4.47)$$

Numerical calculation of the matrix exponentials ($e^{\Delta t B}$) is trivial and can be realized by existing libraries. Integration of the matrix exponentials may not be trivial especially for the stiff cases, however, Gaussian quadrature well performed for our case.

We simply assumed a constant $\Sigma = \zeta_u \mathbf{I}$ for the random force term. This term can be assumed to vary with time depending on a strain dependent stimulus. In every Newton iteration, the random force term can be defined as a ratio of the eigenvalues of Cauchy-Green tensor (equation 4.48). Strain dependent experiments show that the inter-cellular stress fibers (SF) align isotropically when biaxial boundary conditions were applied ($\Lambda_1^H = \Lambda_2^H > \Lambda_3^H$), and show no dispersion when the structure is uniaxially stretched to extreme levels ($\Lambda_{\max}^H > \Lambda_2^H \approx \Lambda_3^H \approx 0$) (see [18]). Then we propose the form,

$$\Sigma = \left(\frac{\Lambda_{\max}^C - 1}{\Lambda_{\max}^C} \right)^\gamma \zeta_u, \quad (4.48)$$

as the random Langevin force for the collagen fiber dispersion. We set $\gamma = 1$ for simplicity, which is a weighting term. ζ_u is an upper bound for the random force.

4.3 Model Parameters and Their Intervals

4.3.1 Problem specification

We validate the theoretical scheme through investigating its predictive abilities on a four-week fibrin based gel experiment, discussed in [14, 5, 49]. The experiments are prepared to track the evolution of chemical signals for the collagen production, evolution of mechanical properties and statistical fiber dispersion. Rectangular strips ($35 \times 5 \times 1 \text{ mm.}$) of polyglycolic acid meshes were coated with a thin layer of poly-4-hydroxybutyrate. The bottom surface of the scaffolds is reinforced by an elastic layer. In the longitudinal direction, the scaffolds are attached to the flexible membranes of 6-well plates at the outer 5mm . Human saphenous vein myofibroblasts were seeded into the fibrin gel compound (10 mg/ml fibrinogen, 10 IU/ml thrombin solution) having the geometry of a rectangular strip at the density of 2×10^6 cells per cm^2 . Two boundary conditions, cyclic and constrained, have been applied for different strips (Figure 4.1a). We only investigate the constrained case here. In the constrained case, the outer 5mm of the engineered scaffold with rectangular geometry has been statically

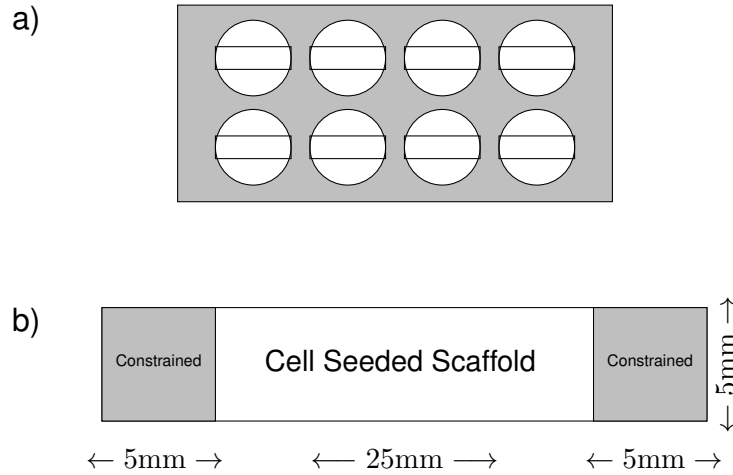


Figure 4.1: A sample drawing of the experiment samples and strip geometry. (a) Experimental design of a set of strips located on a fibrin block. (b) Rough geometry of the samples and their constrained regions.

conditioned and no displacement occurs on this partition. The $25mm$ interior region of the scaffold block is free to compact due to contractility (Figure 4.1b). The strip samples were assumed to be the same in their chemical composition and any material properties. Then the strip samples ($n = 5$) were analyzed to determine the statistical properties of the chemical composition and material properties at predetermined times. In the following sections, through utilizing the qualitative and quantitative information presented in these experiments, we show that a locally linear evolution model for the statistical fiber orientation depending on the transition stretch can be used as an efficient tool to explain a four-week evolution of the collagen concentration in fibrin gels.

4.3.2 Material parameters for fibrin-based engineered tissue

The experimental setup includes the process of myofibroblast seeding using 10 mg/ml fibrinogen and 10 IU/ml thrombin solution as the cell carrier. Although the chemical composition and production procedures influence the mechanical properties, tensile stiffness of the fibrin-based scaffolds is known to be highly correlated with the concentration of fibrinogen and thrombin. For our investigations, the young modulus of isotropic matrix component will be set to an acceptable approximate value which is supposed to represent the properties of the matrix component. Although some publications in the literature support evidence for nonlinear material behavior ([53]), for simplicity, we assume that isotropic matrix component could be modeled by a

nonlinear hyperelastic material. Previous works ([53, 54, 55, 5, 56, 57]) have shown that the linear modulus of fibrin-based scaffolds is on the order of kPa's. We consider that E_M describes the stiffness of isotropic fibrin-based structure without collagen. The linear modulus of collagen scaffolds has shown to be approximately 10 times higher than the fibrin scaffolds which were created by the same production techniques ([55]). The exact value depends on the production process and concentrations, especially the fibrinogen level. It is reasonable to select the variation of elastic modulus E_M to be lying in the interval $5 < E_M < 30$ kPa for our case. We support this assumption by presenting a list of previous experimental measurements gathered by the experiments on fibrin scaffolds (Table 4.1), which focuses on mechanical parameters. The observations point out that without collagen fibers the fibrin-based scaffolds may be described by an isotropic weak matrix where collagen structure takes place by the cellular activities, and mature with time. By this way, in order to decrease the complexity of the problem, we assume that the overall time-dependent strength of the material largely depends on the collagen level and we exclude any temporal change in the mechanics of isotropic matrix. Thus, we set shear modulus of the matrix as 20kPa and $C_1 \approx 10$ kPa.

We have roughly determined the representative stress-strain model by using the (uniaxial extension) data of experimental UTS and linear modulus reported in [5] for the 2nd, 3rd, 4th weeks. A rough power law description of the strain-stress relationship can be given by the function $\sigma = \nu_1 (\lambda - 1)^{\nu_2}$. The linear modulus is placed as the slope of the curve at $\lambda = 1.25$. The estimated coefficients for ν_1, ν_2 have been given in Figure 4.4 where the nonlinear relationship matures with time. We use the representative model for 4th week in order to determine a plausible estimate of the parameters. The components of the Cauchy stress is determined by,

$$\boldsymbol{\sigma}' = C_1 \det(\mathbf{F})^{-5/3} \left(\mathbf{F} \mathbf{F}^T - \frac{\text{tr}(\mathbf{F})}{3} \mathbf{I} \right), \quad (4.49)$$

$$\begin{aligned} \sigma_{11} = & \left(\lambda^2 - \frac{1}{\lambda} \right) \times \left((1 - \varphi_{coll}) C_1 \right. \\ & \left. + \varphi_{coll} \frac{k_1}{3} \left(\left(\lambda^2 + \frac{2}{\lambda} \right) / 3 - 1 \right)^{k_2 - 1} \right). \end{aligned} \quad (4.50)$$

The theoretical uniaxial model in equation 4.50, which represents an incompressible anisotropic nonlinear elastic media with Neo-Hookean isotropic contribution, assumes

a homogenous distribution of the collagen volume fraction which was set to $\varphi_{coll} = 0.015$. The statistical distribution of the fibers has been (experimentally) observed to be almost isotropic at week 4, then ($\mathbf{H} \approx \mathbf{I}/3$). Incompressibility has been utilized in order to simplify the expression equation 4.50, because of the uniaxial extensions $\mathbf{F} = \text{diag}(\lambda, 1/\sqrt{\lambda}, 1/\sqrt{\lambda})$ and $\det(\mathbf{F}) = 1$. The nonlinear fitting of the expression in equation 4.50 supplies the overall variation of the boundaries of two anisotropic parameters. We conclude that $k_1 = 2.2$ GPa and $k_2 > 2.0$ are strictly required for this model to be in accordance with both the UTS and linear modulus data at week 4 (Figure 4.4). The constraint $k_2 > 2.0$ is required not only for fitting purposes but also for the stability of the simulations. Isotropic parameters do not have much effect on the variation of k_1 and k_2 when $C_1 < 30$ kPa. This calibration of parameters is expected to be sufficient for simulating the 30 days of evolution.

4.3.3 Collagen remodeling and transition stretch

Initial estimations of the collagen remodeling parameters can be realized by means of a nonlinear curve fitting applied on to experimental data. The collagen levels are related to the existing hydroxyproline concentration since many collagen types include this molecule at a certain fraction of the collagen content. To estimate the evolution of hydroxyproline, we replace the evolution equation by the logistic type growth curve as in equation 4.51

$$\frac{d\vartheta}{dt} = \frac{1}{\tau_{coll}} \vartheta \left(1 - \frac{\vartheta}{\vartheta_{ss}} \right). \quad (4.51)$$

ϑ_{ss} is the steady state concentration and τ_{coll} is characteristic remodeling time for hydroxyproline production. The exact solution for the incremental update procedure is available,

$$\vartheta(t + \Delta t) = \frac{\vartheta_{ss} \vartheta(t) e^{\Delta t / \tau_{coll}}}{\vartheta_{ss} + \vartheta(t) (e^{\Delta t / \tau_{coll}} - 1)}. \quad (4.52)$$

Parameter estimations for equation 4.52 are $\tau_{coll} = 6.045$ days, $\vartheta_{ss} = 7.3548$, and $\vartheta(t = 0) = 0.3357$. This kind of initial analysis without solving the boundary value problem supplies strong quantitative information such as the characteristic remodeling time for the hydroxyproline content, and weak information about the steady state concentration ϑ_{ss} . Steady state target concentration depends on the evolution of the mechanical magnitudes such as the transition stretch and principal strain. The

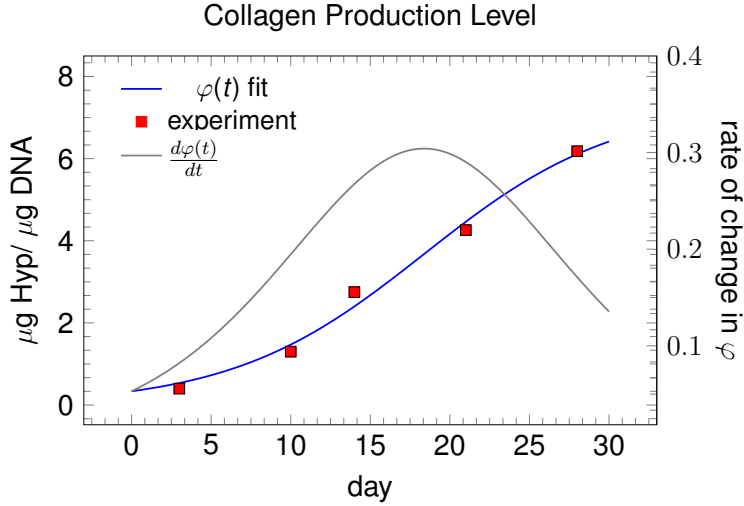


Figure 4.2: Experimentally observed hydroxyproline concentration data [5] and the best logistic type nonlinear growth fitting curve.

time-dependent dimensionless fiber volume fraction $\varphi_{coll}(t)$ can be estimated directly from the dimensionless density variable $\vartheta(t)$ for the hydroxyproline. Since the hydroxyproline data is given in terms of $\mu\text{gHyp}/\mu\text{gDNA}$, the total amount of DNA is required. It can be estimated by multiplying the total number of cells $N_{cell}(V)$ in a volume V by the amount of DNA in a single cell $M_{DNA} = 7.2\text{pg}/\text{cell}$ (see [58]). The mass of the collagen content can be calculated by the mass ratio $R_{hyp}^{coll} = 100.0/13.0$ ([59]), where the mass of the collagen in $\mu\text{gHyp}/\mu\text{gDNA}$ is given by $M_{coll} = R_{hyp}^{coll} \times \vartheta$. Finally, the collagen volume fraction φ_{coll} can be calculated by the technique described in [60], and when there is no variation in the number of cells per unit volume it could be formulated as equation 4.53.

$$\varphi_{coll}(t) \approx \xi M_{DNA} R_{hyp}^{coll} \left(\frac{N_{cell}(V)}{V} \right) \vartheta(t), \quad (4.53)$$

$$\approx \eta \vartheta(t). \quad (4.54)$$

The conversion parameter from hydroxyproline in to collagen concentration in equation 4.54 is $\eta = 0.0024$. $\xi \approx 1.44$ is a constant conversion parameter which relates the volumetric fraction to the density of the chemical composites (see [60] for details). This conversion is used to estimate the final ϑ_{coll} for the mechanical model. We expect this model to predict the Hyp concentration (also volume fraction) of five experimental observations from [49] as $\vartheta(t = 3) \approx 0.4$, $\vartheta(t = 10) \approx 1.3$ and from [5], we have $\vartheta(t = 14) = 2.75$, $\vartheta(t = 21) = 4.26$, $\vartheta(t = 28) = 6.18$ (Figure 4.2).

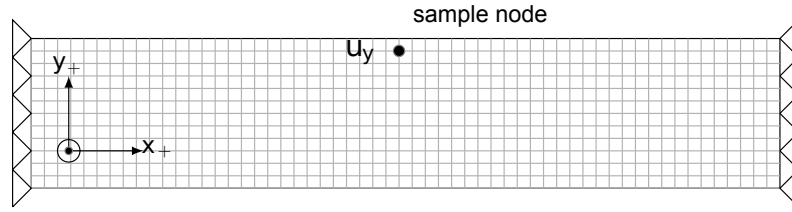


Figure 4.3: Representation of the finite element discretization of strip geometry with 1848 hexahedral 8-node elements. A single node has been selected for data demonstration purposes. u_y is the displacement variable that belongs to the sample node.

The target *homeostatic stretch* was determined as $\lambda_h = 1.01$ which has been used for the collagen compaction models in [30]. It gave satisfactory compaction levels in our simulations.

4.3.4 Rotation rate

Characteristic remodeling time for the mean fiber orientation has been qualitatively determined and set to be in the interval $3.0 \leq \tau_\omega \leq 6.0$ days, due to some experimental results that are given in [11] for collagen gels. For this case, uniaxially strained samples have shown a characteristic rotation time of $t_\omega \approx 72$ hours. Additionally, we test the situation for $t_\omega \approx 6.0$ days.

4.4 Numerical Implementation: Solution Method and Software

The boundary value problem has been solved by an integration point based finite element method where we apply an incremental update procedure for the nonlinear Newton iterations. The basics of the integration point based approach for the growth and remodeling equations can be found in [36]. The whole algorithm and the discretisation of the problem domain have been implemented by using the fortran subroutines located in *Elmer Multiphysics* Library ([61]). The rectangular block domain of the real problem has been partitioned into 1848 hexahedral 8–node elements constructed by 2736 nodes. The displacement boundary conditions of Dirichlet type $\mathbf{u} = 0$ have been applied from both left and right faces of the rectangular block (see Figure 4.3). For the post-processing, the interpolation of local variables has been obtained by the related subroutines in Elmer library. Additional modules to compute the anisotropic stress, collagen production, calculations of the transition stretch and

numerical estimations of the algorithmic tangent moduli have been written and adapted for the incremental update process. The solution procedure is applied both in local and global newton iterations, and there is supposed to be no inertial effects acting on the body,

$$\nabla \cdot \boldsymbol{\sigma} = 0. \quad (4.55)$$

In this case, at every time step, $\Delta t = 0.5$ days, the balance of momentum equation 4.55 is solved by the Total Lagrangian (TL) approach until the convergence is achieved.

In the TL approach, we formulate the remodeling processes to update the internal variables in the intermediate remodeled configuration. For each time step, the local update equations 4.14,4.44,4.52 are solved simultaneously. The updated Green-Lagrange strain (E) in the intermediate configuration is assumed to be the source of elastic strain energy, which can be solved by the global Newton iterations to calculate the stress and strain measures, for the new updated reference configuration. The new estimations of the internal variables ($\lambda_g, \boldsymbol{\alpha}_\mu, \mathbf{H}, \varphi_{coll}$) are stored at the integration point level at the end of each global Newton iteration. The global Newton iteration proceeds until the norm of the global displacement increment vector satisfies the condition $\Delta \mathbf{u} < 10^{-6}$. We numerically estimate the local algorithmic tangent modulus matrix by the approach given by [39]. The evolution of the concentration and other mechanical magnitudes are tracked for 30 days.

4.5 Results and the Validation of the Algorithm

In this section, we briefly represent our simulation results and analyze them in order to improve the estimations. We estimate the optimal parameter interval by successive fine-tuning approaches by means of investigating the sensitivity of the parameters $\varphi_{max}, \tau_\omega, \tau_g$ listed in Table 4.2. We followed a two-stage fine-tuning strategy. In the first part, we use arbitrary initial parameters in order to determine their effects on the deformation level and chemical concentration. Secondly, we fine-tune the parameters for a better estimation of the experimental data. Initial simulation results have certainly shown that φ_{max}, τ_g have a direct consequence on compaction level and collagen production. The remodeling time τ_ω for the fiber dispersion evolution did not affect the simulation results meaningfully ($\zeta = 1$). This interpretation can be followed from Figure 4.5. It is expected to be affecting the results quite weakly even if the parameters

are set to higher values. The reason of the insensitivity may be related to the isotropic distribution of fibers over the domain (see Figure 4.9). Although the dispersion at the beginning of the process is close to isotropy, the evolution of mean fiber direction \mathbf{a}_μ has shown a usual, expected rotation (Figure 4.10). The mean fiber direction is always flat at the middle of the fibrin bar, whereas it has the maximum rate of rotation at spatial positions close to the corners of strips. The influence can probably be seen for $\zeta_u \ll 1.0$ when the random force is relatively small. The experimental observations support the existence of a high level of dispersion for the constrained cases ([14]). The investigation has been continued for $\tau_\omega = 6.0$ days, assuming a similar characteristic remodeling time of the collagen production $\tau_\omega \approx \tau_{coll}$, for the rest of the analysis. On the other hand, remodeling time for transition stretch τ_g has been understood to be very effective on mechanical magnitudes independent from φ_{max} , (Figure 4.5, 4.6, 4.7 and 4.8). Observations of the sample node states that the characteristic time for the

Table 4.1: Previous works that describe the mechanical properties of fibrin gels (*NA* : Not Available).

Fibrinogen (<i>Fb</i>) (mg ml ⁻¹)	Thrombin (<i>Tb</i>) (UI/ml <i>Fb</i>)	E_M (kPa)	V/V_0	Description	Ref.
0.5 – 3.0	0.2 UI/ml	1.04 – 5.92	<i>NA</i>	Analytical description of elastic modulus as a function of <i>Fb</i> , $E_M^\infty = 2.04(Fb)^{0.97}$	[53]
2.0 4.0 40.0	0.1 0.5	28.0 19.0 5.95	0.954 0.816 <i>NA</i>	Pure fibrin gels at day 6 Uncompressed samples at day 0	[55] [56]
4.0	1.0 0.1 0.01 0.001	9.93 8.86 18.9 28.2	$V/V_0 < 0.1$ for all	The influence of <i>Tb</i> concentration on measurements at day 7	[57]
17.8 – 26.5	<i>NA</i>	12.0 ± 1.0	<i>NA</i>		[54]

transition stretch increases when the hydroxyproline production decreases. There is an undoubted trade between τ_g and φ_{max} evolution where the effects of a decrease in τ_g can be counterbalanced by a decrease in φ_{max} . The trade-off exists among φ_{max} , τ_g and λ_g . Since the compaction levels depend on the magnitude of the transition stretch λ_g , it is a functionally dependent variable of both φ_{max} and τ_g . As a result, in order to reach the exact compaction levels, the parameters should be determined through

Table 4.2: The predefined parameters, their descriptions and test intervals that are used in simulations.

Parameter	Value	Description	Test Interval
Material Model			
C_1	10.0 kPa	Shear Modulus	-
D_1	40.0 kPa	Bulk Modulus (Poisson ratio $\nu \approx 0.4$, $D_1 = \frac{C_1 2\nu}{1-2\nu}$)	-
k_1	2.2×10^6 kPa	Fiber Stiffness Parameter	-
k_2	2.1	Exponential Fiber Parameter	-
Transition Stretch			
λ_h	1.01	Homeostatic Stretch	$1.01 \leq \lambda_h$
τ_g	3 days	Characteristic Time for the Transition Stretch	$1.0 \leq \tau_g \leq 3.0$
Fiber Remodeling			
τ_ω	6.0 days	Characteristic Time for Fiber Reorientation	$3.0 \leq \tau_\omega \leq 6.0$ days
γ	1.0	Dispersion parameter	-
ζ_u	1.0	Upper Bound for Random Langevin Force	-
Collagen Remodeling			
φ_{max}	490.0 $\mu\text{g Hyp}/\mu\text{g DNA}$	Target Concentration (Max)	$50.0 \leq \varphi_{max}$
φ_{min}	0.1 $\mu\text{g Hyp}/\mu\text{g DNA}$	Target Concentration (Min)	-
λ_u	1.1	Upper bound for Fiber stretch to activate φ_{max}	-
λ_l	1.0	Lower bound for Fiber stretch to activate φ_{min}	-
τ_{coll}	6.0 days	Characteristic Time for Hydroxyproline Synthesis	-
Fiber Volume Fraction			
η	0.0024	Constant coefficient for the direct conversion of hydroxyproline concentration in to collagen volume fraction	-

analyzing λ_g . Experiments show that, the amount of static strain generated due to tissue compaction is in the order of 4% after four weeks [5]. Here, we assume that $\lambda_g - 1$ is an indicator variable for the static fiber strain generated by myofibroblasts. Although $\varphi_{max} = 100$ and $\tau_g = 2.5$ supply better λ_g estimations, the level of φ_{max} does not fulfill the collagen production criteria (Figure 4.5). For $\varphi_{max} = 100$, $\tau_g = 1.0$, the static stretch generated by the cellular activities reach to a level of nearly 15%, where the estimation has been improved to $\lambda_g - 1 \approx 8\%$, as being the final and satisfactory static stretch level in our simulations (Figure 4.11).

4.5.1 Evaluation of the experimental validation of the framework

In the second stage of the analysis τ_g has been set to 3.0 days. In this case, it can be seen from Figure 4.5 that the static strain levels do not depend on φ_{max} (also Figure 4.11). The effects of varying φ_{max} are shown in Figure 4.12. Our numerical tests prove the inexistence of the evidences for supporting the strong impact of the fiber anisotropy evolution. The evolution of the anisotropy ratio weakly couples with the mechanical rate of change. This is understandable since the statistical dispersion data obtained

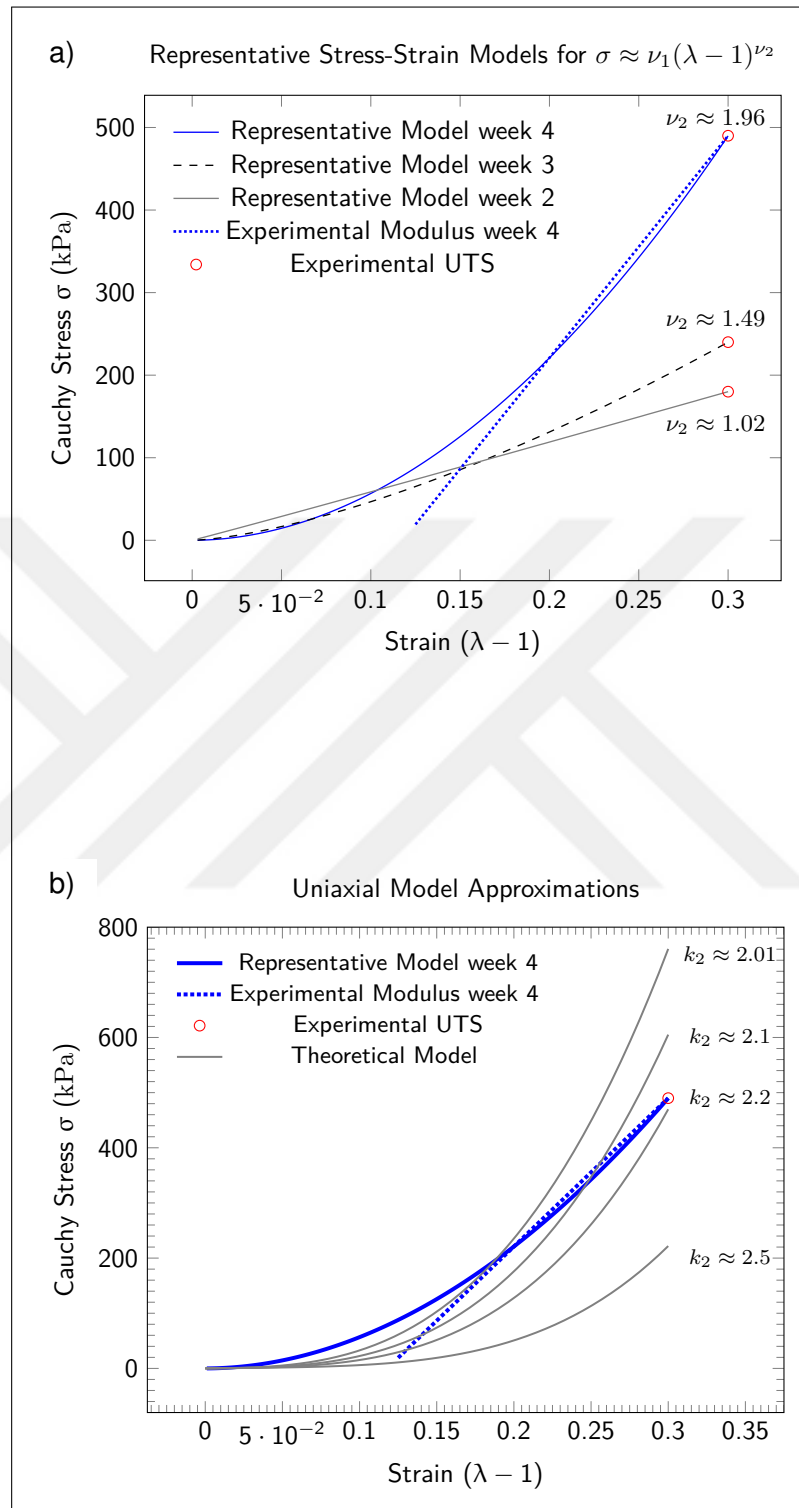


Figure 4.4: Representative True stress - Engineering strain curves for experimental UTS and modulus (a). The effect of the variation of anisotropic parameter k_2 compared with the layout of experimental UTS and modulus (b).

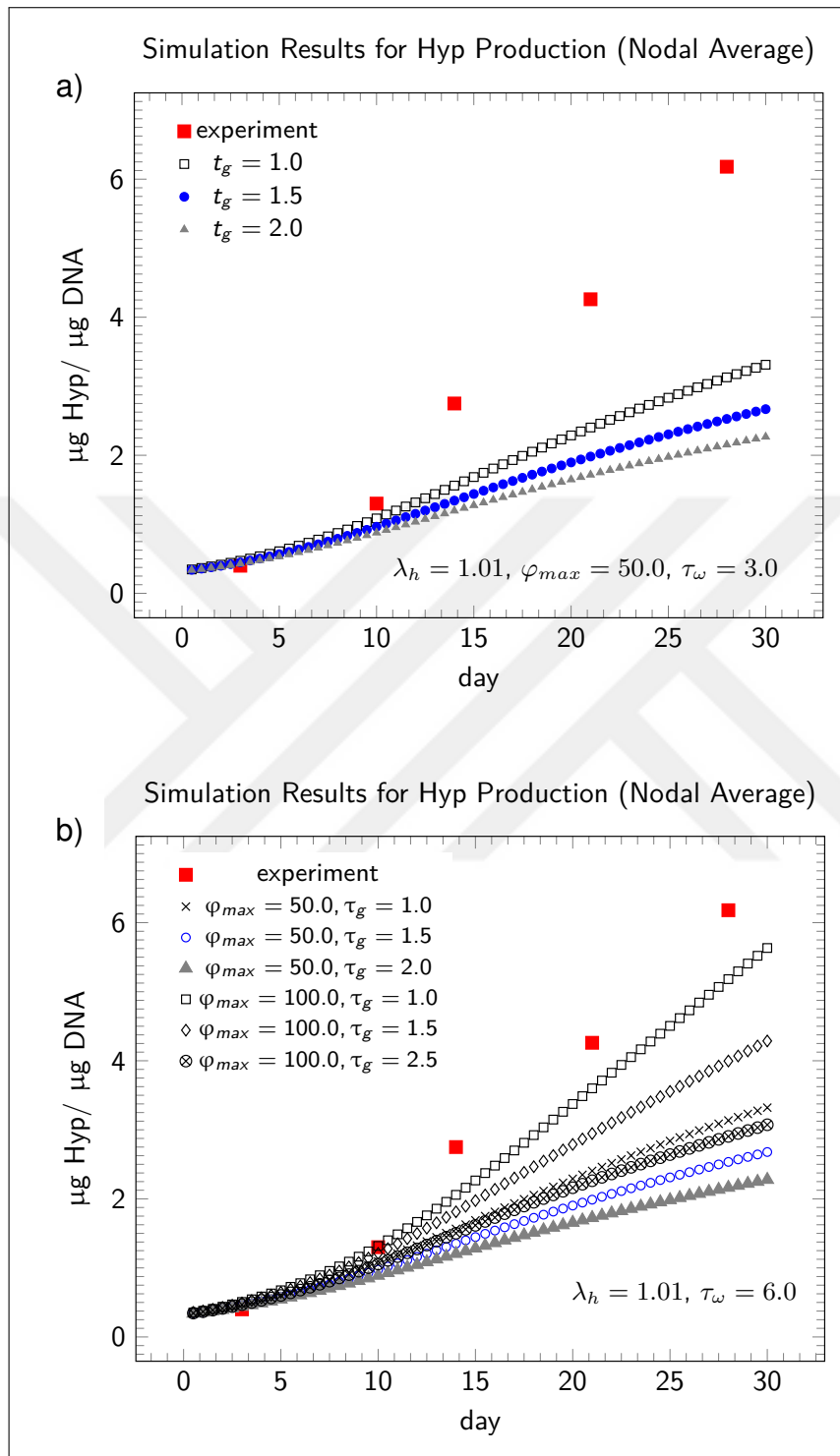


Figure 4.5: Simulation results for the hydroxyproline production. The effects of varying φ_{max} , τ_g and t_ω on the evolution of hydroxyproline concentration (a and b).

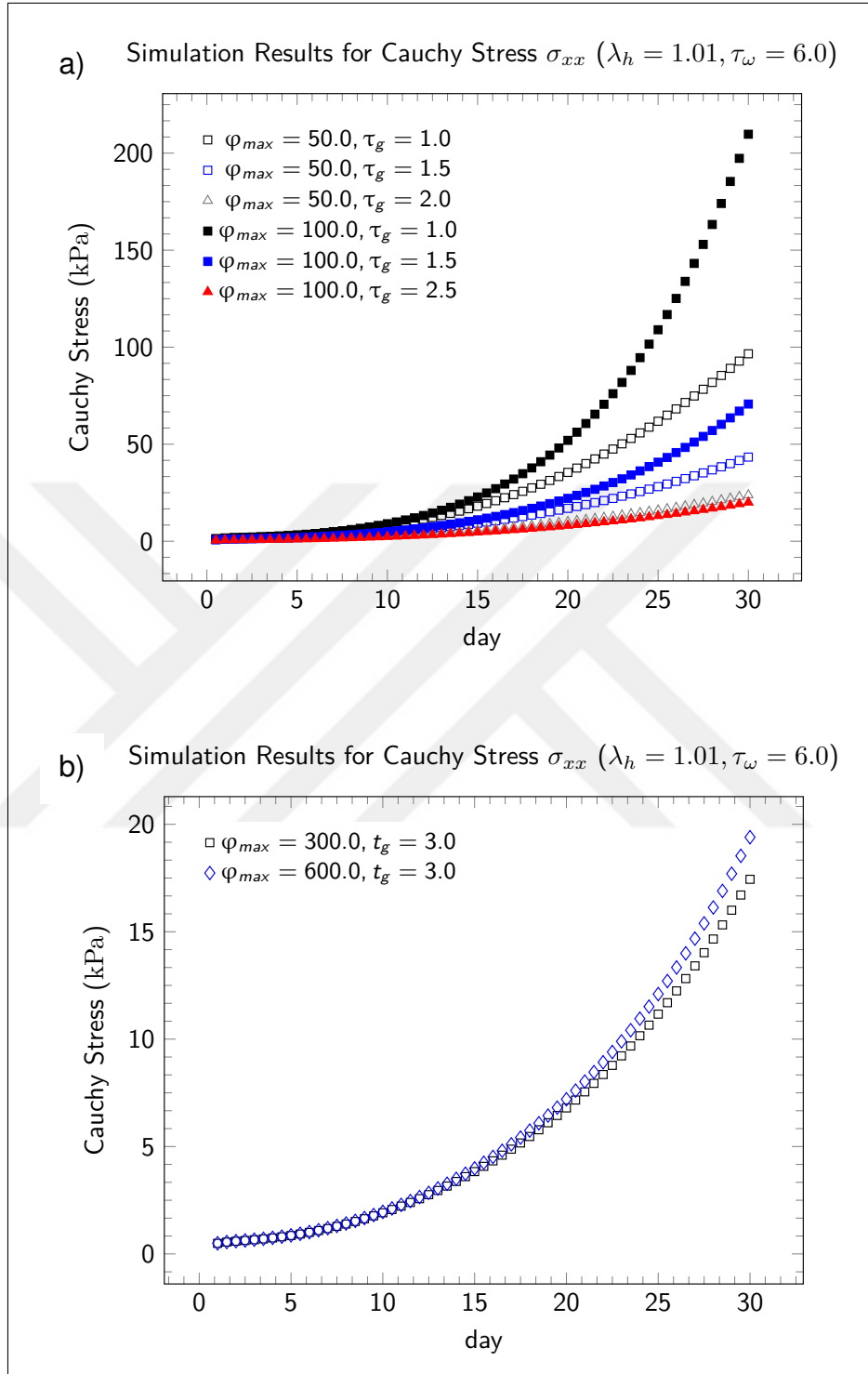


Figure 4.6: Simulation results for the Cauchy Stress σ_{xx} element. The effects of varying τ_g and φ_{max} on the evolution of stress measurements while λ_h and τ_ω are fixed (a). The effects of varying φ_{max} while φ_{max} τ_ω are fixed (b).

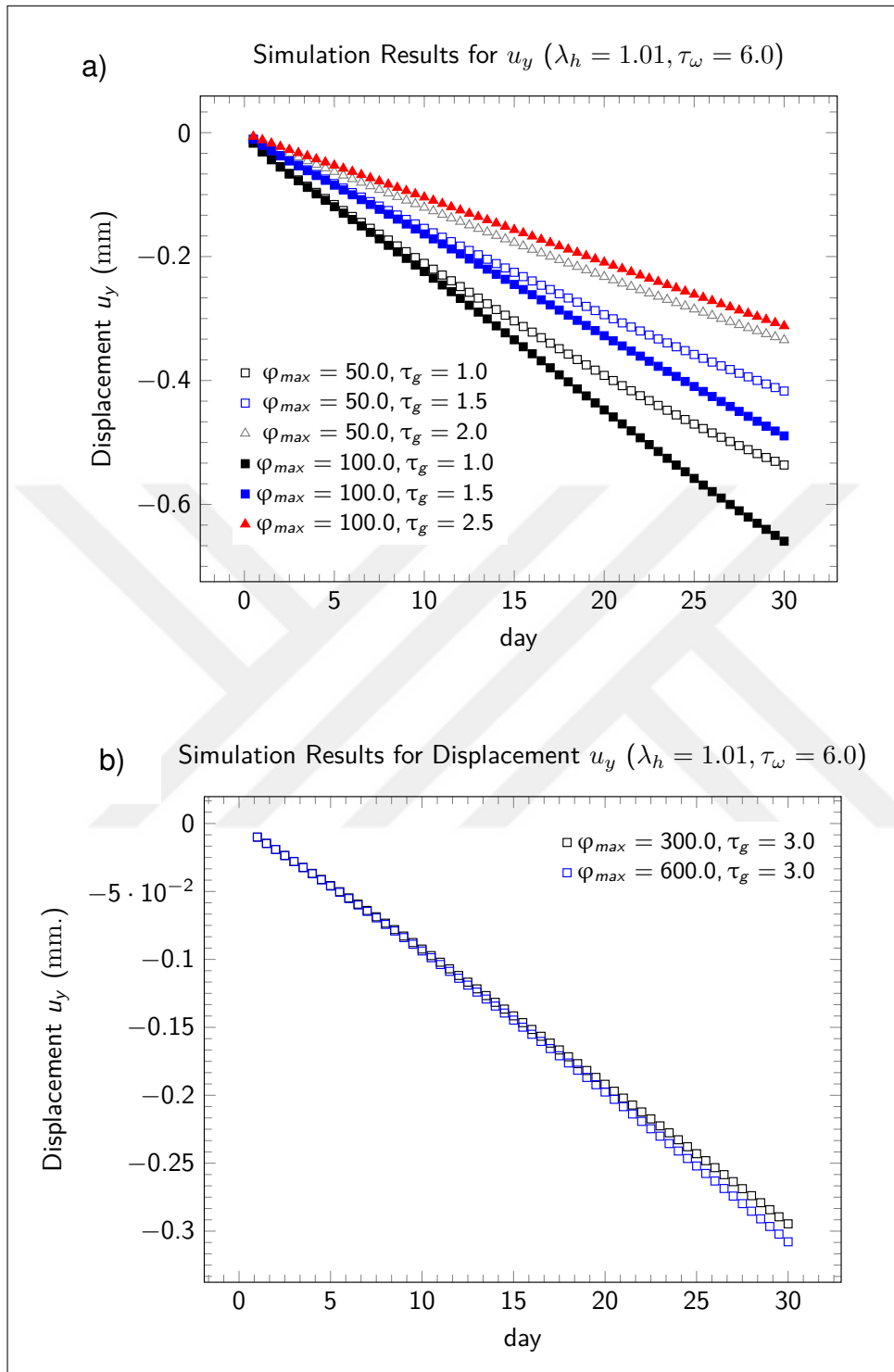


Figure 4.7: Simulation results for the Cauchy Stress u_y element. The effects of varying τ_g and φ_{max} on the evolution of displacement measurements while λ_h and τ_ω are fixed (a). The effects of varying φ_{max} while $\varphi_{max} \tau_\omega$ are fixed (b).

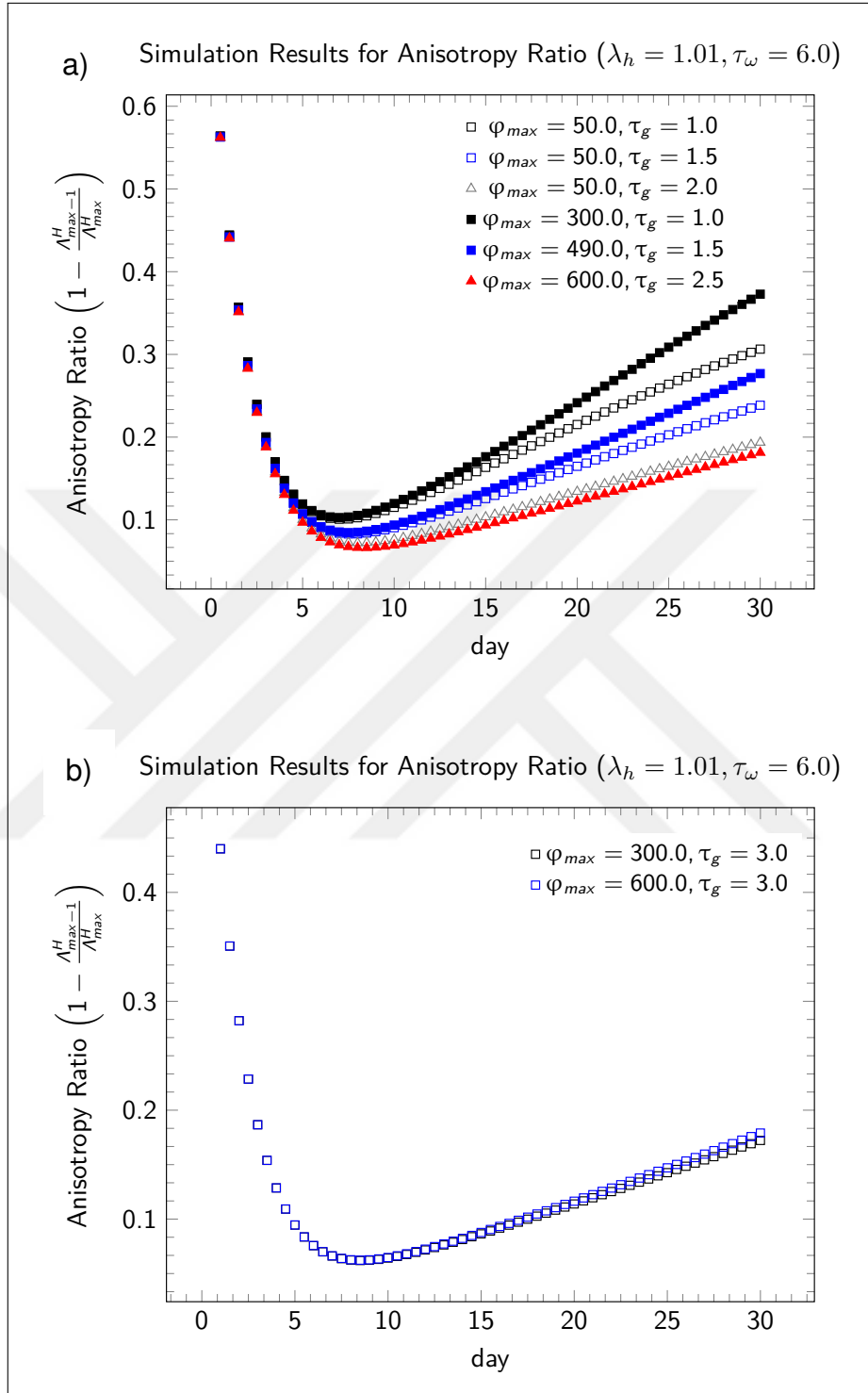


Figure 4.8: Simulation results for the anisotropy ratio $(1 - \Lambda_{max-1}^H / \Lambda_{max}^H)$. The effects of varying τ_g and φ_{max} on the evolution of anisotropy ratio while λ_h and τ_ω are fixed (a). The effects of varying φ_{max} while φ_{max} and τ_ω are fixed (b).

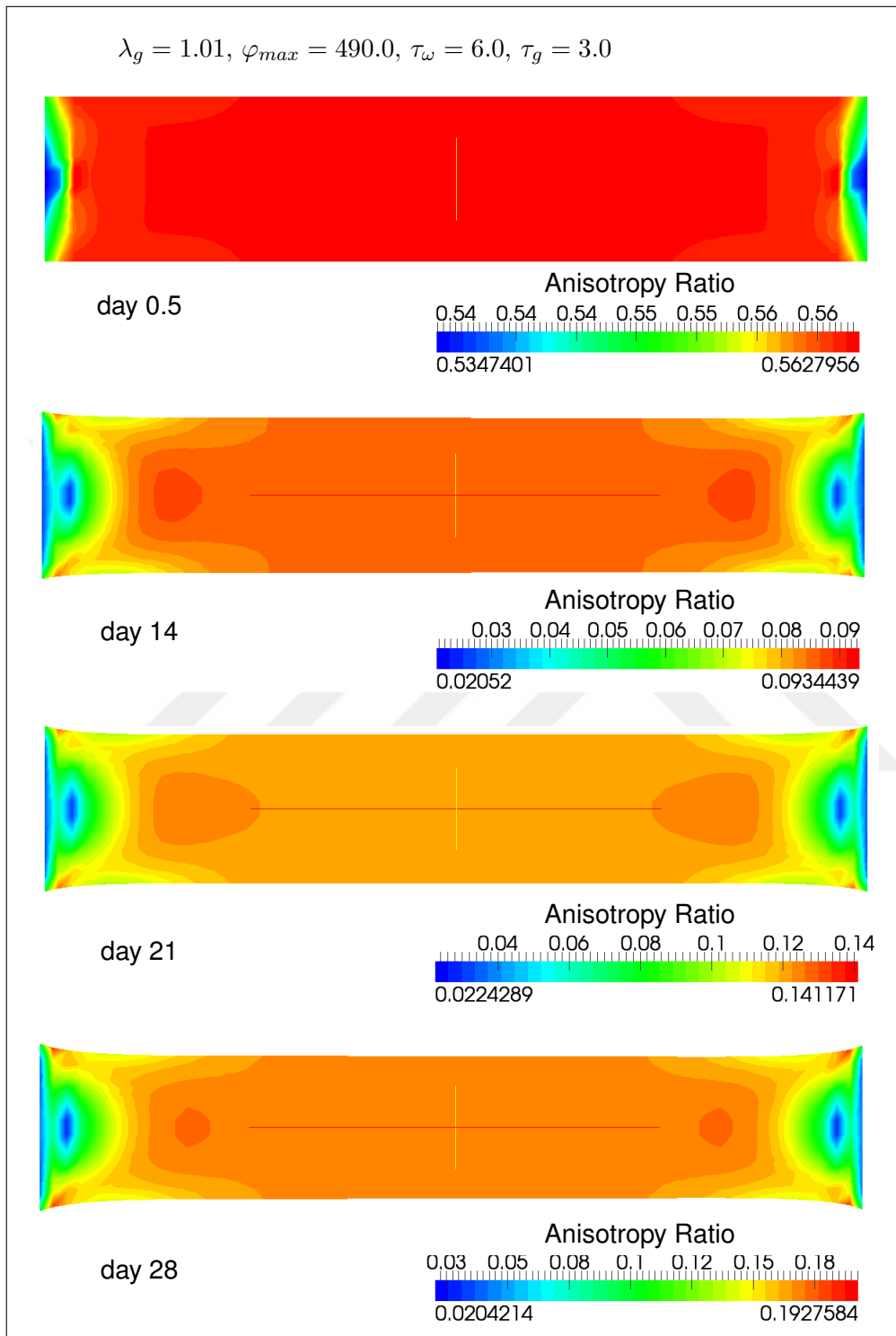
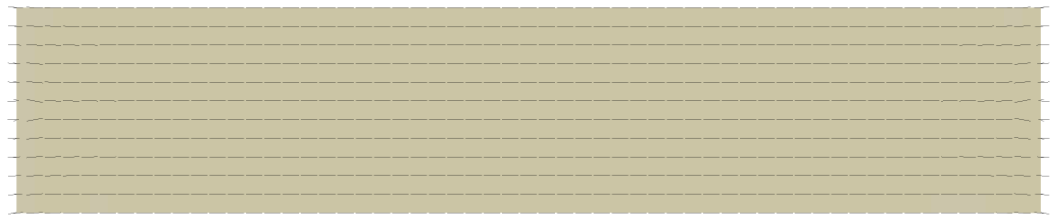


Figure 4.9: Simulation results for the evolution of the anisotropy ratio at days 0.5,14,21 and 28.

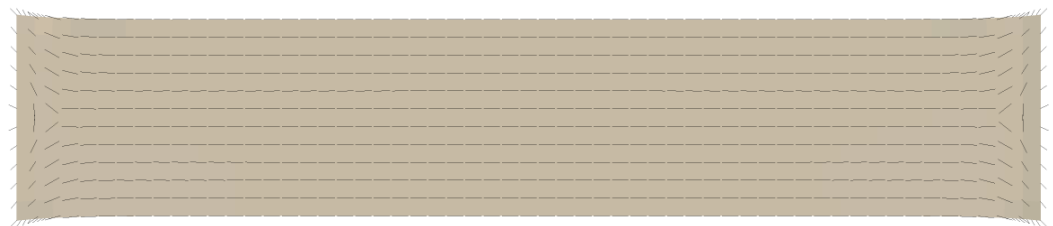
$$\lambda_g = 1.01, \varphi_{max} = 490.0, \tau_\omega = 6.0, \tau_g = 3.0$$



t=0.5



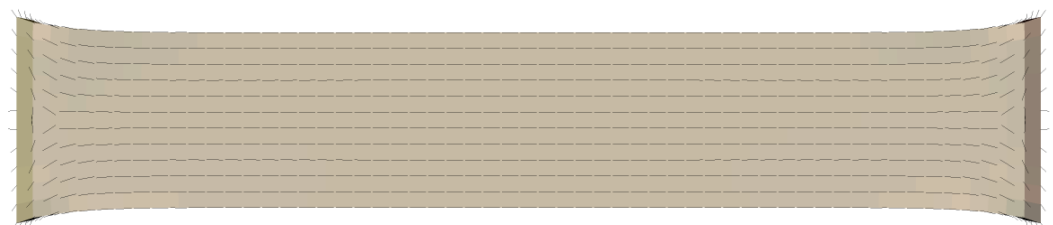
t=14



t=21



t=28



t=30

Figure 4.10: Simulation results for the evolution of mean fiber direction α_μ at days 0.5, 2, 10, 20 and 30.

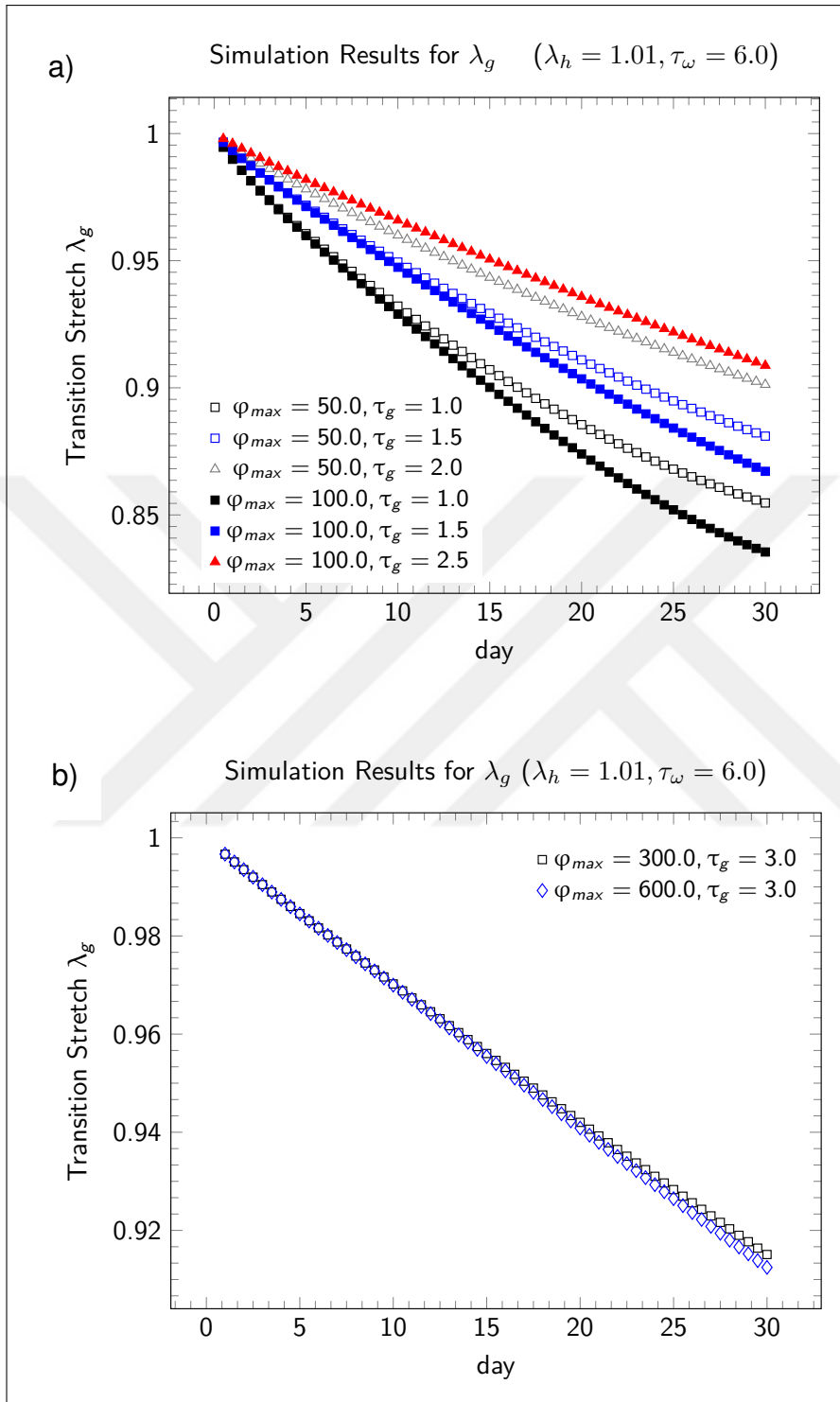


Figure 4.11: Simulation results for the transition stretch λ_g . The effects of varying τ_g and φ_{max} on the evolution of λ_g while λ_h and τ_ω are fixed (a). The effects of varying φ_{max} while τ_g and τ_ω are fixed (b).

Simulation Results for Hyp Production (Nodal Average)

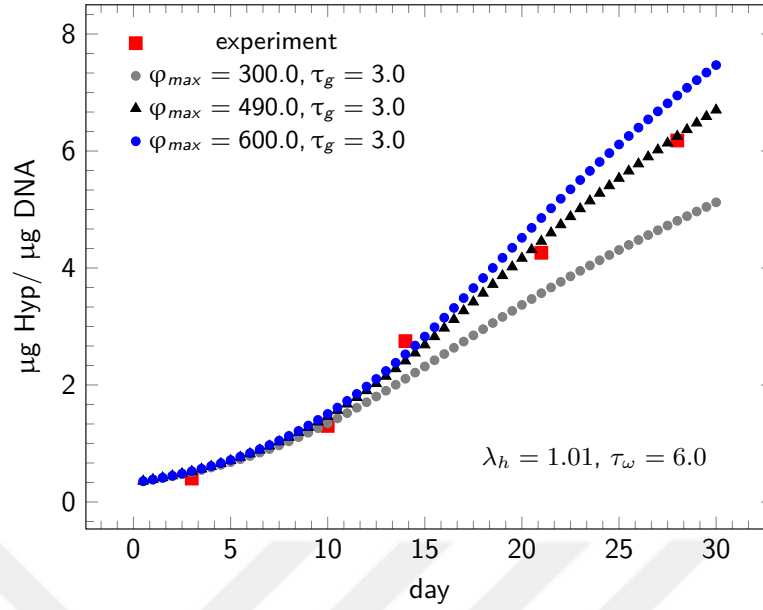


Figure 4.12: Experimental validation of the model framework in accordance with the hydroxyproline production. The model could explain the experimental data for $\varphi_{max} = 490$ and the parameters can be fine-tuned in order to obtain exact compaction levels.

from for this experimental design (constrained case) is so high preventing one from a meaningful analysis to describe the effects of fiber anisotropy. The predictions made by the simulations well describe the qualitative experimental features that are given in [14]. Hydroxyproline levels obtained from each simulation can be determined by changing the maximum concentration level, and an optimal level has been determined as $\varphi_{max} = 490$ supplying an optimal fitting for 4 weeks of evolution. We want to emphasize that the optimal parameters gave a very close description of not only the concentration itself but also the rate of change in it. We think that this predictability is highly related to the evolution function in equation 4.51, where its characteristic curvature is transferred to the predictions realized by the fine-tuning. Therefore, we came to a conclusion that the main effects have been reflected by the fiber strain (through τ_g) and target maximum level of the Hydroxyproline concentration, We could have been able to utilize their parametric tradeoff in order to satisfy an approximate level of compaction. The discussions of the results are given under the conclusion section.



5. A NOVEL FIBER REMODELING FORMULATION BASED ON LANGEVIN FORCE

5.1 Purpose

In previous chapter we have constructed a preliminary version of a probabilistic evolution framework. The algorithm has been shown to supply valid quantitative information extracted from the published experimental data. Also we have represented a sensitivity analysis on parameters. The bounds of the constitutive model parameters are determined by considering the experimental modulus and ultimate tensile stress data. We have validated the consistency of the whole algorithm by determining the optimal model parameters that explain a four-week evolution of the Hydroxyproline concentration in a fibrin gel experiment. In this section we extend and modify our approach in to its final form as an algorithmic scheme. The algorithmic scheme is computationally advantageous for inverse analysis and it is the first model in the literature that can extract the information coming from the random perturbations. First, we develop and modify the algorithm to its final form. Then we tried show the effects of Langevin force approach on the magnitudes of characteristic time evolution via analyzing a collagen scaffold based experiment. In a second numerical simulation, we see that a strain dependent evolution form supplies quantitative information close to experimental values.

5.2 Theoretical Framework

5.2.1 Essential kinematics and constitutive equations

Deformation from the undeformed initial configuration \mathcal{B}_0 to the deformed current configuration \mathcal{B}_t at time t is described by the one-to one mapping Π . Then, transformation (mapping) of the coordinates of material particles $\mathbf{X} \in \mathcal{B}_0 \subset \mathbb{E}^3$ to the spatial coordinates $\tilde{\mathbf{x}} \in \mathcal{B}_t \subset \mathbb{E}^3$ is represented by $\tilde{\mathbf{x}} = \Pi(\mathbf{X}, t)$.

The deformation gradient (\mathbf{F}) for this transformation is defined by $\mathbf{F}(\mathbf{X}) = \nabla \Pi = \partial \Pi(\mathbf{X}) / \partial \mathbf{X}$. Deformation will be considered as incompressible giving rise to the multiplicative decomposition of \mathbf{F} in to its spherical ($J^{1/3} \mathbf{I}$) and unimodular parts $\overline{\mathbf{F}}$, where $J = \det(\mathbf{F}) = 1$. The Cauchy-Green tensor which is based on the isochoric component $\overline{\mathbf{F}}$ is denoted by $\overline{\mathbf{C}}$ as

$$\mathbf{F} = J^{1/3} \overline{\mathbf{F}} \quad \overline{\mathbf{C}} = \overline{\mathbf{F}}^T \overline{\mathbf{F}}, \quad (5.1)$$

where J is the Jacobian of the mapping. The fibers are assumed to be embedded in an isotropic nonlinear hyperelastic matrix and their angular orientation is characterized by the reference unit vector defined on the surface of the unit sphere $\mathbb{S}^2 = (\mathbf{a} \in \mathfrak{R}^3, \|\mathbf{a}\| = 1)$. The deformation gradient maps the orientation from the material to the spatial configuration $\tilde{\mathbf{a}}$ by equation 5.2.

$$\lambda \tilde{\mathbf{a}} = \overline{\mathbf{F}} \mathbf{a} \quad \lambda = \sqrt{\mathbf{a}^T \overline{\mathbf{C}} \mathbf{a}}, \quad (5.2)$$

where λ is the fiber stretch associated with direction of \mathbf{a} . In material space, stretch λ defined in equation 5.2 is supposed to be applied on the current preferred direction of collagen orientation \mathbf{a} . For an anisotropic behavior of the material with statistically dispersed fiber orientations, we considered the definition of [22] based on the additive splitting of the strain energy density function in to its isotropic and anisotropic components originally described by [48]. In this case, the strain energy function including the isochoric and volumetric contributions for the dispersed structure can be defined as,

$$\begin{aligned} \psi(\mathbf{C}, \mathbf{H}_p) &= U(J) + \overline{\psi}_{iso}(\overline{\mathbf{C}}) \\ &+ \sum_{p=1}^{N_f} \overline{\psi}_{aniso}(\overline{\mathbf{C}}, \mathbf{H}_p(\mathbf{a}_\mu^{(p)}, \kappa_p)), \end{aligned} \quad (5.3)$$

in which \mathbf{H}_p is the p^{th} structural tensor of N_f fiber families with a mean orientation $\mathbf{a}_\mu^{(p)}$ and for a dispersion parameter κ_p . The volumetric contribution is related to the energy function $U(J)$. The symmetric generalized structural tensor \mathbf{H} is defined as a function of the orientation density $\rho(\mathbf{a}) = \rho(-\mathbf{a})$ integrated over the surface of the unit sphere $\Omega(\Theta, \Phi) \in \mathbb{S}^2$, where $\Theta \in (0, \pi)$, $\Phi \in (0, 2\pi)$. κ lies on the interval $\kappa \in [0, 1/3]$ when $\mathbf{a} \in \mathfrak{R}^3$ and

$$\mathbf{H} = \frac{1}{4\pi} \int_{\mathbb{S}^2} \rho(\mathbf{a}(\Theta, \Phi)) \mathbf{a}(\Theta, \Phi) \otimes \mathbf{a}(\Theta, \Phi) dS. \quad (5.4)$$

In equation 5.4, $\boldsymbol{\alpha}(\Theta, \Phi) = \sin \Theta \cos \Phi \mathbf{e}_1 + \sin \Theta \sin \Phi \mathbf{e}_2 + \cos \Theta \mathbf{e}_3$ is defined in terms of Eulerian angles where $\mathbf{e}_{1,2,3}$ are the Cartesian bases. Thus, $[\mathbf{H}]_{k,l} = b_{k,l} \mathbf{e}_k \otimes \mathbf{e}_l$ for some $b_{k,l}$ define the orientation-based average quantities. The explicit mathematical form of the total potential can be determined as a function of the Green-Lagrange strain-like quantity $\bar{\mathbf{E}} = \mathbf{H} : \bar{\mathbf{C}} - 1$. In order to prevent initial strains in the undeformed initial configuration, $\text{tr}(\mathbf{H}) = 1$ should be satisfied. In three dimensions, this constraint is unconditionally satisfied for $0 \leq \kappa \leq 1/3$. For a number of p fiber families, without considering volume fractions, the isochoric overall strain energy is defined by,

$$\bar{\psi}(\bar{\mathbf{C}}, \mathbf{H}_p) = \bar{\psi}_{iso}(\bar{\mathbf{C}}) + \sum_{p=1}^N \mathcal{H}(\bar{E}_p) \bar{\psi}_{aniso}(\bar{\mathbf{C}}, \mathbf{H}_p, \boldsymbol{\nu}), \quad (5.5)$$

where $\boldsymbol{\nu} = (c, k_1, k_2)$ represents the set of material parameters and $\bar{E}_p = \mathbf{H}_p : \bar{\mathbf{C}} - 1$. For incompressible materials,

$$\bar{\psi}_{iso} = \frac{c}{2} (\text{tr}(\bar{\mathbf{C}}) - 3), \quad (5.6)$$

$$\bar{\psi}_{aniso} = \frac{k_1}{k_2} (\exp(k_2 \bar{E}_p^2) - 1), \quad (5.7)$$

$\bar{\psi}_{aniso}$ is the ‘‘isochoric-anisotropic’’ fiber potential activated by the Heaviside step function \mathcal{H} , whereas $\bar{\psi}_{iso}$ is the ‘‘isochoric-isotropic’’ potential ([22, 24]). It is possible to define the equations via invariant definition. $\mathcal{I}_4^* = \mathbf{H} : \bar{\mathbf{C}}$ is an invariant of $\bar{\mathbf{C}}$. The first derivative of the scalar function $\bar{\psi}_{aniso}(\mathcal{I}_4^*(\bar{\mathbf{C}}, \mathbf{H}))$ of \mathcal{I}_4^* , $\mathbf{H} \in \mathfrak{R}^{M \times M}$, with respect to $\bar{\mathbf{C}}$ is given by,

$$\frac{\partial \bar{\psi}_{aniso}(\mathcal{I}_4^*(\bar{\mathbf{C}}, \mathbf{H}))}{\partial \bar{\mathbf{C}}} = \frac{\partial \bar{\psi}_{aniso}(\mathcal{I}_4^*(\bar{\mathbf{C}}, \mathbf{H}))}{\partial \mathcal{I}_4^*} \mathbf{H}. \quad (5.8)$$

Here we define M as the spatial dimension of a problem in Cartesian/Cylindrical coordinate systems. The identity in equation 5.8 can be utilized to obtain the second order Cauchy stress tensor ($\boldsymbol{\sigma}$),

$$\boldsymbol{\sigma} = \boldsymbol{\sigma}_{vol} + \mathbb{P} : (\bar{\boldsymbol{\sigma}}_{iso} + \bar{\boldsymbol{\sigma}}_{aniso}), \quad (5.9)$$

$$\boldsymbol{\sigma}_{vol} = -p_h \mathbf{I}, \quad (5.10)$$

$$\bar{\boldsymbol{\sigma}}_{iso} = J^{-1} c \bar{\mathbf{F}} \bar{\mathbf{F}}^T, \quad (5.11)$$

$$\bar{\boldsymbol{\sigma}}_{aniso} = J^{-1} \bar{\mathbf{F}} \left(2 \frac{\partial \bar{\psi}_{aniso}(\mathcal{I}_4^*(\bar{\mathbf{C}}, \mathbf{H}))}{\partial \bar{\mathbf{C}}} \right) \bar{\mathbf{F}}^T, \quad (5.12)$$

$$\bar{\boldsymbol{\sigma}}_{aniso} = 2J^{-1} k_1(\bar{E}) \exp(k_2 \bar{E}^2) \bar{\mathbf{F}} \mathbf{H} \bar{\mathbf{F}}^T,$$

where p_h is the hydrostatic pressure to be determined. The Eulerian projection operator \mathbb{P} in equation 5.9 is defined as

$$\mathbb{P} = \mathbb{I} - \frac{1}{3} \mathbf{I} \otimes \mathbf{I}, \quad (5.13)$$

where \mathbb{I} is the fourth-order and \mathbf{I} is the second order identity tensors. The projection operator is required for incompressible materials to ensure that the constraint $[\mathbb{P} : (\cdot)] : \mathbf{I} = 0$ (see [22]).

Equation 5.12 has the short mathematical form showing that the stress can be represented as the product of a scalar with the generalized structure tensor. The implication points that the stress evolution corresponding to the anisotropic remodeling depends directly on the evolution of \mathbf{H} . The convexity of a potential for arbitrary functional forms of ψ is important. For the polynomial type potentials with similar considerations, convexity has been investigated by [24].

5.2.2 A locally linear fiber remodeling formulation based on a Langevin force

The remodeling process includes a deterministic driving force which drifts the overall mechanism towards a mechanically governed direction. The microscopic description of a stochastic dynamics disturbed by a random Langevin force including a deterministic drift term can be represented by the *Langevin Equation*. A general form of the nonlinear Langevin equation for an M -dimensional state vector $\boldsymbol{\xi}$ variable is given by ([50, 51]),

$$\frac{d \boldsymbol{\xi}(t)}{dt} = \mathbf{h}(\boldsymbol{\xi}(t), t) + \mathbf{G}(\boldsymbol{\xi}(t), t) \boldsymbol{\Gamma}(t), \quad (5.14)$$

where $\boldsymbol{\xi} = \boldsymbol{\xi}(t)$ for $\boldsymbol{\xi} \in \mathfrak{R}^M$ is a stochastic variable and $\mathbf{h}(\boldsymbol{\xi}, t) : \mathfrak{R}^M \rightarrow \mathfrak{R}^M$, and $\mathbf{G}(\boldsymbol{\xi}, t) \in \mathfrak{R}^{M \times M}$ are drift and diffusion terms consecutively. $\boldsymbol{\Gamma}(t) \in \mathfrak{R}^M$ is the random Langevin force and its components are assumed to be of Gaussian type with zero mean and δ -correlation having the following properties

$$\langle \Gamma_k(t) \rangle = 0, \quad \text{and} \quad \langle \Gamma_l(t) \Gamma_k(t') \rangle = \delta_{lk} \delta(t - t'). \quad (5.15)$$

The evolution of $\boldsymbol{\xi}$ depends on the applied random force $\boldsymbol{\Gamma}(t)$ where $\mathbf{G}(\boldsymbol{\xi})$ determines the magnitude and the rotation of this random force vector.

To obtain the microscopic description of the time dependent remodeling of collagen orientation, we used the heuristic derivation approach explained by [50]. Since the

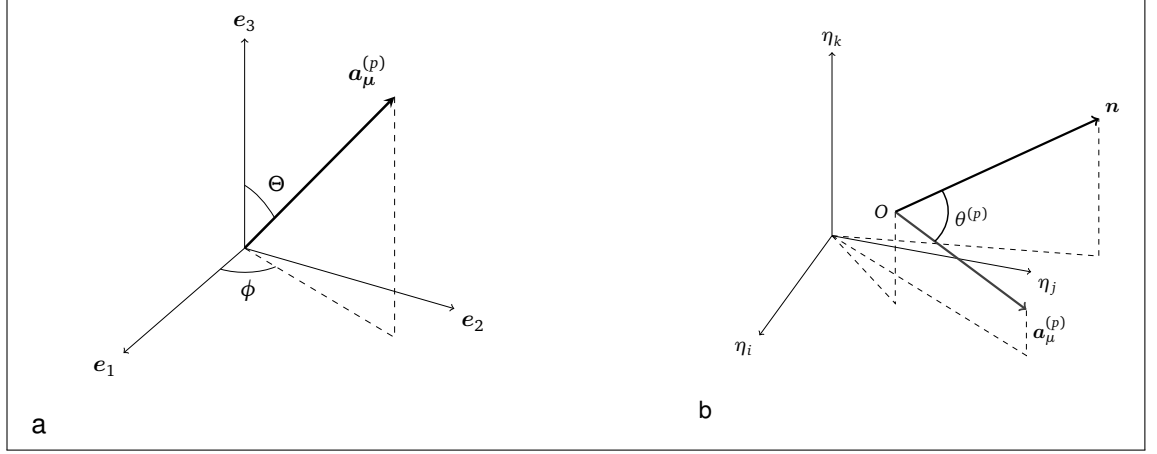


Figure 5.1: (a) Statistical mean vector \mathbf{a}_μ of dispersed fiber bundle family in spherical parameterization $\mathbf{a}_\mu = \mathbf{a}_\mu(\Theta, \phi)$ according to the Cartesian basis $(\mathbf{e}_1, \mathbf{e}_2, \mathbf{e}_3)$ on reference configuration. (b) Rotation path of p^{th} fiber cluster accumulated \mathbf{a}_μ towards its desired homeostatic position vector \mathbf{n} , where $\cos^{-1}(\mathbf{a}_\mu \cdot \mathbf{n}) = \theta^{(p)}$ and $\theta^{(p)} < \pi/2$, according to arbitrary orthogonal basis (η_i, η_j, η_k) .

remodeling process outcomes with the observed statistical quantities are represented by probability distributions, the probability distribution of collagen orientations can be obtained by investigating the effects of a microscopic Langevin force on the drifting mechanism. Eventually, we have a microscopic definition of the remodeling process driven by the deterministic drift (h). The functional form of h is $h : \mathfrak{R}^M \rightarrow \mathfrak{R}^M$, $h = h(\mathbf{a}, \mathbf{C}, t)$. $\mathbf{a} \in \mathfrak{R}^M$ can be selected to give the rate of rotation as described by [44],

$$h(\mathbf{a}, \mathbf{C}, t) = f(\mathbf{a}, \Lambda_{max}^{\mathbf{C}}) (\mathbf{I} - \mathbf{a} \otimes \mathbf{a}) \mathbf{n}_{max}^{\mathbf{C}}, \quad (5.16)$$

where f is a scalar function and $\Lambda_i^{\mathbf{C}}$ is the i^{th} eigenvalue of \mathbf{C} corresponding to the eigenvector $\mathbf{n}_i^{\mathbf{C}}$. Then, an initial attempt for the probabilistic evolution of \mathbf{a} can be made in Cartesian coordinates as in equation 5.17. Here, the random perturbation $\mathbf{G}(\mathbf{a}(t), t)$ $\mathbf{\Gamma}(t)$ can be applied in Cartesian or spherical coordinates through appropriate transformations.

$$\frac{d\mathbf{a}(t)}{dt} = f(\mathbf{a}, \mathbf{C}) (\mathbf{I} - \mathbf{a} \otimes \mathbf{a}) \mathbf{n}_{max}^{\mathbf{C}} + \mathbf{G}(\mathbf{a}(t), t) \mathbf{\Gamma}(t), \quad (5.17)$$

The dimension of the problem can be reduced via the determination of the evolution of a single angular parameter $\theta^{(p)}$ where the p^{th} dispersed fiber bundle rotates towards a homeostatic position vector \mathbf{n} (Figure 5.1). Additionally, Figure 5.1a gives the statistical mean vector \mathbf{a}_μ of a dispersed fiber bundle family in the spherical parameterization $\mathbf{a}_\mu = \mathbf{a}_\mu(\Theta, \phi)$ according to the Cartesian basis $(\mathbf{e}_1, \mathbf{e}_2, \mathbf{e}_3)$ on the

reference configuration. Figure 5.1b illustrates the rotation path of the p^{th} fiber cluster accumulated around \mathbf{a}_μ towards its desired homeostatic position vector \mathbf{n} . Here, $\cos^{-1}(\mathbf{a}_\mu \cdot \mathbf{n}) = \theta^{(p)}$ and $\theta^{(p)} < \pi/2$, are based on an arbitrary orthogonal basis (η_i, η_j, η_k) .

Instead of computing the rotation in Cartesian coordinates, the evolution of a mean angular measurement $\theta^{(p)}$ of the p^{th} fiber bundle supplies information about the infinitesimal rotation increment $\Delta \theta^{(p)}$ which should be followed by an update procedure utilizing the Rodriguez rotation (equation 5.18) ([62]),

$$\begin{aligned} \mathbf{a}_\mu(t + \Delta t) &= \mathbf{a}_\mu(t) \cos(\Delta\theta^{(p)}) \\ &+ (\boldsymbol{\omega} \times \mathbf{a}_\mu(t)) \sin(\Delta\theta^{(p)}) \\ &+ \boldsymbol{\omega}(\boldsymbol{\omega} \cdot \mathbf{a}_\mu(t))(1 - \cos(\Delta\theta^{(p)})), \end{aligned} \quad (5.18)$$

where $\boldsymbol{\omega}$ is a unit vector describing the axis of rotation. The rotation around $\boldsymbol{\omega}$ is considered as a damped motion towards the steady state position. Usually, the governing drift function \mathbf{h} in equation 5.14 has a trigonometric character, ([44, 63]). The probabilistic evolution equation can be given by,

$$\frac{d \boldsymbol{\theta}(t)}{dt} = -\tau^{-1} \sin(\boldsymbol{\theta}(t)) + \mathbf{G}(\boldsymbol{\theta}(t), t) \boldsymbol{\Gamma}(t), \quad (5.19)$$

$$\mathbf{h}(\boldsymbol{\theta}, t) = -\tau^{-1} \sin(\boldsymbol{\theta}(t)), \quad (5.20)$$

where $\boldsymbol{\theta} = (\theta^{(1)}, \dots, \theta^{(p)}, \dots, \theta^{(M)})^T$ is the vector of angular measurements of rotating individual fiber bundles with their own random perturbation vector $\mathbf{G}(\boldsymbol{\theta}(t), t) \boldsymbol{\Gamma}(t)$, $\tau^{-1} \in \mathfrak{R}^+$, and $\sin(\boldsymbol{\theta}) = (\sin(\theta^{(1)}), \dots, \sin(\theta^{(p)}), \dots, \sin(\theta^{(M)}))^T$. Later we will show that, it is possible to represent the time dependent evolution of \mathbf{H} through equation 5.19. Integrating over a unit sphere to calculate the overall effects of individual fibers has been recently used in many studies ([19, 30, 47, 27]). However, we focused, in this study, on the homogenized average effects of the process by directly computing the evolving first and second moments of the probability distribution $\rho(\mathbf{a})$. For transversally isotropic fiber orientation distributions, $\rho(\mathbf{a})$ depends only on θ , where $\rho(\mathbf{a}) = \rho(\theta)$. It may be worth considering more complex distributional schemes, however they are supposed to include mathematical derivations similar to the transverse case. Derivation of the new remodeling algorithm and the $\kappa - s$ function are presented in Appendices.

5.2.3 Interpretation of the functional forms of drift and diffusion terms

For small angular measurements $\theta \ll \pi/4$, the drift function can be selected as $h(\theta(t)) \approx -\tau^{-1}\theta(t)$ which is the Ornstein-Uhlenbeck process for $\tau^{-1} < 1$,

$$\frac{d\theta(t)}{dt} = -\tau^{-1}\theta + \Sigma\Gamma(t). \quad (5.21)$$

As mentioned in the introduction, it should be emphasized that the first term of the right hand side in equation 5.21 is well settled in the literature and the linear assumption has also given satisfactory results in our experimental analysis. On the other hand, the second diffusive term of the equation has not been widely investigated and usually mechanical stimulus postulations made by [20] have been adopted by other researchers.

From a modeling point view, selection of the basic stimulus of fiber remodeling does not change its mathematical description much. It is expected that the “long term” remodeling of the structure, which is in balance with the external mechanical conditions, starts the variation in physical characteristics of fibers. Computation of the maximum principal stresses/strains and the hypothesization that the collagen fibers will align along the related direction, are considered to be meaningful assumptions. Therefore, the elongation of principal direction and relative position of fibers to that direction have been common in many modeling perspectives. The main difference is the equations that are used to determine the rate of the process. For example, the remodeling rate can be linked to the strain rate formulation ([19]) for gels. On the other hand, since macroscopic living structures, such as artery, have very complex dynamics at every measurement scale, phenomenological approaches are much more widely used for the remodeling rate. In this case, strain or stress dependent formulations are almost the same and they both use the principal direction of related mechanical tensors (see [20] and [4]). The *reductionism* as a philosophical motivation could also lead the current studies towards much more complex models, where every individual model of specific length scales is linked to a single multi-scale mechanism. We did not follow such a reductionist approach in this work and took variables as global determiners, such as the diffusion mechanism and its parameters (for some discussions about mechanistic approaches, see [9]).

According to the hypothesis, the magnitude of a mechanical stimulus is governed by the ratio of first two eigenvalues $\sigma_{1,2}$ of the stress tensor $\boldsymbol{\sigma}$ in spatial configuration. The eigenvalues satisfy the inequality $\sigma_1 \geq \sigma_2 \geq \sigma_3$ for $\boldsymbol{\sigma} \in \mathfrak{R}^{3 \times 3}$. Additionally, the mean fiber orientation moves towards a position in between the two corresponding eigenvectors weighted by the principal stresses. These assumptions give satisfactory experimental results in systems with active collagen fiber dynamics (see [64] and [46]). We follow the same postulation in [46] satisfying the stimulus assumptions in [46] and [20] that governs κ to see whether the diffusive component Σ has a functional form or not. According to [46], the homeostatic value of $\kappa \in [0, 1/3]$ is a linear function of the principal stress ratio $\sigma_2/\sigma_1 \in [0, 1]$. Hence, it is natural to approximate the functional form of Σ , that satisfies the linear relationship through evaluating the asymptotic prediction of κ , by using the proposed scheme when $t \rightarrow \infty$. The results should give a linear relationship in σ_2/σ_1 . The final standard deviation of the process depends on the external mechanical stimulus σ_2/σ_1 . We consider the limiting case, where $\lim_{t \rightarrow \infty} s(t) = \Sigma(\sigma_2/\sigma_1)/\sqrt{2\tau^{-1}}$ is estimated by equation 5.21. Considering the $\hat{\kappa}$ function in Table A.1, $\Sigma(\sigma_2/\sigma_1)$ can be approximated by the polynomial model with coefficients a_i, b_i as,

$$\hat{\kappa} \left(\Sigma \left(\frac{\sigma_2}{\sigma_1}, \tau^{-1} \right), \tau^{-1} \right) = c_0 \chi_{CDF}^2 \left(c_1 \left(\Sigma / \sqrt{2\tau^{-1}} \right)^{c_2}, \nu \right), \quad (5.22)$$

where we used the approximation for Σ in equation 5.21 as

$$\Sigma \left(\frac{\sigma_2}{\sigma_1}, \tau^{-1} \right) \approx 2\pi \sqrt{2\tau^{-1}} \sum_{i=0}^2 a_i \left(\frac{\sigma_2}{\sigma_1} \right)^{b_i} + \epsilon. \quad (5.23)$$

To remove the dependency on the parameter $\sqrt{2\tau^{-1}}$ (τ is the remodeling constant), the same term is added as a multiplier in equation 5.23, thus $\hat{\kappa}$ is a function of mechanical stimulus,

$$\hat{\kappa} \left(\frac{\sigma_2}{\sigma_1} \right) = c_0 \chi_{CDF}^2 \left(c_1 \left(2\pi \sum_{i=0}^n a_i \left(\frac{\sigma_2}{\sigma_1} \right)^{b_i} \right)^{c_2}, \nu \right). \quad (5.24)$$

Approximation yields an absolute error of $\max(|\epsilon|) < 4.0 \times 10^{-3}$, with the coefficients: $a_0 = 0.13084$, $a_1 = 0.13710$, $a_2 = 0.18333$, $b_0 = 2.8099$, $b_1 = 16.17847$, $b_2 = 0.49707$. With this approximation, we complete our explanation on the relationship between mechanical stimulus and random Langevin force, depending on the assumptions made in [46] and [20].

5.2.4 Comparison of the proposed algorithm with existing modeling approaches

In this section, we present some analytical results to give a better understanding of the proposed scheme compared to other approaches.

5.2.4.1 Ornstein-Uhlenbeck interpretation of the evolution of statistical dispersion

Since few analytical solutions of a closed form for probability distributions exist, our investigation is limited to the linear Langevin equation instead of the nonlinear one. We consider the same form given in equation 5.21, and then we simplify the approximations to the evolution of fiber mean and dispersion. In the one dimensional case, analytical update equations A.12 and A.13 reduce to first order differential equations for a single fiber family, that is,

$$\dot{\theta}_\mu(t) = -\tau^{-1} \theta_\mu(t), \quad (5.25)$$

$$\dot{V}(t) = -2\tau^{-1} V(t) + \Sigma, \quad (5.26)$$

where again τ^{-1} and Σ are constants. It should be noted that equations A.12-A.13 show continuous representations of the stochastic evolutions, which intrinsically assumes the evolution of infinitely many number of fiber directions affected by random perturbations. Each fiber direction evolves according to the Langevin equation. The initial conditions $IC(\theta)$ for all fiber directions are again infinite dimensional, which can only be given by their probability distribution $IC(\theta(t')) \sim \mathcal{N}(\theta_\mu(t'), s^2(t'))$ at time t' . The analytical solutions to the equations 5.25 and 5.26 for an initial mean $\theta_\mu(t')$ and initial variance $V(t')$ are given by,

$$\theta_\mu(t) = e^{-\tau^{-1}(t-t')} \theta_\mu(t'), \quad (5.27)$$

$$V(t) = e^{-2\tau^{-1}(t-t')} V(t') + \frac{\Sigma^2}{2\tau^{-1}} (1 - e^{-2\tau^{-1}(t-t')}). \quad (5.28)$$

In the literature, initial conditions are set according to a *continuous Markov process* where the evolution of a probability distribution $Pr(\theta_\mu(t), V(t))$ between time steps (states) are given by Chapman-Kolmogorov equation,

$$Pr(\theta, t) = \int_{-\infty}^{\infty} \widetilde{Pr}(\theta, t|\theta', t') Pr(\theta', t') d\theta'. \quad (5.29)$$

Here, $\widetilde{Pr}(\theta, t|\theta', t')$ is the normal transition probability density function from state t' to t . Equations A.12 and A.13 are the evolution equations for mean and variance

functions belonging to the transition density, not the probability density itself. However, for an *Ornstein-Uhlenbeck process* defined by equation 5.21, it can be shown that the analytical solutions in equations 5.27,5.28 are identical to the evolution pattern obtained by taking the integration in equation 5.29.

The evolution of a mean fiber direction and fiber dispersion has different characteristic evolution equations. The difference should be evaluated as an evidence for the existence of a randomly perturbed feedback, whereas many algorithms in the literature suppose that mean and dispersion as identical physical phenomena obey the same physical characteristics (such as orientation time), in fact they obey physical constraints forced by equations 5.25-5.26. If there is such an evolution of mentioned feedback type, then the experimental observations are expected to exhibit a certain ratio between the characteristic remodeling time of a mean orientation and dispersion. In order to understand whether the model proposed here has better qualitative and quantitative features or not compared to algorithms in the literature, two remodeling approaches are compared based on the experimental data. The equality of remodeling speeds are proposed by [64] and based on the same assumption, [46] predicted the collagen fibril organization on a cornea-scleral region.

We have worked on two kinds of data: one is the mean orientation measurement θ_μ of either cell (θ_μ^{cell}) or collagen fiber alignment (θ_μ^{coll}), and second is the dispersion measurement in terms of the *mean vector lengths* ρ^{cell} and ρ^{coll} . The mean vector length (ρ) measurements are the deviation statistics for the circular wrapped normal distribution. Thus, ρ should be transformed to the standard deviation s of a normal distribution by using the identity $\rho = \exp(-s^2/2)$ proposed by [65]. The corresponding evolution equation for $\rho(t)$ yields,

$$\rho(t) = \exp \left(-\frac{1}{2} (e^{-(\tau_s)^{-1}(t-t')} V(t') + \Sigma^2 \tau_s (1 - e^{-(\tau_s)^{-1}(t-t')})) \right), \quad (5.30)$$

where $\tau^{-1} = 2/\tau_\mu$ and τ_s is the characteristic remodeling time for dispersion, $\tau_s = \tau_\mu/2$.

To analyze the characteristic remodeling times for mean and variance evolution of the collagen fiber distribution in cellular scale, we have tried to estimate the model parameters on experimental data. The collagen and cellular orientation data are gathered from [11], which focuses directly on the evolution of a cellular orientation

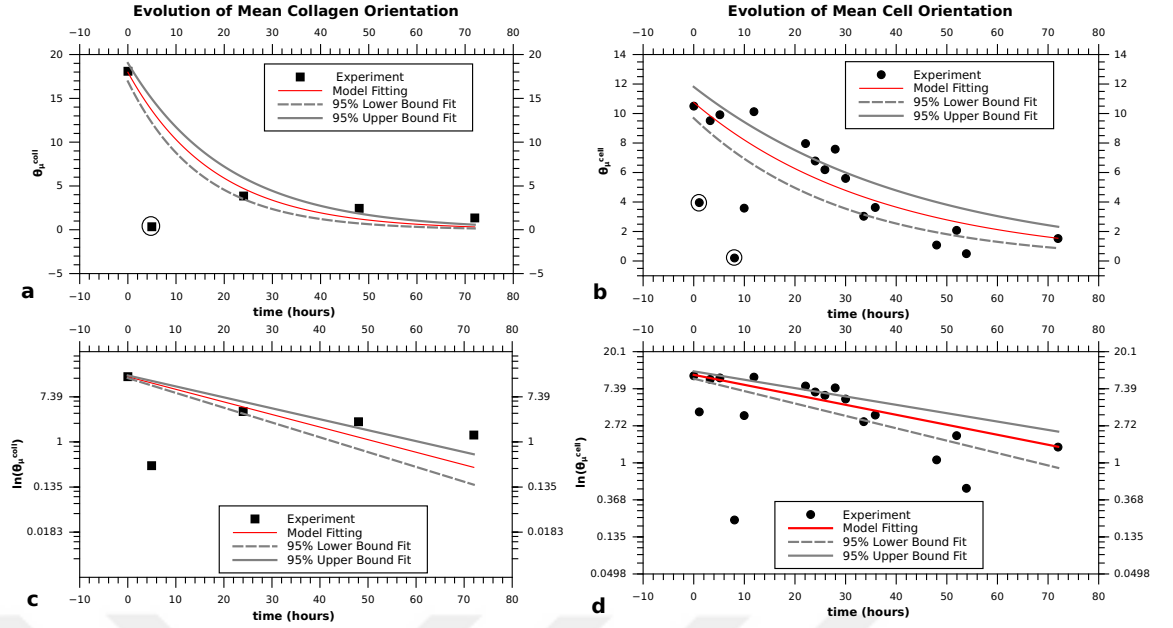


Figure 5.2: Model fitting results of the mean collagen (θ_{μ}^{coll}) and mean cell (θ_{μ}^{cell}) orientation by using two parameter relationship $\theta_{\mu}(t) = \theta_0 \exp(-t/\tau_{\mu})$. (a) best model fit ($\theta_0 = 17.98^{\circ}$, $\tau_{\mu}^{coll} = 17.93\text{h}$) for the mean collagen orientation and (c) natural logarithm of the dependent axis of the same analysis. (b) best model fit ($\theta_0 = 10.75^{\circ}$, $\tau_{\mu}^{cell} = 37.08\text{h}$) for the mean cell orientation and (d) natural logarithm of the dependent axis of the same analysis. The data in circles ((a)-(b)) are evaluated as the statistical outliers for the analysis by performing a Cook's distance analysis (from [6]).

and simultaneous collagen fiber orientation distribution. The main motivation for us to work on a collagen orientation distribution for prepared scaffolds is to see the pure effects of mechanical conditions on a cellular orientation as much as possible and minimize the effects of other variables.

We estimate the remodeling time parameters based on the experimental observations given in [11]. For the experimental setup of collagenous media, cell culture and boundary conditions, we refer the reader to the same work.

Our analysis depends on fitting the mentioned evolution equations that source from the Langevin equation and compares the characteristic time assumptions made in [64] and [46]. Model fitting results of a mean collagen (θ_{μ}^{coll}) and mean cell (θ_{μ}^{cell}) orientation by using two parameter relationship $\theta_{\mu}(t) = \theta_0 \exp(-t/\tau_{\mu})$ with the characteristic remodeling time τ_{μ} (hours) are shown in Figure 5.2a and 5.2d. The best model fit ($\theta_0 = 17.98^{\circ}$, $\tau_{\mu}^{coll} = 17.93\text{h}$) for a mean collagen orientation and natural logarithm of the dependent axis of the same analysis are given in Figure 5.2a and 5.2c. The best model

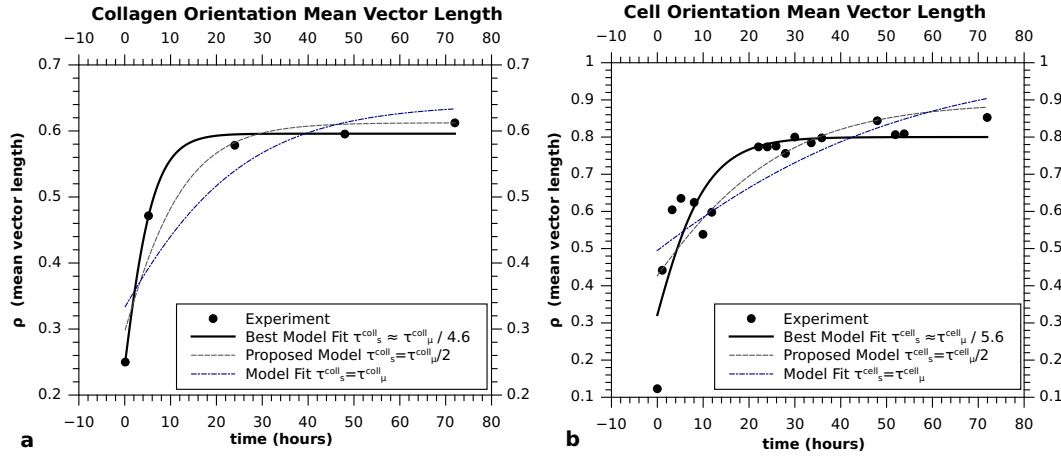


Figure 5.3: Model fitting results of the collagen (ρ^{coll}) and cell (ρ^{cell}) mean vector lengths by using the relationship in equation 5.30 with fixed characteristic remodeling time τ_μ (obtained from the previous analysis). (a) best model fits for the collagen orientation dispersion: comparison of the proposed approach and existing assumption of “equal characteristic times”. (b) best model fit for the cell orientation dispersion: comparison of the proposed approach and existing assumption of equal characteristic times (from [6]).

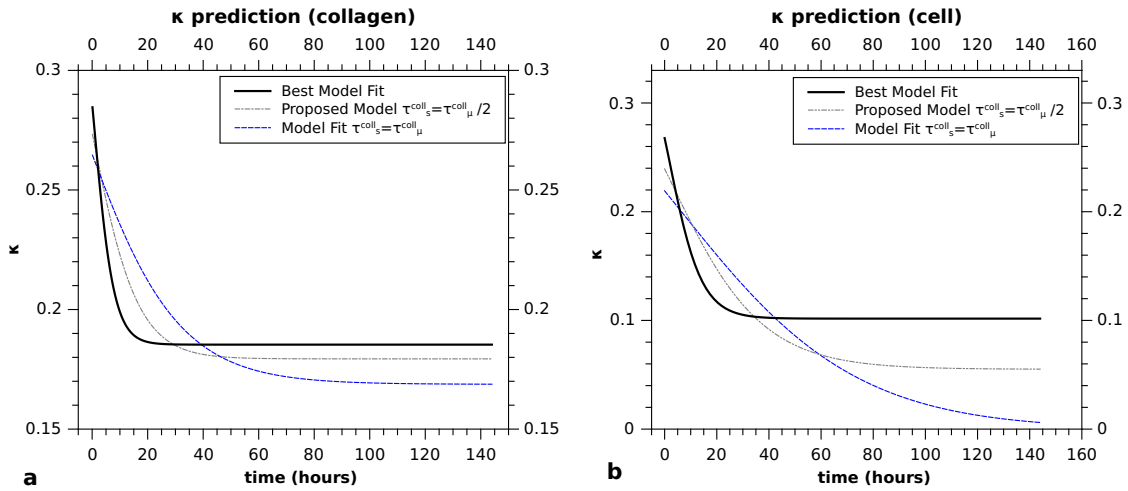


Figure 5.4: Model fitting results of the collagen (κ^{coll}) and cell (κ^{cell}) structural parameters by using the approximation in Table A.1. (a) Best model fits for the collagen orientation κ parameter: comparison of the proposed approach and existing assumption of equal characteristic times. (b) Best model fit for the cell orientation κ parameter: comparison of the proposed approach and existing assumption of “equal characteristic times” (from [6]).

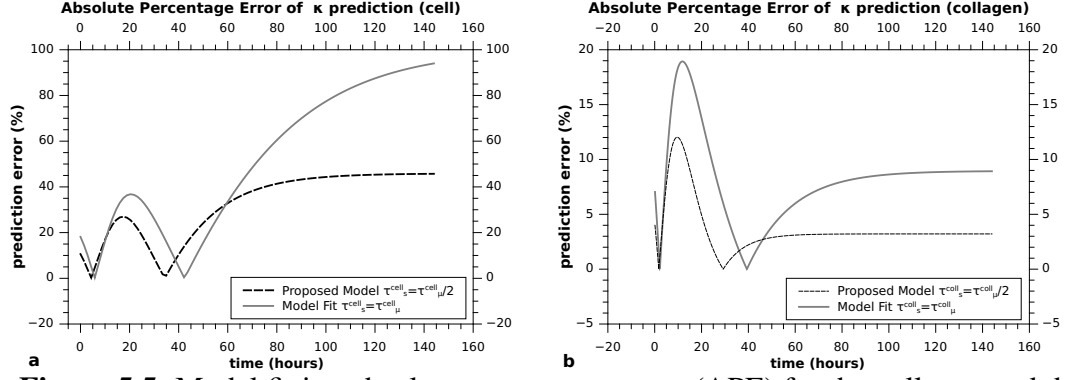


Figure 5.5: Model fitting absolute percentage errors (APE) for the collagen and the cell orientation κ parameter: (a) comparison of the proposed approach and the existing assumption of “equal characteristic times” for cell, (b) comparison of the proposed approach and the existing assumption of “equal characteristic times” for collagen orientation (from [6]).

fit ($\theta_0 = 10.75^\circ$, $\tau_\mu^{cell} = 37.08\text{h}$) for a mean cell orientation and natural logarithm of the dependent axis of the same analysis are given in Figure 5.2b and 5.2d. The data in circles given in Figures 5.2a and 5.2b are evaluated as the statistical outliers for the analysis by performing a Cook’s distance analysis. All possible curve combinations lie in between (95%) upper and lower bound curve estimations. Experimental data show that the natural logarithm of a mean fiber direction θ_μ^{coll} and a mean cell orientation θ_μ^{cell} have a linear decay pattern towards its homeostatic position at $\theta = 0$ which is determined by the applied mechanical strain in that direction (see Figure 5.2c). The linear decay patterns in Figure 5.2c-5.2d are clearly visible, however the corresponding remodeling times significantly differ where collagen fibers evolve faster.

The estimated characteristic times τ_μ for mean orientations are $\tau_\mu^{coll} = 17.93\text{h} \pm 2.68\text{h}$ (Adj- $R^2=0.97$) and $\tau_\mu^{cell} = 37.08\text{h} \pm 7.18\text{h}$ (Adj- $R^2=0.68$). The parameter estimations are settled as fixed (pre-estimated) time parameters for the mean vector length (ρ) model fitting. We calculate the best nonlinear least square fits for the data while we kept τ_s (the characteristic time for κ evolution) fixed depending on the estimations made for a mean orientation. Based on the results in Figure 5.3a-5.3b, the evolution of statistical dispersion (ρ) is well aligned with the proposed approach, since it can predict the underlying viscosity in statistical evolution much better compared to the “equal assumption $\tau_s = \tau_\mu$ ” made in [64] and [46]. In fact, it should be at least $\tau_s = \tau_\mu/2$, which is an estimation depending on very few initial assumptions, such as statistical evolution being Markovian.

Our aim here is not to give a complete and exact understanding of the underlying dynamics of collagen dispersion phenomena, which is not feasible if we consider the complexity of the dynamics and cellular level interactions. Instead, we give the simplest form of evolution equation under the assumption that the current time step orientation density distribution is predicted by the previous time step. The final κ value in cell orientation highly differs from the experimental observations, if this approach is not considered. We believe that, this approach gives a better explanation for a real situation, since it has lower absolute percentage error rates compared to “equal evolution time parameters” assumption (Figure 5.4-5.5). Figure 5.5 shows a notable relative decrease on error levels, especially for the cell orientation. Additionally, the dynamics of cell and collagen orientation is understood to be similar in terms of the ratio of time parameters, where $\tau_{\mu}^{coll}/\tau_s^{coll} = 4.6$ and $\tau_{\mu}^{cell}/\tau_s^{cell} = 5.6$. Since the observed ratios are greater than the one we propose, it points out that the process is not a Markovian and the tissue environment may have disordered fractal properties (see discussions in [66]). In this case, it is cumbersome to construct the governing equations through investigating the characteristic time parameters alone. We note that the simplification in approaches is also required for the stability of computational algorithms.

5.2.4.2 Computational efficiency of the algorithm

The algorithm proposed has the ability to model the evolution of a probability distribution having time dependency. In that sense, the probability should be classified as a viscous one. The remodeling algorithm presented here is computationally advantageous compared to the angular integration (AI) schemes, since the evolution of a generalized structural tensor (GST) \mathbf{H} can be obtained directly without angular integration of the contribution of individual fibers. Existing approaches in the literature, such as [19, 30, 29, 27], deal with the evolution of distribution via supplying a large number of fiber direction vectors, whose dispersions supply information on the evolution of a orientation density distribution. In that sense, modeling the evolution of distribution is analogous to the kernel density based modeling of probability distribution. What we show here is a distinctive branch of a new type of statistical evolution concept in which the angular integration (AI) scheme is replaced by the phenomenological evolution equation of a single fiber perturbed by noise. Thus,

'multiple directions' assumption of the AI schemes are no longer required, since the number of randomly perturbed single fibers can be taken to be infinite and their asymptotic properties are known. In this case, the computation of a generalized structure tensor is fast, because an underlying individual fiber direction set is not required. The limitations of the proposed approach are discussed in chapter 6.

5.3 Numerical Implementation

5.3.1 Deformation of a “single layered” and “internally pressurized” axisymmetric cylindrical artery tube

We qualitatively tested the theoretical scheme by investigating its predictive abilities on the radial deformation of a single layered (adventitia) artery structure which is set up for 30 days of random evolution. In the following sections, utilizing the qualitative and quantitative information presented in the previous published works, we discuss how a linear evolution model for statistical fiber orientation depending on the magnitude of a random Langevin force can be used as a remodeling tool. We expect that an algorithm of this kind could explain the evolution of the collagen dispersion, and radial deformation, in **biaxially strained** soft tissue. The biaxiality assumption is emphasized for numerical accuracy of the simulations. For this purpose, we used the analytical description of an axisymmetric artery deformation discussed in [1]. The deformation problem is formulated by using the strain energy density function based on principal stretches. The mechanics of a helically arranged dispersed fiber family embedded in an isotropic matrix environment for adventitia layer is characterized by the energy functions given in equation 5.31. In this section, the variable λ with or without an index always represents the stretch level in the tissue. Specifically, $\lambda_{r,\tilde{\Theta},z}$ are the stretch levels given in cylindrical coordinates seen in Figure 5.6 ([1]), where $r, \tilde{\Theta}, z$ denote the radial, circumferential and axial directions respectively. We consider the additive splitting of the energy function into its isotropic and anisotropic components, where the isotropic matrix media is considered to be a Neo-Hookean material. The remodeling algorithm formulated in this work is linked to the anisotropic model by embedding the time dependent dispersion of the evolution equations. The kinematics and geometry of the mechanical model are displayed in Figure 5.6. Figure

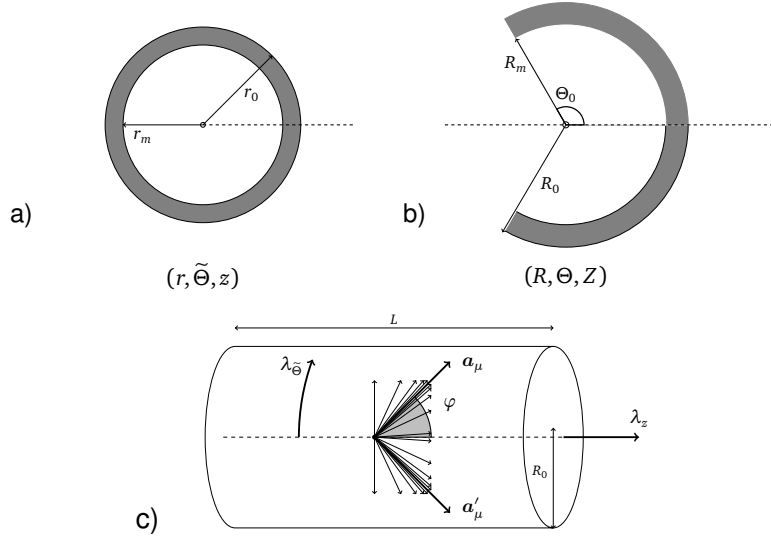


Figure 5.6: (a) Kinematics of an arterial wall with respect to final deformed configuration under internal pressure. (b) Geometry of the stress free configuration in cylindrical coordinates (R, Θ, Z) with an opening angle of Θ_0 and internal radius R_m . (c) Solution domain of the internally pressurized thick cylinder and corresponding principals $\lambda_{\tilde{\Theta}}$ and λ_z . For each artery layer, it is assumed that the dispersion of fibers are clustered around a mean direction which is very close to the reference vector \mathbf{n} and \mathbf{n}' (from [6]).

5.6 a explains the kinematics of an arterial wall compared to the deformed final configuration with internal pressure. The “stress free” reference configuration in cylindrical coordinates is characterized by the variables (R, Θ, Z) with an opening angle of Θ_0 , internal radius R_m and outer radius R_0 . The final configuration is an updated geometry carrying an active residual stretch and its geometry is defined by the coordinate variables $(R, \tilde{\Theta}, z)$ represented in Figure 5.6b. In the long term, the fibers are clustered close to the reference vectors \mathbf{n} and \mathbf{n}' which show the direction of the mechanical stimuli that governs the remodeling process. A common definition of the strain energy function depends on the additive splitting of isotropic and anisotropic components,

$$\Psi(\lambda_r, \lambda_{\tilde{\Theta}}, \lambda_z) = \Psi_{iso}(\lambda_r, \lambda_{\tilde{\Theta}}, \lambda_z) + \Psi_{aniso}(\lambda_{\tilde{\Theta}}, \lambda_z). \quad (5.31)$$

The strain energy density function of the adventitia layer that is composed of an isotropic Neo-Hookean ground-matrix component and for an anisotropic collagen fiber

material is given by,

$$\Psi_{iso} = \frac{c}{2}(I_1 - 3), \quad (5.32)$$

$$\Psi_{aniso} = \frac{k_1}{k_2}(\exp(k_2(I_4^* - 1)^2) - 1), \quad (5.33)$$

where c is the shear modulus for the ground-matrix material, k_1 and k_2 are the anisotropic potential parameters. The dispersion related fiber strain invariant I_4^* is defined by $I_4^* = \kappa I_1 + (1 - 3\kappa)I_4$, $I_1 = \lambda_r^2 + \lambda_{\tilde{\Theta}}^2 + \lambda_z^2$, $I_4 = \mathbf{a}_\mu \mathbf{C} \mathbf{a}_\mu$ and $\mathbf{a}_\mu = [0 \ \sin(\varphi) \ \cos(\varphi)]$ is the mean orientation vector of a dispersion which rotates to the stimulus direction $\mathbf{n} = [0 \ \sin(\beta) \ \cos(\beta)]$ as shown in Figure 5.7. Geometric boundaries for the investigated problem are defined as,

$$R_m \leq R \leq R_0 \quad 0 \leq \Theta \leq 2\Theta_0 \quad 0 \leq Z \leq L, \quad (5.34)$$

$$r_m \leq r \leq r_0 \quad 0 \leq \tilde{\Theta} \leq 2\pi \quad 0 \leq z \leq l. \quad (5.35)$$

The deformation is described over a transformation from R_m to r_m where the principal stretches depend strictly on r_m and R_m ,

$$r = r(R) > 0 \quad \tilde{\Theta} = \frac{\pi}{\Theta_0}\Theta \quad z = \lambda_z \Lambda Z, \quad (5.36)$$

due to incompressibility (see Figure 5.6). The principal stretches are defined as functions of the reference position variable R on radial direction as,

$$\begin{aligned} \lambda_{\tilde{\Theta}} &= \frac{\pi}{\Theta_0} \left(\frac{r_m^2}{R^2} + \frac{\Theta_0}{\pi \lambda \Lambda} \left(1 - \frac{R_m^2}{R^2} \right) \right)^{1/2}, \\ \lambda_z &= \lambda \Lambda, \quad \lambda_r = (\lambda_{\tilde{\Theta}} \lambda_z)^{-1}, \quad r_m \leq r \leq r_0. \end{aligned} \quad (5.37)$$

The stretch λ_r in the r direction is calculated by the incompressibility relation, where $\lambda_r \lambda_{\tilde{\Theta}} \lambda_z = 1$. $\Lambda = \text{diag}(\lambda_r, \lambda_{\tilde{\Theta}}, \lambda_z)$ is the residual stress definition characterized by the explicit stretch level.

The stretches are used directly to calculate the diagonal components $\sigma_{\tilde{\Theta},r,z}$ of the Cauchy stress tensor. The equilibrium equation for the deformed artery tube, depending on the diagonal components of stress tensor is [67]

$$\frac{d\sigma_{rr}}{dr} + \frac{1}{r}(\sigma_r - \sigma_{\tilde{\Theta}}) = 0 \quad r_m \leq r \leq r_0, \quad (5.38)$$

and boundary conditions for the radial stress is $\sigma_r = -P_0; r = r_m$, $\sigma_r = 0; r = r_0$, where P_0 is the applied internal pressure. The components of Cauchy stress are defined

by,

$$\sigma_r(r) = -p_h(r) + c\lambda_r^2, \quad (5.39)$$

$$\begin{aligned} \sigma_{\tilde{\Theta}}(r) &= -p_h(r) + c\lambda_{\tilde{\Theta}}^2 \\ &+ 4k_1(I_4^* - 1) \exp(k_2(I_4^* - 1)^2) (\kappa + (1 - 3\kappa) \sin^2(\varphi)) \lambda_{\tilde{\Theta}}^2, \end{aligned} \quad (5.40)$$

$$\begin{aligned} \sigma_z(r) &= -p_h(r) + c\lambda_z^2 \\ &+ 4k_1(I_4^* - 1) \exp(k_2(I_4^* - 1)^2) (\kappa + (1 - 3\kappa) \cos^2(\varphi)) \lambda_z^2. \end{aligned} \quad (5.41)$$

The Cauchy stress can be related to the strain energy function as,

$$\sigma_i(r) = -p_h(r) + \lambda_i(r) \frac{\Psi(\lambda_r, \lambda_{\tilde{\Theta}}, \lambda_z)}{\lambda_i(r)} \quad i = r, \tilde{\Theta}, z, \quad (5.42)$$

$$\bar{\sigma}_i(r) = \lambda_i(r) \frac{\Psi(\lambda_r, \lambda_{\tilde{\Theta}}, \lambda_z)}{\lambda_i(r)} \quad i = r, \tilde{\Theta}, z, \quad (5.43)$$

here its components are derived from the exponential strain energy function. The hydrostatic pressure $p_h(r)$ can be calculated by integrating the balance equation 5.38, yielding,

$$p_h(r) = \lambda_r \frac{\Psi(\lambda_r, \lambda_{\tilde{\Theta}}, \lambda_z)}{\lambda_r} + \int_r^{r_0} (\bar{\sigma}_{\tilde{\Theta}}(r) - \bar{\sigma}_r(r)) \frac{dr}{r}, \quad (5.44)$$

where $p_h(r_m) = P_0$. For a given internal pressure P_0 , the unknown deformed internal radius r_m is definite and can be found by solving,

$$P_0 = \int_r^{r_0} (\bar{\sigma}_{\tilde{\Theta}}(r) - \bar{\sigma}_r(r)) \frac{dr}{r}, \quad (5.45)$$

by means of fixed point iterations.

The remodeling process is determined by the strain/stress stimulus which governs the deformation mapping from the undeformed reference configuration to the deformed current configuration. The evolution of dispersion is not related to the geometric framework and is widely effected by the shape of the stimulus function depending on mechanical magnitudes. In our study, the stimulus function is characterized by the ratio of principal stretches and stresses. There are two fiber evolution parameters. First, the mean orientation vector of dispersion, \mathbf{a}_μ rotates to the stimulus direction $\mathbf{n} = [0 \ \sin(\beta) \ \cos(\beta)]$ as shown in Figure 5.7. In this case, β is determined by the selected stimulus function. Second, the Langevin force parameter, Σ determines the evolution of dispersion. Both functions depend on strain, symbolized by $(\beta_\lambda, \Sigma_\lambda)$, or stress, symbolized by $(\beta_\sigma, \Sigma_\sigma)$. The \wedge symbol stands for the logical 'or' operator

which gives the information about the stimuli, $(\sigma \wedge \lambda)$, that is currently being used in the formulation. The mean direction stimulus $\beta_{\lambda, \sigma}$ is defined by the trigonometric arctan function as

$$\beta_{\sigma} = \arctan\left(\frac{\sigma_{\tilde{\Theta}}}{\sigma_z}\right) \quad \beta_{\lambda} = \arctan\left(\frac{\lambda_{\tilde{\Theta}} - 1}{\lambda_z - 1}\right). \quad (5.46)$$

For the stress dependent evolution, the ratio of principal stresses $\sigma_{\tilde{\Theta}}/\sigma_z$ is used as stimulus. In strain dependent case, which is the preferred case for this work, the stretch dependent ratio $(\lambda_{\tilde{\Theta}} - 1)/(\lambda_z - 1)$ is utilized. The preferred direction stimuli based on stress and strain are given by,

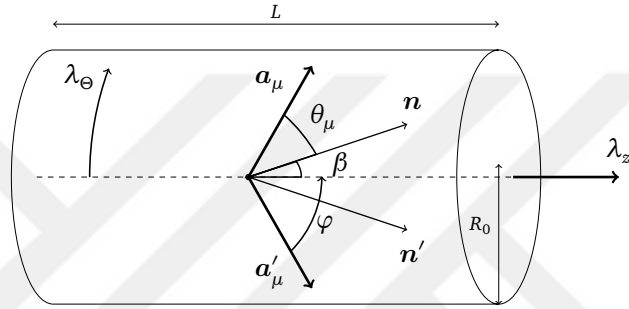


Figure 5.7: The layout of mean fiber orientation vector \mathbf{a}_{μ} , spatial stimulus direction vector $\mathbf{n}^{\lambda \wedge \sigma}$ and angular measurement θ_{μ} between these two vectors (from [6]).

The angle $\theta_{\mu}(t')$ between the mean fiber orientation vector \mathbf{a}_{μ} and the stimulus direction vector $\mathbf{n}^{\sigma \wedge \lambda}$ at time t' is updated to $\theta_{\mu}(t)$ by the linear evolution equation (Figure 5.7)

$$\theta_{\mu}(t') = |\varphi(t') - \beta_0(t')_{(\sigma \wedge \lambda)}| \quad 0 < \varphi < \pi/2, \quad 0 < \beta_0 < \pi/2, \quad (5.47)$$

$$\theta_{\mu}(t) = \exp(-\tau_{\mu}^{-1} \Delta t) \theta_{\mu}(t'), \quad (5.48)$$

where $\Delta t = t - t'$ is the time step. In this study, we use the remodeling approach discussed in [46] for evolution of stimulus. Since $0 < \varphi < \pi/2$, and $0 < \beta_0 < \pi/2$, a new mean fiber orientation angle φ is updated by

$$\varphi = \beta_0 + \theta_{\mu} \quad \text{if } \varphi \geq \beta_0, \quad \varphi = \beta_0 - \theta_{\mu} \quad \text{if } \varphi < \beta_0, \quad (5.49)$$

where β_0 is the angular measurement between the pull back of spatial stimulus direction vector $\mathbf{n}^{\lambda \wedge \sigma}$ and axial direction E_z , in undeformed initial configuration, i.e. $\beta_0 = \angle(\mathbf{n}_0^{\lambda \wedge \sigma}, E_z)$. The material stimulus $\mathbf{n}_0^{\lambda \wedge \sigma}$ is obtained by the pull back of the

spatial stimulus vector $\mathbf{n}^{\lambda,\sigma}$ to the material configuration via deformation mapping,

$$\mathbf{n}_0^{\lambda\wedge\sigma} = \frac{\|\mathbf{n}_0^{\lambda\wedge\sigma}\|}{\|\mathbf{F}^{-1}\mathbf{n}^{\lambda\wedge\sigma}\|} \mathbf{F}^{-1}\mathbf{n}^{\lambda\wedge\sigma}, \quad (5.50)$$

which supplies an objective definition of the remodeling stimulus. In equation 5.50 \mathbf{F} is the deformation gradient and $\|\cdot\|$ is the norm of (\cdot) . Finally, the new dispersion parameter $\kappa(t)$ at time t is estimated from the variance $s^2(t')$ at time t' using,

$$s(t)^2 = \exp(-2\tau_\mu^{-1}\Delta t)s(t')^2 + \frac{\Sigma_{(\lambda\wedge\sigma)}^2}{2\tau_\mu^{-1}}(1 - \exp(-2\tau_\mu^{-1}\Delta t)). \quad (5.51)$$

Then s^2 is converted to κ by the $\hat{\kappa}$ function given in equation 5.52.

$$\kappa(t) = \hat{\kappa}(s(t)), \quad (5.52)$$

where $\Sigma_{(\lambda\wedge\sigma)}$ represents stimulus dependent variable. The stimulus functions in equation 5.51, whether they depend on strain or stress, are described by the same functional forms:

$$\Sigma_\sigma(\sigma_{\tilde{\Theta}}, \sigma_z) = 2\pi\sqrt{2\tau_\mu^{-1}} \sum_{i=0}^2 a_i \left(\frac{\min(\sigma_{\tilde{\Theta}}, \sigma_z)}{\max(\sigma_{\tilde{\Theta}}, \sigma_z)} \right)^{b_i}, \quad (5.53)$$

$$\Sigma_\lambda(\lambda_{\tilde{\Theta}}, \lambda_z) = 2\pi\sqrt{2\tau_\mu^{-1}} \sum_{i=0}^2 a_i \left(\frac{\min(\lambda_{\tilde{\Theta}} - 1, \lambda_z - 1)}{\max(\lambda_{\tilde{\Theta}} - 1, \lambda_z - 1)} \right)^{b_i}, \quad (5.54)$$

where a_i, b_i are constant coefficients and their values are presented in theoretical section.

For general coding purposes, we summarize the total remodeling stimuli definitions as (E_z is the Cartesian basis)

$$\beta^\sigma = \angle(\mathbf{n}^\sigma, E_z) =, \quad \begin{cases} \arctan\left(\frac{\sigma_\Theta}{\sigma_z}\right) & \epsilon \leq \frac{\sigma_\Theta}{\sigma_z} < \infty \\ \beta^\sigma = \beta^0 & \sigma_\Theta, \sigma_z < \epsilon \\ \beta^\sigma = \epsilon & \sigma_\Theta < \epsilon, \sigma_z > \epsilon \\ \beta^\sigma = \pi/2 - \epsilon & \sigma_z < \epsilon, \sigma_\Theta > \epsilon \end{cases}, \quad (5.55)$$

$$\beta^\lambda = \angle(\mathbf{n}^\lambda, E_z) = \begin{cases} \arctan\left(\frac{\lambda_\Theta - 1}{\lambda_z - 1}\right) & \epsilon \leq \frac{\lambda_\Theta - 1}{\lambda_z - 1} < \infty \\ \beta^\sigma = \beta^0 & \lambda_\Theta, \lambda_z < 1 + \epsilon \\ \beta^\sigma = \epsilon & \lambda_\Theta < 1 + \epsilon, \lambda_z > 1 + \epsilon \\ \beta^\sigma = \pi/2 - \epsilon & \lambda_z < 1 + \epsilon, \lambda_\Theta > 1 + \epsilon \end{cases}, \quad (5.56)$$

which are the stimuli for mean fiber orientation. Instead of absolute zero measurements, $\epsilon \approx 10^{-16}$ the machine epsilon is applied for any undesired singularity. It is also possible to set $10^{-16} < \epsilon \ll 1$. the numerical results are not effected.

Compression in all directions (including the r axis) lead to hydrostatic pressure, so no stretch based remodeling occurs. In this case, $\beta^\sigma = \beta^0$; $\sigma_\Theta, \sigma_z < 0$, where β^0 is the previous position of the orientation vector. The modulation function restricts the stimulus magnitude to position in the interval $\mathcal{M}^{\lambda^\sigma} \in [0, 1]$. We eliminate the remodeling stimulus that is sourced from the r axis,

$$\mathcal{M}^\sigma(\sigma_\theta, \sigma_z) = \begin{cases} \frac{\min(\sigma_\Theta, \sigma_z)}{\max(\sigma_\Theta, \sigma_z)} \in [0, 1] & \text{if } \sigma_\Theta, \sigma_z > \epsilon \\ 1 - \epsilon & \text{if } \sigma_\Theta, \sigma_z < \epsilon \\ \epsilon & \text{if } \sigma_\Theta < \epsilon, \sigma_z > \epsilon \\ \epsilon & \text{if } \sigma_\Theta > \epsilon, \sigma_z < \epsilon \end{cases}, \quad (5.57)$$

$$\mathcal{M}^\lambda(\lambda_\theta, \lambda_z) = \begin{cases} \frac{\min(\lambda_\Theta - 1, \lambda_z - 1)}{\max(\lambda_\Theta - 1, \lambda_z - 1)} \in [0, 1] & \text{if } \lambda_\Theta, \lambda_z > 1 + \epsilon \\ 1 - \epsilon & \text{if } \lambda_\Theta, \lambda_z < 1 + \epsilon \\ \epsilon & \text{if } \lambda_\Theta < 1 + \epsilon, \lambda_z > 1 + \epsilon \\ \epsilon & \text{if } \lambda_\Theta > 1 + \epsilon, \lambda_z < 1 + \epsilon \end{cases} \quad (5.58)$$

are our modulation functions. $\mathcal{M}^{\sigma, \lambda}(\lambda_\Theta, \lambda_z) = 1$ is defined for the bulk compression cases where stresses are the hydrostatic pressures for incompressible material. Naturally there is no dominant stimulus direction. A typical example is the articular cartilage, where multiaxial compression leads to highly dispersed collagen fiber orientations.

5.3.2 Model parameters

Constitutive parameters for isotropic and anisotropic parts of the strain energy density function are gathered from [1] and the parameters are listed in Table 5.1. The angle parameter φ points the direction of \mathbf{a}_μ in the adventitia layer which may change during the remodeling process. According to the referred study, the dispersion parameter κ , in Table 5.1, is reported to be the statistical average of nine different human adventitia measurements (published in [68]). The second set of parameters defining the geometry of an artery, and residual stress, are presented in Table 5.2. The remodeling parameter in this simulation is chosen as τ_μ which determines the speed of a mean orientation evolution. The characteristic time for κ evolution is a function of τ_μ and it is not listed here. Since a single layered model is adopted, τ_μ is fixed to $\tau_\mu = 5$ days by evaluating the previous collagen and fibrin based studies focusing on the collagen remodeling and cell rotation. Depending on the experimental setups, the whole process may converge in hours or in weeks. As we have discussed the experimental data in which are limited by the constraints and procedures of the work in [11], a typical guess of τ_μ is $1 <$

Table 5.1: Constitutive parameters for isotropic and anisotropic contributions in the strain energy density function according to [1].

Layer	c (kPa.)	k_1 (kPa.)	k_2	φ ($^\circ$)	κ
Adventitia	2.7	5.1	15.4	40.0	0.226

Table 5.2: Parameter set used for media and adventitia, and remodeling simulation (see [1]).

Parameter	Description	Value
R_m	interface for media and adventitia	3.795 mm.
R_0	outer radius	4.042 mm.
Θ_0	opening angle for adventitia	120 $^\circ$
Λ	residual stress	1
λ	prestretch in axial direction	1.265
p_0	internal pressure	0 – 30 kPa.
Remodeling	Description	Value
τ_μ	characteristic remodeling time	$\tau_\mu = 5$ days

$\tau_\mu < 2$ days which is shorter than the time parameter of cell rotation. In fact, some qualitative works, such as [14] and [5], reported much larger evolution times for the maturation of scaffold sample where the highest degree of collagen fiber alignment observed in 4 weeks. We tested the remodeling speed for 5 days since the process is quasi-static and larger values do not contribute to the results of the simulation. On the other hand, we simulated the model for different axial stretches with the additional residual stress component. The axial pre-stretches in the artery wall are set to $\lambda_z = \lambda = 1.265$ and $\Lambda = 1.0$ for the simulations. Additionally, we analyzed the evolution of mechanical magnitudes with respect to changes in internal pressure between $0 < p_0 < 30$ kPa.

5.4 Application and Results

In order to observe its usefulness and effectiveness, we simulated the remodeling algorithm using the parameters in Table 5.1 and 5.2. The software used for the simulations is written in the `Octave` language and the results are reported in Figure 5.8 through Figure 5.11. In summary, the simulation includes the calculation of the stress measurements and a final internal radius r_m which determines the whole history of nonlinear solutions. Previously, the deformation problem was reduced to the

Table 5.3: Initial condition sets that are used for simulating six trial cases.

simulation case (Σ_λ)	initial conditions				
	P_0 (kPa)	κ_0	s_0	φ_0	λ
case 1	2	0.1	0.1π	5°	1.25
case 2	5	0.2	0.3π	45°	1.25
case 3	10	0.3	0.5π	85°	1.25
case 4	15	0.1	0.1π	5°	1.25
case 5	20	0.2	0.3π	45°	1.25
case 6	30	0.3	0.5π	85°	1.25

solution of equation 5.45 to obtain stresses using the calculated stretches depending on r_m . Solutions are obtained via Octave's `fzero` function using fixed-point iterations. Stress components, satisfying the boundary conditions $\sigma_r = -P_0$ and $R = R_m$ include hydrostatic pressure terms. Remodeling stimuli of an artery depend on the internal stress/strain and the whole remodeling event is self-directing since no external constraints are defined. Remodeling variables are the dispersion parameter κ , and the fiber direction angular measurement φ , that are free to evolve along with the modified stresses/strains at each time step. At this point, we constructed our algorithm using an explicit scheme, which means the remodeled parameters determine the stresses explicitly such that there is no feedback at the same time interval. The solutions are calculated under the assumption of finite deformation of a thick-walled cylinder, where remodeling variables are inhomogenously distributed over wall thickness. The internal mechanical variable distributions (stress, stretch and remodeling variables) through the thickness are interpolated for the next calculation step. Three information nodes are selected for interpolations: the inner radius R_i , the outer radius R_0 and middle radius $R_m = (R_0 + R_i)/2$. This assumption simplifies the algorithm and observations still supply the information at the desired level. We investigated the effects of stimulus functions for a mean fiber orientation on the deformation of an axisymmetric artery tube under internal blood pressure. We have also tested the stability of the model under different initial conditions to observe that the final converged internal variables are the same. To obtain some quantitative clues for the evaluation of the existence and uniqueness of the remodeling solutions, we select six parameter set combinations as initial conditions (see Table 5.3). Every parameter set corresponds to an internal pressure step. Then, the convergence behavior of all variables are observed for every parameter set. The evolution of the internal radius r_m , the dispersion parameter κ

and remodeling stimuli variables for the adventitia have been tracked for 30 days for strain (Σ_λ) and 100 days for the stress stimulus case. The stress case is supplied just for illustration. The analysis of varying internal pressure between $0 < p_0 < 30$ kPa gives us information on the hardening of a material under pressure increment. As can be seen from Figure 5.8, the maturation of the internal radius measurement completes around 5 to 10 kPa, and we observed that no meaningful change appears beyond this pressure limit. The dispersion evolves to $0 < \kappa < 0.2$ interval along with the pressure increment. The final stress and stretch stimuli show that the stabilization of the final dispersion level is related to the ratio $(\lambda_{\bar{\theta}} - 1)/(\lambda_z - 1)$ showing the minor increment beyond 5 days. On the other hand, stress measurements do not saturate and show a linear pattern with respect to p_0 . Both circumferential stress and strains preserve the linearity, thus their ratio is close to a constant value. We observed that the final κ values are close to experimental results ([68]).

The second set of simulations present the evolution of internal variables with respect to time. Both stress and strain dependent cases are tested. We observed experimental validation for stretch based stimulus (Σ_λ). For stretch based simulations, the parameter set $\lambda = 1.265$ and $\Lambda = 1$ are used with different initial conditions. It can be seen from Figure 5.9 that the saturation of κ completes much faster than the saturation of the angular variable φ . The fast convergence of κ is a characteristic output of stochastic evolution of fiber dispersion. The final κ value, in this example, is $\kappa \approx 0.22$ and $\varphi \approx 0.25\pi$ which are close to the experimental observations. Naturally, these close approximations depend on p_0 , λ and Λ . For example, for $\lambda = 1.15$ and $\Lambda = 1.05$, the final κ is close to $\kappa \approx 0.18$. Thus, we consider that the results of simulations based on Σ_λ give smooth and stable evolution patterns where the final values are close to expected observations.

For a stress based evolution (Σ_σ), we use the parameter set $\lambda = 1.25$ and $\Lambda = 1$ with initial conditions $s_0 = 0.9\pi$ and $\varphi = 70^\circ$. The evolution paths of a stress based results represented fluctuating complex patterns and sharp turning points. The solution paths of strain based (Σ_λ) cases are smoother (see Figure 5.11). For a small initial dispersion parameter $\kappa \approx 0$, the process reaches its stabilized position around 30 days. The convergence is faster in the evolution of κ compared to φ magnitudes. The initial condition set exhibit a more complex pattern compared to the strain based

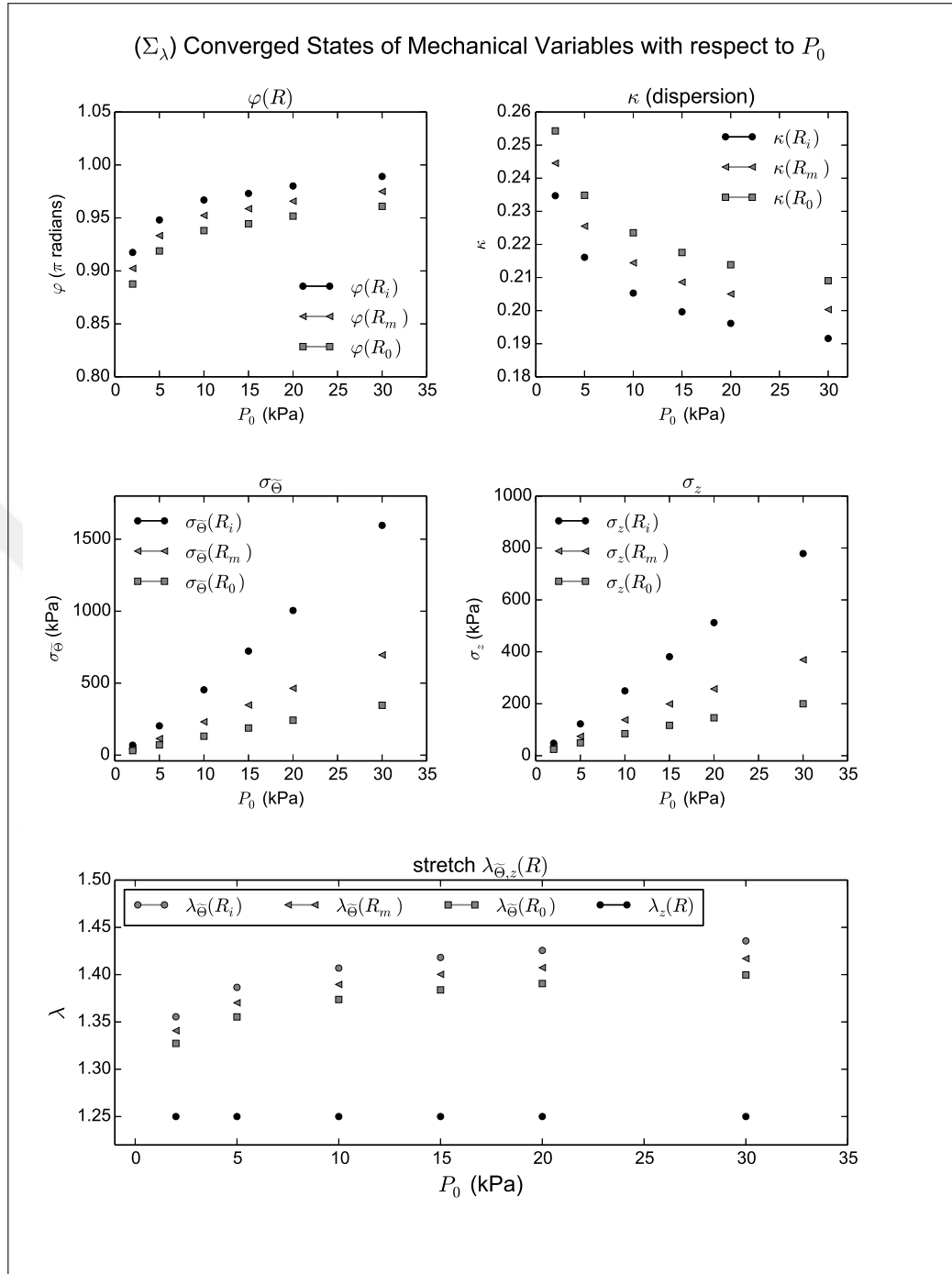


Figure 5.8: Converged mechanical magnitudes with respect to the changes in the applied internal pressure P_0 based on the strain stimulus (Σ_λ) . The internal pressure steps for the simulation are $P_0 = 2, 5, 10, 15, 20, 30$ (kPa). At every pressure step, the evolution of mechanical magnitudes are tracked for 30 days, and final converged values are represented in the graphics. Initial condition sets for the six simulation cases corresponding to the six pressure steps are given in Table 5.3. The time step for the simulation is set as $\Delta t = 0.2$ days (from [6]).

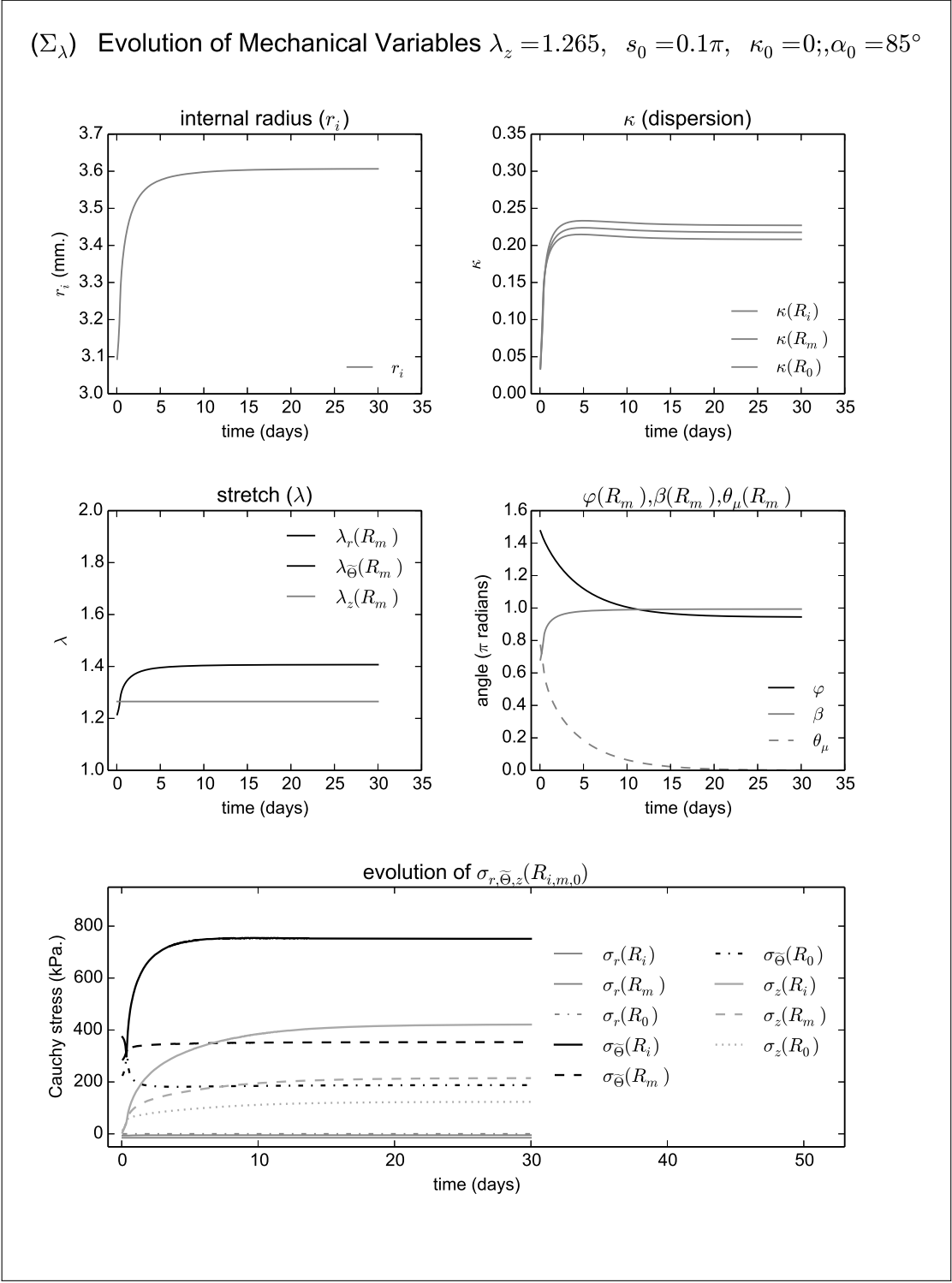


Figure 5.9: Evolution of mechanical magnitudes in time based on strain stimulus (Σ_λ). The model parameters for this simulation are $\lambda = 1.265$ and $\Lambda = 1.0$, with the initial conditions $s_0 = 0.1\pi$ and $\varphi_0 = 85^\circ$. The time step for the simulation is $\Delta t = 0.04$ days (from [6]).

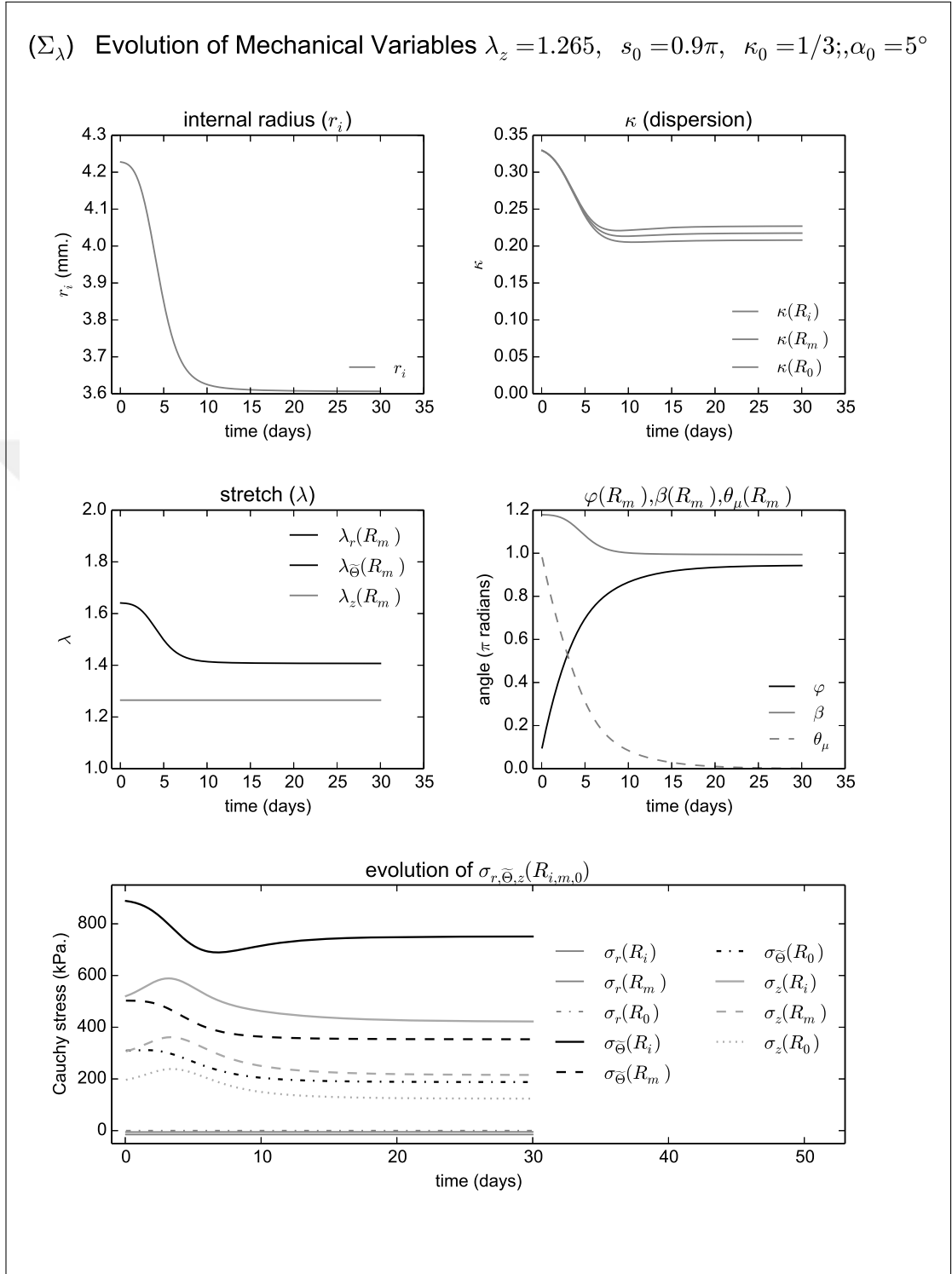


Figure 5.10: Evolution of mechanical magnitudes in time based on strain stimulus (Σ_λ). The model parameters for this simulation are $\lambda = 1.265$ and $\Lambda = 1.0$, with the initial conditions $s_0 = 0.9\pi$ and $\varphi_0 = 5^\circ$. The time step for the simulation is $\Delta t = 0.04$ days.

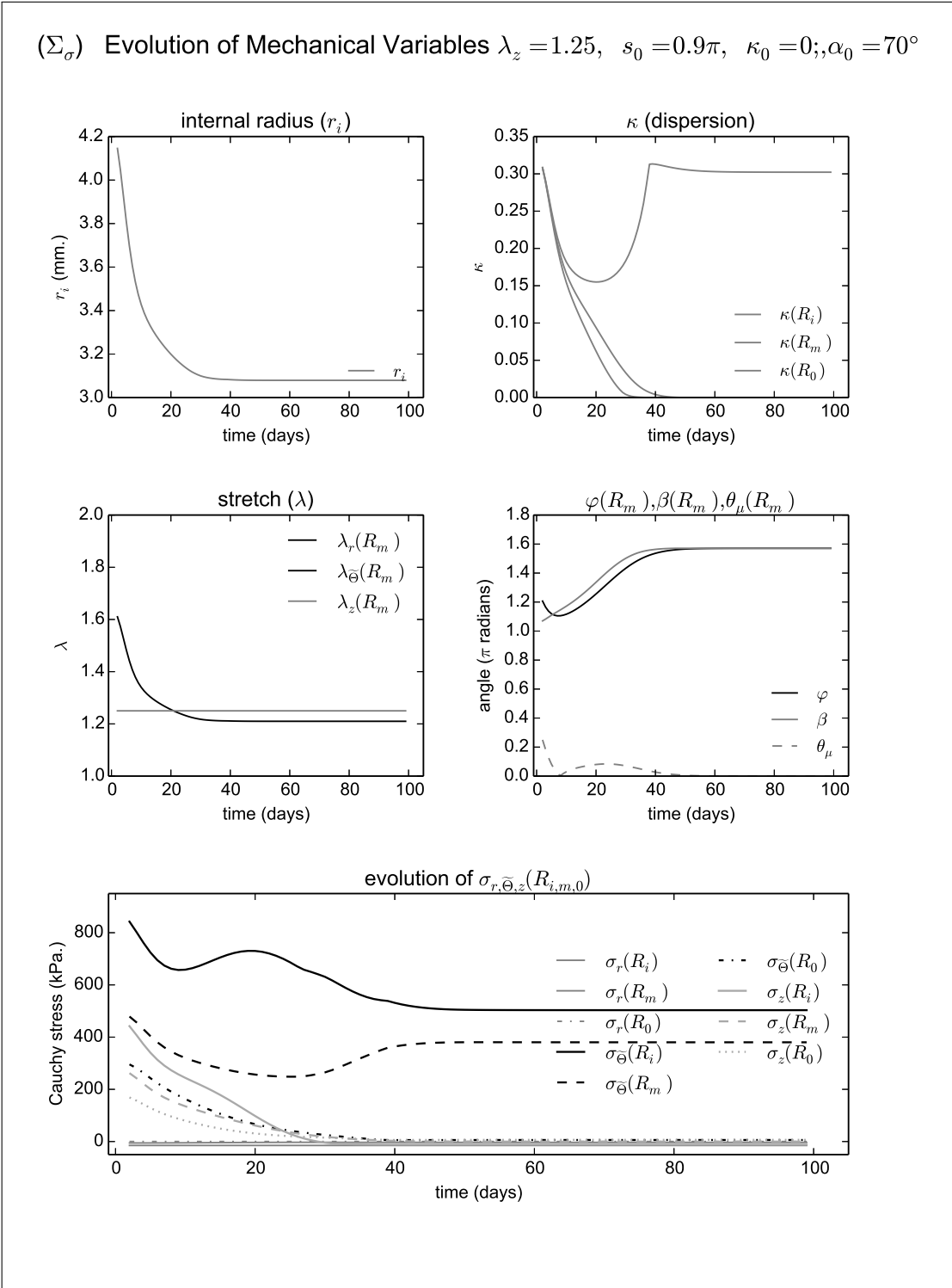


Figure 5.11: Evolution of mechanical magnitudes in time based on stress stimulus (Σ_σ). The model parameters for this simulation are $\lambda = 1.265$ and $\Lambda = 1.0$, with the initial conditions $s_0 = 0.9\pi$ and $\varphi_0 = 70^\circ$. The time step for the simulation is $\Delta t = 1$ days (from [6]).

simulations. The κ evolution shows a rapid decay form from $\kappa \approx 0.33$ to $\kappa \approx 0.0$, resulting with a non-homogeneous κ distribution. There is also a linear increment in φ evolution in between 5 – 30 days (Figure 5.11). For stress based evaluations based on Σ_σ , unlike our observation for strain based cases, uniqueness of the evolution is questionable. Our simulation setup has shown that there always exists a solution for stress based remodeling, however, the convergence can be effected by the initial parameter sets. This was not observed for strain stimuli cases. Thus, we can conclude that initial conditions may greatly effect the evolution pattern in stress based situations. The parameter settings give final κ and φ estimations that are far from experimental observations reported in ([68]).





6. CONCLUSION AND FUTURE PERSPECTIVES

In this thesis work, a novel computational modeling framework that incorporates the probabilistic nature of collagen fiber remodeling and evolutionary effects on structural tensors have been proposed. The random effects are assumed to be additive perturbations which inherently states that the perturbations are actually forces, forces that are analogous to Cauchy tractions inside the material domain, and they give rise to the time-dependent structural modification of the medium in a statistical sense. The statistical information is processed by cellular structures in order to evaluate the feedback process where the reaction of the structure is a continuous modification until a homeostatic position is reached. In this final chapter, we extend our discussions on the results of simulations. Then we give our conclusion and future perspectives on growth and remodeling simulations, numerical problems, experimental considerations and reflections that may be possible in other scientific fields.

6.1 General Comments on Simulations, Numerical Problems and Future Perspectives

In this study, we proposed a new mathematical approach to model the time-dependent evolution of collagen fiber orientation distribution using the concept of random Langevin force. The mathematical and physical assumptions we made should be considered as phenomenological, in other words, we have modeled only the mean fiber direction and dispersion based on stress stimulus. There are two main distinctions of the proposed algorithm from the existing approaches.

First, characteristic remodeling time for mean fiber direction and dispersion are bounded mathematically following a certain ratio for the processes called Markovian. In this case, the probability distribution depends only on the previous time step. Our initial analysis of the system has shown some potential modeling capabilities compared to the existing approaches assuming the equal remodeling times for both mean fiber direction and dispersion. The characteristic times can be estimated separately by

other approaches (see [4] and [46]) where remodeling of κ has been considered as a distinct process. We have explained this concept in detail in the theoretical and experimental sections that these two processes should be evaluated as correlated events and new theoretical models should consider this fact. One of the modeling perspectives presented here is an example of this formalism. The model described in this paper inherently include this estimation by definition stating that $\tau_\mu/\tau_s \approx 2.0$, which is an outcome of the proposed scheme. The main motivation for this first contribution is valid for only “feedback systems with random perturbation” such as cell systems producing fiber materials based on their misperceived signal transduction. The misperception is obvious and has been discussed in [63]. The main limitation for experimental validation is the lack of so-called “transient stretch” (recruitment stretch) which is the plastic part of the fiber evolution keeping the internal strains at much lower value than expected. The collagen remodeling algorithm discussed here have the potential to describe the evolution of fibrous structure in artery systems similar to the computational finite element approaches applied in [64].

Second, the algorithm discussed here is computationally advantageous compared to the angular integration based schemes, such as [30] and [19] or microsphere approaches proposed by [27]. In these algorithms, the underlying probability distribution is tried to be characterized by the sum of distinct fiber/mean directions or distinct distribution kernels (such as Gaussian). The basic idea, in these cases, is analogous to the kernel density based representation of the original probability distribution. We replaced this idea for feedback systems with the random Langevin approach, in which the evolution is given by the original distribution. The algorithm proposed in this study has been selected to be linear to eliminate the complexity in equations and to gain computational efficiency. We have described the solution schemes not as a partial differential equation but a system of differential equations which makes the solution procedure easier to implement. However, to achieve that, the Langevin equation is assumed to be linear too. This requirement seems to be the main drawback of the algorithm restricting the underlying fiber distribution to Gaussian. This limitation is not crucial for artery systems since the fiber dispersion is proved to be circular Gaussian.

Soft tissue can nevertheless be assumed to maintain its equilibrium configuration through a set of random events. The reason for this interpretation may be associated

with the random structure of biological environments shaped by random nature of the evolution equations, i.e. random rotation of cells as a Brownian event. A soft tissue can be considered as a complex system composed of a tremendous number of microscopic subsystems that irregularly vary on fast time scales ([51] and [50]). At the very small scales, random fluctuations are a natural part of particle motions which give rise to the *Brownian motion*. In spatially larger scales, the statistical results of underlying dynamics can still be followed to large temporal scales, for our case, it is the anisotropic dispersion of collagen fibers. Consequently, one may follow the mechanical modeling perspective through observing the outcomes of the underlying probabilistic process. In this work, we have interested in the random structure of the rotation concept. Essentially, the mathematical description of the random nature of collagen remodeling is not a new concept and has been well investigated by the community of mathematical biology. For instance, basic governing equations have been presented in close works by [69] and [70]. The cellular migration pattern modifying the matrix environment has been proposed to be governed by a set of vector stochastic differential equations including the perturbation term called random *Langevin force* ([71]). Probabilistic dynamics of the rotation of cells can be described by the continuous form of stochastic dynamics, namely the Fokker-Planck equation ([63]). However, the representation of mechanical models explaining anisotropic remodeling in soft tissue through the complex evolution of stochastic differential equations has not been given. Thus, unlike the existing modeling strategies, we assumed that the source of the statistical dispersion remodeling at a micro or macro scale is the driving Langevin force, which is a random perturbation.

We considered the observed dispersion characteristics of collagen fiber orientations as not being a static structure of the soft tissue but as a stationary state of a transient dynamic mechanism. Our main goal is to derive the macroscopic remodeling of fiber dispersion and give a consistent evolution equation for the time-dependent evolution of generalized structural tensor \mathbf{H} . An evolution form has been previously given by [26] whereas, we have been focused on the analytical form to account the random force term. In this case, the overall collagen remodeling problem at hand intrinsically assumes the existence of an underlying spatially dependent diffusion mechanism that can be originated from a random force acting on the fast time scale. *The fast time*

scale is considered as a feed-back error between cell's automatic actions that source from a complex signal-transduction chain and its cellular environment. Thus, the main consideration in this study was a feed-back model with error, where biological environment utilizes this error in order to reach a biological equilibrium.

Simulation results for axisymmetric deformation problem pointed out one crucial property of randomly perturbed systems obviously: the evolution of κ is so fast compared to the results gathered for internal radius measurement changes. The rate of dispersion formation directly depends on the internal stresses, thus any change in stress pattern is reflected by the dispersion without significant delay. Our analysis has shown that the evolution of κ has a notable effect on the internal radius measurements. We believe that there is a strong need for this algorithm to be implemented on a large sample set to observe the effects of characteristic time and internal stresses in detail. We have seen that the internal radius measurements have a sensitive dependence to the characteristic remodeling times.

At this point, we should mention that there is also a need for an important algorithmic extension to the work which may be considered as a future direction. In equation 5.5 we have pointed out that index p represents the number of fiber families that are modeled simultaneously. This intrinsically represents that a larger number of fiber families with narrow dispersions may be utilized to obtain the whole fiber dispersion behavior. Every fiber family could have its own remodeling parameters which may differ. This could be useful for highly dispersed fiber media. The algorithmic extension probably would result in more efficient representations of the fact with smaller error percentages. This perspective is recommended to the interested readers as a future work.

For numerical simulations, we have stated that the algorithm developed can be used for biaxially strained tissue environments. This is due to the work of [72]. They have shown that in uniaxially extended fibrous structures the GST definition of transversally isotropic \mathbf{H} tensor (see equation A.19) usually represents a strong *negative* bias in the estimations of positive second Piola-Kirchhoff stress tensor. The bias is relative to the ones that are estimated by the angular integration schemes (AI) given in [72]. The problem can be disregarded for biaxially strained cases. For uniaxially strained cases, the remodeling approach derived here *cannot be used for $\kappa > 0.05$* in three

dimensions, due to extremely high error rates on stress estimations. This constraint should be considered as a numerical limitation of the proposed algorithm.

Finally, we aim to emphasize the validity of stress based remodeling stimuli. Limited with the work and approaches utilized here, a nonlinear remodeling stimuli governed by Brownian effects should be linked to a strain based stimulus. According to the proof derived by Trabuco in ([73]), a large class of nonlinear remodeling algorithms based on strain stimulus supplies existing unique solutions. The solution path is also stable. Although the existence and uniqueness can be assumed for small strains, for an approach similar to ours, should depend on strain for large deformation case at first guess. Computational results validate such an assumption.

In our preliminary formulation, we have tested the uniaxial case on the collagen gel remodeling. Modeling of collagen evolution in living organisms is a highly active research area due to its role in mechanical maturation and adaptation of the organism towards environmental changes. In this work, we formulated a collagen fiber remodeling algorithm that incorporates the random evolution of single fibers resulting with a macroscopic mechanical description of anisotropic evolution. In order to get simplified matrix forms of non-iterative local update procedures eliminating the drawbacks of nonlinear solutions, the evolution equations are linearized. With this form, one could separate the functional dependency of overall dispersion evolution from a single fiber rotation. The separation simplifies the application of complex processes which is computationally advantageous not only usable for collagen, but also any other dispersed quantity. Additionally, the algorithm utilizes the exact mathematical forms of fiber rotations used in the cellular scale model. By this way, physically correct mathematical forms are implemented while modeling the cellular scale random rotations. It should be noted that the algorithm can be used for only biaxially strained tissues due to previously discussed algorithmic reasons. This was the main reason why we have only considered the artery deformation model which is known to be biaxial. We also presented a continuum mechanical framework for the evolution equations and how they could be coupled with time-dependent axisymmetric evolution of the artery deformation under internal blood pressure. From an algorithmic point of view, the phenomenological model developed here gave us an insight into the nature of the cellular level Langevin force parameters. The whole evolution process

is governed by one important parameter τ_μ where its value affects the steady state solution of mechanical deformation. We can conclude that a linear evolution algorithm gave consistent and acceptable results from both numerical and biological point of views.

The remodeling framework developed here can be used for fast implementation and improve the prediction accuracy. Especially for situations, where the characteristic evolution times of mean fiber orientation and dispersion are of crucial importance, and when there is a strong need to consider the effects of stochastic nature at the very small scale. This model can be adapted to future algorithmic schemes dealing with the nature of statistical evolution and it can play a useful role for finite element implementation of scaffold designs or vascular system modeling.

6.1.1 Perspectives on growth and remodeling models

In this work, we extended the macroscopic evolution parameters by considering them a randomly perturbed state of an ideal situation. And, we could be able to link the random force with the final structural magnitude via the “Transfer function concept”. One natural question that would arise is to ask whether there exist similar functions for not only collagen remodeling but also isotropic-anisotropic growth cases. Then, the extension and testing of newly developed forms should be analyzed.

Similar to the forms discussed in the text, the nonlinear extensions of the random perturbation will inevitably affect the derived quantities. However, derivations may result with the loss of computational efficiency. The issue is not so much critical if very small time steps are selected. The most important extensions of the derived methodology here would be in the investigation of diseased situations. The model can be used in order to extract the random force level and give the ability to see how it propagates in the medium as the tissue evolves. However, many critical questions should be answered before the application of such models to the prediction of disease situations. We discuss these circumstances in perspectives on experiments section.

6.1.2 Perspectives on numerical problems

κ -based evolutionary approaches depend on a generalized structural tensor H . However, GST based formulations suffer from the excessive generalization of the

orientation density by assuming that the total fiber bundles can be represented by their mean value. Surely, this is not correct as there exist fiber bundles that are not spatially close to the mean value. This results with spurious mechanical magnitudes in simulations. Proposals that aims to solve this problem have recently been made. A novel extension could be the application of these techniques on the probabilistic framework discussed in this work. Since computational efficiency is required, we advocate κ -based solution procedures.

As previously mentioned, the growth and remodeling models may include so many internal variables giving rise to an increase in computational complexity. Then, new kind of solution techniques which demands smaller time steps but which are suitable for large deformation problem should be in consideration. One typical approach could be the formulation and adaptation of existing explicit-implicit hybrid computational methods to remodeling problems. Simulation algorithms based on CPU-GPU shared memory applications has been well established for known libraries (cublas, magma etc.). Then, new specialized theoretical schemes targeting for an extreme number of internal variables for GR simulations are welcomed. However, existence and uniqueness of numerical solutions and stability may still affect the solution procedures until abstract analytical proofs for nonlinear large deformation cases are supplied. Investigation of the existence and uniqueness of analytical solutions and necessary and sufficient conditions for uniqueness is a challenging topic. Understanding the challenge is not difficult: biological structures are complex systems and they are supposed to obey sensitive dependence to initial conditions. However, somehow, experiments show that similar mechanical boundary constraints with different initial conditions result with similar final solutions with similar evolution patterns. The enlightenment of such a mathematical phenomena will inevitably impact the future modeling trends and it will encourage new questions to be asked.

6.1.3 Perspectives on experimental validation related issues

Many of the growth and remodeling phenomena are widely understood by designed and controlled in-vitro gel experiments. A future perspective and reflection of this thesis work will inevitably find its position in designing new collagen-based experimentation to search for the source of the random forces, that are created and

destroyed through the growth and remodeling process. The main question is “which parts of the cellular functioning is directly related to the perception of random signals”. Randomness can be utilized in order to reach biological equilibrium, but is there genetic and epigenetic factors that are directly related to the *source of randomness*? Experiments that are directed towards these questions may give insights to the analysis of growth and remodeling phenomena. Some other research links may be found in new visualization techniques of the randomness (like diffusion tensor-based imaging in neurology) that is propagating in remodeling time scales.

6.1.4 Interdisciplinary reflections to other scientific fields (complex systems, social sciences and paleontology)

In this section, we discuss (possible) the interdisciplinary reflections of the potential of growth and remodeling phenomena on other scientific fields including: complex systems, social sciences and paleontology.

6.1.4.1 Profitable utilization by randomness in social systems

Profitable utilization by randomness has been recently introduced into the spatial evolutionary social game theory. This field may be considered as a related field of computational sociology, which tries to analyze collective or individual human behavior on the utility maximization. The utility is maximized by social agents (individuals, establishments) through analyzing their local/global effects of collective and selfish movements. Since behavioral science belongs to social science context, we limit our discussions on this distant topic, however, it is natural to estimate that an inevitable interdisciplinary connection exists.

The concept of game theory has been introduced in to biology by Maynard Smith in 1973 [74]. According to spatial game theory, social agents may interact locally in order to reach a microscopic (individual) and macroscopic (collective behavior) level of utility equilibrium. The concept is analogous to the homeostatic equilibrium where cellular actions do not modify the continuum anymore. Recent publications argue that individuals may choose to behave in a noisy way and in fact, they do not make mistakes [75]. In their words: “Randomness in social systems may play a functional role”. Supporting this idea, Macy and Tsvetkova [76] point that noise can be individually

or collectively beneficial. According to the author, from the defined perspective, the functional relationship between randomness and utility, for both social and biological structures, includes future potential as a research area.

6.1.4.2 Complex systems

Many of the algorithms proposed by the bio-mechanics community on growth and remodeling phenomena achieved successful interpretations about the underlying hidden rules. We declare the governing evolutionary forces as hidden, since the number of interacting chemical agents reaches to an immense level, whereas the outcome of the process could be described by a few global determiner. One example is the isotropic growth of a tumor or volumetric growth of an artery aneurysm. Phenomenological models, we may add mechanistic approaches with a low number of variables, are idealizations of the growth process. Then, how relatively a small number of mechanical internal variables could represent the outcome and extremely complex process? Why the outcome of the processes are so smooth and how it is controlled by the cellular activity? Are these questions are related to the self-organization? According to Nagler and his coworkers [77] a “*self-organized critical system*”, the concept has been introduced by Per Bak in 1987, is a driven dissipative system having properties :

1. a medium
2. where disturbances are propagating through the medium
3. giving rise to the modification of the medium,
4. such that the system reaches critical state,
5. and the modification of the medium is completed, and an unusual balance situation is reached.

which exhibits above-mentioned blocks of modification steps that are similarly observed in remodeling situations. Surely, that similarity requires an analytical background. If collagen remodeling process is a self-organized one, then how can its mathematical governing equations be linked with the continuum mechanical formulations. And if the similarity exists, how it can be linked with the state of the art modeling techniques that are currently being utilized for the description of the diseases

and growth and remodeling changes. These questions have very deep roots towards understanding the underlying processes of biological phenomena and their possible answers via abstract analytical proofs may revolutionize the looking perspective. They require a strong understanding of the current approaches.

6.1.4.3 Separation of evolutionary time scale from the growth and remodeling time scale

The model proposed here could find theoretical applications in paleontology and its interdisciplinary related fields. We will discuss the topic for continuum frameworks developed for general growth and remodeling equations. Biology is a historical science. Unlike social systems, that history is supposed to be stored in the genetic code. As the species evolve in very long time intervals, the mechanical structure of the species reaches to a homeostatic position in an “ecological sense” instead of mechanical equilibrium observed in short time periods governed by the “mechanical sense”.

For short time periods, the growth and remodeling process assumes an intrinsic remodeling time \underline{t} (in months years), which is separated from the short time scale t (in the order of seconds) where remodeling is not observed. Analogously, for very long evolutionary time scales ($\underline{t} > 10^4$ years or so), species reach to a desired mechanical equilibrium which is usually governed by ecological factors and rivals. Thus, for a probabilistic structural evolution of \mathbf{H} from $\underline{t}^1 \rightarrow \underline{t}^2$ requires a continuum formulation of an additional layer framework which should be constructed on the top of the framework derived in this work. In this case, the propagation of the probabilistic magnitudes could be able to be tracked not only in time scales limited by an individual life cycle but the life cycle of the species.

The experimental research linked with these possible formulations are expected to be limited by the investigation of hard tissue (bones itself, the size of soft tissue organs determined by the position of bones) only. On the other hand, any predictive models will have strong potential to explain the mechanical aspects of genetic information, which can not be extracted by controlled short time experiments. Novel continuum formulations should be realized from this perspective.

6.2 Closure

Briefly, the remodeling framework developed here can be used for fast implementation and improve the prediction accuracy. Especially for the situations, where the characteristic evolution times of mean fiber orientation and dispersion are of crucial importance, and when there is a strong need to consider the effects of stochastic nature at the very small scale. This model can be adapted to future algorithmic schemes dealing with the nature of statistical evolution and it can play a useful role for finite element implementation of scaffold designs or vascular system modeling.





REFERENCES

- [1] **Jiu-sheng, R.** (2012). Effects of dispersion of fiber orientation on the mechanical property of the arterial wall, *Journal of Theoretical Biology*, 301, 153–160.
- [2] **Kuhl, E., Maas, R., Himpel, G. and Menzel, A.** (2007). Computational modeling of arterial wall growth, Attempts towards patient-specific simulations based on computer tomography, *Biomechanics and Modeling in Mechanobiology*, 6, 321–331.
- [3] **Holzappel, G.A.** (2009). *Biomechanical Modelling at the Molecular, Cellular and Tissue Levels*, volume 508 of *CISM International Centre for Mechanical Sciences*, Springer-Verlag Wien, 1 edition.
- [4] **Driessen, N.J.B., Cox, M.A.J., Bouten, C.V.C. and Baaijens, F.P.T.** (2008). Remodelling of the angular collagen fiber distribution in cardiovascular tissues, *Biomechanics and Modeling in Mechanobiology*, 7(2), 93–103.
- [5] **Rubbens, M.P., Mol, A., Boerboom, R.A., Bank, R.A., Baaijens, F.P.T. and Bouten, C.V.C.** (2009b). Intermittent Straining Accelerates the Development of Tissue Properties in Engineered Heart Valve Tissue, *Tissue Engineering Part A*, 15(5), 999–1008.
- [6] **Çoban, G. and Çelebi, M.S.** (2016). A novel computational remodelling algorithm for the probabilistic evolution of collagen fibre dispersion in biaxially strained vascular tissue, *Mathematical Medicine and Biology*, doi: 10.1093/imammb/dqw012.
- [7] **Ambrosi, D., Ateshian, G.A., Arruda, E.M., Cowin, S.C., Dumais, J., Goriely, A., Holzappel, G.A., Humphrey, J.D., Kemkemer, R., Kuhl, E., Olberding, J.E., Taber, L.A. and Garikipati, K.** (2011). Perspectives on biological growth and remodeling, *Journal of the Mechanics and Physics of Solids*, 59(4), 863–883, <http://www.sciencedirect.com/science/article/pii/S0022509610002516>.
- [8] **Boerboom, R.A., Driessen, N.J.B., Bouten, C.V.C., Huyghe, J.M. and Baaijens, F.P.T.** (2003). Finite Element Model of Mechanically Induced Collagen Fiber Synthesis and Degradation in the Aortic Valve, *Annals of Biomedical Engineering*, 31, 1040–1053.
- [9] **Baaijens, F.P.T., Bouten, C.V.C. and Driessen, N.J.B.** (2010). Modeling collagen remodeling, *Journal of Biomechanics*, 43, 166–175.
- [10] **Driessen, N.J.B., Wilson, W., Bouten, C.V.C. and Baaijens, F.P.T.** (2004). A computational model for collagen fibre remodelling in

the arterial wall, *Journal of Theoretical Biology*, 226(1), 53–64, <http://www.sciencedirect.com/science/article/pii/S0022519303003199>.

- [11] **Lee, E., Holmes, J.W. and Costa, K.D.** (2008). Remodeling of Engineered Tissue Anisotropy in Response to Altered Loading Conditions, *Annals of Biomedical Engineering*, 36(8), 1322–1334, <http://dx.doi.org/10.1007/s10439-008-9509-9>.
- [12] **Pang, Y., Ucuzian, A.A., Matsumura, A., Brey, E.M., Gassman, A.A., Husak, V.A. and Greisler, H.P.** (2009). The temporal and spatial dynamics of microscale collagen scaffold remodeling by smooth muscle cells, *Biomaterials*, 30(11), 2023–2031, <http://www.sciencedirect.com/science/article/pii/S0142961208010466>.
- [13] **Balestrini, J.L. and Billiar, K.L.** (2009). Magnitude and Duration of Stretch Modulate Fibroblast Remodeling, *Journal of Biomechanical Engineering*, 131(5), 051005–9.
- [14] **Rubbens, M.P., Driessen-Mol, A., Boerboom, R.A., Koppert, M.M.J., van Assen, H.C., TerHaar Romeny, B.M., Baaijens, F.P.T. and Bouten, C.V.C.** (2009). Quantification of the Temporal Evolution of Collagen Orientation in Mechanically Conditioned Engineered Cardiovascular Tissues, *Annals of Biomedical Engineering*, 37(7), 1263–1272, <http://dx.doi.org/10.1007/s10439-009-9698-x>.
- [15] **de Jonge, N., Kanters, F.M.W., Baaijens, F.P.T. and Bouten, C.V.C.** (2013). Strain-induced Collagen Organization at the Micro-level in Fibrin-based Engineered Tissue Constructs, *Annals of Biomedical Engineering*, 41(4), 763–774.
- [16] **Barocas, V.H. and Tranquillo, R.T.** (1997). An Anisotropic Biphasic Theory of Tissue-Equivalent Mechanics: The Interplay Among Cell Traction, Fibrillar Network Deformation, Fibril Alignment, and Cell Contact Guidance, *J Biomech Eng*, 119(2), 137–145.
- [17] **Zhao, L., Sang, C., Yang, C. and Zhuang, F.** (2011). Effects of stress fiber contractility on uniaxial stretch guiding mitosis orientation and stress fiber alignment, *Journal of biomechanics*, 44(13), 2388–2394.
- [18] **Kaunas, R., Usami, S. and Chien, S.** (2006). Regulation of stretch-induced JNK activation by stress fiber orientation, *Cellular Signalling*, 18(11), 1924–1931, <http://www.sciencedirect.com/science/article/pii/S0898656806000453>.
- [19] **Soares, A.L.F., Oomens, C.W.J. and Baaijens, F.P.T.** (2012). A computational model to describe the collagen orientation in statically cultured engineered tissues, *Computer Methods in Biomechanics and Biomedical Engineering*, 0(0), 1–12, <http://www.tandfonline.com/doi/abs/10.1080/10255842.2012.680192>, PMID: 22548258, <http://www.tandfonline.com/doi/pdf/10.1080/10255842.2012.680192>.

- [20] **Hariton, I., deBotton, G., Gasser, T.C. and Holzapfel, G.A.** (2007). Stress-driven collagen fiber remodeling in arterial walls, *Biomechanics and Modeling in Mechanobiology*, 6(3), 163–175.
- [21] **Karsaj, I., Sansour, C. and Soric, J.** (2009). The modelling of fibre reorientation in soft tissue, *Biomechanics and Modeling in Mechanobiology*, 8(5), 359–370, <http://dx.doi.org/10.1007/s10237-008-0142-1>.
- [22] **Gasser, T.C., Ogden, R.W. and Holzapfel, G.A.** (2006). Hyperelastic modelling of arterial layers with distributed collagen fibre orientations, *J. R. Soc. Interface*, 3, 15–35.
- [23] **Schrieffl, A.J., Reinisch, A.J., Sankaran, S., Pierce, D.M. and Holzapfel, G.A.** (2012). Quantitative assessment of collagen fibre orientations from two-dimensional images of soft biological tissues, *J. R. Soc. Interface*, 9, 3081–3093.
- [24] **Federico, S. and Gasser, T.C.** (2010). Nonlinear elasticity of biological tissues with statistical fibre orientation, *J. R. Soc. Interface*, 7, 955–966.
- [25] **Holzapfel, G.A. and Ogden, R.W.** (2010). Constitutive modelling of arteries, *Proc. R. Soc. A*, 466, 1551–1597.
- [26] **Menzel, A., Harrysson, M. and Ristinmaa, M.** (2008). Towards an orientation-distribution-based multi-scale approach for remodelling biological tissues, *Computer Methods in Biomechanics and Biomedical Engineering*, 11(5), 505–524, <http://www.tandfonline.com/doi/abs/10.1080/10255840701771776>, PMID: 19230147, <http://www.tandfonline.com/doi/pdf/10.1080/10255840701771776>.
- [27] **Menzel, A. and Waffenschmidt, T.** (2009). A microsphere-based remodelling formulation for anisotropic biological tissues, *Phil. Trans. R. Soc. A*, 367(1902), 3499–3523.
- [28] **Kuhl, E. and Holzapfel, G.A.** (2007). A continuum model for remodeling in living structures, *Journal of Materials Science*, 42(21), 8811–8823, <http://dx.doi.org/10.1007/s10853-007-1917-y>.
- [29] **Saez, P., Pena, E., Doblare, M. and Martinez, M.** (2011). An Anisotropic Microsphere-Based Approach for Fiber Orientation Adaptation in Soft Tissue, *IEEE TRANSACTIONS ON BIOMEDICAL ENGINEERING*, 58(12), 3500–3503.
- [30] **Nagel, T. and Kelly, D.J.** (2012). Remodelling of collagen fibre transition stretch and angular distribution in soft biological tissues and cell-seeded hydrogels, *Biomechanics and Modeling in Mechanobiology*, 11(3-4), 325–339, <http://dx.doi.org/10.1007/s10237-011-0313-3>.
- [31] **Kroon, M.** (2010). A continuum mechanics framework and a constitutive model for remodelling of collagen gels and collagenous tissues,

Journal of the Mechanics and Physics of Solids, 58(6), 918–933,
<http://www.sciencedirect.com/science/article/pii/S0022509610000530>.

- [32] **Holzappel, G.A.** (2000). *Nonlinear Solid Mechanics, A Continuum Approach for Engineering*, John Wiley & Sons.
- [33] **Lee, E.H.** (1969). Elastic Plastic Deformations at Finite Strains, *Journal of Applied Mechanics*, 1–6.
- [34] **Lubarda, V.A. and Hoger, A.** (2002). On the mechanics of solids with a growing mass, *International Journal of Solids and Structures*, 39, 4627–4664.
- [35] **Lubarda, V.A.** (2004). Constitutive theories based on the multiplicative decomposition of deformation gradient: Thermoelasticity, elastoplasticity, and biomechanics, *Appl. Mech. Rev.*, 57(2), 95–108.
- [36] **Kuhl, E., Menzel, A. and Steinmann, P.** (2003). Computational modeling of growth: A critical review, a classification of concepts and two new consistent approaches, *Computational Mechanics*, 32, 71–88.
- [37] **Kuhl, E. and Steinmann, P.** (2003). Mass- and volume-specific views on thermodynamics for open systems, *Proc. R. Soc. Lond. A*, 459, 2547–2568.
- [38] **Editorial** (2014). Growing matter: A review of growth in living systems, *Journal of the Mechanical Behavior of Biomedical Materials*, 29, 529–543.
- [39] **Miehe, C.** (1996). Numerical computation of algorithmic (consistent) tangent moduli in large-strain computational inelasticity, *Computer Methods in Applied Mechanics and Engineering*, 134(3-4), 223–240, <http://www.sciencedirect.com/science/article/pii/S0045782596010195>.
- [40] **Menzel, A. and Kuhl, E.** (2012). Frontiers in growth and remodeling, *Mechanics Research Communications*, 42(0), 1–14, <http://www.sciencedirect.com/science/article/pii/S0093641312000225>, recent Advances in the Biomechanics of Growth and Remodeling.
- [41] **Menzel, A.** (2007). A fibre reorientation model for orthotropic multiplicative growth, *Biomechanics and Modeling in Mechanobiology*, 6(5), 303–320, <http://dx.doi.org/10.1007/s10237-006-0061-y>.
- [42] **Taber, L.A.** (1995). Biomechanics of Growth, Remodeling, and Morphogenesis, *Appl. Mech. Rev.*, 48(8), 487–545.
- [43] **Qi, N., Gao, H., Ogden, R.W., Hill, N.A., Holzappel, G.A., Han, H.C. and Luo, X.** (2015). Investigation of the optimal collagen fibre orientation in human iliac arteries, *Journal of the mechanical behavior of biomedical materials*, 52, 108–119.

- [44] **Himpel, G., Menzel, A., Kuhl, E. and Steinmann, P.** (2008). Time-dependent fibre reorientation of transversely isotropic continua—Finite element formulation and consistent linearization, *International Journal for Numerical Methods in Engineering*, 73(10), 1413–1433, <http://dx.doi.org/10.1002/nme.2124>.
- [45] **Driessen, N.J.B., Peters, G.W.M., M., H.J., Bouten, C.V.C. and T., B.F.P.** (2003). Remodelling of continuously distributed collagen fibres in soft connective tissues, *Journal of Biomechanics*, 36, 1151–1158.
- [46] **Grytz, R. and Meschke, G.** (2010). A computational remodeling approach to predict the physiological architecture of the collagen fibril network in corneo-scleral shells, *Biomechanics and Modeling in Mechanobiology*, 9(2), 225–235, <http://dx.doi.org/10.1007/s10237-009-0173-2>.
- [47] **Sáez, P., Alastrué, V., Peña, E., Doblaré, M. and Martínez, M.A.** (2012). Anisotropic microsphere-based approach to damage in soft fibered tissue, *Biomechanics and Modeling in Mechanobiology*, 11(5), 595–608, <http://dx.doi.org/10.1007/s10237-011-0336-9>.
- [48] **Holzapfel, G.A., Gasser, T.C. and Ogden, R.W.** (2000). A New Constitutive Framework for Arterial Wall Mechanics and a Comparative Study of Material Models, *Journal of Elasticity*, 61(1-3), 1–48.
- [49] **Rubbens, M.P., Mol, A., van Marion, M.H., Hanemaaijer, R., Bank, R.A., Baaijens, F.P.T. and Bouten, C.V.C.** (2009c). Straining mode-dependent collagen remodeling in engineered cardiovascular tissue, *Tissue Engineering Part A*, 15(4), 841–849.
- [50] **Risken, H.** (1989). *The Fokker-Planck Equation: Methods of Solution and Applications*, Springer-Verlag, Berlin Heidelberg, 2 edition.
- [51] **Friedrich, R., Peinke, J., Sahimi, M. and Tabar, M.R.R.** (2011). Approaching complexity by stochastic methods: From biological systems to turbulence, *Physics Reports*, 506(5), 87–162, <http://www.sciencedirect.com/science/article/pii/S0370157311001530>.
- [52] **Çoban, G. and Çelebi, M.S.** (2015). Exact analytical representation of fiber stress tensor based on angular integration (AI) through cellular level probabilistic equations, *Proceedings of the International Conference on Numerical Analysis and Applied Mathematics 2014 (ICNAAM-2014)*, volume1648, AIP Conf. Proc., pp.320002–1.
- [53] **Benkherourou, M., Gumery, P., Tranqui, L. and Tracqui, P.** (2000). Quantification and macroscopic modeling of the nonlinear viscoelastic behavior of strained gels with varying fibrin concentrations, *IEEE TRANSACTIONS ON BIOMEDICAL ENGINEERING*, 47(11), 1465–1475.
- [54] **Velada, J.L., Hollingsbee, D.A., Menzies, A.R., Cornwell, R. and Dodd, R.A.** (2002). Reproducibility of the mechanical properties of Vivostat – system patient-derived fibrin sealant, *Biomate-*

rials, 23(10), 2249–2254, <http://www.sciencedirect.com/science/article/pii/S0142961201003593>.

- [55] **Cummings, C.L., Gawlitta, D., Nerem, R.M. and Stegemann, J.P.** (2004). Properties of engineered vascular constructs made from collagen, fibrin, and collagen-fibrin mixtures, *Biomaterials*, 25(17), 3699–3706, <http://www.sciencedirect.com/science/article/pii/S0142961203010068>.
- [56] **Haugh, M.G., Thorpe, S.D., Vinardell, T., Buckley, C.T. and Kelly, D.J.** (2012). The application of plastic compression to modulate fibrin hydrogel mechanical properties, *Journal of the Mechanical Behavior of Biomedical Materials*, 16(0), 66–72, <http://www.sciencedirect.com/science/article/pii/S1751616112002676>.
- [57] **Rowe, S.L., Lee, S. and Stegemann, J.P.** (2007). Influence of thrombin concentration on the mechanical and morphological properties of cell-seeded fibrin hydrogels, *Acta Biomaterialia*, 3(1), 59–67, <http://www.sciencedirect.com/science/article/pii/S1742706106000997>.
- [58] **Engelmayr, Jr., G.C., Rabkin, E., Sutherland, F.W.H., Schoen, F.J., Mayer, Jr., J.E. and Sacks, M.S.** (2005). The independent role of cyclic flexure in the early in vitro development of an engineered heart valve tissue, *Biomaterials*, 26(2), 175–187, <http://www.sciencedirect.com/science/article/pii/S0142961204001735>.
- [59] **Ignateva, N.Y., Danilov, N.A., Averkiev, S.V., Obrezkova, M.V., Lunin, V.V. and Sobol, E.N.** (2007). Determination of hydroxyproline in tissues and the evaluation of the collagen content of the tissues, *Journal of Analytical Chemistry*, 62(1), 51–57, <http://dx.doi.org/10.1134/S106193480701011X>.
- [60] **Simha, N.K., Fedewa, M., Leo, P.H., Lewis, J.L. and Oegema, T.** (1999). A composites theory predicts the dependence of stiffness of cartilage culture tissues on collagen volume fraction, *Journal of Biomechanics*, 32(5), 503–509.
- [61] **Råback, P., Malinen, M., Ruokolainen, J., Pursula, A. and Zwinger, T.** (2016). Elmer-Finite element software for multiphysical problems, Elmer Models Manual, CSC – IT Center for Science, release 8.1 edition, <http://www.csc.fi>.
- [62] **Betsch, P., Menzel, A. and Stein, E.** (1998). On the parametrization of finite rotations in computational mechanics: A classification of concepts with application to smooth shells, *Computer Methods in Applied Mechanics and Engineering*, 155(3-4), 273–305, <http://www.sciencedirect.com/science/article/pii/S0045782597001588>.
- [63] **Kemkemer, R., Jungbauer, S., Kaufmann, D. and Gruler, H.** (2006). Cell Orientation by a Microgrooved Substrate Can Be Predicted by Automatic Control Theory, *Biophysical Journal*, 90(12), 4701–4711.

- [64] **Creane, A., Maher, E., Sultan, S., Hynes, N., Kelly, D.J. and Lally, C.** (2011). Prediction of fibre architecture and adaptation in diseased carotid bifurcations, *Biomechanics and Modeling in Mechanobiology*, 10(6), 831–843, <http://dx.doi.org/10.1007/s10237-010-0277-8>.
- [65] **Mardia, K.V. and Jupp, P.E.** (2000). *Directional Statistics*, John Wiley & Sons, Ltd.
- [66] **Viñales, A. and Despósito, M.** (2006). Anomalous diffusion: Exact solution of the generalized Langevin equation for harmonically bounded particle, *Phys. Rev. E*, 73(1), 016111, <http://link.aps.org/doi/10.1103/PhysRevE.73.016111>.
- [67] **Taber, L.A.** (2004). *NONLINEAR THEORY OF ELASTICITY, Applications in Biomechanics*, World Scientific, LONDON.
- [68] **Holzapfel, G.A.**, (2009). Arterial Tissue in Health and Disease: Experimental Data, Collagen-Based Modeling and Simulation, Including Aortic Dissection, **G.A. Holzapfel and R.W. Ogden**, editors, Biomechanical Modelling at the Molecular, Cellular and Tissue Levels, volume 508, chapter CISM International Centre for Mechanical Sciences, Springer Vienna, pp.259–344.
- [69] **Dallon, J.C. and Sherratt, J.A.** (1998). A Mathematical Model for Fibroblast and Collagen Orientation, *Bulletin of Mathematical Biology*, 60, 101–129.
- [70] **Olsen, L., Maini, P.K., Sherratt, J.A. and Dallon, J.** (1999). Mathematical modelling of anisotropy in fibrous connective tissue, *Mathematical Biosciences*, 158, 145–170.
- [71] **Groh, A. and Wagner, M.** (2011). Biased three-dimensional cell migration and collagen matrix modification, *Mathematical Biosciences*, 231(2), 105–119, <http://www.sciencedirect.com/science/article/pii/S0025556411000253>.
- [72] **Cortes, D.H., Lake, S.P., Kadlowec, J.A., Soslowsky, L.J. and Elliott, D.M.** (2010). Characterizing the mechanical contribution of fiber angular distribution in connective tissue: comparison of two modeling approaches, *Biomechanics and Modeling in Mechanobiology*, 9(5), 651–658.
- [73] **Trabucho, L.** (2000). Non-linear Bone Remodelling: An Existence and Uniqueness Result, *Mathematical Methods in the Applied Sciences*, 23, 1331–1346.
- [74] **Killingback, T. and Doebeli, M.** (1996). Spatial evolutionary game theory: Hawks and Doves revisited, *Proc. R. Soc. Lond. B*, 263, 1135–1144.
- [75] **Helbing, D. and Yu, W.** (2010). The future of social experimenting, *PNAS*, 107, 5265–5266.
- [76] **Macy, M. and Tsvetkova, M.** (2015). The Signal Importance of Noise, *Sociological Methods and Research*, 44, 306–328.

[77] **Nagler, J., Hauert, C. and Schuster, H.G.** (1999). Self-organized criticality in a nutshell, *Physical Review E*, 60(3), 2706–2709.



APPENDICES

APPENDIX A.1 : Derivation of the Remodeling Algorithm

APPENDIX A.2 : $\kappa - s$ Transfer Function



Appendix A.1

The evolution equation of \mathbf{H} is reduced to the exact solution of a linear matrix differential equation if a suitable \mathbf{h} has been chosen. In this case, there is no need to convert the whole problem into the continuous Fokker-Planck partial differential equation. A preliminary introduction to the concept is presented in [52] where a simplified analytical form of stress tensor components has been derived. The linearization of $\mathbf{h}(\boldsymbol{\theta}, t)$ around $\boldsymbol{\theta}_0$ at time t yields,

$$\mathbf{h}(\boldsymbol{\theta}) = \mathbf{h}(\boldsymbol{\theta}_0) + \nabla(\mathbf{h}(\boldsymbol{\theta}_0)) \cdot (\boldsymbol{\theta} - \boldsymbol{\theta}_0) + \mathcal{O}(\|\boldsymbol{\theta} - \boldsymbol{\theta}_0\|). \quad (\text{A.1})$$

The linearization is given by,

$$\mathbf{h}(\boldsymbol{\theta}, t) = \nabla(\mathbf{h}(\boldsymbol{\theta}_0))\boldsymbol{\theta} + \mathbf{h}(\boldsymbol{\theta}_0) - \nabla(\mathbf{h}(\boldsymbol{\theta}_0))\boldsymbol{\theta}_0, \quad (\text{A.2})$$

$$\mathbf{h}(\boldsymbol{\theta}, t) = \mathbf{B}(\boldsymbol{\theta}_0)\boldsymbol{\theta} + \mathbf{c}(\boldsymbol{\theta}_0), \quad (\text{A.3})$$

where $\mathbf{B} \in \mathfrak{R}^{M \times M}$ and $\mathbf{c} \in \mathfrak{R}^M$ for $\boldsymbol{\theta} \in \mathfrak{R}^M$. From the continuum mechanics perspective, $\boldsymbol{\theta}_0$ can be considered as an ingredient to the previous direction of fiber in the reference configuration which is updated to a new remodeled direction by incremental Newton iterations. By incorporating the linear form in equation A.2, it is possible to represent the integrated form (equation A.4) and differential form in equation A.5 of the fiber orientation evolution including random effects,

$$\begin{aligned} \boldsymbol{\theta}(t + \Delta t) &= \boldsymbol{\theta}(t) + \int_t^{t+\Delta t} \mathbf{h}(\boldsymbol{\theta}(t'), t') dt', \\ &+ \int_t^{t+\Delta t} \mathbf{G}(\boldsymbol{\theta}(t'), t') \boldsymbol{\Gamma}(t') dt', \end{aligned} \quad (\text{A.4})$$

$$d\boldsymbol{\theta}(t) = (\mathbf{B}(t) \boldsymbol{\theta}(t) + \mathbf{c}(t)) dt + \Sigma d\mathbf{W}(t), \quad (\text{A.5})$$

where $d\mathbf{W}(t)$ is a Wiener process ([50, 51]) with the property,

$$\mathbf{W}(t + \Delta t) - \mathbf{W}(t) = \int_t^{t+\Delta t} \boldsymbol{\Gamma}(t') dt', \quad (\text{A.6})$$

$$d\mathbf{W} = \sqrt{\Delta t} \boldsymbol{\Gamma}(t), \quad (\text{A.7})$$

and $\mathbf{G}(\boldsymbol{\theta}, t)$ as given in equation A.5, is taken to be Σ . In equation A.6, due to the random nature of $\boldsymbol{\Gamma}$, integration is calculated by probabilistic approaches (Itô rule). As previously mentioned, $\boldsymbol{\Gamma}(t) \in \mathfrak{R}^M$ is distributed according to the Gaussian distribution defined by the probability density function $Pr(\boldsymbol{\Gamma})$ as,

$$Pr(\boldsymbol{\Gamma}) = \frac{1}{\sqrt{(2\pi)^M}} \exp\left(-\frac{1}{2} \boldsymbol{\Gamma} \cdot \boldsymbol{\Gamma}\right). \quad (\text{A.8})$$

The angle measurement ($\boldsymbol{\theta}_\mu$) of the expected mean orientation is calculated by utilizing the infinitesimal increase of the expectation function $\mathbb{E}(\boldsymbol{\theta}) = \int_{\boldsymbol{\theta}} Pr(\boldsymbol{\theta}) \boldsymbol{\theta} d\boldsymbol{\theta}$. Since $\mathbb{E}(d\mathbf{W}(t)) = \mathbf{0}$

$$d\boldsymbol{\theta}_\mu = \mathbb{E}(\boldsymbol{\theta} + d\boldsymbol{\theta}) - \mathbb{E}(\boldsymbol{\theta}), \quad (\text{A.9})$$

$$d\boldsymbol{\theta}_\mu = \mathbf{B}(t)\boldsymbol{\theta}_\mu(t)dt + \mathbf{c}(t)dt. \quad (\text{A.10})$$

We want to estimate the expectation of structural tensor through the derived identities in equation A.9. The generalized structure tensor can be defined through the expected value of the variance-covariance matrix $\mathbf{V} = \mathbb{E}(\boldsymbol{\theta} \otimes \boldsymbol{\theta}) - \mathbb{E}(\boldsymbol{\theta}) \otimes \mathbb{E}(\boldsymbol{\theta})$. Using $\mathbb{E}(\Sigma d\mathbf{W}(t) \otimes \Sigma d\mathbf{W}(t)) = \Sigma^2 \mathbf{I} dt$ and assuming a constant dispersion term $\Sigma \in \mathfrak{R}$ and isotropic $d\mathbf{W}$, one obtains the time dependent matrix differential equation for the evolution of \mathbf{V} (and \mathbf{H}) as,

$$\begin{aligned} d\mathbf{V}(t) &= \mathbb{E}((\boldsymbol{\theta} + d\boldsymbol{\theta} - \boldsymbol{\theta}_\mu - d\boldsymbol{\theta}_\mu) \otimes (\boldsymbol{\theta} + d\boldsymbol{\theta} - \boldsymbol{\theta}_\mu - d\boldsymbol{\theta}_\mu)) \\ &\quad - \mathbb{E}((\boldsymbol{\theta} - \boldsymbol{\theta}_\mu) \otimes (\boldsymbol{\theta} - \boldsymbol{\theta}_\mu)), \\ d\mathbf{V}(t) &= \mathbf{B}(t) \otimes \mathbf{V}(t)dt + \mathbf{V}(t) \otimes \mathbf{B}(t)dt + \Sigma^2 \mathbf{I}dt + \mathcal{O}(dt^2). \end{aligned} \quad (\text{A.11})$$

The advantage of linearity is that the internal variable updates can be used analytically. Algorithmically, the update equations from t to $t + \Delta t$ for $\boldsymbol{\theta}_\mu$ and \mathbf{V} are given in

$$\boldsymbol{\theta}_\mu(t + \Delta t) = e^{\Delta t \mathbf{B}} \boldsymbol{\theta}_\mu(t) + \int_0^{\Delta t} e^{(\Delta t - s) \mathbf{B}} \mathbf{c} ds, \quad (\text{A.12})$$

$$\begin{aligned} \mathbf{V}(t + \Delta t) &= e^{\Delta t \mathbf{B}} \mathbf{V}(t) e^{\Delta t \mathbf{B}^T} \\ &\quad + \int_0^{\Delta t} e^{(\Delta t - s) \mathbf{B}} \Sigma^2 \mathbf{I} e^{(\Delta t - s) \mathbf{B}^T} ds. \end{aligned} \quad (\text{A.13})$$

We define the p and q elements of matrix \mathbf{V} as $\mathbf{V}(p, q) = s_{p,q}^2$ where $s_{p,p}^2$ is the variance of the p^{th} angular measurement with a univariate distribution $\mathcal{N}(\theta_\mu, s_{p,p}^2)$. Update equations for mean fiber orientation are,

$$\Delta\theta^{(p)} = \theta_\mu^{(p)}(t + \Delta t) - \theta_\mu^{(p)}(t), \quad (\text{A.14})$$

$$\begin{aligned} \mathbf{a}_\mu(t + \Delta t) &= \mathbf{a}_\mu(t) \cos(\Delta\theta^{(p)}) + (\boldsymbol{\omega} \times \mathbf{a}_\mu(t)) \sin(\Delta\theta^{(p)}) \\ &\quad + \boldsymbol{\omega}(\boldsymbol{\omega} \cdot \mathbf{a}_\mu(t))(1 - \cos(\Delta\theta^{(p)})). \end{aligned} \quad (\text{A.15})$$

Integration of matrix exponentials may not be trivial especially for stiff equations, However, Gaussian quadrature is well performed for our case. We note that equation A.13 is a multidimensional model which does not account for cross relationships of angular variables. It is known that if \mathbf{B} and \mathbf{c} exist, the outcome distribution is multivariate normal in equation A.12.

Appendix A.2

In this section, we will derive the time dependent evolution equation $\dot{\mathbf{H}}(t)$. By definition, presented in [22], the structural tensor \mathbf{H} is given by the following integration over \mathbb{S}^2 with an appropriate normalization as,

$$\mathbf{H} = \frac{1}{4\pi} \int_{\mathbb{S}^2} \rho(\mathbf{a}) \mathbf{a} \otimes \mathbf{a} dS, \quad (\text{A.16})$$

here,

$$\frac{1}{4\pi} \int_{\mathbb{S}^2} \rho(\mathbf{a}) dS = 1. \quad (\text{A.17})$$

For three dimensional transversely isotropic orientation, the dispersion parameter κ is defined as in

$$\kappa = \frac{1}{4} \int_0^\pi \rho(\theta) \sin^3(\theta) d\theta, \quad (\text{A.18})$$

where $\rho(\theta) = n\mathcal{VM}(\theta; \theta_\mu, k)$, and κ is directly related to the structural tensor $\mathbf{H} \in \mathfrak{R}^{3 \times 3}$ as

$$\mathbf{H} = \kappa \mathbf{I} + (1 - 3\kappa) \mathbf{a}_\mu \otimes \mathbf{a}_\mu, \quad (\text{A.19})$$

through a normalized circular von-Mises type probability distribution where $\rho(\mathbf{a}) = \rho(\theta)$.

$$\rho(\theta) = \frac{n}{2\pi I_0(k)} \exp(k (\cos(\theta - \theta_\mu))). \quad (\text{A.20})$$

The normalization, which can be found in [22], converts the probability distribution into an orientation density distribution.

Thus, determination of structural tensor evolution is described by the probability distribution evolution whose outcomes are obtained by solving the probabilistic equation via algorithms given in equations A.12 and A.13. The solution for one dispersed fiber family reduces the dimension of the problem and is given by $\mathbf{V} \in \mathfrak{R}^{1 \times 1}$, and $V_{1,1} = s^2$ where the solution is normally distributed with mean θ_μ and variance s^2 defined by $\mathcal{N}(\theta; \theta_\mu, s^2)$. θ_μ is required only for Rodriguez rotation. In reality, $\theta_\mu = 0$ is taken for distributional properties assuming that individual collagen fiber orientations are clustered around the mean fiber direction $\mathbf{a}_\mu = \mathbf{a}_\mu(\theta_\mu)$. However, angular measurement distribution $\mathcal{N}(\theta; \theta_\mu, s^2)$ cannot be used to calculate the κ directly due to the domain being limited to $0 \leq s \leq \infty$. There should be a transformation from the unbounded domain of s on to a circularly bounded region, in our case, this is the unit circle,

$$\begin{array}{ccc} \varrho & \longrightarrow & k \\ \uparrow & & \downarrow \\ s & \longrightarrow & \kappa \end{array}, \quad (\text{A.21})$$

$$\begin{array}{ccc} \mathcal{WN}(\theta; \theta_\mu, \varrho) & \xrightarrow{\varrho = \frac{I_1(k)}{I_0(k)}} & \mathcal{VM}(\theta; \theta_\mu, k) \\ \uparrow_{\varrho = \exp(-s^2/2)} & & \downarrow \\ \mathcal{N}(\theta; \theta_\mu, s^2) & \xrightarrow{\mathcal{T}^{-1}(s)} & \kappa \end{array}. \quad (\text{A.22})$$

The commutative diagram in equation A.21 explains the transformation path of unbounded variance s^2 in to the circular von Mises variance parameter k . The first step of the transformation includes wrapping the normal distribution (\mathcal{N}) in to a wrapped normal distribution (\mathcal{WN}) on a circular domain. The wrapped distribution includes an infinite sum by definition. Thus, we replaced the wrapped normal distribution by one of the known approximation by the von Mises distribution (\mathcal{VM}) (see [65]), where a parameter transformation is required from wrapped normal's ϱ to von Mises' k . Equation A.22 describes this transformation in detail. Since the transformations are one-to-one and on-to, there is a single transformation function for $s \rightarrow k$ and for $\mathcal{N}(\theta; \theta_\mu, s^2) \rightarrow \kappa$. For numerical purposes, we have defined this transformation function as $s = \mathcal{T}(k)$ where $\mathcal{T} : \mathfrak{R}^+ \rightarrow \mathfrak{R}^+$ to benefit from the definition $\kappa = \kappa(\theta, k)$ as in equation A.18. Then, parameter k is defined using the inverse function as $k = \mathcal{T}^{-1}(s)$. As a result, $\kappa = \kappa(s)$ and its integral form is given as,

$$\kappa = \frac{n}{4} \int_0^\pi \mathcal{VM}(\theta; \theta_\mu, \mathcal{T}^{-1}(s)) \sin^3(\theta) d\theta. \quad (\text{A.23})$$

Table A.1: Approximating $\hat{\kappa}(s)$ functions for $\kappa - s$ transformation. ϵ represents the global error statistics.

$\hat{\kappa}(s) = c_0 \chi_{CDF}^2(c_1 s^{c_2}, \nu) + \epsilon$		$\hat{\kappa}(s) = \left(\frac{1}{3} - c_0\right) \chi_{CDF}^2(c_1 s^{c_2}, \nu_1) + c_0 \chi_{CDF}^2(c_3 s^{c_4}, \nu_2) + \epsilon$	
c_0	1/3	c_0	0.3001596405288
c_1	3.8328011433268	c_1	6.8198674774904
c_2	1.1983102095583	c_2	2.5076967412147
ν	4.1770029065574	ν_1	3.5312593631438
		c_3	2.0108360373395
		c_4	1.5646949492399
		ν_2	2.5742566697292
$\max \epsilon < 2 \times 10^{-3}$		$\max \epsilon $	$< 4 \times 10^{-4}$
		$\max \epsilon \%$	$< 2 \times 10^{-1} \%$

We call the transformation from normal variance s^2 to transversely isotropic dispersion parameter κ via \mathcal{T}^{-1} over the parameterization of k the $\kappa - s$ function. Its parametric representation on the (s, κ) domain through parameterization of k is given by,

$$s = \left(-2 \ln \left(\frac{I_1(k)}{I_0(k)} \right) \right)^{1/2}, \quad (\text{A.24})$$

$$\kappa = n \int_0^\pi \mathcal{VM}(2\theta; 0, k) \sin^3(\theta) d\theta, \quad (\text{A.25})$$

$$n = \left(2 \int_0^\pi \mathcal{VM}(2\theta; 0, k) \sin(\theta) d\theta \right)^{-1}. \quad (\text{A.26})$$

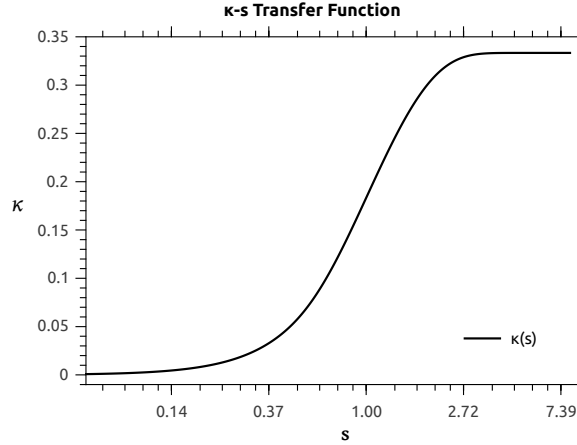


Figure A.1: The graph of $\kappa - s$ function which transforms the normal variance parameter s into the transversally isotropic dispersion parameter κ by \mathcal{T}^{-1} by means of the parameterization of k .

Parametric representations of the equations, such as A.24 and A.26, are cumbersome. The $\kappa - s$ function can be well approximated by χ_{CDF}^2 , which is the cumulative

distribution function (CDF) of the scaled- χ^2 distribution. This approximation is preferred in our work since it has fewer parameters compared to the locally adaptive polynomial approaches. In Table A.1, two simple approximations to the $\hat{\kappa}(s)$ function are presented. The first approximation to $\hat{\kappa}(s)$ with 4 parameters is used in our simulations. It should be noted that precision can be increased arbitrarily by increasing the number of χ_{CDF}^2 functions used for the $\kappa - s$ approximation.

When the time-dependent variance parameter $s = s(t)$ is obtained from numerical simulations, it is directly converted to the time-dependent dispersion parameter $\kappa(t)$ (see in Figure A.1). By using the identity in equation A.19, the evolution equation of the structural tensor can be directly given by the integral form representation,

$$\begin{aligned}
 \mathbf{H}(t) &= \left(\frac{n}{4} \int_0^\pi \mathcal{VM}(\theta; \theta_\mu, \mathcal{T}^{-1}(s(t))) \sin^3(\theta) d\theta \right) \mathbf{I} \\
 &+ \left(1 - 3 \left(\frac{n}{4} \int_0^\pi \mathcal{VM}(\theta; \theta_\mu, \mathcal{T}^{-1}(s(t))) \sin^3(\theta) d\theta \right) \right) \\
 &\times \mathbf{a}_\mu(t) \otimes \mathbf{a}_\mu(t). \tag{A.27}
 \end{aligned}$$

CURRICULUM VITAE

Name Surname : Gürsan ÇOBAN

Place and Date of Birth : Silivri 1981

E-Mail : grsncoban@gmail.com, grscbn@yahoo.com

EDUCATION:

- **B.Sc.** : Istanbul Technical University, Department of Management Engineering (2004)
- **M.Sc.** : Yıldız Technical University, Department of Statistics (2007)

PUBLICATIONS/PRESENTATIONS ON THE THESIS

PRESENTATIONS

- **Çoban, Gürsan** and Çelebi, M. Serdar, 2015: Exact analytical representation of fiber stress tensor based on angular integration (AI) through cellular level probabilistic equations, *Proceedings of the International Conference on Numerical Analysis and Applied Mathematics 2014 (ICNAAM-2014)*, AIP Conf. Proc., 1648 (320002-1).

PUBLICATIONS

- **Çoban, Gürsan** and Çelebi, M. Serdar, 2016: A novel computational remodeling algorithm for the probabilistic evolution of collagen fiber dispersion in biaxially strained vascular tissue, *Mathematical Medicine and Biology*, doi:10.1093/imammb/dqw012

